STRUCTURAL PERFORMANCE OF RC BEAMS STRENGTHENED WITH NSM (SOFFIT AND SIDE)

MD. AKTER HOSEN

DISSERTATION SUBMITTED IN FULFILMENT OF THE REQUIREMENTS FOR THE DEGREE OF MASTER OF ENGINEERING SCIENCE

FACULTY OF ENGINEERING
UNIVERSITY OF MALAYA
KUALA LUMPUR

2015

ORIGINAL LITERARY WORK DECLARATION

Name of the candidate: **Md. Akter Hosen**

Registration/Matric No:

Name of the Degree: **Master of Engineering Science**

Title of Project Paper/Research Report/Dissertation/Thesis (This Work):

STRUCTURAL PERFORMANCE OF RC BEAMS STRENGTHENED WITH NSM (SOFFIT AND SIDE).

Field of Study: **Structural Engineering**

I do solemnly and sincerely declare that:

(1) I am the sole author/writer of this work;

(2) This work is original;

(3) Any use of my work in which copyright exists was done by way of fair dealing and for permitted purposes and any excerpt or extract from, or reference to or reproduction of any copyright work has been disclosed expressly and sufficiently and the title of the work and its authorship have been acknowledged in this work;

(4) I do not have any actual knowledge nor do I ought reasonably to know that the making of this work constitutes an infringement of any copyright work;

(5) I hereby assign all and every rights in the copyright to this work to the University of Malaya ("UM"), who henceforth shall be owner of the copyright in this work and that any reproduction or use in any form or by any means whatsoever is prohibited without the written consent of UM having been first had and obtained;

(6) I am fully aware that if in the course of making these works I have infringe any copyright whether intentionally or otherwise, I may be subject to legal action or any other action as may be determined by UM.

Candidate's Signature Date:

Subscribe and solemnly declare before,

Witness Signature Date:

Name :

Designation :

ABSTRACT

RC structures around the world require rehabilitation or strengthening for various reasons, such as increased load, the repair of damaged members, modification of the structural system, improvement of the structure, or errors in design and construction. In recent decades, strengthening has inevitably been a good choice in terms of structural efficacy as well as from an economic point of view. The near surface mounted (NSM) and the proposed side near surface mounted (SNSM) with steel or carbon fibre reinforced polymer (CFRP) bars provide suitable approaches for the enhancement of the flexural performance of RC beams. However, the NSM-steel technique has only been implemented in very few existing research, and, hence, is still an interesting issue. Furthermore, the SNSM approach to strengthening is a new concept. The main goal of this study is to investigate the experimental behaviour of RC rectangular beams strengthened using the NSM and newly developed SNSM techniques.

To strengthen RC beams, CFRP composites (bars and fabric) and steel bars were used as the strengthening materials. Twenty-five (25) RC beams were fabricated for the experimental programme. The RC beams were cast in the concrete laboratory and divided into seven groups. The first group consisted of one unstrengthened beam as the control beam (CB) to represent the existing structural member. The other groups were strengthened by incorporating NSM, NSM with end anchorage (CFRP fabrics) and the proposed SNSM technique, with different configurations of CFRP and steel bars subjected to gradually increasing static load. All the representative RC beams were tested by a highly precise Instron Universal testing machine and the results were recorded using an automatic data logger.

The experimental results showed that the ultimate capacity of the RC beams strengthened with NSM steel bars increased 96% more than the control beam. When the RC beams were strengthened using NSM steel bars and end anchorage using CFRP fabric, the ultimate capacity was enhanced by 132%. Moreover, a 93% and 138% increase in the ultimate capacity was achieved by strengthening the RC beams with SNSM steel and CFRP bars, respectively. An improvement of 130% in the ultimate capacity was achieved once the pre-cracked beams were strengthened with SNSM CFRP bars. An analytical model has been developed to predict the load, deflection and compressive strain in concrete; the tensile strain in the main reinforcement; and the strain in the NSM bars of the RC beams (control and strengthened) under static loading using sectional analysis. The flexural crack spacing of the RC beam specimens was predicted from existing models. The experimental results showed good agreement with the results obtained from the analytical models. It has been revealed that the deflection of the strengthened beams was significantly smaller than that of the unstrengthened beams. In addition, strengthening using the NSM and SNSM technique decreased the spacing of the cracks and increased the number of cracks. The crack widths also reduced with the increasing number of cracks.

ABSTRAK

Struktur RC di seluruh dunia memerlukan pemulihan atau pengukuhan atas pelbagai sebab, seperti beban meningkat, pembaikan ahli yang rosak, pengubahsuaian sistem struktur, pembaikan struktur, atau kesilapan dalam reka bentuk dan pembinaan. Dalam dekad kebelakangan ini, pengukuhan pasti telah menjadi pilihan yang baik dari segi keberkesanan struktur dan juga dari sudut ekonomi. Permukaan dipasang berhampiran (NSM) dan bahagian yang dicadangkan berhampiran permukaan dipasang (SNSM) dengan keluli atau karbon bertetulang gentian polimer (CFRP) bar menyediakan pendekatan yang sesuai untuk peningkatan prestasi lenturan rasuk RC. Walau bagaimanapun, teknik NSM yang hanya dilaksanakan dalam satu penyelidikan yang sedia ada, dan, dengan itu, masih satu isu yang menarik. Tambahan pula, pendekatan SNSM untuk pengukuhan merupakan satu konsep baru. Matlamat utama kajian ini adalah untuk menyiasat tingkah laku eksperimen rasuk segi empat tepat KM diperkukuhkan menggunakan NSM dan teknik SNSM yang baru dibangunkan.

Untuk mengukuhkan rasuk RC, komposit CFRP (bar dan kain) dan bar keluli telah digunakan sebagai bahan pengukuhan. Dua puluh lima rasuk (25) KM telah direka untuk program uji kaji. RC rasuk dibuang di makmal konkrit dan dibahagikan kepada tujuh kumpulan. Kumpulan pertama terdiri daripada satu rasuk unstrengthened sebagai rasuk kawalan untuk mewakili anggota struktur yang sedia ada. Kumpulan-kumpulan lain telah diperkukuh dengan memasukkan NSM, NSM dengan akhir berlabuh (fabrik CFRP) dan teknik SNSM yang dicadangkan, dengan konfigurasi yang berlainan CFRP dan keluli bar tertakluk kepada secara beransur-ansur meningkatkan beban statik. Semua RC rasuk wakil telah diuji oleh yang sangat tepat Instron Universal mesin ujian dan keputusan direkodkan menggunakan data logger automatik.

Keputusan eksperimen menunjukkan bahawa kapasiti muktamad rasuk RC diperkukuh dengan batang keluli NSM meningkat 96% lebih daripada rasuk kawalan. Apabila rasuk RC telah diperkukuhkan dengan menggunakan batang besi NSM dan akhir berlabuh menggunakan fabrik CFRP, kapasiti utama telah dipertingkatkan dengan 132%. Selain itu, peningkatan 93% dan 138% dalam kapasiti muktamad telah dicapai dengan mengukuhkan RC rasuk bar keluli dan CFRP SNSM masing-masing. Peningkatan sebanyak 130% dalam kapasiti muktamad telah dicapai sekali rasuk pra-retak telah diperkukuhkan dengan bar SNSM CFRP. Model analisis telah dibangunkan untuk meramalkan beban, pesongan dan terikan mampatan dalam konkrit; terikan tegangan dalam tetulang utama; dan terikan dalam bar NSM RC rasuk (kawalan dan diperkukuhkan) di bawah muatan statik menggunakan analisis keratan. Jarak retak lenturan RC spesimen rasuk telah diramalkan daripada model sedia ada. Keputusan eksperimen menunjukkan perjanjian yang baik dengan keputusan yang diperolehi daripada model analisis. Ia telah mendedahkan bahawa pesongan rasuk diperkuatkan adalah lebih kecil berbanding rasuk unstrengthened. Di samping itu, mengukuhkan menggunakan NSM dan SNSM teknik mengurangkan jarak retak dan meningkatkan bilangan retak. Lebar retak juga berkurangan dengan peningkatan jumlah retak.

ACKNOWLEDGEMENTS

First of all, all praise to Allah SWT for giving me the strength and the patience to have this work completed. I would like to express my sincere thanks and deep appreciation to my supervisor Professor Ir. Dr. Mohd Zamin Jumaat for his valuable guidance, encouragement, patience, and for his precious time spent on the fruitful discussion during the research work, which has been extremely valuable in conducting this study.

My research work could be conducted with the full financial support of the University of Malaya High Impact Research Grant under Account No UM.C/HIR/MOHE/ENG/36 (D000036-160001).

My profound appreciation and sincere thanks to all staff members from the Department of Civil Engineering and also Faculty of Engineering. Special thanks go to Mr. Md. Moshiur Rahman, Dr. A.B.M. Saiful Islam, Mr. Kh. Mahfuz ud Darain, Mr. M. Obaydullah, Mr. Mahmudur Rahman Soeb, Mr. Nazmul Huda and Mr. Mohamed Kamruzzaman for helping me for conducting this research. All the technicians at concrete lab and heavy structure lab in Department of Civil Engineering are greatly thanked for helping me at every stage of the experimental work.

Finally, I would like to express all my gratitude to my parents for their supported, encouraged, and guided me with unconditional love. I believe there is no more important thing than my family. Without their love and support, my M. Eng. Sc research could not be completed. I would like to dedicate my dissertation to them.

Md Akter Hosen

University of Malaya, Malaysia

July, 2015

TABLE OF CONTENTS

LIST OF FIGURES

LIST OF TABLES

LIST OF SYMBOLS

A_s	Cross sectional area of main reinforcement
A_{NSM}	Cross sectional area of NSM reinforcement
A_{ts}	Transformed area of steel bar
A_{tNSM}	Transformed area of NSM reinforcement
A_c	Area of concrete
A_{ceff}	Area of the concrete in tension
A_t	Total area
b	Width of beam
C	Total compressive force of concrete
c	Concrete cover
d	Effective depth of beam
d_b	Diameter of bar
d_c	Distance between the C.G. of NSM bar and the surface of main steel bar
d_{NSM}	Distance between the C. G. of NSM bar and compression face of beam
E_c	Modulus of elasticity of concrete
E_s	Modulus of elasticity of steel bar
E_{NSM}	Modulus of elasticity of NSM reinforcement
f'_c	Compressive strength of concrete
f_{cr}	Concrete modulus of rupture
f_{NSM}	Yield strength of NSM reinforcement

f_{NSMu} Ultimate strength of the NSM reinforcement

f_y Yield strength of steel bar

h Depth of beam

I_A Moent of inertia at section A

I_g Gross moment of inertia

I_{cr} Cracking moment of inertia

I_e Effective moment of inertia

k_1 Bond coefficient

k_2 Strain distribution coefficient

L Span length

L_a Shear span length

L_s Distance from the support to NSM bar cut off point

M_A Moment at point A

M_B Moment at point B

M_{cr} Cracking moment

M_y Yield moment

M_u Ultimate moment

n Modular ratio of steel bar

n_{NSM} Modular ratio of NSM reinforcement

P Applied load

P_{cr} Cracking load

P_y Yield load

P_u Ultimate load

S_{max} Maximum crack spacing

T_s Total tensile force of tension steel

T_{NSM} Total tensile of NSM reinforcement

y Depth of N. A. from compression face of beam

y_t Distance of N. A. from tension face of beam

y_y Depth of N. A. from compression face of beam at yield load

y_u Depth of N. A. from compression face of beam at ultimate load

ε_c Strain of the top fibre of concrete

ε_{cu} Ultimate strain of concrete

ε_s Strain in the tension steel

ε_y Yield strain of steel bar

ε_{NSM} Strain in the NSM reinforcement

ε_{NSMu} Ultimate strain in the NSM reinforcement

ϕ Curvature behind first yielding of the steel bar

ϕ_y Yield curvature of steel bar

ϕ_u Ultimate curvature of steel bar

σ_A Tensile stress at point A

σ_{NSM} Stress in the NSM bar

Δ_{cr} Deflection of uncracking stage

Δ_y Deflection of cracking stage

Δ_u Deflection of postcracking stage

Δ_{max} Maximum deflection

ρ_{eff} Effective reinforcement ratio

LIST OF NOTATIONS

ACI	American Concrete Institute
AASHTO	American Association of State Highway and Transportation Officials
AFRP	Aramid Fibre Reinforced Polymer
CC	Concrete Cover Separation Failure
CFRP	Carbon Fibre Reinforced Polymer
EBR	Externally Bonded Reinforcement
FL	Flexural Failure
FRP	Fibre Reinforced Polymer
GFRP	Glass Fibre Reinforced Polymer
GPa	Gigapascal
kN	Kilo Newton
LVDT	Linear Variable Displacement Transducer
MPa	Megapascal
NSM	Near Surface Mounted
OPC	Ordinary Portland Cement
PL	Peeling-off Failure
RC	Reinforced Concrete
SNSM	Side Near Surface Mount
SRP	Steel Reinforced Polyme

1. INTRODUCTION

1.1 RESEARCH BACKGROUND

Nowadays, the strengthening of reinforced concrete (RC) structures and bridges is the major challenge facing structural engineers, and has become a dynamic sector of interest in structural engineering. The increasing use of retrofitting, repairing and strengthening systems of RC structures to enhance load carrying has become common in recent years.

The crucial factors for strengthening structural elements comprise:

- upgrading live and dead loads
- corrosion of materials
- functional change of structures
- construction weakness
- error in existing design of structure

Most of the structures that were built more than several decades ago may need to be strengthened and upgraded to meet the current service load demands. The repairing or strengthening of RC structures is one of the greatest challenges and essential responsibilities of civil engineering. In addition, the use of strengthening techniques is expected to grow rapidly over the next few years. Several methods for strengthening RC structures using various materials have been studied and applied in the rehabilitation field (Eberline, Klaiber & Dunker, 1988); (MacDonald & Calder, 1982).

Ferrocement, sprayed concrete, externally bonded steel reinforcement or carbon fibre reinforced polymer (CFRP) and near surface mounted (NSM) steel or FRP bars or strips are available in the global market for the strengthening of structures. Externally bonded steel plates were primarily used for the strengthening of structures. However, the strengthening of structures using steel plates has certain disadvantages, i.e. the handling and installation of heavy plates are difficult. Moreover, supplementary dead loads are added to the structure by using steel plates and they require protection from environmental action. By using FRP laminates, these problems can be overcome for strengthening structures. However, the externally bonded plates or laminates often suffer from premature failure. This could be due to plate end debonding, intermediate crack induced debonding or shear failure (El-Mihilmy and Tedesco, 2001). Such plate end debonding failures are the most common for both steel plate and CFRP laminate strengthened reinforced concrete beams (Smith and Teng, 2002).

Recently, the near surface mounted (NSM) technique has been the subject of increasing research as well as practical usage because it is less prone to premature debonding (L De Lorenzis & Teng, 2007). However, it has some limitations in application. Sometimes, the width of the beam may not be wide enough to provide the necessary edge clearance and clear spacing between two adjacent NSM grooves. ACI (ACI 440, 2008) recommends that the minimum edge clearance and the clear spacing of the NSM groove should be four and two times the groove depth. However, this recommendation has also proven to be inadequate by De Lorenzis & Nanni (2002). In addition, the concrete cover should be deeper to provide sufficient groove depth.

The application of NSM steel bars for the strengthening of RC structures started in Europe in the early 1950s (Asplund, 1949). Where steel rebars with cement grout were used to strengthen a concrete slab in the field construction work. Masonry buildings and arch bridges were strengthened with NSM stainless steel bars (Garrity, 2001). More recently, the experimental and numerical behaviour of RC beams flexurally strengthened with NSM steel or GFRP bars has been investigated (Almusallam, Elsanadedy, Al-Salloum & Alsayed, 2013). Most of the experimental studies were conducted to investigate the behaviour of flexurally strengthened RC beams using the NSM technique with FRP bars or strips (Al-Mahmoud et al., 2009; Badawi & Soudki, 2009; De Lorenzis et al., 2000; El-Hacha & Gaafar, 2011; El-Hacha & Rizkalla, 2004; Soliman et al., 2010). The experimental test results showed that NSM FRP bars significantly enhance the flexural strength of RC members. Also, improve the serviceability of RC structures.

1.2 PRESENT STATE OF THE PROBLEM

Though the repair or rehabilitation of reinforced concrete structural elements with different techniques are studied, there are several issues that are yet to be explored and investigated. Following are the important aspects required to be addressed.

a) Very few experimental investigations were found concerning reinforced concrete beams flexurally strengthened with NSM steel bars. The application of the technique needs to study further.

b) The U-wrap end anchorage with CFRP fabrics to prevent the concrete cover separation for flexurally strengthened beam specimens by NSM technique is rarely employed.

c) No experimental investigation was found pertaining to RC beams flexurally strengthened with side near surface mounted (SNSM) with steel or CFRP bars.

1.3 OBJECTIVES OF RESEARCH

In view of the literature reviewed some important areas of further research with their future scope of applications are identified. The focus of the present study is, therefore, on the following objectives:

a) To study the performance of RC beams flexurally strengthened with the NSM technique using steel bars.

b) To investigate the effect of the number of grooves and the amount of NSM reinforcement on the RC beams flexurally strengthened with NSM steel bars.

c) To evaluate the experimental behaviour of RC beams flexurally strengthened with the SNSM technique using steel and CFRP bars.

d) To prevent the cover separation of NSM strengthened RC beams with U-wrap anchorage using CFRP fabric.

e) To assess the experimental behaviour of pre-cracked RC beams strengthened with the SNSM technique using CFRP bars.

f) To develop analytical models to predict the flexural responses of RC strengthened beams and compare with the experimental results.

1.4 SCOPE OF THE WORK

The research addresses experimental and analytical investigations of flexurally strengthened beam specimens. The studies have been carried out considering the following constraints:

a) To enhance the flexural strength, the representative RC rectangular beam specimens are strengthened with different diameter of steel bars in NSM technique.

b) The end anchorage with CFRP fabric are used to eliminate the concrete cover separation failure. U-wrap anchorage are placed at the end of the NSM curtailment of flexurally strengthened beam.

c) The innovative SNSM strengthening method has been employed to investigate the flexural behaviour of RC beam specimens with steel and CFRP bars. In addition, the performance of SNSM technique is examined for pre-cracked beam specimens strengthened with CFRP bars.

d) All specimens are subjected to static loading until failure. The distinctive instruments are used for measuring the loads, deflection, strains, crack width and spacing.

e) The analytical models are developed to predict the flexural responses of all beam specimens which have been validated with the experimental results.

1.5 ORGANIZATION OF THESIS

The present thesis is structured into six chapters.

Chapter 1 provides a brief introduction of strengthening RC beam elements. The research background on recent advancement of the strengthening techniques has been given. Accordingly the problem statement, research objectives and scope of work are discussed. The chapter is concluded with an outline of the thesis.

Chapter 2 presents a brief review of the existing research works related to this research until now. A concise survey is given of the recent literature concerning the usage of the NSM techniques for the strengthening of reinforced concrete elements under the static loading condition. Finally, the research gap is identified from the literature review.

Chapter 3 includes the experimental programme, specimen construction, test instrumentation and loading the test set-up. The choices for the different loading parameters is explained and justified. A methodology for the design of RC beams strengthened by the NSM technique (soffit and side) using steel and CFRP bars is also presented.

Chapter 4 includes the proposed model based on sectional analysis to predict the flexural behavior of strengthening RC beams. The analytical models for load-deflection, compressive strain of concrete, tensile strain of main rebar, tensile strain of strengthening reinforcement and spacing of crack have been described.

Chapter 5 illustrates the results of the research and a discussion of the results. A description of the performance of the strengthened beams under test conditions is qualitatively compared to the behaviour of an unstrengthened control beam.

Finally the Chapter 6 summarizes the main findings of the research work and the final conclusions have been outlined point to point. Furthermore, several important research aspects beyond the scope of the present study are recommended for future work.

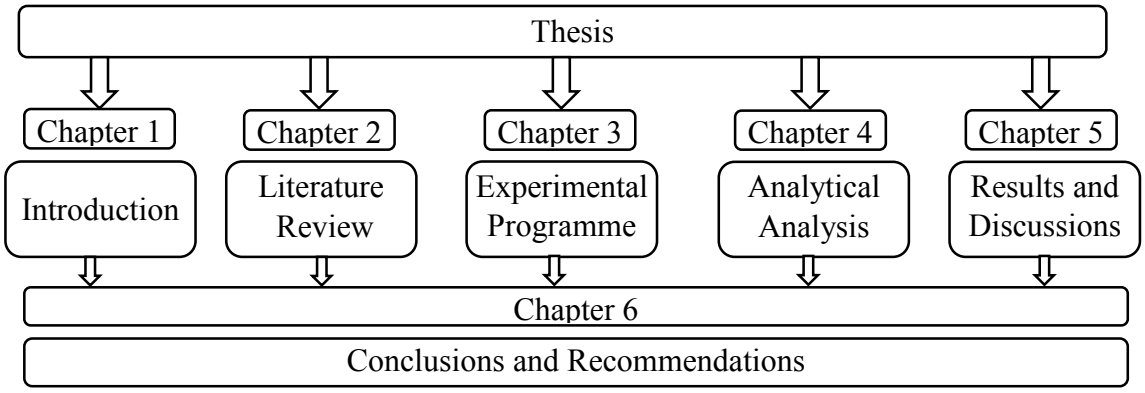

Figure 1.1: Thesis structure

2. LITERATURE REVIEW

2.1 INTRODUCTION

The experimental investigation of RC structures strengthened using the near surface mounted (NSM) technique is well documented in the literature. This chapter deliberates on the existing works that are relevant to the objectives of this study, and identifies the research gaps in the existing research that will be reported in this study.

2.2 THE NSM TECHNIQUE

The NSM technique involves cutting a groove in the surface of the structural member, roughening and cleaning the groove, filling the groove halfway with a structural adhesive, installing the strengthening bar, filling the groove completely with structural adhesive, and levelling the surface. NSM FRP bars and laminates are being increasingly used as a substitute for externally bonded FRP laminates.

Asplund (1949) studied reinforced concrete beam specimens reinforced using steel reinforcement and others using NSM steel bars. The specimens were strengthened with the NSM technique using steel bars and cement mortar. The experimental results exhibited that the behaviour of both beam specimens were identical. This NSM technique was applied in the strengthening of bridge deck slabs, as shown in Figure 2.1.

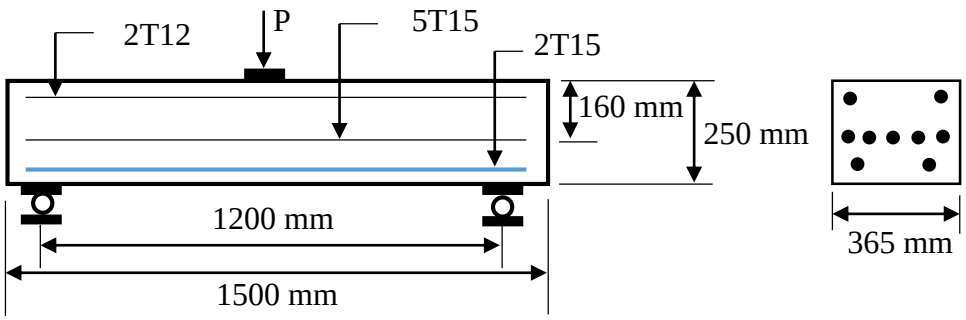

Figure 2.1: Test specimen (Asplund, 1949)

Blaschko and Zilch (1999) investigated the bond behaviour of concrete blocks using NSM CFRP strips. The size of concrete block specimens were 200 x 200 x 450 mm in width, depth and length, respectively. The experiment was executed using EB and NSM CFRP strips to compare the two techniques. The experimental test results showed that the NSM CFRP strips had superior capacity to the EBR strips.

Gentile and Rizkalla (1999) studied the feasibility of flexurally strengthening timber bridge stringers using NSM GFRP bars. The timber stringers had NSM grooves cut longitudinally and GFRP bars inserted with an epoxy resign. The results of the experimental investigation revealed that the NSM technique achieved the load carrying capacity required according to the AASHTO design. The NSM GFRP bars technique only cost 15% of the cost of the replacement of the bridge.

De Lorenzis et al. (2000) conducted research on RC beams strengthened using the NSM technique with CFRP or GFRP bars. This research investigated both flexural and shear strengthening. The flexural strengthened RC beams increased the bending capacity by up to 44% compared to the control beam. The shear strengthened RC beams enhanced the shear capacity by up to 106% more than the

control beam. The test results also revealed that the NSM FRP bars were very efficient for enhancing the flexural and shear capacity of the RC beams. This study found that premature debonding of FRP bars occurred as a result of splitting the epoxy cover. NSM bars with a large bonded length along the beam flange may eliminate premature debonding.

Nordin et al. (2001) performed an experimental study on flexurally strengthened reinforced concrete beams using prestressed NSM CFRP strips. A total of 15 full-scale RC beams were examined until failure. The dimensions of the beams were 200 mm x 300 mm x 4000 mm in width, depth and length, respectively. Four-point bending tests were performed with a loading rate of 0.02 mm/s under static condition. The experimental results presented that strengthened specimens significantly increased the cracking and failure loads. Prestressing NSM CFRP strips had no effect on the mode of failure. Furthermore, the specimens strengthened with prestressed FRP had considerably smaller deflections at failure.

Hassan and Rizkalla (2002) studied the practicability of flexural strengthening of half scale prestressed concrete beams by different strengthening systems with different types of FRP. Two cantilevers and one simple span were examined in this study. NSM leadline bars, CFRP strips, C-bars and EB CFRP strips and sheets were used for flexural strengthening. The experimental results confirmed that the NSM FRP was feasible and more cost-effective than EBR for the strengthening of prestressed concrete bridge members. In addition, the experimental test results were compared to the predictions of a nonlinear finite model, which showed reasonable agreement.

Yost et al. (2004) investigated the structural performance of retrofitted concrete flexural members using the NSM technique with CFRP reinforcement. They reported an increase of 30% and 78% in the yield load and ultimate strength, respectively, when compared to the control beam. They also found that the bonds between the CFRP reinforcement, the epoxy and the adjacent concrete were strong enough to improve the tensile strength of the CFRP reinforcement.

El-Hacha et al. (2004) investigated and compared the structural performance of RC T-beams flexurally strengthened using NSM FRP bars or strips to those using externally bonded FRP strips. A total of eight simply supported RC T-beams were used with a width of 150 mm, depth 300 mm and a span length of 2700 mm (one reference and seven strengthened using CFRP bars or strips as well as GFRP strips). The specimens were tested under a statically applied load at midspan by a loading rate of 1.07 mm/min. The study found that complete composite action between the NSM strips and the concrete was achieved. The flexural strength of the strengthened RC beams significantly increased and NSM FRP strips delivered greater strength capacity than the EB FRP strips.

El-Hacha and Rizkalla (2004) also investigated the flexural behaviour of RC beam specimens strengthened with NSM technique utilizing FRP. The variables examined were the number of FRP bars or strips; the form of FRP, either strips or bars; and the type of FRP, either glass or carbon. They found that using NSM reinforcement with CFRP strips for flexural strengthening resulted in beams that had a higher flexural strength than those strengthened using CFRP bars with similar axial stiffness. The results were explained as debonding probably occurring earlier between the CFRP bar and the epoxy interface.

Rosenboom et al. (2004) conducted research on the strengthening of twelve 9.14 m long C-channel prestressed concrete girders using several CFRP schemes and tested them under static (seven girders) and fatigue (five girders) loading. The NSM CFRP bars and strips strengthened girders achieved a 20% improvement in the ultimate flexural strength compared to the control girder when monotonically loaded to failure. The NSM strengthened girders also performed well under fatigue loading conditions, enduring over two million cycles of increased service loading with little degradation and reduced crack widths.

Kishi et al. (2005) performed an experimental investigation of RC beams flexurally strengthened with NSM and externally bonded technique using AFRP bars and sheets, respectively. Six RC beams were used with a span length of 3000 mm, a depth of 250 mm and a width of 150 mm. The tests were conducted using the four-point bending condition. The experimental results indicated that the load capacity increased as the bond length increased and that two types of failure mode occurred. One was debonding in the concrete epoxy interface and the other was debonding in the CFRP rod epoxy interface.

Barros and Fortes (2005), and Barros et al. (2006) investigated the effectiveness of using CFRP laminates as NSM reinforcement for structural strengthening. They tested two sizes of beam (120 mm x 170 mm x 1000 mm for flexural strengthening and 150 mm x 300 mm x 1600 mm for shear strengthening). The different variables examined were the number of CFRP laminate strips, different steel reinforcement ratios, and different depths of the cross section. The results exhibited a maximum load increase of 91%. It was also found that the

strengthened RC beams demonstrated more deflection at failure. A serviceability limit state analysis showed an increase in the rigidity of the beam by 28%.

Tang et al. (2006) conducted a study on the performance of RC beams flexurally strengthened using NSM GFRP bars, in which normal and lightweight polystyrene concrete was used as a variable. The cross-section of the tested beams was 180 mm x 250 mm and with a total length of 1500 mm (effective span length of 1200 mm) and two 9.5 mm or 16 mm GFRP were used with the same beam configuration for the NSM strengthening purpose. The shear span by depth ratio of the tested beams was 2.47. The experimental test variables were the ratio of steel or composite reinforcing bars subjected to four-point bending until failure. The GFRP bars strengthened beams demonstrated an enhancement of flexural rigidity, bending capability and improvement of moment ranging from 23% to 53%. However, the dominant failure mode of these strengthened beams was debonding, which can be designated as shear, splitting of adhesive layer and rupture of the strengthening bars (GFRP).

Jung et al. (2006) performed research on the flexural behaviour of NSM CFRP bars and externally bonded reinforcement strengthened RC beams. A total of eight specimens (one control, two strengthened with externally bonded reinforcement, three with NSM CFRP bars and two with NSM and mechanical interlocking grooves) were tested with a shear span to depth ratio of 3.89. The dimensions of the specimens were 200 mm width, 300 mm depth and 3400 mm span length (effective span length of 3000 mm). They compared the NSM CFRP strengthened beams to externally bonded CFRP strengthened beams. The NSM strengthened specimens utilized the CFRP reinforcement more efficiently than the externally

strengthened beams. The NSM CFRP bars and EB reinforcement strengthened specimens failed by deonding, and the mechanical interlocking grooves eliminated the debonding failure.

Kang et al. (2006) conducted an experimental and analytical evaluation of NSM strengthened RC beams using CFRP strips. They tested five beams. The first beam was left unstrengthened as the control, while the second and third beams were strengthened with different NSM groove depths of strips, and the remaining two beams were strengthened with a different spacing of NSM strips. The dimensions of the beams were 200 x 300 x 3400 mm and with a shear span/depth ratio 3.89. The study focused on the relation between the ultimate load of the beam and the depth of the NSM groove and the spacing between the CFRP strips. They concluded that the minimum spacing between the NSM groove (for multiple CFRP strips) and from the edge of the beam should exceed 40 mm to ensure that each CFRP strip behaved independently.

Aidoo et al. (2006) conducted a full-scale experimental investigation on the repairing of the RC interstate bridge using CFRP material. They studied eight RC bridge girders. The three types of strengthening methods investigated were externally bonded reinforcement, NSM reinforcement, and powder actuated fasteners. All three methods improved the load-carrying capacity of bridge girders. In particular, the externally bonded CFRP and NSM CFRP behaved better than the powder actuated fasteners. However, the NSM reinforcement showed a significantly higher ductility, which was explained as being due to the better bond characteristics.

Nordin and Täljsten (2006) experimentally examined the use of prestressed NSM CFRP to strengthen RC beams under static loading. Fifteen full-scale RC beams (4000 mm x 200 mm x 300 mm) were tested with two types of CFRP (medium modulus of elasticity 160 GPa and a high modulus of elasticity 250 GPa) and different bonded lengths. The results demonstrated that prestressed quadratic CFRP bars significantly increased the structural load (crack, yield and ultimate) capacity of the strengthened beams when compared to the reference beam. They concluded from the monotonic test results (no fatigue tests were conducted), that the fatigue life of prestressed NSM CFRP strengthened RC beams might be improved. They also concluded from the combination of a higher cracking load and smaller crack widths, that the durability of the structure was enhanced. Furthermore, the force transfer between the structure and the CFRP bars worked well in the laboratory conditions without the need for a mechanical anchor device. The loss in strain (stress) ranged from 2.8–14.5% at the centre and 35.3–100% at the ends. This expert use combines the advantage of CFRP laminate passive bonded systems with the benefits related to external prestressing. Through applying a prestress to the CFRP, the material may be used more efficiently since a superior portion of its tensile aptitude is engaged.

Badawi and Soudki (2009) studied the flexural behaviour of prestressed NSM CFRP bars strengthened reinforced concrete beams. The experimental programme consisted of four beams. One beam was unstrengthened, which was taken as a reference beam, and one beam strengthened using NSM CFRP bars, while the other two beams were strengthened using prestressed NSM CFRP bars of different levels (40% and 60% ultimate strength of the CFRP bars). The size of the tested beams was 152 mm of width, 254 mm of depth and 3500 mm of span length. The

groove size was 15 mm x 25 mm and the shear span to depth ratio 4.91. The experimental test results of the strengthened beams demonstrated that the prestressed NSM CFRP bars effectively enhanced the flexural capacity and reduced the deflection compared to the reference beam. The strengthened beams failed by rupture of the CFRP bar, i.e. flexural failure.

R. Capozucca (2009) investigated the static and dynamic behaviour of damaged beam specimens strengthened with the NSM technique using CFRP bars. He tested three RC beams with dimensions of 150 mm x 250 mm x 3750 mm. Loads were applied to produce damaged beams with different degrees of cracking and then strengthened with the NSM technique. The experimental static results indicated that the NSM CFRP bars improved the load deflection response and ultimate load capacity. All the strengthened beams failed by concrete cover delamination. Dynamic tests were conducted to validate the safety of damaged reinforced concrete and strengthened beams using a non-destructive method. The use frequency is the correlation between the degree of damage and strengthening at different loadings. The dynamic test results established that the beams strengthened with NSM CFRP bars prevented the development of cracking.

Al-Mahmoud et al. (2009) conducted an experimental programme that consisted of eight RC beams (one control and seven strengthened). They performed a four-point bending test to evaluate the flexural strength of RC beam specimens strengthened with NSM CFRP bars where the testing variables were CFRP diameter (6 mm and 12 mm), concrete composition (conventional and high strength) and filling materials (resin and mortar). The tested beam cross-section was 150 mm × 280 mm with a span length of 3000 mm and shear span to depth

ratio 2.98, in which 1–12 mm or 2–6 mm diameter CFRP bars were inserted into the groove (2 d_b x 2 d_b). The flexural strength was enhanced irrespective of the groove filler and concrete strength, and even though the failure mode for all the beams was debonding (pullout with splitting and peeling-off). The analytical model to predict the debonding load was a very conservative approach.

In addition, Al-Mahmoud et al. (2010) studied the behaviour of cantilever RC beams that were flexurally strengthened using 2–6 mm diameter NSM-CFRP bars. They tested seven (two reference and five strengthened) beams with a cross-section of 150 mm x 280 mm. The specimens strengthened using NSM CFRP bars were tested under the four-point bending condition and the results were compared to the reference specimens. Both beams failed by the pull out of the bars (splitting resin and concrete adjacent the groove) while the CFRP bar was longer than the cracked span length and the peeling-off failure occurred when some cracks reached to the end.

Costa and Barros (2010) performed experimental, analytical and numerical studies, concerning the flexural strength of RC beams strengthened using NSM CFRP strips. They tested three RC beams with different span lengths (1500 mm, 1900 mm and 2200 mm respectively) and cross-section (200 mm x 250 mm, 200 mm x 320 mm and 200 mm x 380 mm, respectively). Grooves (1.4 mm x 20 mm) were cut into the bottom arm of the steel stirrups and to avoid shear failure U-wrap with CFRP sheets was used. The failure modes of the strengthened specimens were premature shear and concrete cover.

F. Ceroni (2010) reported on a comparative study of NSM FRP bars and externally bonded RC beams strengthened with FRP laminates under static and cyclic loading conditions, in which the experimental and theoretical failure loads were also compared. The experimental tests consisted of twenty-one beams (two control, sixteen EBR strengthened and three NSM strengthened). The beam dimensions were 100 mm x 180 mm x 2000 mm. The NSM groove dimensions and bonded length were 15 mm x 15 mm and 1600 mm, respectively, and the externally bonded FRP laminate had a width of 100 mm and was applied in two bonded lengths of 1400 mm and 1200 mm, respectively. Eleven externally bonded strengthened beams were tested under cyclic conditions and the remaining strengthened beams were tested under static conditions. The results of this study indicated that the two methods significantly increased the strength over the control beam under static conditions. However, all the EBR strengthened beams failed by debonding and the NSM FRP strengthened beams failed in flexure.

Kalayci et al. (2010) investigated the effect of the near surface mounted groove size on the strengthened RC beams using FRP. Twelve RC T-beams (flange size – 305 mm x 76mm and web size – 152 mm x 229 mm) were tested under the three point bending conditions. Half the beams were strengthened with NSM FRP strips and the others were strengthened with NSM FRP bars using different sizes of NSM groove for the bars (11 mm x 11 mm, 14 mm x 14 mm and 17 mm x 17 mm, respectively) and strips (11 mm x 25 mm, 14 mm x 25 mm and 17 mm x 25 mm, respectively). The experimental test results showed that the strengthening technique had little or no effect on the flexural strength of NSM FRP and that all the strengthened beams failed in premature debonding.

Rasheed et al. (2010) examined the flexural performance of RC beams strengthened with NSM CFRP strips and stainless steel bars and externally bonded SRP sheets and CFRP sheets. Six RC beams (254 mm x 457 mm x 4880 mm) were tested with a shear span to depth ratio of 5.71. Two beams were kept as reference beams, one beam strengthened with CFRP sheets (longitudinal and transverse direction), one beam strengthened with NSM CFRP longitudinal strips [6 mm x 19 mm] and transverse strips [3 mm x 19 mm], one beam strengthened with L-shape SRP sheets (longitudinal and transverse direction) and one beam strengthened with NSM stainless steel bars (longitudinal direction) and NSM CFRP strips (transverse direction). Third point bending tests were conducted until failure of beams with a loading rate of 8.9 kN/min. The results of this study indicated that all the strengthened beams increased the ultimate loads and that the NSM strengthened beams modes of failure confirmed core crushing while the EBR strengthened beams were partial to the delamination of sheets.

Soliman et al. (2010) investigated the behaviour of reinforced concrete beams flexurally strengthened using NSM FRP bars. This study used twenty RC rectangular beams, 200 mm width, 300 mm depth and 3010 mm span length, to ensure a shear span/depth ratio of 3.10. Different variables including internal steel reinforcement ratio (0.40%, 0.80% and 1.60%), type of FRP bar (CFRP and GFRP), diameter of FRP bar (9.5 mm and 12.7 mm), bonded length (12*d*, 18*d*, 24*d*, 48*d* and 60*d*) and groove size (2*d* x 2*d* and 1.5*d* x 1.5*d*) were examined in this research. The test results indicated that the application of NSM FRP bars was useful for improving the flexural strength of the RC beams. However, all strengthened beams failed by concrete cover splitting.

Choi et al. (2011) focused on the effect of RC T-beams flexurally strengthened with the NSM technique using partially bonded CFRP bars. Six RC beams (one control and other five strengthened) were tested under static load conditions using a loading rate of 1.0 mm/min. The test variables were strengthening bars unbonded length (one strengthened beam fully bonded and other beams unbonded lengths of 1300 mm, 1500 mm, 1700 mm and 2100 mm at midspan, respectively). The test results indicated that the mode of failure of the strengthened beams was by concrete crushing at the compression zone.

Almusallam et al. (2013) conducted experimental and numerical studies on RC beams strengthened in flexure using NSM steel and GFRP bars. They tested sixteen RC beams with dimensions of 150 mm width, 200 mm depth and 2200 mm length (2000 mm effective span). One or two NSM bars were placed in a beam with a shear span to depth ratio of 5.73. The fixed groove size for strengthening was 30 mm x 30 mm. Most of the beams failed by internal steel yield and crushing of the compression concrete.

In addition, R. Capozucca (2014) performed experimental and analytical studies on RC beams strengthened with the NSM technique using GFRP bars. The dimensions of the beams and NSM grooves were 150 mm x 200 mm x 1700 mm, and 20 mm x 20 mm, respectively. Four-point bending tests were conducted under the static load state until failure of the beams. In addition, vibration tests were executed for the dynamic response of the strengthened and unstrengthened beams.

Sharaky et al. (2014) investigated the flexural behaviour of NSM strengthened RC beams using CFRP and GFRP bars. A total of eight RC rectangular beams (160

mm x 280 mm x 2600 mm) were tested, to ensure a shear span to depth ratio of 3.40. The test variables were NSM bar diameter (8 mm and 12 mm), number of NSM bars (1 or 2), FRP bar type (CFRP and GFRP) and epoxy type (mbrace and polyfixer ep). All the strengthened beams failed by debonding. Among the double grooved strengthened beams, the CFRP supported beam displayed concrete cover separation whereas the GFRP exhibited concrete splitting. In general, the strengthening scheme considerably increased the stiffness and ultimate load behaviour.

Table 2.1: Summary of research progress in flexural strengthening

Researchers	Strengthening materials	Variables
Asplund (1949)	Steel bars	Feasibility of using NSM strengthening
Blaschko and Zilch (1999)	CFRP strips	Strengthening techniques
Gentile and Rizkalla (1999)	GFRP bars	Feasibility of using NSM strengthening
De Lorenzis et al. (2000)	FRP bars	Types of FRP
Nordin et al. (2001)	CFRP strips	Prestressing force on the NSM bars
Hassan and Rizkalla (2002)	CFRP bars and strips	Strengthening techniques and types of CFRP
Yost et al. (2004)	CFRP bars	Effect of strengthening
El-Hacha et al. (2004)	FRP bars and strips	Strengthening techniques and types of FRP
El-Hacha and Rizkalla (2004)	FRP bars or strips	Number, form and type of FRP
Rosenboom et al. (2004)	CFRP bars and strips	Types of CFRP and loading
Kishi et al. (2005)	AFRP bars and sheets	Strengthening techniques and types of AFRP
Barros and Fortes (2005) and Barros et al. (2006)	CFRP laminates	Number of strips, steel reinforcement ratio and depth of cross section
Tang et al. (2006)	GFRP bars	Ratio of steel and GFRP bars
Jung et al. (2006)	CFRP bars and laminates	Strengthening techniques
Kang et al. (2006)	CFRP strips	Size and spacing of grooves
Aidoo et al. (2006)	CFRP bars and laminates	Strengthening techniques

Researchers	Strengthening materials	Variables
Nordin and Täljsten (2006)	CFRP bars	Strength and bonding length of CFRP bars, and types of loading
Badawi and Soudki (2009)	CFRP bars	Prestressing force on the NSM bars
R. Capozucca (2009)	CFRP bars	Degree of damage beams
Al-Mahmoud et al. (2009)	CFRP bars	Size of CFRP bars and filling materials
Al-Mahmoud et al. (2010)	CFRP bars	Types of beams and position of NSM
Costa and Barros (2010)	CFRP strips	Length and cross-section of specimens
F. Ceroni (2010)	CFRP bars and laminates	Strengthening techniques and types of loading
Kalayci et al. (2010)	CFRP bars and laminates	Groove size
Rasheed et al. (2010)	CFRP strips and steel	Groove size and direction of strips
Soliman et al. (2010)	FRP bars	Steel reinforcement ratio, type and diameter of FRP bars, bonded length and groove size
Choi et al. (2011)	CFRP bars	Unbonded length of strengthening bars
Almusallam et al. (2013)	Steel and GFRP bars	Reinforcement ratio of steel and GFRP bars
R. Capozucca (2014)	GFRP bars	Dynamic test and frequency
Sharaky et al. (2014)	FRP bars	Number and diameter of FRP, and epoxy

2.3 IDENTIFICATION OF RESEARCH GAPS AND SIGNIFICANCE OF THIS STUDY

NSM is a new and promising technique in the field of structural strengthening. A number of experimental research works have been conducted on the NSM strengthening method. From the existing literature, it was revealed that the NSM technique with steel bar reinforcement has rarely been incorporated. It is worth mentioning that the NSM steel technique may be an effective alternative because of the numerous advantages of steel bars compared to FRP bars. However, no literature has been found on the SNSM technique.

Therefore, the main contribution of the current study is to examine the performance of the SNSM technique for the flexural strengthening of reinforced concrete (RC) beams under the static loading system. In addition, the behaviour of pre-cracked beams for flexural strengthening using the SNSM technique is investigated.

To provide a more economical strengthening solution, experimental studies of RC beam strengthened with the NSM technique using steel bars is completely characterized. To develop an analytical model to predict the flexural response (load, deflection, strains and crack spacing) of RC beams, the experimental results are verified using the predicted results.

3. EXPERIMENTAL PROGRAMME

3.1 INTRODUCTION

The design and materials used for the fabrication of the RC rectangular beams, strengthening techniques, instrumentation of the specimens, experimental setup and test procedures are described in this chapter. The experimental methodology are shown in flow chart (Figure 3.1).

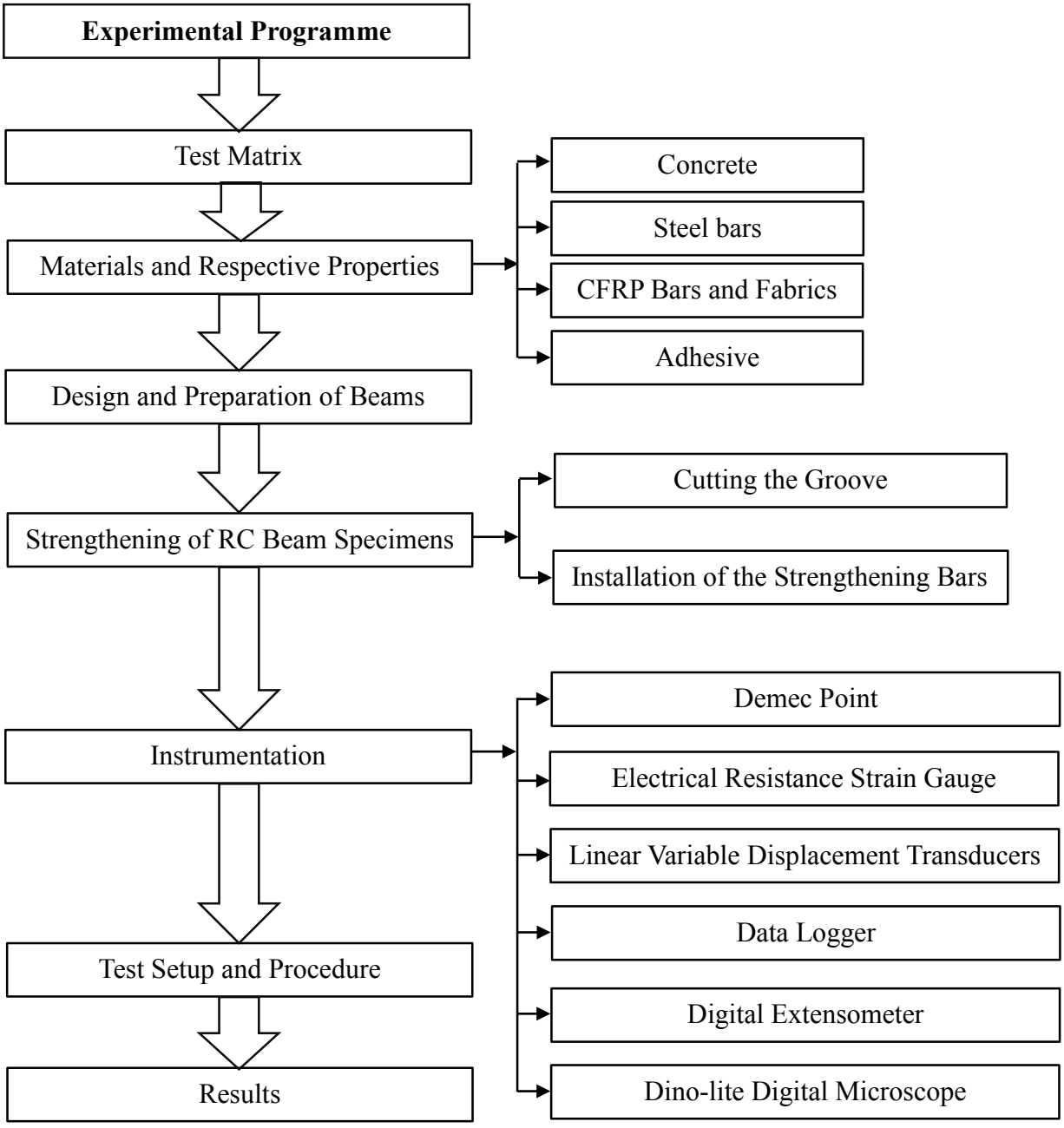

Figure 3.1: Flow chart of experimental methodology

3.2 TEST MATRIX

The experimental programme consisted of twenty-five RC beams. The RC beams were constructed and tested according to the text matrix given in Table 3.1. Four-point bending tests were conducted until failure of the specimens. The beams were divided into seven groups. The first group consisted of one beam as the control specimen. The five specimens in the second group were strengthened using a single NSM steel bar. The five beams in the third group were strengthened using two NSM steel bars and FRP bars.

The four beams in the fourth group were strengthened using NSM steel bars and end anchorage with CFRP fabric. The four beams in the fifth group were strengthened using SNSM steel bars. The three beams in the sixth group were strengthened using SNSM CFRP bars.

In addition, the three pre-cracked beams in the seventh group were strengthened using SNSM CFRP bars. This chapter provides a description of the test specimens and the different construction steps, the method used to strengthen the RC beams, the instrumentation and the experimental set-up.

Table 3.1: Text matrix

Group	Specimens	Strengthen-ing system	Groove size	Bar size	No. of bar	Bar type	End anc.	Beam type
1st	CB	-						
2nd	N1S6	NSM	$1.5d_b$ x $1.5d_b$	6 mm	1	steel	-	-
	N1S8	NSM	$1.5d_b$ x $1.5d_b$	8 mm	1	steel	-	-
	N1S10	NSM	$1.5d_b$ x $1.5d_b$	10 mm	1	steel	-	-
	N1S12	NSM	$1.5d_b$ x $1.5d_b$	12 mm	1	steel	-	-
	N1S16	NSM	$1.5d_b$ x $1.5d_b$	16 mm	1	steel	-	-
3rd	N2S6	NSM	$1.5d_b$ x $1.5d_b$	6 mm	2	steel	-	-
	N2S8	NSM	$1.5d_b$ x $1.5d_b$	8 mm	2	steel	-	-
	N2S10	NSM	$1.5d_b$ x $1.5d_b$	10 mm	2	steel	-	-
	N2S12	NSM	$1.5d_b$ x $1.5d_b$	12 mm	2	steel	-	-
	N2C12	NSM	$1.5d_b$ x $1.5d_b$	12 mm	2	FRP	-	-
4th	N2S8U3	NSM	$1.5d_b$ x $1.5d_b$	8 mm	2	steel	CFRP fabric	-
	N2S10U3	NSM	$1.5d_b$ x $1.5d_b$	10 mm	2	steel	CFRP fabric	-
	N2S12U3	NSM	$1.5d_b$ x $1.5d_b$	12 mm	2	steel	CFRP fabric	-
	N2S12U4	NSM	$1.5d_b$ x $1.5d_b$	12 mm	2	steel	CFRP fabric	-
5th	SN2S6	SNSM	$1.5d_b$ x $1.5d_b$	6 mm	2	steel	-	-
	SN2S8	SNSM	$1.5d_b$ x $1.5d_b$	8 mm	2	steel	-	-
	SN2S10	SNSM	$1.5d_b$ x $1.5d_b$	10 mm	2	steel	-	-
	SN2S12	SNSM	$1.5d_b$ x $1.5d_b$	12 mm	2	steel	-	-
6th	SN2C8	SNSM	$1.5d_b$ x $1.5d_b$	8 mm	2	CFRP	-	-
	SN2C10	SNSM	$1.5d_b$ x $1.5d_b$	10 mm	2	CFRP	-	-
	SN2C12	SNSM	$1.5d_b$ x $1.5d_b$	12 mm	2	CFRP	-	-
7th	PSN2C8	SNSM	$1.5d_b$ x $1.5d_b$	8 mm	2	CFRP	-	Pre-crack
	PSN2C10	SNSM	$1.5d_b$ x $1.5d_b$	10 mm	2	CFRP	-	Pre-crack
	PSN2C12	SNSM	$1.5d_b$ x $1.5d_b$	12 mm	2	CFRP	-	Pre-crack

* description of strengthening specimens notation:

N1S6 – N = near surface mounted technique, 1= number of bars, S = steel bar, 6 = diameter of bar; **N2C12** – N = = near surface mounted technique, 2 = number of bars, C = CFRP bar, 12 = diameter of bar; **N2S8U3** – N = near surface mounted technique, 2 = number of bars, S = steel bar, 8 = diameter of bar, U = U-wrap end anchorage, 3 = number of CFRP fabric layers; **SN2S6** – SN = side near surface mounted technique, 2 = number of bars, S = steel bar, 6 = diameter of bar; **SN2C8** – SN = side near surface mounted technique, 2 = number of bars, C = CFRP bar, 8 = diameter of bar; **PSN2C8** – P = pre-cracked beam, SN = side near surface mounted technique, 2 = number of bars, C = CFRP bar, 8 = diameter of bar.

3.3 MATERIALS AND RESPECTIVE PROPERTIES

The materials used in the construction of the RC beams were concrete and reinforcing steel bars. The engineering properties of these materials are given in the following sections.

3.3.1 CONCRETE

In this research, the normal cement was used in casting the beam specimens, prisms, cylinders and cubes. Crushed stone (granite) was used as a coarse aggregate and the maximum size was 20 mm. It was air-dried in the concrete laboratory. Natural river sand was used for the fine aggregate. The sieve analysis was done in accordance with BS 882 to determine the grading of the aggregate and the grading zone of the fine aggregate was found to be 2. Coarse and fine aggregates were washed with water and air dried in the concrete laboratory. All the beams were cast with the same amount of cement, water coarse and fine aggregate. Steel moulds were used for casting purposes. Before casting, all the moulds were cleaned by air jetting and oil was applied for easy demoulding. Fresh tap water was used in the hydration of the concrete mix during casting and curing of the beams, prisms, cubes and cylinders. The concrete mix was designed for 40 MPa compressive strength according to the DOE method (Neville & Brooks, 1987). The calculation of the mix design is shown in Appendix A. The mix proportion is given in Table 3.2.

Table 3.2: Concrete mix proportion

Slump (mm)	**W/C ratio**	**Water (kg/m^3)**	**Cement (kg/m^3)**	**Coarse aggregate (kg/m^3)**	**Fine aggregate (kg/m^3)**
60	0.50	224	420	892	889

3.3.2 STEEL BARS

The beam specimens used five types of steel bar. The 12 mm bars were used as flexural reinforcement with both ends bent (90^0) to satisfy the anchorage conditions. The 10 mm bars were used as hanger bars up to the shear span zone. The 6 mm bars were used for stirrups, while the 6 mm, 8 mm, 10 mm, 12 mm and 16 mm steel bars were employed for strengthening of the specimens. The tensile

strength of all bars (three pieces) were tested based on ASTM A615/A6156M-09b in ELE (Engineering Laboratory Equipment) testing machine with a load capacity of 5000 kN. The average yield, ultimate strength and modulus of elasticity of all the steel bars are shown in Table 3.3.

Table 3.3: Properties of reinforcing bars

Bar size (dia), mm	Yield strength, (MPa)	Ultimate strength, (MPa)	Modulus of elasticity, (GPa)
16	550	570	200
12	550	640	200
10	520	572	200
8	379	536	200
6	520	570	200

3.3.3 CFRP BARS AND FABRICS

The CFRP bars were used for the RC beam specimens flexurally strengthened by the NSM and SNSM techniques. According to manufacturer's product results (Haining Anjie Composite) the tensile strength and modulus of elasticity of the bars are shown in Table 3.4. CFRP fabric was used for U wrapping the end anchorage of the NSM beams strengthened using steel bars. The thickness of the fabric was 0.17 mm. The CFRP fabric had a tensile strength of 4900 MPa, a modulus of elasticity of 230 GPa, and elongation at the break of 2.1% (SikaWrap®- 301C, 2012).

Table 3.4: Properties of CFRP bars

Bar size (dia), mm	Yield strength, (MPa)	Ultimate strength, (MPa)	Modulus of elasticity, (GPa)
12	1260	1870	132
10	1250	1860	132
8	1250	1860	132

3.3.4 ADHESIVE

Sikadur® 30 epoxy was used as a bonding mediator between the strengthening bars and concrete substrate of the specimens (Sikadur®-30, 2014). Sikadur® 30 epoxy adhesive has two parts, namely, part A and part B. Part A is white in colour

and consists of the epoxy resin, while part B is black in colour and consists of the hardener. The two parts were mixed together in a ratio of 3:1 until a uniform grey colour was achieved. The density was 1.65 kg/L at 23°C after mixing. The bond strength with steel and concrete were 21 MPa and 4 MPa respectively. The compressive, tensile and shear strengths, and modulus of elasticity of the adhesive are shown in Table 3.5. Furthermore, Sikadur 330 was used to bond the CFRP fabrics to the concrete substrate (Sikadur®-330, 2012). The properties of Sikadur 330 were also shown in Table 3.5.

Table 3.5: Properties of Sikadur® 30 and 330

Properties	Strength (MPa)	
	Sikadur 30	**Sikadur 330**
Compressive strength	95	-
Tensile strength	31	30
Shear strength	19	-
Modulus of elasticity	11200	4500

3.4 THE PROPOSED SIDE NEAR SURFACE MOUNTED (SNSM) TECHNIQUE

In the side near surface mounted (SNSM) strengthening technique, installation of the strengthening bars (CFRP/steel) began by cutting grooves into the concrete cover in the longitudinal direction on both sides of the beam specimen (25 mm above the tension face). The grooves had dimensions of 1.5d_b x 1.5d_b (where d_b is the diameter of the strengthening reinforcement). The details of the dimensions of the grooves are shown in Figure 3.2.

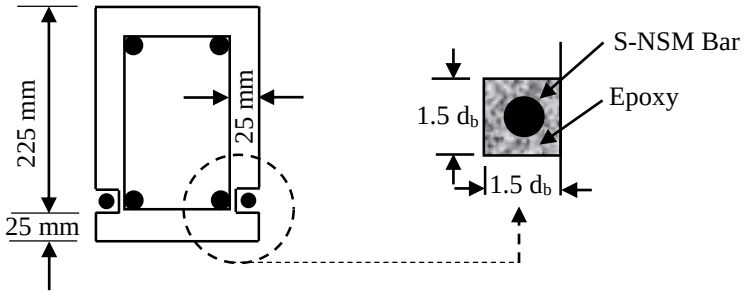

Figure 3.2: SNSM grooves details

3.5 DESIGN AND PREPARATION OF BEAM SPECIMENS

The dimensions of all the beam specimens were 125 mm x 250 mm x 2300 mm, as shown in Figure 3.3. The beam specimens were reinforced with two 12 mm diameter steel bars as main reinforcement and two 10 mm diameter steel bars were used as hanger bars up to the shear span zone, which was located at the top of the specimen. The diameter of the shear reinforcement, which was placed symmetrically, was 6 mm and the spacing of the shear reinforcement was 50 mm. The reinforcement detailing for all the beam specimens is shown in Figure 3.3.

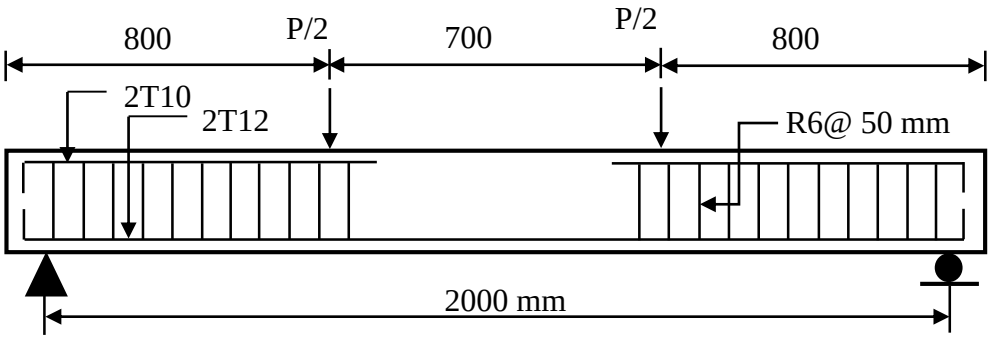

Figure 3.3: Details of beam specimen

The cement, coarse aggregate, fine aggregate and water with appropriate quantity were mixed using a laboratory drum mixer of 500 kg capacity, as shown in Figure 3.4. The steel moulds were cleaned and greased before placing of the concrete. After placing of the concrete, it was compacted using an electric internal vibrator machine. The beam specimens were cast in three layers, in which each layer was compacted using a vibrator machine to confirm sufficient compaction. To prevent the bleeding and segregation of the concrete during vibration, each penetration nozzle was made at a realistic distance from each other.

Figure 3.4: Laboratory drum mixer

The prisms (100 mm x 100 mm x 500 mm) and cubes (100 mm x 100 mm x 100 mm) were also cast with the same fresh concrete that was used for the beams. These were cured and tested in accordance with the BS EN 12390-5 (2009) and BS EN 12390-3 (2009) to determine the flexural strength (modulus of rupture) and concrete compressive strength respectively, as shown in Figure 3.5.

Figure 3.5: Flexural and compressive strength test

The curing was performed by covering with wet hessian cloths for at least two weeks, as shown in Figure 3.6.

Figure 3.6: Curing of specimens

3.6 STRENGTHENING OF RC BEAM SPECIMENS

3.6.1 CUTTING THE GROOVE

The RC beams specimens strengthened using the NSM technique, had either one or two grooves cut along the length of the tension faces for the placement of the NSM bars. After completion of 28 days curing, the beams were ready for structural strengthening. First, the position of the groove on the tension side of the beams was marked. The installation of the strengthening bars began with the cutting of grooves into the concrete cover of the beam specimens while maintaining the dimensions 1.5 d_b x 1.5 d_b (where d_b is the diameter of the tension reinforcement). The preferred depth for the NSM groove was made by constructing two parallel cuts with a special diamond concrete saw.

Then, the concrete between the two cuts was chopped out and removed from the beam. A hammer and a hand chisel were used to remove any remaining concrete lugs and to roughen the lower surface of the groove. The grooves were cleaned

using a wire brush and high-pressure air jet. The remaining specimens were strengthened using the SNSM technique. The dimension and construction of the grooves were the same as for the NSM technique. The groove of specimens are shown in Figure 3.7.

Figure 3.7: NSM groove of specimen

3.6.2 INSTALLATION OF THE STRENGTHENING BARS

The groove was half filled with epoxy and then a strengthening bar was placed inside each groove and pressed lightly. This forced the epoxy to flow around the inserted strengthening bar. More epoxy was used to fill the groove and the surface was levelled. The installation of the NSM bar is shown in Figure 3.8. To allow the epoxy to cure and achieve full strength, the beam specimens were not disturbed for one week.

Figure 3.8: Placing of NSM bar

3.6.3 APPLICATION OF END ANCHORAGE

After curing period of applied NSM steel bars, the concrete surface was prepared based on epoxy adhesive (Sikadur 330) specifications at the end of NSM steel. The soffit and two sides of width 100 mm of the specimens were prepared for end anchoring (Figure 3.9). Then, the surface was cleaned using brush and air jet. Finally, acetone was used to remove the dust and any other materials, which affect the bonding. A thin layer of adhesive was applied on the concrete surface to make sure that the adhesive fully covers the concrete surface. Later on, CFRP fabrics layers were placed on the beam as like as U (soffit and two sides) and covered with epoxy adhesive. To achieve full strength of the epoxy, the beam was kept for one week of curing time.

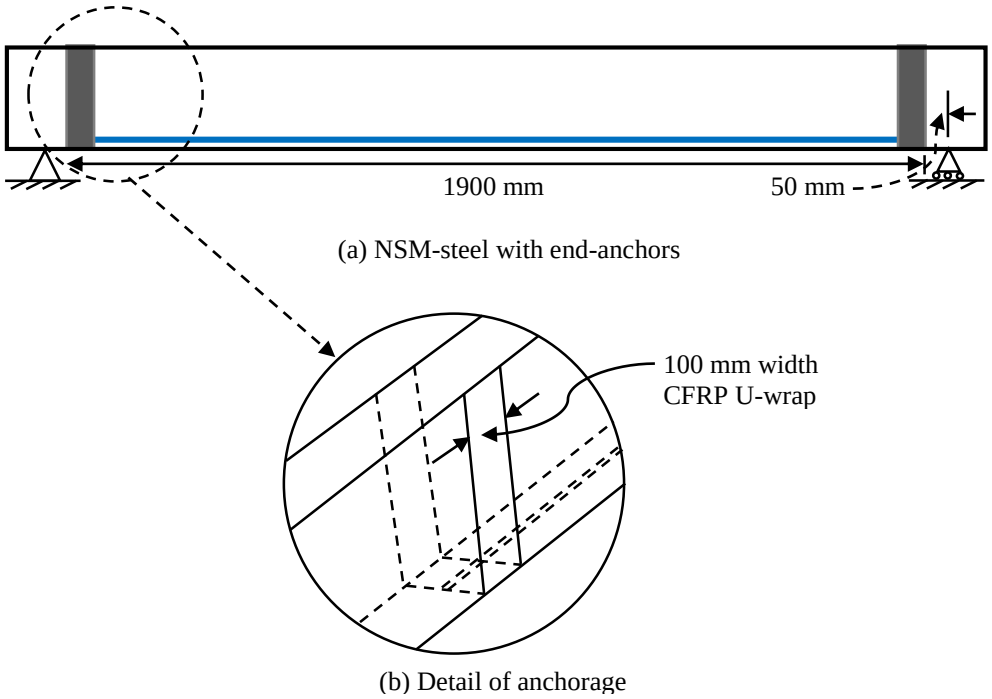

(a) NSM-steel with end-anchors

(b) Detail of anchorage

Figure 3.9: End anchorage strengthening

3.7 INSTRUMENTATION

3.7.1 DEMEC POINT

Demec gauges were installed on the side surface of the RC beam specimen to compute the strain and then to determine the position of the neutral axis of the RC beam section. The two demec gauges were placed at a horizontal distance of 200 mm. The concrete surface was ground where each demec gauge was to be installed to ensure proper bonding. Then, it was cleaned using acetone to remove the dust. After preparation of the concrete surface, the demec gauges were installed using adhesive, as shown in Figure 3.10 and left for at least 24 hours to set.

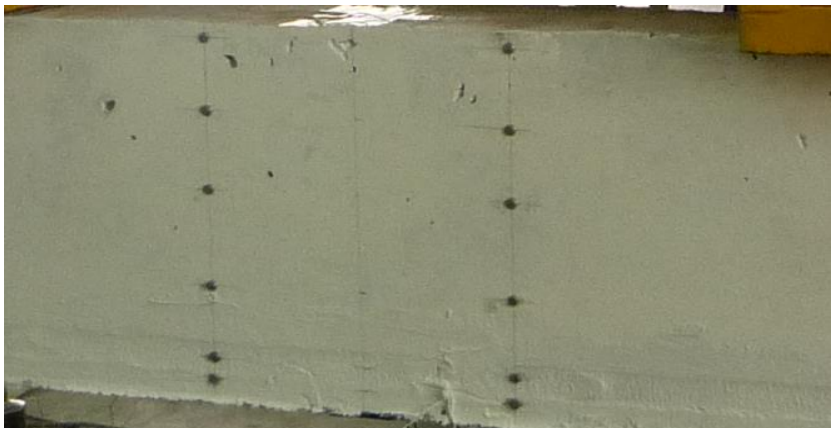

Figure 3.10: Position of demec points on concrete beam

3.7.2 ELECTRICAL RESISTANCE STRAIN GAUGE

Electric resistance strain gauges were used to measure the strain in the reinforcing bars and the concrete. The two 5 mm strain gauges were fixed in the middle of the rebars of each beam specimen to measure the tensile strain of the rebars. Before fixing the strain gauges, the surface of the rebars was smoothed using a grinding machine and the surface was cleaned with acetone, as shown in Figure 3.11.

Figure 3.11: Surface preparation of steel bar for strain gauge

The araldite glue (adhesive) set properly, the attached strain gauges were left for a few hours. The strain gauge wires were then connected with a special cable by soldering, as shown in Figure 3.12.

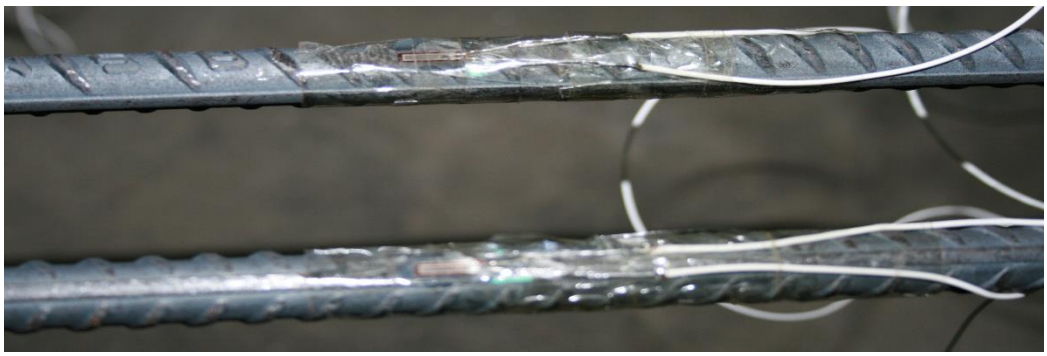

Figure 3.12: Strain gauges connect with wire

The connection of the strain gauge wires and cable was checked using a multi-meter. After wiring, the strain gauges were coated with silicon to prevent and protect from damage during the placement of the concrete, as shown in Figure 3.13.

Figure 3.13: Strain gauges covered with silicone gel

Then, the reinforcing cage was placed into the steel mould. Precautions were taken to avoid damaging the strain gauges while the specimen was cast. Two 30 mm strain gauges were placed at the middle of the top surface of the reinforced concrete specimen, to measure the concrete compressive strain of the specimen.

3.7.3 LINEAR VARIABLE DISPLACEMENT TRANSDUCERS (LVDT)

The LVDT (perform transverse range of 50 mm) was applied to measure the displacement of the specimen at the central position, as shown in Figure 3.14. The transducer was connected to a moveable Data Logger to collect the reading for deflection of the specimen during testing.

Figure 3.14: LVDT

3.7.4 DATA LOGGER

The data logger utilized in this research is TDS-530, as shown in Figure 3.15. It was employed to record the data of several strain gauges placed at different positions, one LVDT and the load from the Instron testing machine. The strain gauges were connected as 1G3W120 Ω to the data logger and the unit of strain measurement is in micro-strains. The LVDT was connected as 4 GAGE to the data logger and the unit of deflection measurement is mm.

Figure 3.15: TDS-530 data logger

3.7.5 DIGITAL EXTENSOMETER

The deformation at the sides of the beam were measured from the demec points using a digital extensometer to estimate the strain profile of the beam section, and, subsequently, to measure the position of the neutral axis. The attachment of the demec point on the side surface of the beam specimen is described in section 3.7.1. However, the vertical distance of the demec points is shown in Figure 3.16.

Figure 3.16: Digital extensometer

3.7.6 DINO-LITE DIGITAL MICROSCOPE

This instrument was used to measure the crack width of the concrete beams during testing, as shown in Figure 3.17 and Figure 3.18. Using this device, the crack width can be measured up to 0.001 mm. The lens was adjustable to obtain the sharpest picture of the crack, and, consequently, the crack width can be estimated accurately. However, the crack spacing along the beam length was measured manually.

Figure 3.17: Dino-lite digital microscope for crack width measurement

Figure 3.18: Measuring crack width using Dino-lite digital microscope

3.8 TEST SETUP AND PROCEDURE

All beam specimens (control and strengthened) were conducted to test under four-point bending until failure of the specimens as a simple support, as shown in Figure 3.19. The centre-to-centre distance between two supports and two loading points of the spreader were 2000 mm and 700 mm, respectively. The resulting shear span to depth ratio was 3.0. During testing, the actuator of the Instron Machine was loaded at a low rate, therefore the readings for load, deflection and

strain values from the data logger can be recorded easily and the visible crack width measured effortlessly using the dino-lite digital microscope.

Figure 3.19: Instrumentation and loading set-up.

All the beam specimens were lifted and positioned on the two supports. The LVDT was placed to ensure that the transducer touched the bottom face of the specimen. The LVDT and strain gauges were connected to the data logger and the data logger was calibrated.

The experiments were carried out employing two types of controlling technique. The first was the load control, which was used up to the strain hardening. Commencing from the strain softening region, the displacement control loading was maintained until failure of the beam specimens. All data were recorded by the data logger at 10 second intervals. The rate of the actuator was set to 5 kN/min during load control and 1.5 mm/min during displacement control.

4. ANALYTICAL ANALYSIS

4.1 INTRODUCTION

This chapter presents the theoretical model to predict the flexural response (loads, deflection, strains and crack spacing) of the RC beams (control and strengthened). The theoretical model predicts the crack, yield and ultimate loads, deflection, concrete compressive strain, internal steel bar strain and NSM bar strain at different loading stages. In addition, it predicts the concrete cover separation failure loads.

4.2 THEORETICAL MODEL FOR LOAD PREDICTION

The following assumptions are considered for the theoretical model (Rethnasamy, Rajagopal, & Muthuraj, 2013):

a) Afterward bending, plane sections same as before,
b) The strains (tensile and compressive) are directly proportional to the neutral axis distance,
c) No slip occurs between strengthening reinforcement and concrete,
d) The maximum concrete compressive strain is 0.003,
e) The concrete tensile strength is ignored.

4.2.1 CONTROL BEAM

4.2.1.1 CRACKING LOAD

The cracking load of the control beam can be obtained from the transformed section, as shown in Figure 4.1.

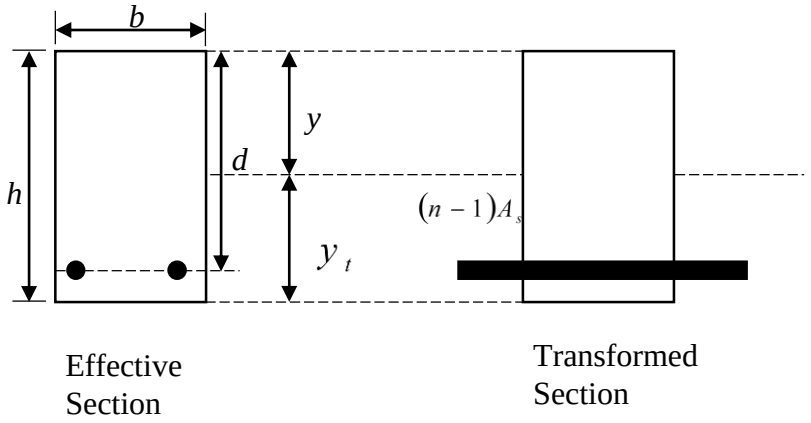

Figure 4.1: Transformed section of the control beam before cracking

Concrete compressive strength = f_c'

Concrete modulus of elasticity, $E_c = 4700\sqrt{f'_c}$ (4.1)

Concrete modulus of rupture, $f_{cr} = 0.70\sqrt{f'_c}$ (4.2)

Steel modulus of elasticity = E_s

Modular ratio of steel bar, n = $\frac{E_s}{E_c}$ (4.3)

Area of concrete, $A_c = bh$ (4.4)

Net transformed area of steel bar, $A_{ts} = A_s(n-1)$ (4.5)

Total area, $A_t = A_c + A_{ts}$ (4.6)

Depth of neutral axis (N.A.) from compression face of beam,

$$y = \frac{A_c.\frac{h}{2} + A_{ts}.d}{A_t} \quad (4.7)$$

Where, *b* is the beam width, *h* is the beam depth, A_s is the area of steel bar, and *d* is the beam effective depth.

Distance of N.A. from tension face of beam, $y_t = h - y$ (4.8)

Gross moment of inertia, $I_g = \frac{bh^3}{12} + A_c\left(\frac{h}{2} - y\right)^2 + A_{ts}(d-y)^2$ (4.9)

Cracking Moment, $M_{cr} = \frac{I_g f_{cr}}{y_t}$ (4.10)

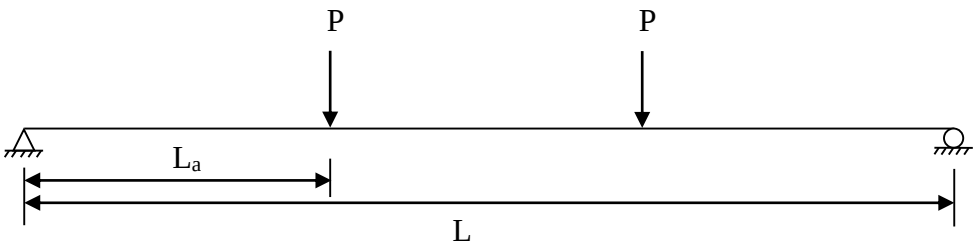

Figure 4.2: Loading position

Therefore, Cracking Load of beam under two points load (Figure 4.2),

$$P_{cr} = \frac{2M_{cr}}{L_a} = \frac{2I_g f_{cr}}{L_a y_t} \quad (4.11)$$

Where, L_a = Shear span and L = Total span length.

4.2.1.2 YIELD LOAD

The yield load of control beam can be estimated from the crack transformed section, as shown in Figure 4.3.

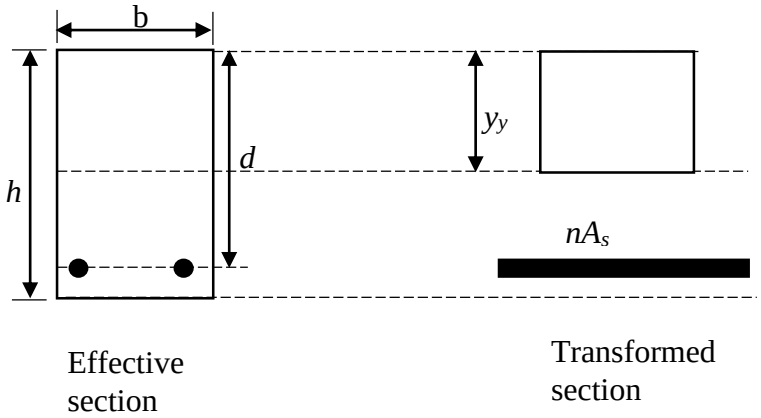

Figure 4.3: Transformed section of control beam after crack

Depth of N.A., $y_y = \frac{-(nA_s) + \sqrt{(nA_s)^2 + 2.b(nA_s d)}}{b}$ (4.12)

Cracking moment of inertia, $I_{cr} = \frac{by_y^3}{3} + nA_s(d - y_y)^2$ (4.13)

Steel bar yield strain, $\varepsilon_y = \frac{f_y}{E_s}$ (4.14)

Steel bar yield curvature, $\phi_y = \frac{\varepsilon_y}{d - y_y}$ (4.15)

Yield moment, $M_y = \phi_y E_c I_{cr}$ (4.16)

Therefore, yield load of control beam, $P_y = \frac{2M_y}{L_a}$ (4.17)

Where, I_{cr} is the cracking moment inertia, y_y is the depth of neutral axis, f_y is the steel bar yield strength, ε_y is the steel bar yield strain, ϕ_y is the steel bar yield curvature, M_y is the control beam yield moment and P_y is the control beam yield load.

4.2.1.3 ULTIMATE LOAD

The ultimate load capacity of control beam was determined by the strain compatibility and force equilibrium requirements, as demonstrated in Figure 4.4. The iteration procedure was adopted to achieve equilibrium.

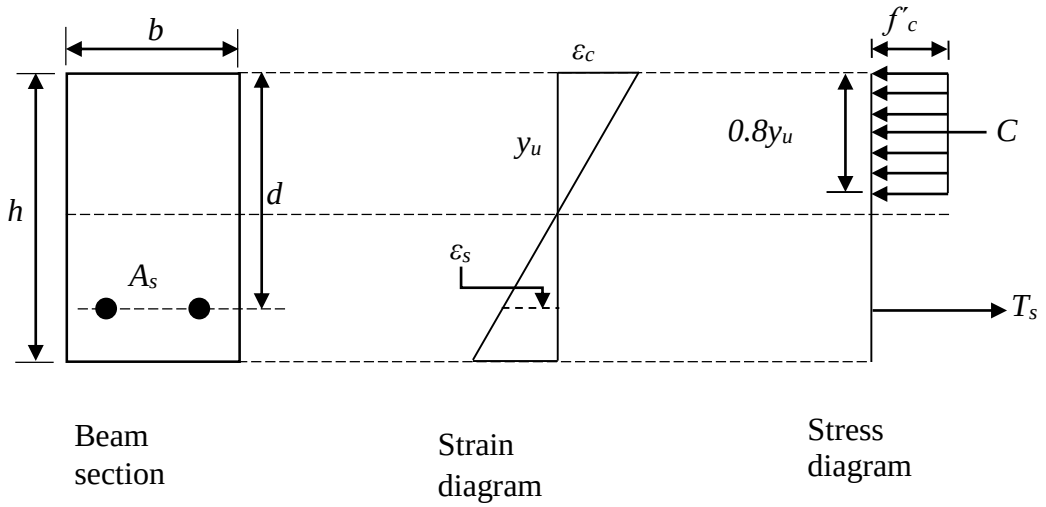

Figure 4.4: Beam section with strain and stress distribution

From Figure 4.4, T_s = C (4.18)

$$(0.8bf_c')y_u^{\,2} + (-A_s f_y)y_u = 0 \tag{4.19}$$

$$M_u = A_s f_y (d - 0.4y_u) \tag{4.20}$$

$$P_u = \frac{2M_u}{L_a} \tag{4.21}$$

Where, y_u is depth of neutral axis, ε_c is strain of the top fibre of concrete, ε_s is strain in the tension steel, f_c' is concrete compressive strength, A_s is the tension main reinforcement area, C is the total concrete compressive force, T_s is the tensile force of the tension steel, M_u is the ultimate moment and P_u is the ultimate load.

4.2.2 STRENGTHENED BEAM

4.2.2.1 CRACKING LOAD

The cracking load of strengthened beam can be calculated based on the transformed section of the strengthened beam, as shown in Figure 4.5.

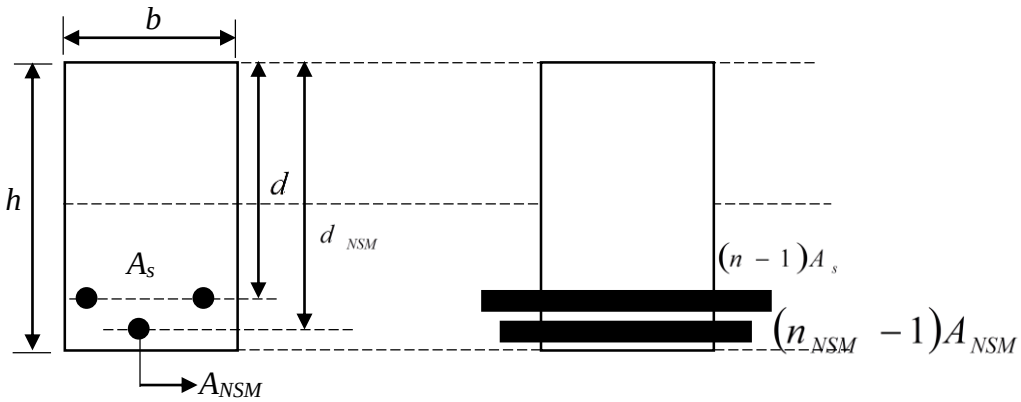

Figure 4.5: Transformed section of strengthened beam before cracking

Modular ratio of NSM bar, $n_{NSM} = \frac{E_{NSM}}{E_c}$ (4.22)

Net transformed area of NSM bar, $A_{tNSM} = (n_{NSM} - 1)A_{NSM}$ (4.23)

Total area, $A_t = A_c + A_{ts} + A_{tNSM}$ (4.24)

Depth of N.A. from compression face of beam,

$$y = \frac{A_C \frac{h}{2} + A_{ts}d + A_{tNSM}d_{NSM}}{A_t} \quad (4.25)$$

Where, d_{NSM} is the distance between the centre of gravity of NSM bar and top compression fibre, E_{NSM} is the modulus of elasticity of the NSM bar.

Gross moment of inertia,

$$I_g = \frac{by^3}{3} + \frac{b(h-y)^3}{3} + nA_s(d-y)^2 + n_{NSM}A_{NSM}(d_{NSM}-y)^2 \quad (4.26)$$

Therefore, the cracking moment and load of strengthened beam can be obtained from Equations 4.10 and 4.11, respectively.

4.2.2.2 YIELD LOAD

The yield load of the strengthened beam can be obtained from the crack transformed section, as shown in Figure 4.6.

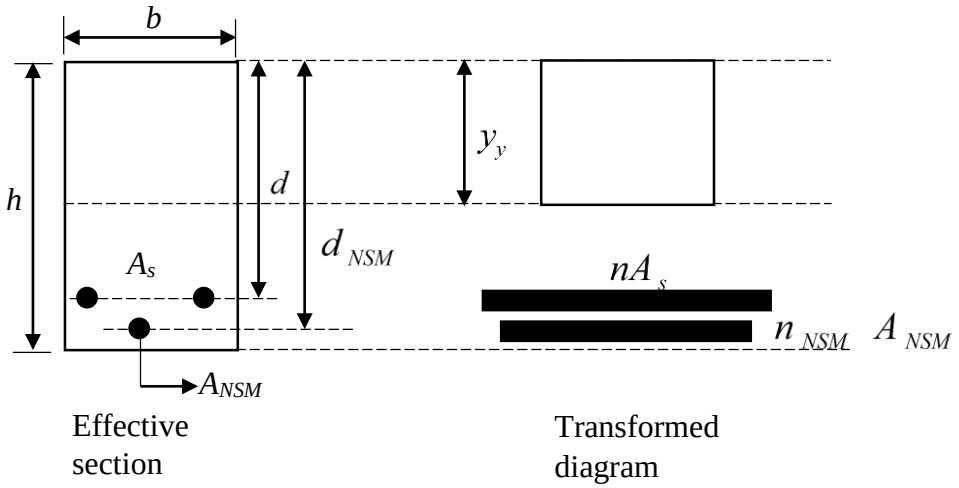

Figure 4.6: Transformed section of strengthened beam after crack

Depth of N.A. from compression face of beam,

$$y_y = \frac{-(nA_s + n_{NSM}A_{NSM}) + \sqrt{(nA_s + n_{NSM}A_{NSM})^2 + 2.b(nA_s d + n_{NSM}A_{NSM}d_{NSM})}}{b} \quad (4.27)$$

Cracking moment of inertia,

$$I_{cr} = \frac{by_y^{\,3}}{3} + nA_s(d - y_y)^2 + n_{NSM}A_{NSM}(d_{NSM} - y_y)^2 \quad (4.28)$$

Therefore, the yielding moment and load of strengthened beam can be obtained from Equations 4.14, 4.15, 4.16 and 4.17, respectively.

4.2.2.3 ULTIMATE LOAD

The ultimate load capacities of the strengthened beams were determined by the strain compatibility and force equilibrium requirements, as demonstrated in Figure 4.7. The iteration procedure was adopted to achieve equilibrium.

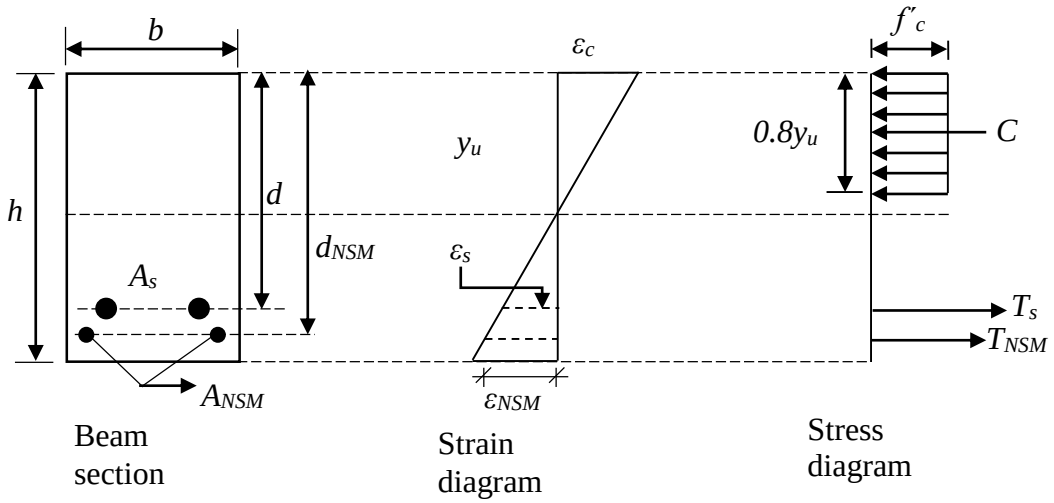

Figure 4.7: Strengthened beam section with strain and stress distribution

From Figure 4.7:

$$T_s + T_{NSM} = C \tag{4.29}$$

$$(0.8bf'_c)y_u^{\,2} + (\varepsilon_{NSM}E_{NSM}A_{NSM} - A_s f_y)y_u - \varepsilon_c E_{NSM}A_{NSM}d_{NSM} = 0 \tag{4.30}$$

$$\varepsilon_{NSM} = \varepsilon_c \frac{d_{NSM} - y_u}{y_u} \le \varepsilon_{NSMu} \tag{4.31}$$

$$f_{NSM} = E_{NSM}\varepsilon_{NSM} \le f_{NSMu} \tag{4.32}$$

$$M_u = A_s f_y(d - 0.4y_u) + A_{NSM} f_{NSM}(d_{NSM} - 0.4y_u) \tag{4.33}$$

Where, M_u is the ultimate load of strengthened beam, ε_{NSM} is the strain in the NSM reinforcement, ε_{NSMu} is the ultimate strain in the NSM reinforcement, f_{NSM} is the yield strength of NSM bar, f_{NSMu} is the ultimate strength of the NSM reinforcement.

Therefore, the ultimate load of strengthened beam can be obtained from Equation 4.21.

4.3 CONCRETE COVER SEPARATION MODEL

The analytical model for predicting concrete cover separation is illustrated in Figure 4.8. The basic concept is that a concrete tooth is created between adjacent cracks (Al-Mahmoud, Castel, François, & Tourneur, 2010) when external loading is imposed. To determine concrete cover separation failure loads, this prediction model depends on stabilized crack spacing.

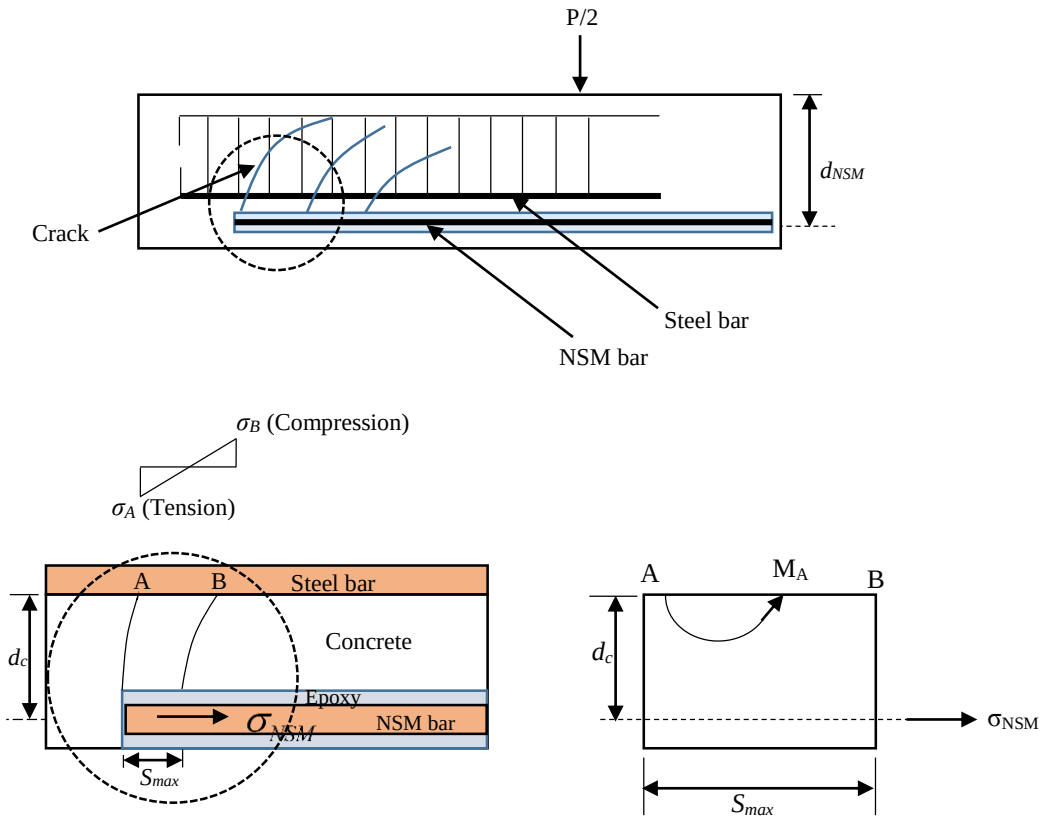

Figure 4.8: Distribution of stress in the NSM bars and concrete between the last two adjacent cracks at the end of the NSM bars

The tensile stress at the critical point A (σ_A) can be calculated by bending moment:

$$\sigma_A = \frac{M_A\left(S_{\max}/2\right)}{I_A} \tag{4.34}$$

Where I_A is moment of inertia of the section (b x S_{max}):

$$I_A = \frac{b \times S_{\max}^{\ 3}}{12} \tag{4.35}$$

And $M_A = \sigma_{NSM} A_{NSM} d_c$ (4.36)

$$\sigma_A = \frac{6A_{NSM} d_c}{bS_{\max}^{\ 2}} \sigma_{NSM} \tag{4.37}$$

With, $\sigma_{NSM} = n_{NSM} \frac{d_{NSM} - y}{I_{cr}} M_B$ (4.38)

Where, M_A is the moment at point A, b is beam width, S_{max} is the maximum crack spacing, d_c is the distance between the centre of gravity of the NSM bars and the surface of the main steel bars, σ_{NSM} is the stress in NSM bar, and M_B is the moment at point B. The other symbols designate the usual meaning.

From Equations 4.37 and 4.38 the following equation was obtained:

$$\sigma_A = \frac{6n_{NSM} A_{NSM} d_c}{bS_{\max}^{\ 2}} \frac{(d_{NSM} - y)}{I_{cr}} M_B \tag{4.39}$$

Concrete cover separation occurs when the tensile strength at point A attains the ultimate tensile strength of the concrete f_{ct} and the bending moment at point B (M_B) is heading towards the beam failure load:

$$M_B = \frac{f_{ct} I_{cr} bS_{\max}^{\ 2}}{6n_{NSM} A_{NSM} d_c (d_{NSM} - y)} \tag{4.40}$$

4.4 DEFLECTION PREDICTION MODEL

The load-midspan deflection curve for RC beams strengthened with NSM reinforcement can be divided into three distinct linear stages (Figure 4.9) as:

a) Un-cracked phase ($P < P_{cr}$)

b) Cracking phase ($P_{cr} \leq P \leq P_y$)

c) Post-cracking phase ($P_y < P < P_u$)

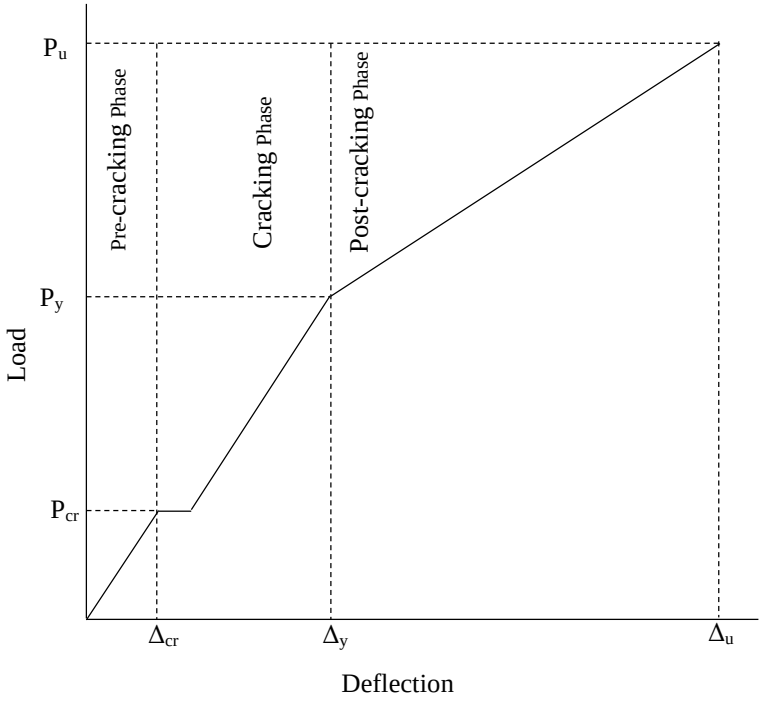

Figure 4.9: Schematic model of load-midspan curve for the strengthened beams

a) Un-cracked phase: Elastic equations are applied to determine the deflection of the strengthened beams utilizing the gross transformed moment of inertia I_g, which contains the contribution of the NSM reinforcement.

Therefore, the deflection of uncracked phase:

$$\Delta_{cr} = \frac{(P_{cr}/2)L_a}{24E_cI_g}(3L^2 - 4L_a{}^2) \tag{4.41}$$

b) Cracking phase: When applied load P is greater than the cracking load P_{cr}, the section of the concrete in the locality of the midspan cracks, then the flexural stiffness of the beam reduces. In the lower moment location, where there are no cracks in the concrete, the moment of inertia is almost equal to the gross moment of inertia (I_g). Where the flexural cracks are located, the moment of inertia of that section is almost equal to the transformed cracked moment of inertia (I_{cr}). The moment of inertia lies between the two values of I_g and I_{cr}. When the tensile forces develop between the concrete and cracks, then the flexural rigidity EI refers to the tension stiffening. In this period, the beam no

longer has a constant moment of inertia along its length, and the effective moment of inertia (I_e) is used. The effective moment of inertia (I_e) according to the ACI Code (Committee, Institute & Standardization, 2008).

$$I_e = I_{cr} + \left(I_g - I_{cr}\right)\left(\frac{M_{cr}}{M}\right)^3 \tag{4.42}$$

Hence, deflection of cracking phase, $\Delta_y = \frac{(P_y/2)L_a}{24E_cI_e}(3L^2 - 4L_a{}^2)$ (4.43)

c) Post-cracking phase: In this phase, the deflection is determined using the curvature along the beam length. The curvature is calculated by linear interpolation between the curvature at the first yield of tension steel ϕ_y and the ultimate curvature ϕ_u. The depth of the neutral axis and the ultimate moment can be obtained for the ultimate load capacity section.

$$\phi_u = \frac{\varepsilon_{cu}}{y_u} \tag{4.44}$$

$$\phi = \phi_y + \frac{M - M_y}{M_u - M_y}\left(\phi_u - \phi_y\right) \tag{4.45}$$

$$I_e = \frac{M}{E_c\phi} \tag{4.46}$$

Therefore, the deflection of post-cracking phase can be estimated from Equation 4.43. Where, *M* is the post-cracking of any service moment.

4.5 CRACK SPACING PREDICTION MODEL

The maximum flexural crack spacing is reliant on the modular ratio and position of the neutral axis for the composite section (Beeby & Narayanan, 1995). Following this ideology, the crack spacing for the present strengthened beams uses the consequent prediction model.

$$S_{\max} = 3.4c + 0.425k_1k_2\frac{d_b}{\rho_{eff}} \tag{4.47}$$

$$\rho_{eff} = \frac{A_s + n_{NSM}A_{NSM}}{A_{ceff}} \tag{4.48}$$

$$A_{ceff} = \min\begin{Bmatrix} 2.5\times b\times c \\ b\times(h-y)/3 \end{Bmatrix} \tag{4.49}$$

Where, c is the concrete cover, k_1 is the bond coefficient (0.80 and 1.6 for high bond and plain rebar, respectively), k_2 is the strain distribution coefficient (0.50 and 1.0 for bending and pure tension, respectively) d_b is the diameter of the rebar, ρ_{eff} is the effective reinforcement ratio and A_{ceff} is the area of the concrete in tension.

4.6 CONCRETE COMPRESSIVE STRAIN PREDICTION MODEL

The concrete top fibre strain of the RC beam specimen is predicted using the following equation:

$$\varepsilon_c = \frac{(P/2)\times L_a \times y}{E_c I} \tag{4.50}$$

Where, ε_c is the concrete top fibre strain and the other symbols designate the usual meaning.

4.7 INTERNAL REINFORCEMENT TENSILE STRAIN PREDICTION MODEL

The following equation is used to predict the tensile strain in the main internal reinforcement:

$$\varepsilon_s = \frac{(P/2)\times L_a \times (d-y)}{E_c I} \tag{4.51}$$

Where, ε_s is the tensile strain in the internal main reinforcement and the other symbols are designating the usual meanings.

4.8 NSM BAR STRAIN PREDICTION MODEL

The NSM bar strain can be predicted using the following equation:

$$\varepsilon_{NSM} = \frac{(P/2)\times L_a \times (d_{NSM} - y)}{E_c I} \tag{4.52}$$

Where, ε_{NSM} is the NSM bar strain and the other symbols designate the usual meaning.

5. RESULTS AND DISCUSSIONS

5.1 INTRODUCTION

The experimental test results of twenty-five RC beams (control and strengthened) are described. This chapter demonstrates the flexural strength, load-midspan deflection behaviour, failure modes, strain characteristics and crack features of all the tested beam specimens. The influence of strengthening on their first crack, yield and ultimate loads are discussed. The variation in the load vs. strain in the main steel rebar, concrete top fibre and strengthened bars as a result of strengthening are also described.

5.2 TEST RESULTS

5.2.1 PROPERTIES OF CONCRETE

All the tested beam specimens were cast using the same mix design. The compressive strength tests were determined according to BS EN 12390-3 (2009) using three 100 mm x 100 mm x 100 mm cube specimens and modulus of rupture tests were performed according to BS EN 12390-5 (2009) using three 100 mm x 100 mm x 500 mm prism specimens. An ELE (Engineering Laboratory Equipment) testing machine with a load capacity of 3000 kN was used in the compression and flexure test, and the loading rate was 2.4 kN/s and 0.067 kN/s respectively. The average concrete compressive strength and modulus of rupture for 28 days of all tested beams are shown in Table 5.1.

Table 5.1: Strength properties of concrete

No. of beam specimens	Compressive strength (MPa)	Modulus of rupture (MPa)
25	40.00	4.43

5.2.2 FLEXURAL PERFORMANCE OF NSM STEEL BAR STRENGTHENED RC BEAMS (SINGLE GROOVE)

This section presents the results of the experimental investigation of six beam specimens. The results of the strengthened beams are compared with the control beams.

5.2.2.1 FLEXURAL STRENGTH AND DEFLECTION BEHAVIOUR

The experimental performance of all the tested beam specimens in relation to flexural strength, deflection and failure modes are demonstrated in Table 5.2. The beams strengthened with NSM single steel bar increased the first cracking load by 7.94%, 26.98%, 39.68%, 46.03% and 52.38% for N1S6, N1S8, N1S10, N1S12 and N1S16, respectively, compared to the control beam specimen. The use of NSM steel bars increased the yield load of the strengthened specimens by 7.14%, 28.57%, 50.00% and 57.14% for N1S6, N1S8, N1S10 and N1S12, respectively, over the control beam. The ultimate load increased by 7.57%, 35.81%, 53.02%, 70.45% and 47.32% for N1S6, N1S8, N1S10, N1S12 and N1S16, respectively, over the control beam.

Table 5.2: Summary of test results for single groove

Beam ID	P_{cr} (kN)	$\%P_{cr}$	P_y (kN)	$\% P_y$	P_u (kN)	$\%P_u$	Δ_{max} (mm)	Failure mode
CB	15.75	-	70.00	-	74.37	-	33.61	FL
N1S6	17.00	7.94	75.00	7.14	80.00	7.57	41.68	FL
N1S8	20.00	26.98	90.00	28.57	101.00	35.81	40.23	FL
N1S10	22.00	39.68	105.00	50.00	113.80	53.02	39.13	FL
N1S12	23.00	46.03	110.00	57.14	126.76	70.45	38.65	FL
N1S16	24.00	52.38	-	-	109.56	47.32	8.26	CC

The load versus deflection curves for all the beam specimens are shown in Figure 5.1. As can be seen from the figure, the curves exhibit tri-linear characteristics, as defined by elastic, concrete cracking to steel yielding and steel yielding to failure phases, except the N1S16 specimen due to premature failure. In the first phase, the behaviour of all the beam specimens was linear and elastic. Earlier, the first

crack, the bond into the steel bar, adhesive and the concrete were perfect. In the second phase, cracking was initiated in the concrete cross-section of the maximum moment zone of the beam specimen. At the beginning of this phase, the cracks did not pass through the integrant materials because of their higher tensile strength and low elastic modulus. As the loading increased, the cracks became more widespread and new flexural cracks arose. In the third phase, the internal tension steel reinforcement yielded and the NSM steel bar controlled the cracks and the width of the cracks up to failure of the beam.

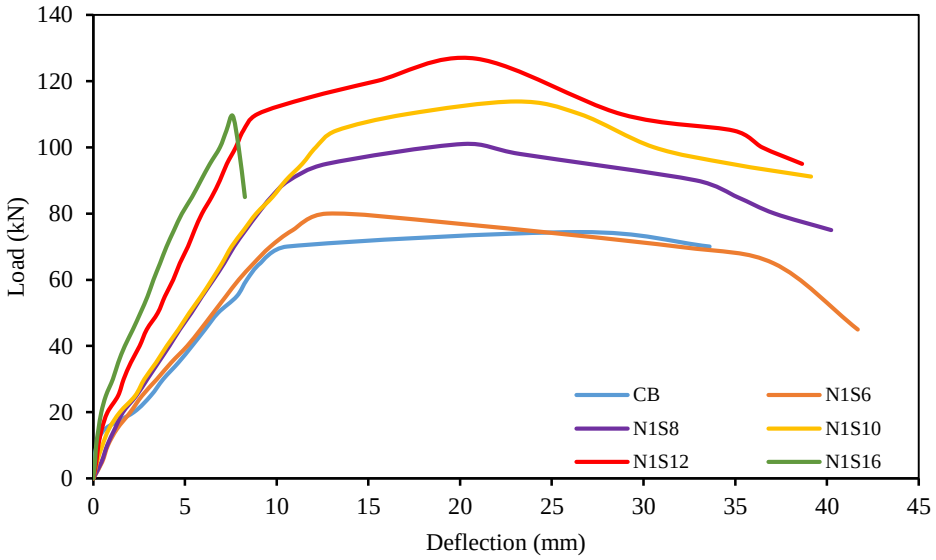

Figure 5.1: Load-midspan deflection

5.2.2.2 MODE OF FAILURE

The modes of failure for all specimens are shown in Figure 5.2. The beam specimens exhibited two types of failure. The extreme fibre concrete crushing of the RC beam cross-section after the yielding of the tension reinforcement. This failure mode was seen in the control specimen. When the NSM steel bar was used for strengthening of the beams, the failure mode was rupture of the NSM bar after the yielding of the main tension rebar, except for the N1S16 beam specimen. The cracking pattern was similar for all specimens. At first, a fine flexural crack

developed at the midspan of the beam. As the applied load increased, extra cracks appeared at the neutral axis or beyond the neutral axis, with a notable increase in the deflection of the beam specimen. Therefore, all the strengthened beam specimens showed narrower and finer cracks compared to the control specimen. This is due to the greater stiffness of the strengthened beam specimens. However, for the N1S16 specimen, stress overlap due to the limited width of beam, high strengthening reinforcement ratio, and the tensile strengths of both the epoxy and the concrete. Therefore, the concrete cover separation failure occurs at the end of the NSM bar.

5.2 (a) CB

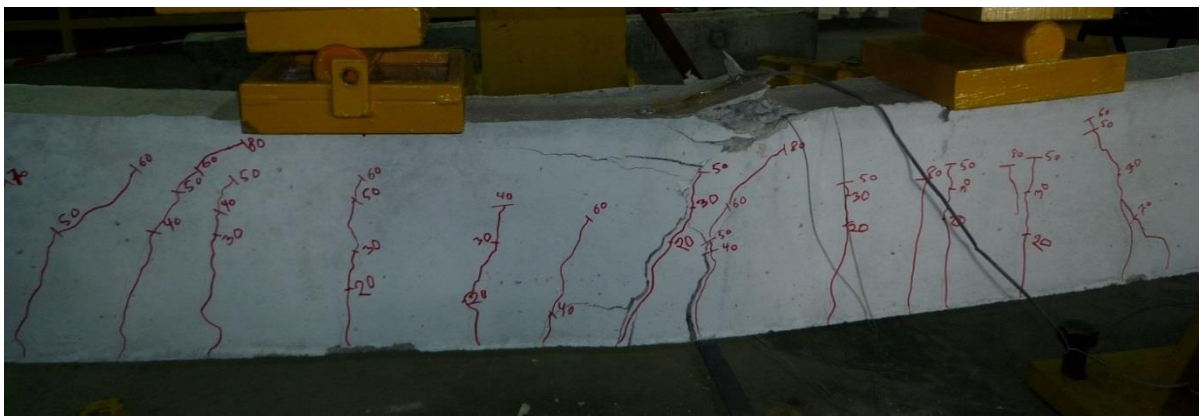

5.2 (b) N1S6

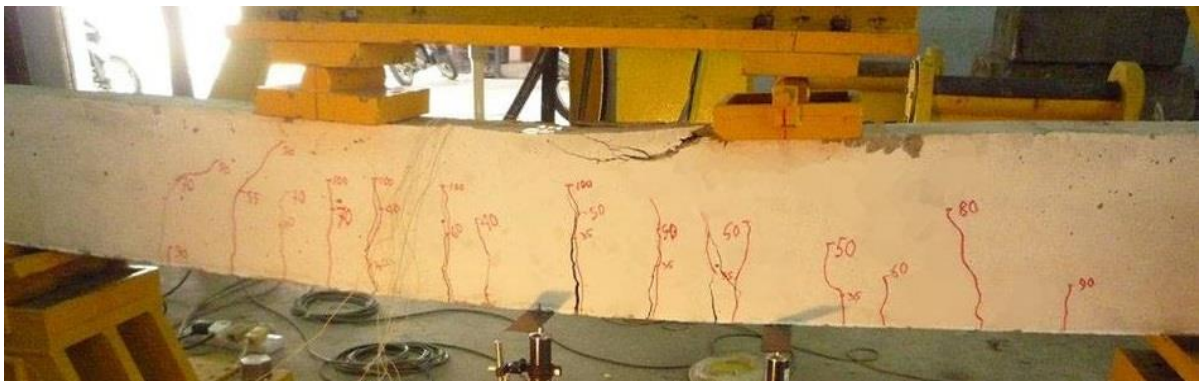

5.2 (c) N1S8

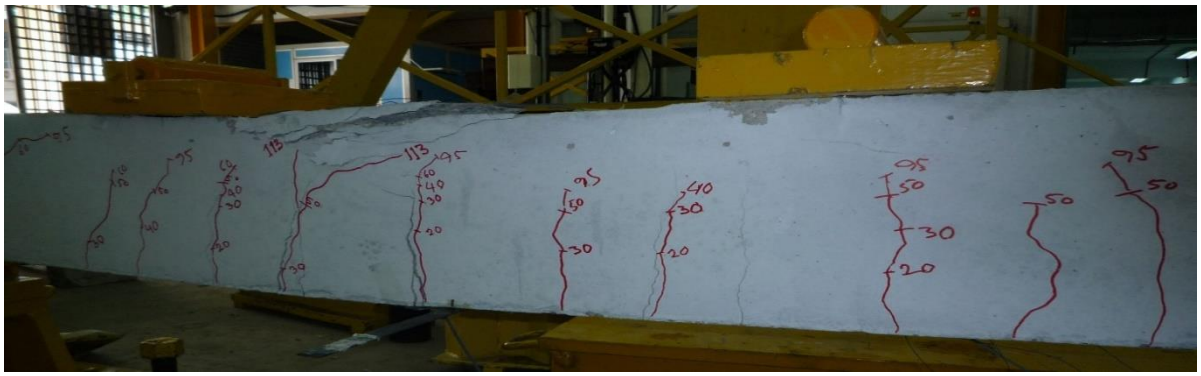

5.2 (d) N1S10

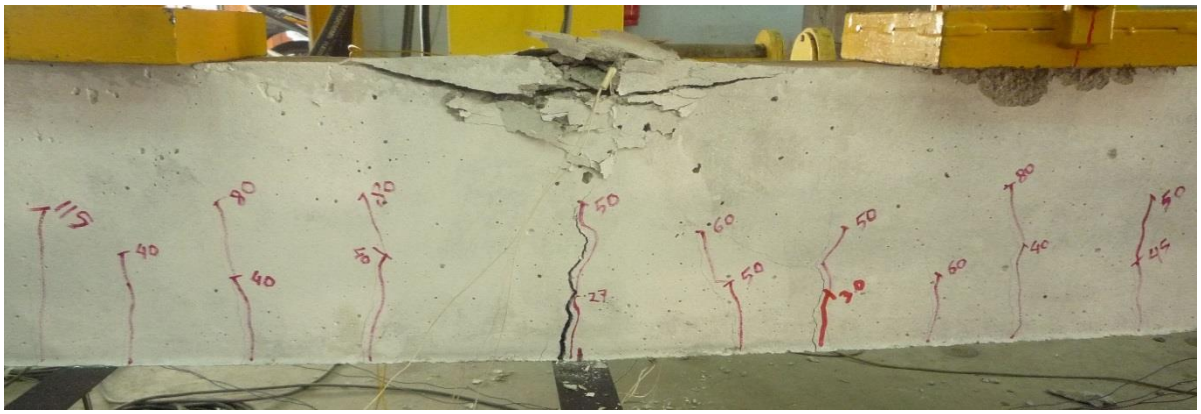

5.2 (e) N1S12

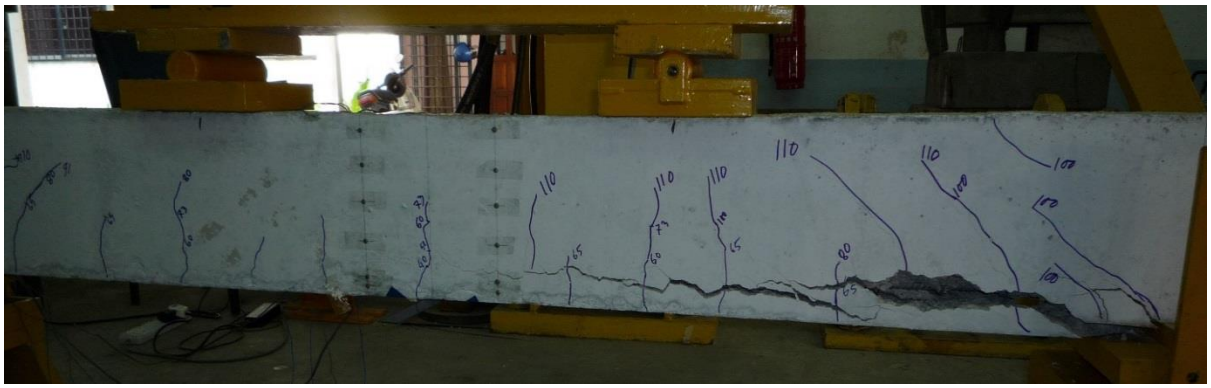

5.2 (f) N1S16

Figure 5.2: Failure modes of beam specimens

5.2.2.3 COMPRESSIVE STRAIN OF CONCRETE

The loads versus concrete compression strains at the extreme fibre of the beam specimens are shown in Figure 5.3. The concrete compressive strains of all the strengthened specimens were smaller than the concrete compressive strains of the control specimen because of the greater stiffness of the strengthened specimens. All the strengthened specimens showed linear variation in strain up to steel yielding. After steel yielding, the concrete strains rapidly increased as a result of strain compatibility. This shows that concrete compression failure occurred first and was then followed by flexural failure, except for the N1S16 specimen due to less cracks occurred at the compressive zone.

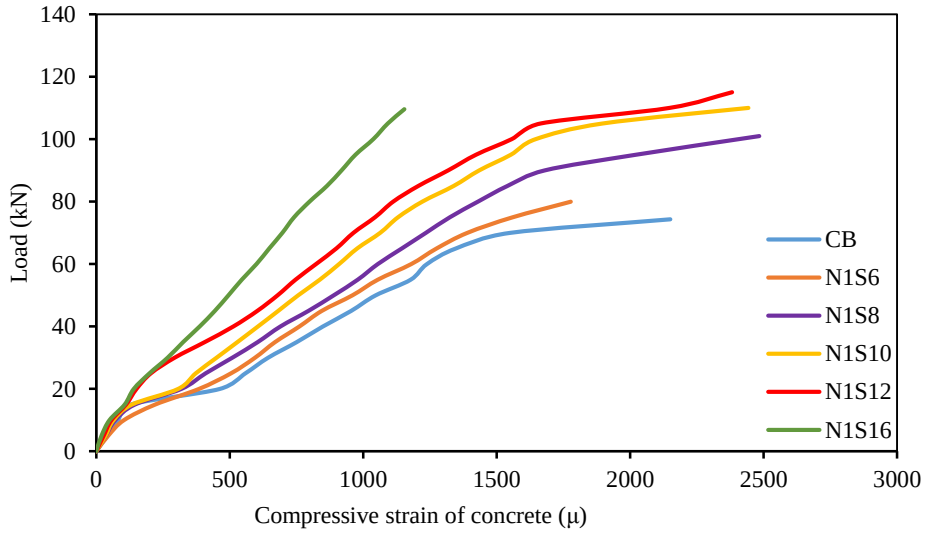

Figure 5.3: Load-compressive strain of concrete

5.2.2.4 TENSILE STRAIN OF MAIN REBARS

The loads versus the strains in the internal tension steel bars during loading are shown in Figure 5.4. The tension steel bar strains for all the strengthened beam specimens were smaller than the tension steel bar strains of the control specimen. After the first crack in a concrete section, the tensile stress was transferred to the

steel bars. Therefore, there was an abrupt increase in the strain in the tension steel bars after the first crack. This rate of increment was greater for the control specimen than for the strengthened beam specimens because the control beam had larger crack widths. All the strengthened beams showed linear variation in strain from the first crack to steel yielding except N1S16. After yielding of the steel, the tension bar strains increased rapidly due to greater crack width.

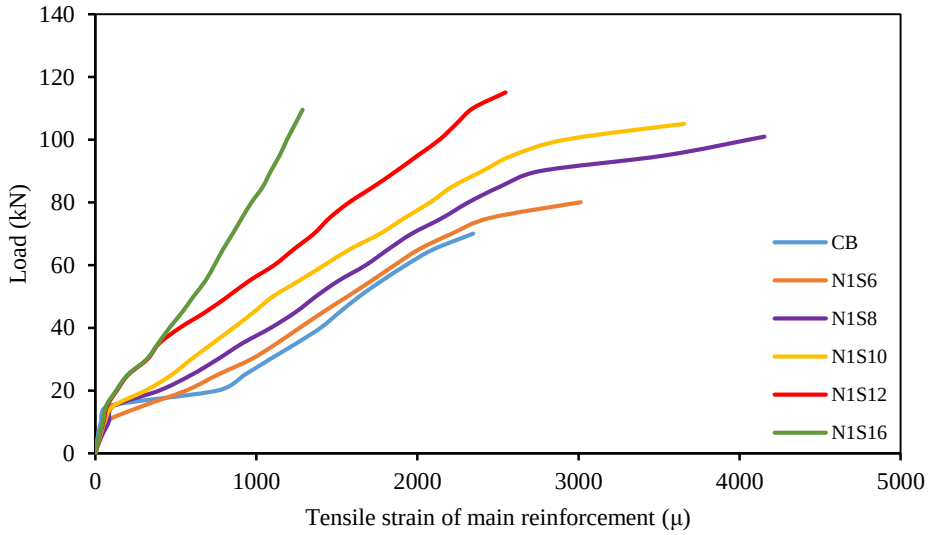

Figure 5.4: Load-tensile strain of main reinforcement

5.2.2.5 TENSILE STRAIN OF NSM REINFORCEMENT

The loads versus the strains in the NSM steel bars during loading are shown in Figure 5.5. It was found that the N1S16 beam had less NSM bar strain compared to the other specimens due to higher stiffness and premature failure. At the failure stage, the NSM bar strains of beams N1S6, N1S8, N1S10, and N1S12 were found to be 0.0055, 0.0052, 0.0066, 0.0056 and 0.0028, respectively. It was observed that the concrete cover separation of the N1S16 specimen was initiated at the NSM strain of around 0.0028.

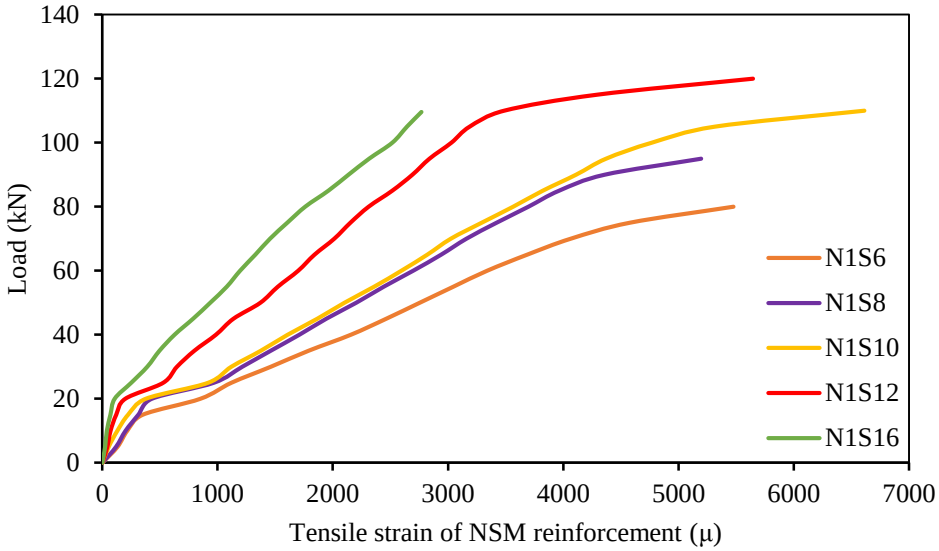

Figure 5.5: Load-tensile strain of NSM reinforcement

5.2.2.6 SECTIONAL STRAIN VARIATION

The variation in strain over the depth of the strengthened beams N1S6, N1S8, N1S10, N1S12 and N1S16 at different load levels is shown in Figure 5.6. The strain variation was linear at the commencement of loading and the variation increased with the upper load levels. For all the strengthened beam specimens, the strain variation increased at the NSM bar level. The position of the neutral axis and the strain variation of all the strengthened beam specimens were very similar because of the stiffness of the beam specimens. It was found that the increase in the NSM reinforcement reduced the sectional strain.

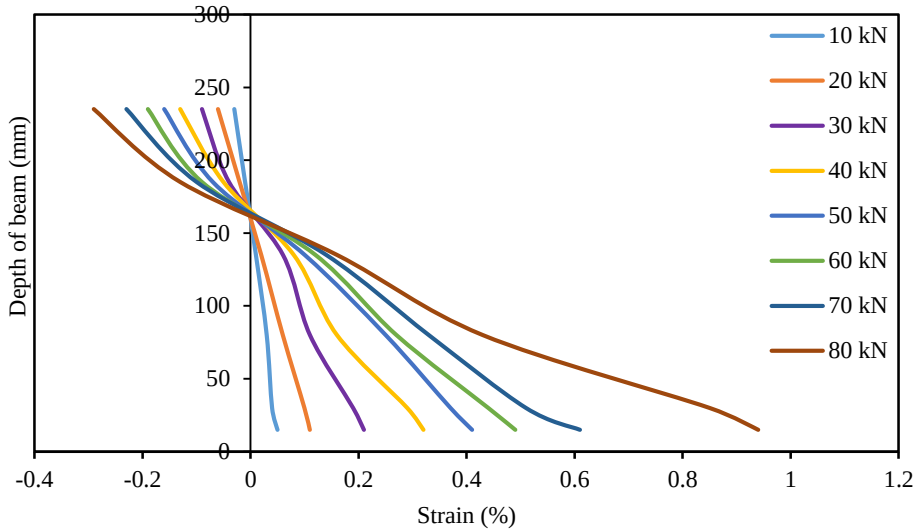

5.6 (a) N1S6

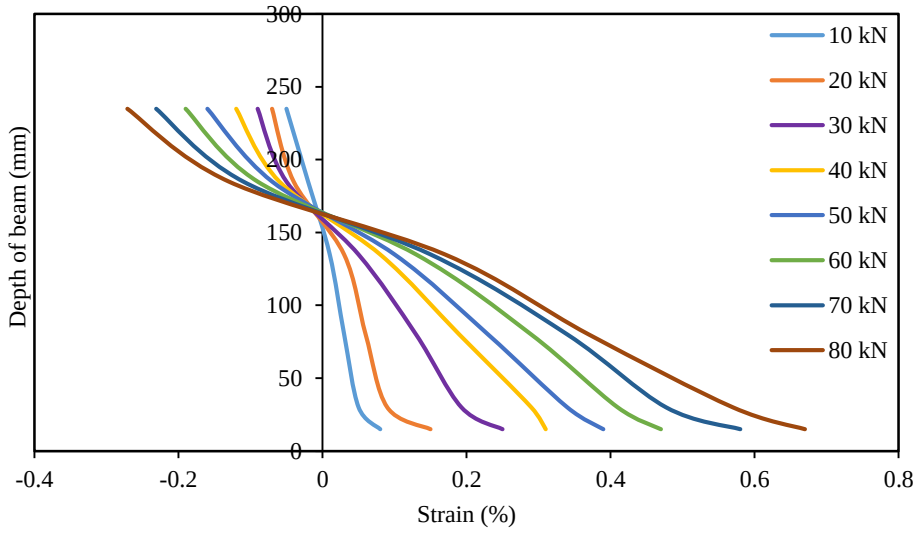

5.6 (b) N1S8

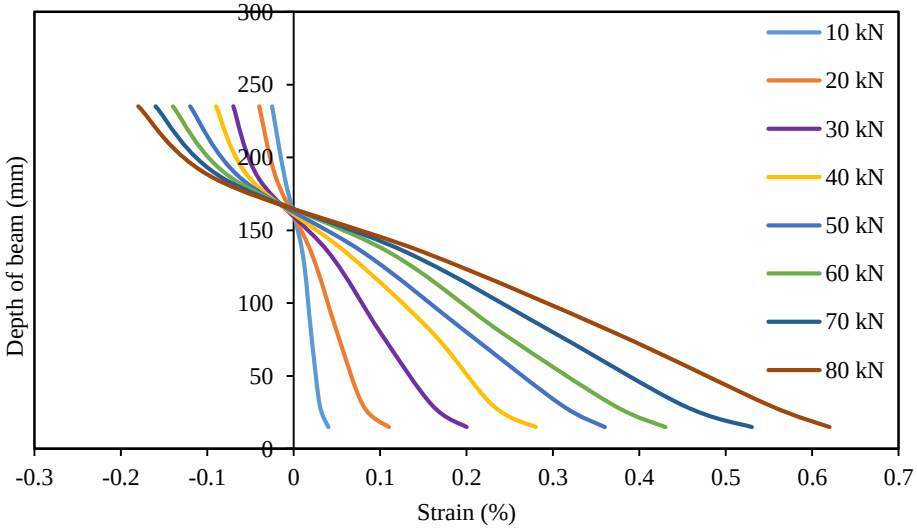

5.6 (c) N1S10

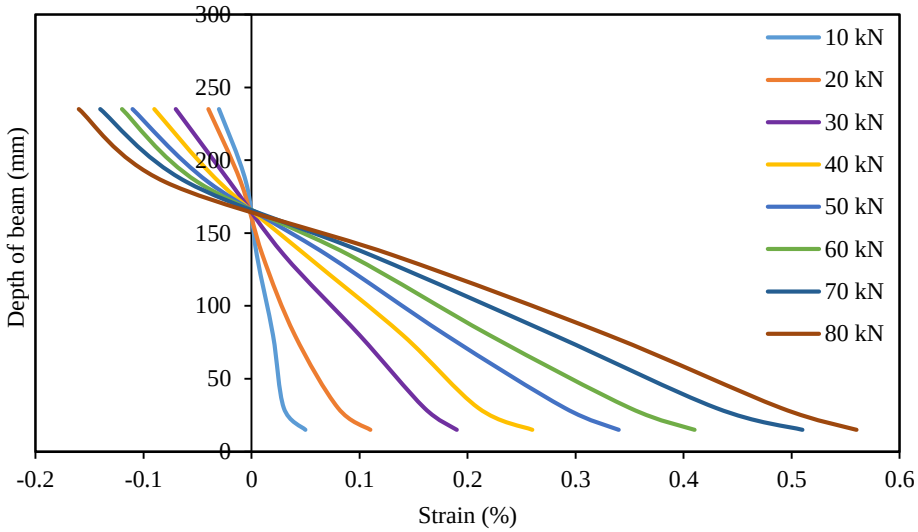

5.6 (d) N1S12

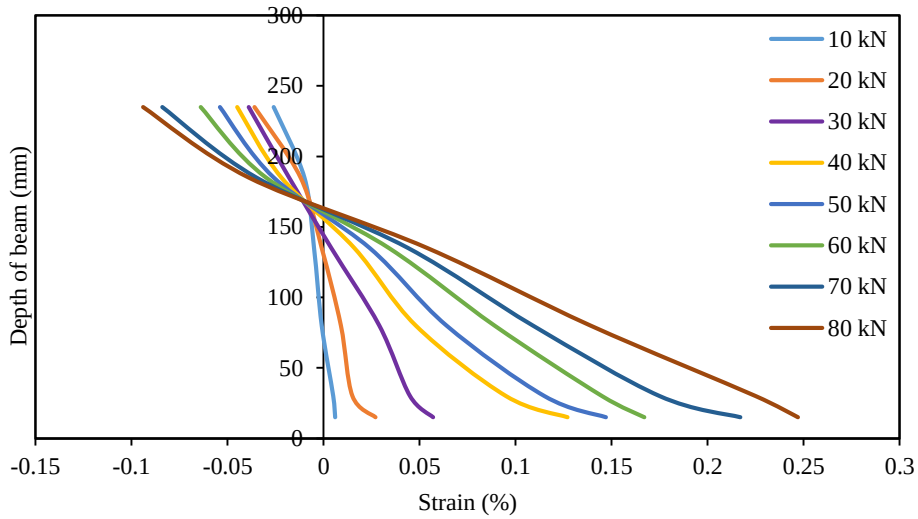

5.6 (e) N1S16

Figure 5.6: Sectional strain variation at midspan of strengthen beams

5.2.2.7 CRACK CHARACTERISTICS

The loads versus crack widths of the beam specimens are shown in Figure 5.7. The first crack load of CB, N1S6, N1S8, N1S10, N1S12 and N1S16 were 15.75 kN, 17 kN, 20 kN, 22 kN, 23 kN and 24 kN, respectively. All the strengthened beam specimens showed higher first crack loads compared to the control specimen. Thus, the use of NSM steel bars increased the first crack load. The total number of cracks of CB, N1S6, N1S8, N1S10 N1S12 and N1S16 were 11, 16,

17, 19, 22 and 19, respectively, and the average crack spacing of each beam was 180 mm, 115 mm, 125 mm, 100 mm, 90 mm and 107 mm, respectively.

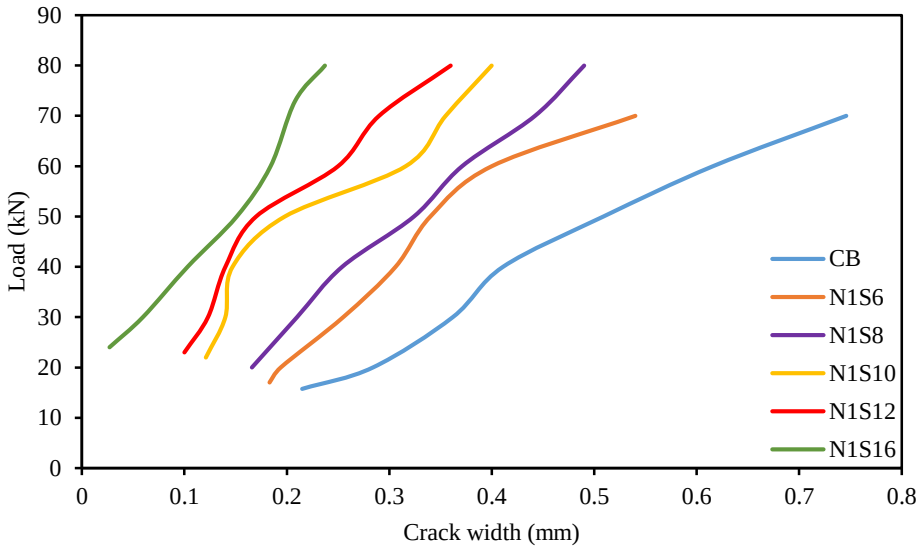

Figure 5.7: Load-crack width

However, N1S8 had a wider crack spacing than N1S6 and N1S16 had fewer cracks and wider crack spacing than N1S12. This was because N1S8 was strengthened with a low strength steel bar and the N1S16 specimen failed before achieved the full strength due to debonding. However, all the strengthened beam specimens showed a smaller crack spacing compared to the control specimen. Thus, it can be understood that beam specimens strengthened with NSM steel bars exhibited more and finer cracks with closer spacing than the unstrengthened beams.

5.2.2.8 THE EFFECTIVENESS OF NSM-STEEL TECHNIQUE

The reduction in deflection due to strengthening using the NSM-steel bar technique at 30 kN, 50 kN and 70 kN service loadings are shown in Figure 5.8. The deflection of the strengthened beam specimens was reduced by a maximum of about 72%, 62% and 62% at 30 kN, 50 kN and 70 kN, respectively,

compared to the control beam specimen, which was due to the increased stiffness of the strengthened beam specimen. The compressive strain of concrete at the top fibre of the specimens and the reduction of the strain due to strengthening at 30 kN, 50 kN and 70 kN service loading are shown in Figure 5.9.

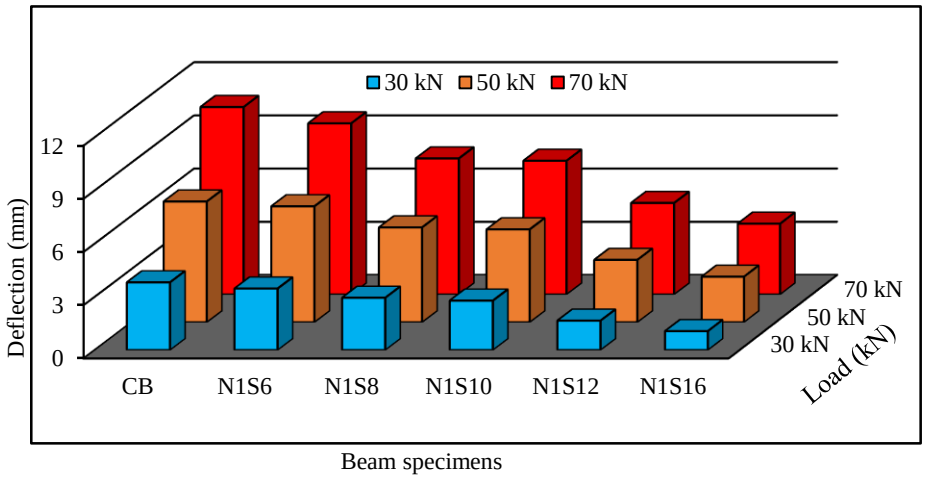

Figure 5.8: Reduction in deflection due to NSM-steel strengthening

The concrete compressive strain of the strengthened beam specimens was reduced by a maximum of about 58%, 53% and 55% at 30 kN, 50 kN and 70 kN, respectively, compared to the control beam specimen. The extreme fibre concrete strain of the strengthened beam specimens was significantly decreased. The internal reinforcing tension steel bar strain and reduction of the strain due to strengthening at 30 kN, 50 kN and 70 kN service loading is shown in Figure 5.10. The strain in the reinforcing bars of the strengthened beam specimens was reduced by a maximum of about 71%, 63% and 64% at 30 kN, 50 kN and 70 kN, respectively, compared to the control beam specimen.

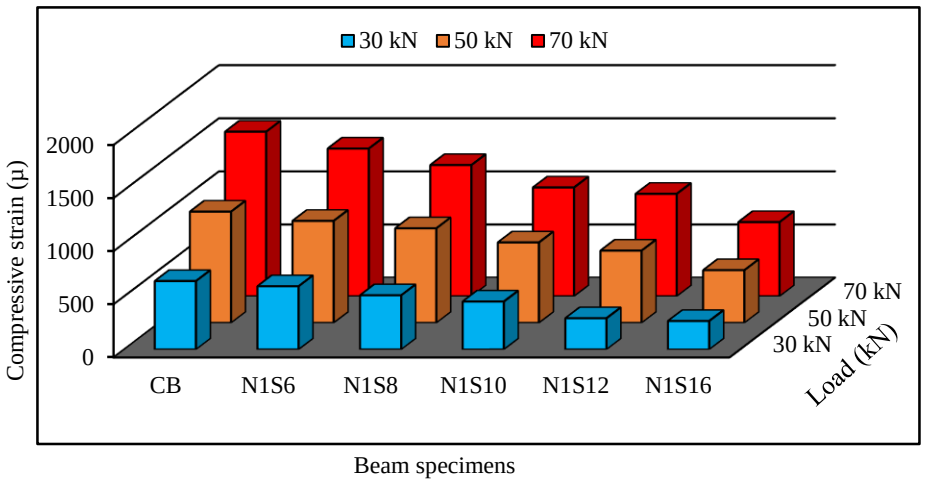

Figure 5.9: Reduction in concrete top fibre strain due to NSM-steel strengthening

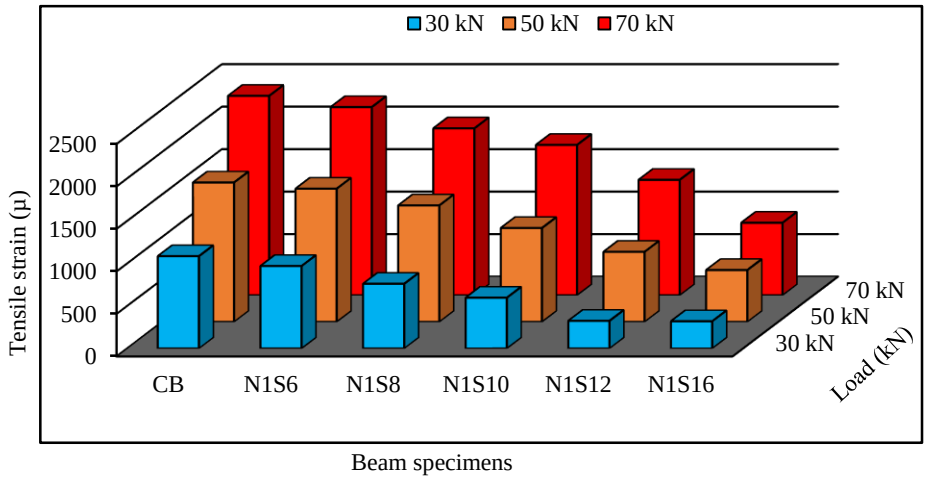

Figure 5.10: Reduction in main steel bar strain due to NSM-steel strengthening

5.2.3 FLEXURAL PERFORMANCE OF NSM STEEL OR CFRP BARS STRENGTHENED RC BEAMS (DOUBLE GROOVE)

This section presents the experimental results obtained from the RC beam specimens strengthened with NSM steel or CFRP bars compared with the control beam. The results of these beams are presented as shown below.

5.2.3.1 FLEXURAL STRENGTH AND DEFLECTION BEHAVIOUR

The experimental performance of the tested specimens in terms of flexural strength, maximum deflection and modes of failure are revealed in Table 5.3. The

beams strengthened with NSM steel or CFRP bar increased the first cracking load by 23.41%, 26.98%, 33.33%, 68.89% and 58.73% for N2S6, N2S8, N2S10, N2S12 and N2C12, respectively, compared to the control beam. The yield load of the beam was not distinguished because of early debonding or concrete crushing without yielding. It is important to note that the first crack loading of the strengthened beams increased most significantly compared to the control specimen. Also, the ultimate load significantly increased by 44.12%, 42.85%, 58.33%, 83.88% and 96.36% for N2S6, N2S8, N2S10, N2S12 and N2C12, respectively, over the control beam.

Table 5.3: Summary of test results for double groove

Beam ID	P_{cr} (kN)	$\%P_{cr}$	P_u (kN)	$\%P_u$	Δ_{max} (mm)	Failure mode
CB	15.75	-	74.37	-	33.61	FL
N2S6	19.50	23.81	107.18	44.12	38.95	FL
N2S8	20.00	26.98	106.24	42.85	14.14	CC
N2S10	21.00	33.33	117.75	58.33	15.62	CC
N2S12	26.60	68.89	136.75	83.88	11.95	CC
N2C12	25.00	58.73	146.03	96.36	12.93	CC

The load versus midspan deflection curves for beams CB, N2S6, N2S8, N2S10, N2S12 and N2C12 are shown in Figure 5.11. The CB and N2S6 beam specimens demonstrated a tri-linear response specified by cracking, yielding and ultimate stages due to flexural failure. The N2S8, N2S10, N2S12 and N2C12 beam specimens revealed a bi-linear response specified by cracking and ultimate stages due to concrete cover separation failure. In the cracking stage, the strengthened beam specimens followed a linear elastic shape similar to the control specimen. In this stage, the NSM steel bars induced an insignificant influence on the stiffness of the load-deflection curves, but a slight reduction in the deflection and enhanced first cracking load. In the second stage, cracking started at the maximum moment zone of the concrete cross-section of the beam specimens. With a further increase in the applied load, the cracks became wider and fresh flexural cracks occurred.

Cracking increased according to the applied load. After yielding of the internal reinforcement, the NSM steel bars controlled the crack width until failure of the beam. The N2S8, N2S10, N2S12 and N2C12 strengthened beams failed by premature debonding; the ultimate load was reached rapidly after separation of the concrete cover with a quick decrease in the load. However, N2C12 showed more deflection than the N2S10 and N2S12 beam specimens.

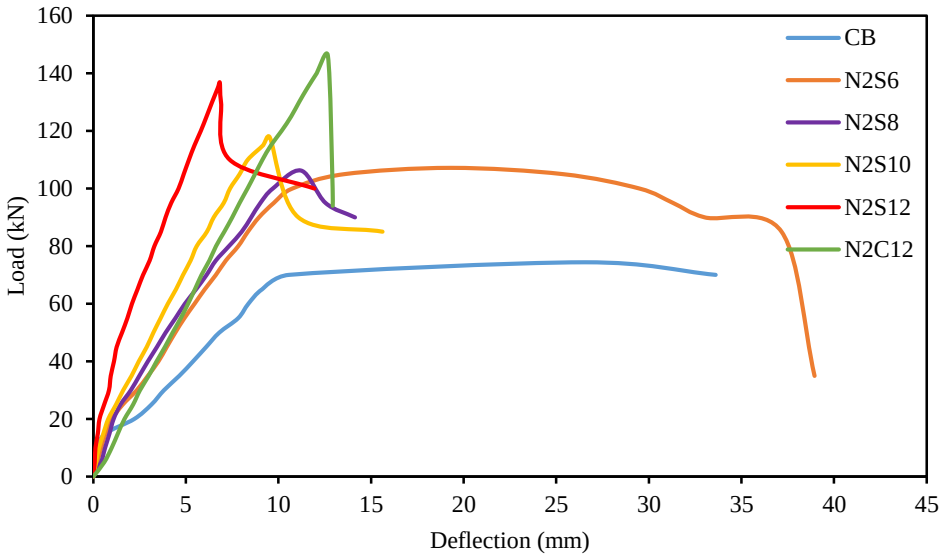

Figure 5.11: Load-Midspan deflection

5.2.3.2 MODE OF FAILURE

The failure modes of the N2S6, N2S8, N2S10, N2S12 and N2C12 beam specimens are shown in Figure 5.12. The failure mode of the N2S6 specimen showed that the beam failed in flexure, with rupture of the NSM bars followed by crushing of the concrete. Hence, the beam exhibited a ductile mode of failure. In contrast, beams N2S8, N2S10, N2S12 and N2C12 failed owing to concrete cover separation. After yielding of the internal main reinforcement, the shear crack initiated at the end of NSM bars and rapidly increased the crack width. When the shear crack and flexural crack intersected, the exposed concrete cover separated.

5.12 (a) N2S6

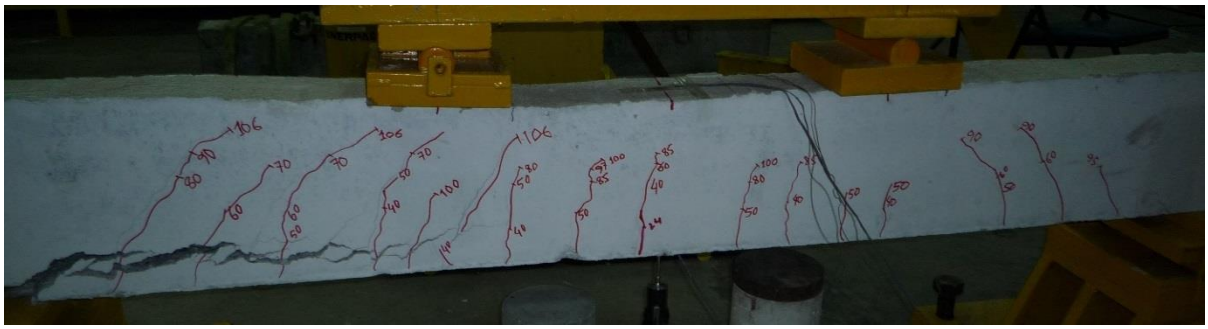

5.12(b) N2S8

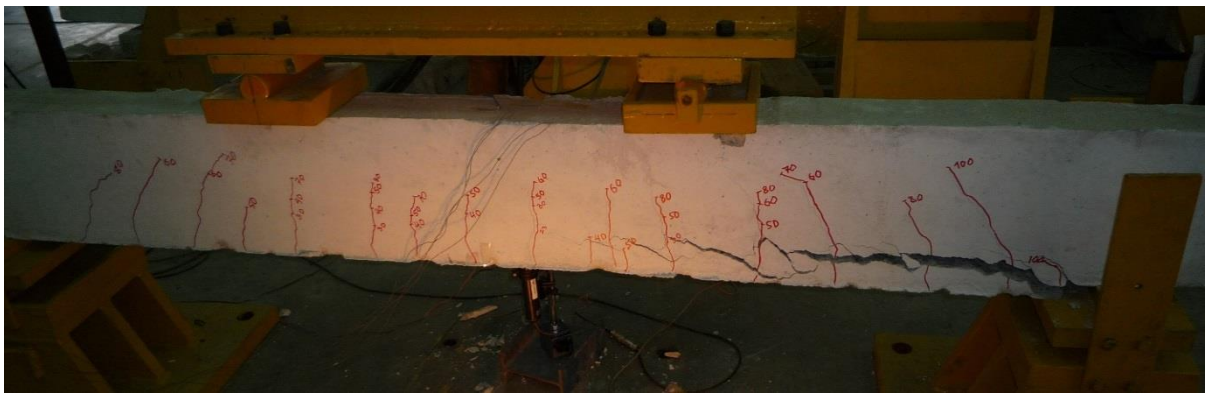

5.12 (c) N2S10

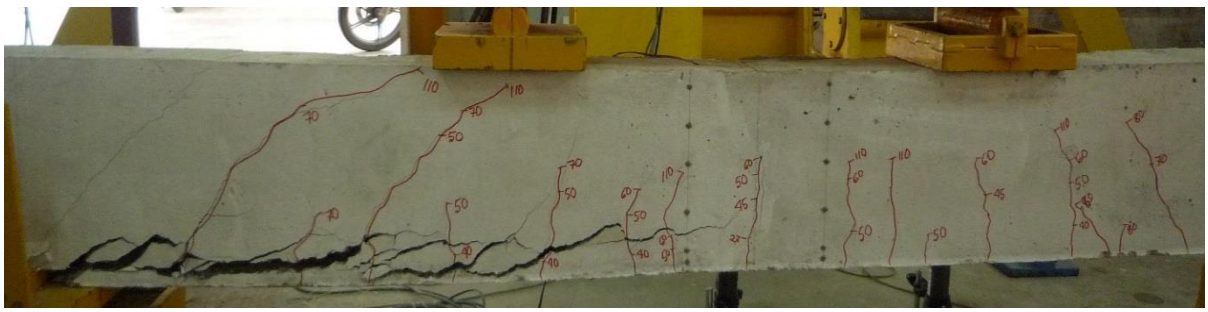

5.12 (d) N2S12

5.12 (e) N2C12

Figure 5.12: Failure modes of beam specimens

5.2.3.3 COMPRESSIVE STRAIN OF CONCRETE

The load versus the compressive strain of the concrete at the top most fibre of the specimens is demonstrated in Figure 5.13. All the strengthened specimens had less concrete compressive strain compared to the control specimen because of the greater rigidity of the strengthened specimens. In the first cracking zone, the strengthened specimens had a similar concrete strain compared to the control specimen. Subsequently, all the strengthened specimens showed linear compressive strain up to the yielding of the main reinforcement. After yielding of the steel, the concrete strain rapidly increased as a result of strain compatibility.

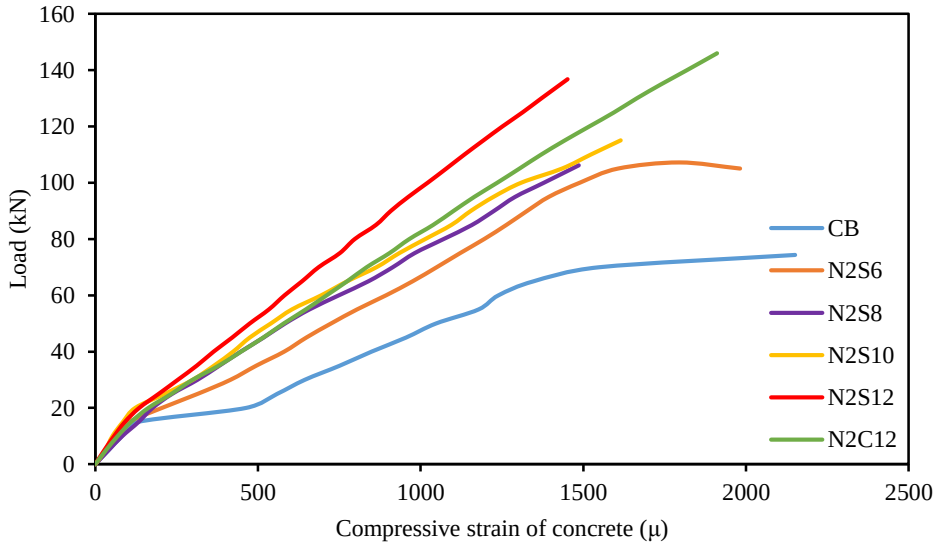

Figure 5.13: Load-compressive strain of concrete

5.2.3.4 TENSILE STRAIN OF MAIN REBARS

The load versus tensile strain of the main reinforcement throughout loading is presented in Figure 5.14. The tensile strains of the main reinforcement of all the strengthened specimens were smaller than the tensile strain of the main reinforcement of the control specimen. The internal main reinforcement strain of all the NSM steel strengthened specimens were found to be identical. However, the N2C12 specimen showed more bar strain than the N2S12 specimen.

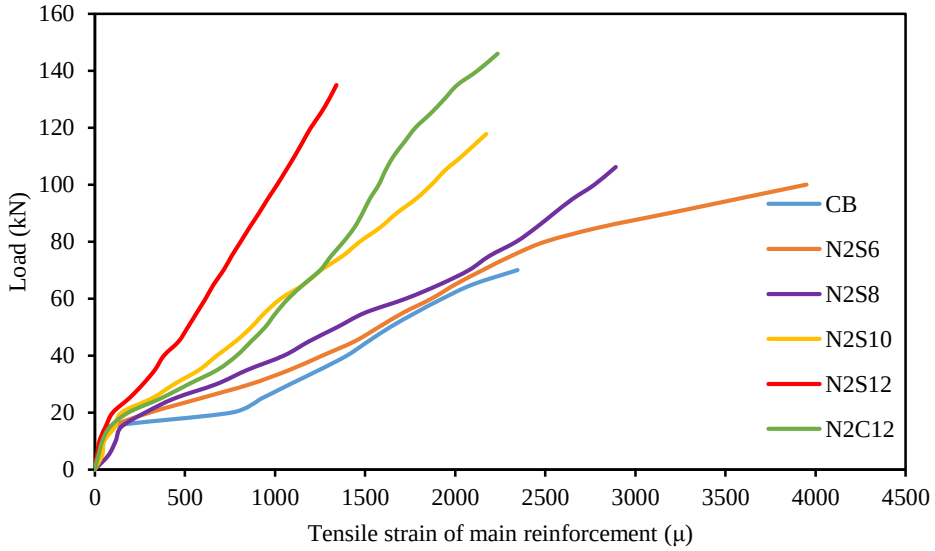

Figure 5.14: Load-tensile strain of main reinforcement

5.2.3.5 TENSILE STRAIN OF NSM REINFORCEMENT

The load versus tensile strain of the NSM steel bars during loading is shown in Figure 5.15. It was found that the N2S12 beam had less NSM bar strain compared to the other specimens due to higher stiffness. At the failure stage, the NSM bar strains of beams N2S6, N2S8, N2S10, N2S12 and N2C12 were found to be 0.0096, 0.0032, 0.0036, 0.0026 and 0.0034, respectively. It was found that the concrete cover separation of the N2S12 specimen was initiated at the NSM strain of around 0.0026. However, the N2S6 specimen was supposed to fail by flexure at the NSM bar strain of 0.0096.

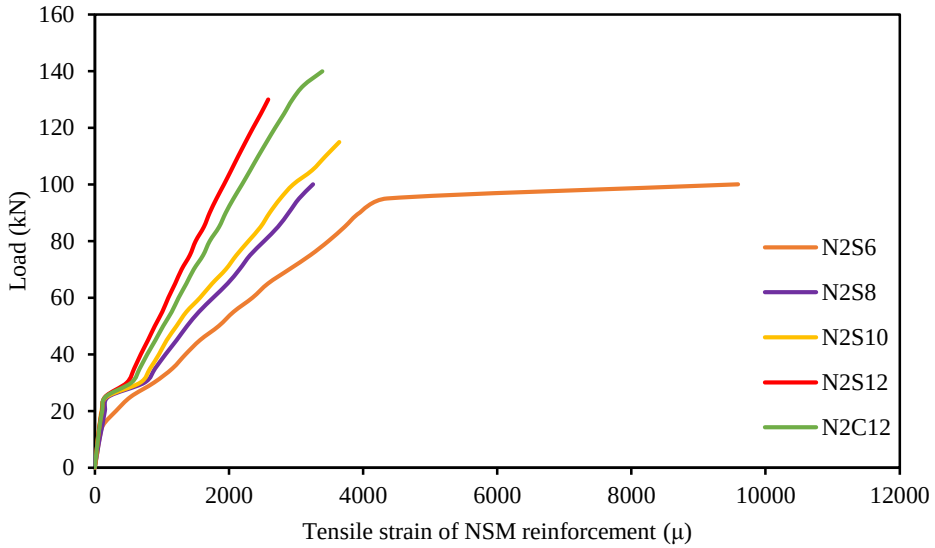

Figure 5.15: Load-tensile strain of NSM reinforcement

5.2.3.6 SECTIONAL STRAIN VARIATION

The variation in strain over depth of the strengthened specimens N2S6, N2S8, N2S10, N2S12 and N2C12 at different load levels is shown in Figure 5.16. The strain variation was linear at the beginning of loading and the variation increased with higher load levels. For all the strengthened specimens, the strain variation increased at the NSM bar level. The strain of the strengthened specimens was less than the control specimen and the depth of the neutral axis for these specimens was higher than the control specimen.

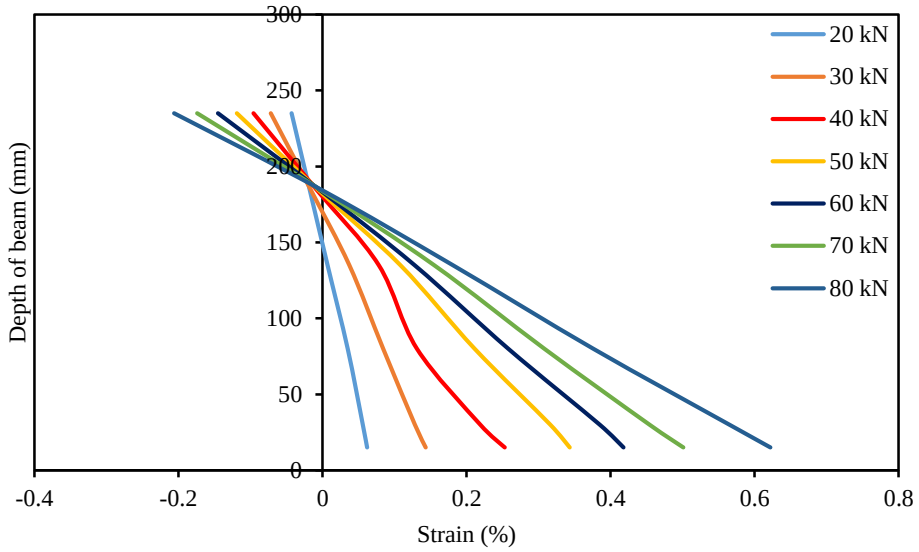

5.16 (a) N2S6

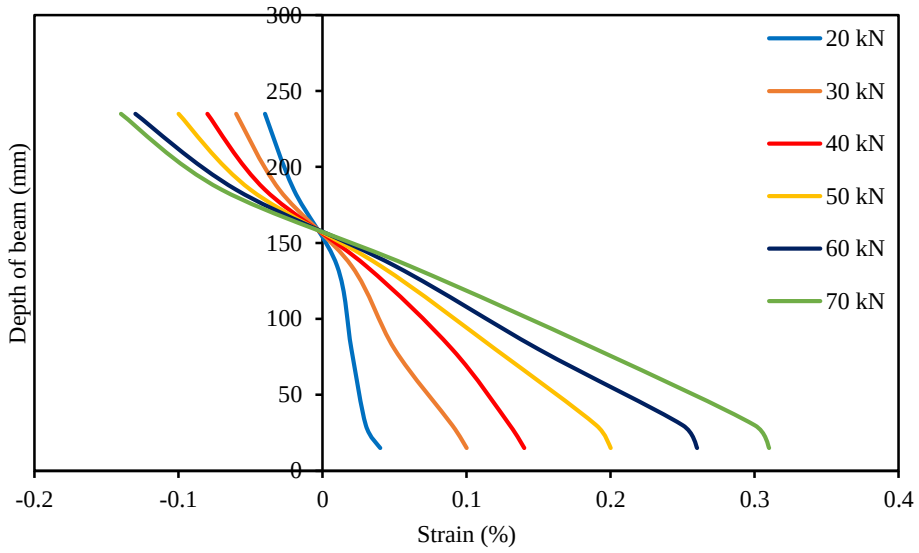

5.16 (b) N2S8

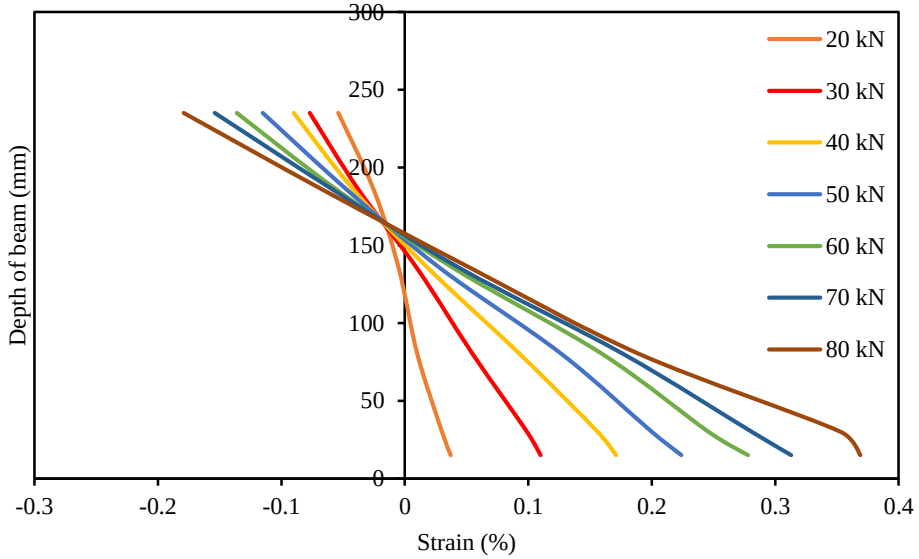

5.16 (c) N2S10

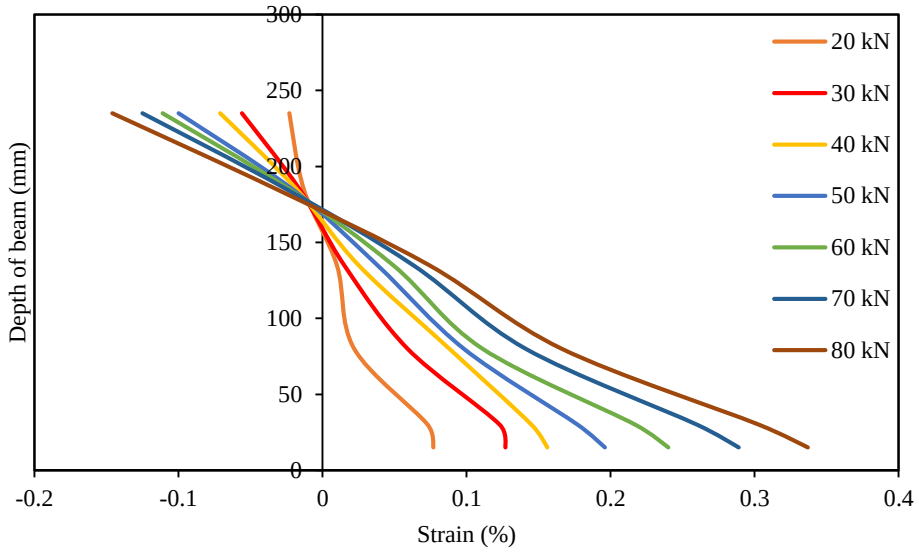

5.16 (d) N2S12

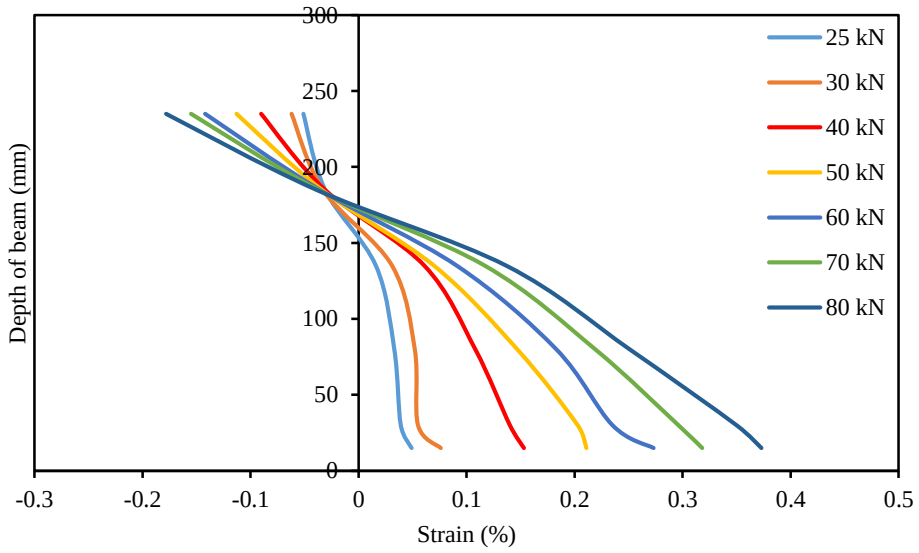

5.16 (e) N2C12

Figure 5.16: Sectional strain variation at midspan of strengthened beams

5.2.3.7 CRACK CHARACTERISTICS

The load versus crack widths of the beam specimens are shown in Figure 5.17. The first crack load of CB, N2S6, N2S8, N2S10, N2S12 and N2C12 were 15.75 kN, 19.50 kN, 20 kN, 21 kN, 26.6 kN and 25 kN, respectively. All the strengthened beam specimens presented a greater first crack load compared to the control beam specimen. The total number of cracks of CB, N2S6, N2S8, N2S10, N2S12 and N2C12 were 11, 14, 15, 17, 20 and 17, respectively, and the average

crack spacing of each specimen was 180 mm, 130 mm, 125 mm, 115 mm, 95 mm and 100 mm, respectively. However, N2C12 had wider crack spacing and fewer cracks than N2S12. This was because N2C12 was strengthened with a CFRP bar. However, all the strengthened beam specimens showed smaller crack spacing than the control specimen.

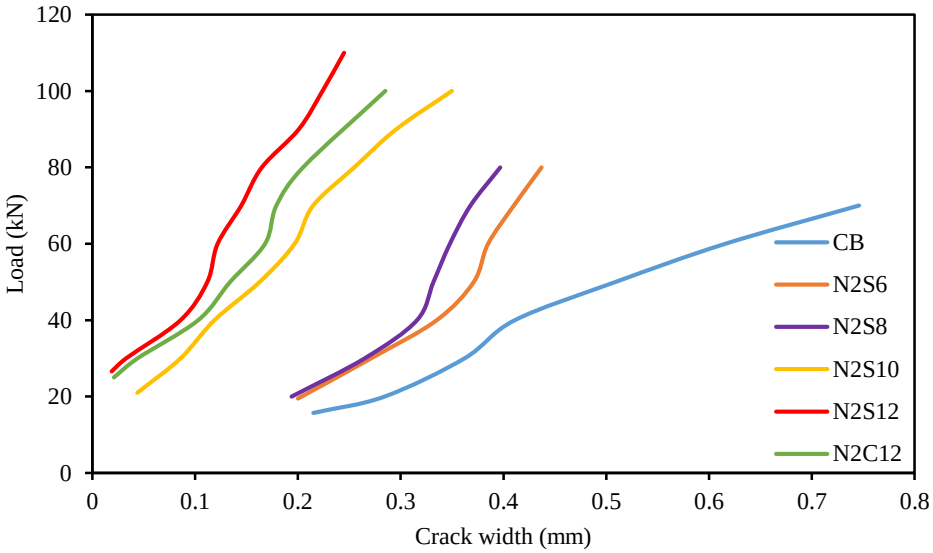

Figure 5.17: Load-crack width

5.2.3.8 THE EFFECTIVENESS OF NSM-STEEL TECHNIQUE

The reduction of deflection due to strengthening with NSM steel or CFRP bars at 30 kN, 50 kN and 70 kN service loadings are presented in Figure 5.18. The deflection of the strengthened beam specimens was reduced by a maximum of about 78%, 77% and 75% at 30 kN, 50 kN and 70 kN, respectively, compared to the control specimen, which was due to the increased stiffness of the strengthened specimens. The compressive strain of concrete at the top fibre of the specimens and reduction of strain due to strengthening at 30 kN, 50 kN and 70 kN service loading are shown in Figure 5.19.

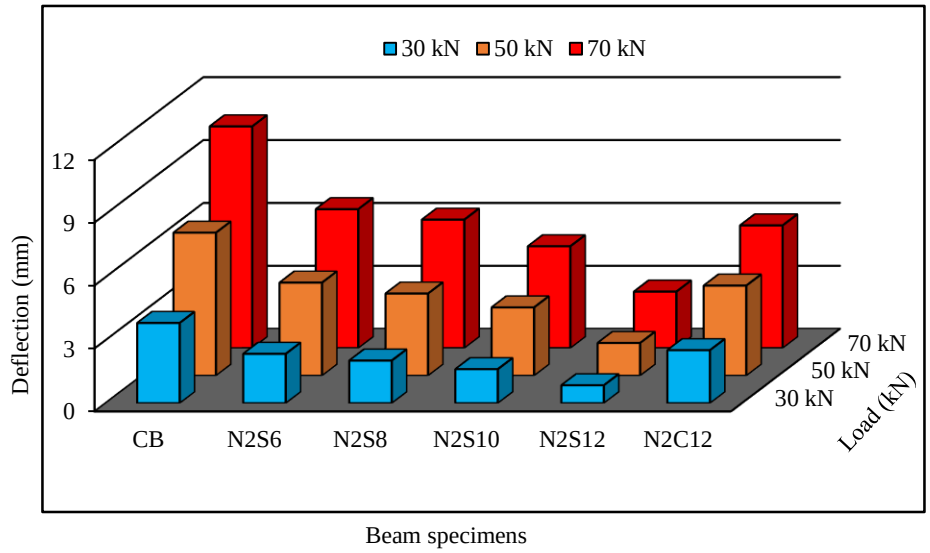

Figure 5.18: Reduction in deflection due to NSM-steel strengthening

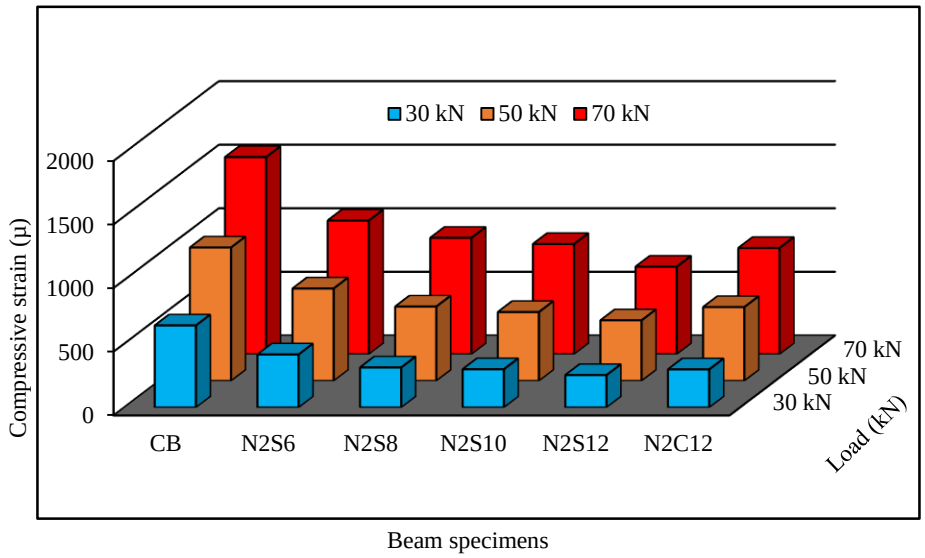

Figure 5.19: Reduction in concrete top fibre strain due to NSM-steel strengthening

The compressive strain of the strengthened beam specimens was reduced by a maximum of about 61%, 55% and 56% at 30 kN, 50 kN and 70 kN, respectively, compared to the control specimen. The extreme fibre concrete strain of the strengthened beam specimens was significantly decreased. The internal reinforcing tension steel bar strain and reduction of strain due to strengthening at 30 kN, 50 kN and 70 kN service loading is revealed in Figure 5.20. The strain in the reinforcing bars of the strengthened beams was reduced by a maximum of

about 75%, 69% and 70% at 30 kN, 50 kN and 70 kN, respectively, compared to the control specimen.

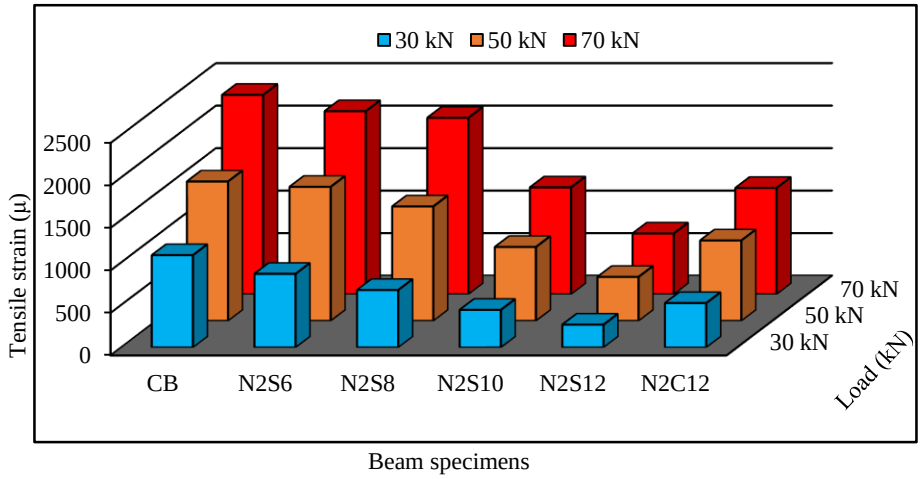

Figure 5.20: Reduction in main steel bar strain due to NSM-steel strengthening

5.2.4 THE EFFECT OF THE NUMBER OF GROOVES ON THE PERFORMANCE OF NSM STRENGTHENED RC BEAMS

A groove is needed for the placing of a strengthening bar in concrete. The effect of the number of grooves on the performance of NSM strengthening technique with the same amount of reinforcement is shown in Figure 5.21. The experimental data for N1S8 and N2S6 specimens were used to investigate the effect of the number of grooves. Hence, the amount of NSM reinforcement of these specimens were almost similar (56 mm^2). The increase in the number of groove provides an additional amount of groove filler (adhesive) in RC beams. Therefore, an increase in the number of grooves, increases the ultimate load carrying capability of reinforced concrete beams.

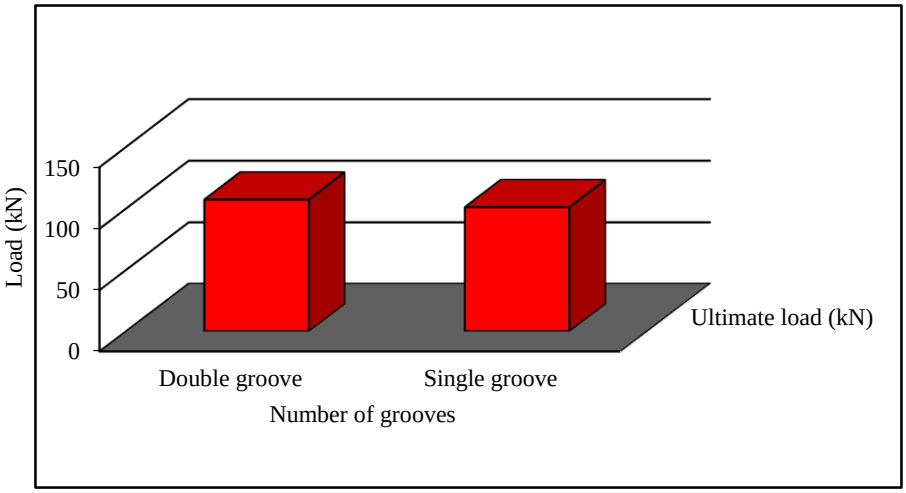

Figure 5.21: The effect of the number of grooves

5.2.5 THE EFFECT OF THE AMOUNT OF NSM REINFORCEMENT ON THE PERFORMANCE OF NSM STRENGTHENED RC BEAMS

The amount of NSM reinforcement is an important constraint for the flexural strengthening of RC structural elements. The influence of the amount of NSM reinforcement on the flexural strength of RC beams is revealed in Figure 5.22. It was found that an increase in the amount of NSM reinforcement significantly increased the ultimate load.

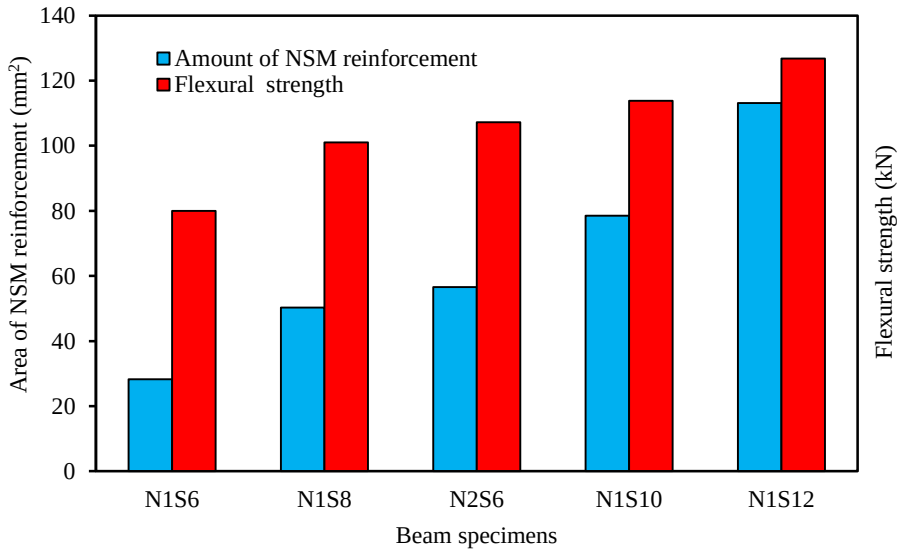

Figure 5.22: The effect of the amount of NSM reinforcement

5.2.6 INNOVATIVE SNSM TECHNIQUE FOR ENHANCING THE FLEXURAL PERFORMANCE OF RC BEAMS STRENGTHENED WITH STEEL BARS

In this section, the experimental results obtained from RC beams strengthened with steel bars using the innovative side near surface mounted (SNSM) technique are compared to the control beam. The results for these beams are presented as shown below.

5.2.6.1 FLEXURAL STRENGTH AND DEFLECTION BEHAVIOUR

The experimental study of the tested specimens in terms of flexural strength, maximum deflection and modes of failure are shown in Table 5.4. The beams strengthened with SNSM steel bars significantly influenced the stiffness of the strengthened beams in the pre-cracking stage. The first crack load showed a remarkable increase of 71.43%, 120.32%, 122.22% and 217.46% for SN2S6, SN2S8, SN2S10 and SN2S12, respectively, over the control beam. The yield load increased by 28.57%, 42.86%, 78.57% and 100.00% for SN2S6, SN2S8, SN2S10 and SN2S12, respectively, over the reference beam. The ultimate load increased by 34.46%, 46.17%, 76.05% and 93.05% for SN2S6, SN2S8, SN2S10 and SN2S12, respectively, compared to the control beam.

Table 5.4: Summary of test results for SNSM steel bars

Beam ID	P_{cr} (kN)	$\%P_{cr}$	P_y (kN)	$\%P_y$	P_u (kN)	$\%P_u$	Δ_{max} (mm)	Failure mode
CB	15.75	-	70.00	-	74.37	-	33.61	FL
SN2S6	27.00	71.43	90.00	28.57	100.00	34.46	41.74	FL
SN2S8	34.70	120.32	100.00	42.86	108.71	46.17	47.05	FL
SN2S10	35.00	122.22	125.00	78.57	130.93	76.05	38.56	FL
SN2S12	50.00	217.46	140.00	100.00	143.57	93.05	35.98	PL

The load versus midspan deflection curves for beams CB, SN2S6, SN2S8, SN2S10 and SN2S12 are shown in Figure 5.23. The curves show an approximate

tri-linear response defined by the pre-cracking, cracking and post-cracking stages. In the pre-cracking stage the strengthened beams showed linear elastic behaviour similar to the control beam. In the cracking stage, from first cracking to steel yielding, the SNSM steel bars increased the stiffness of the beam specimens, and, consequently, increased the yield load. In the post-cracking stage, from steel yielding to failure of the beam, the load increased and the deflection increased at a higher rate than in the previous stages. In this stage, the SNSM steel bars controlled the cracks and crack widths up to failure of the beams.

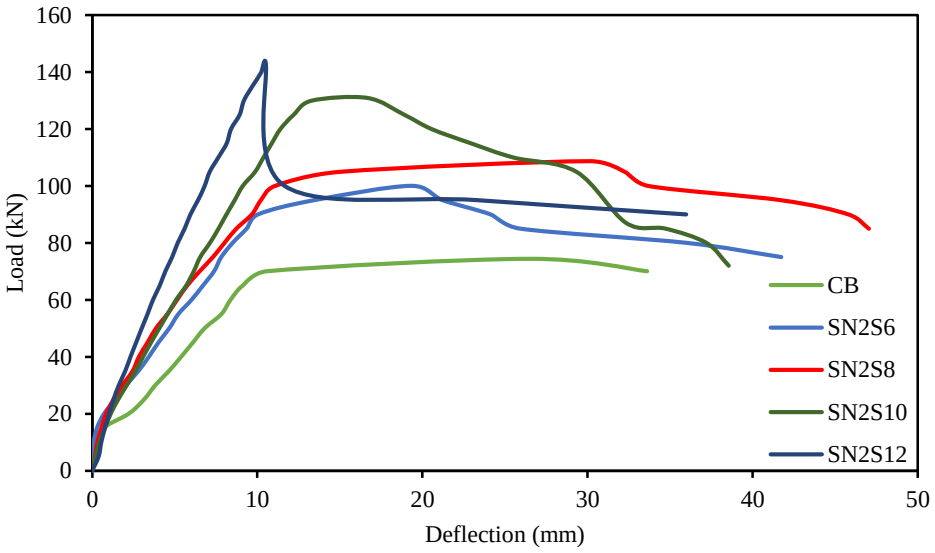

Figure 5.23: Load-midspan deflection

5.2.6.2 MODE OF FAILURE

The modes of failure of the tested specimens are shown in Figure 5.24. The SN2S6, SN2S8 and SN2S10 strengthened beam specimens failed in flexure. Flexural failure happened towards the midspan of the beam by the spreading of a vertical crack. Additional cracks developed when the external applied load was increased. A hair crack first formed at midspan, and, gradually, spread towards the neutral axis of each specimen. Eventual failure occurred by concrete crushing at the extreme fibre of the specimen after yielding of the tension steel

reinforcement and rupture of the SNSM reinforcement. However, the SN2S12 specimen failed through the peeling off of the SNSM steel bars. After yielding of the internal main steel reinforcement, the shear crack initiated at the end of SNSM bars and the crack width quickly increased. Although the shear crack and flexural crack meet, peeling off of the SNSM steel bars occurred, which induced premature failure of the specimen.

(a) SN2S6

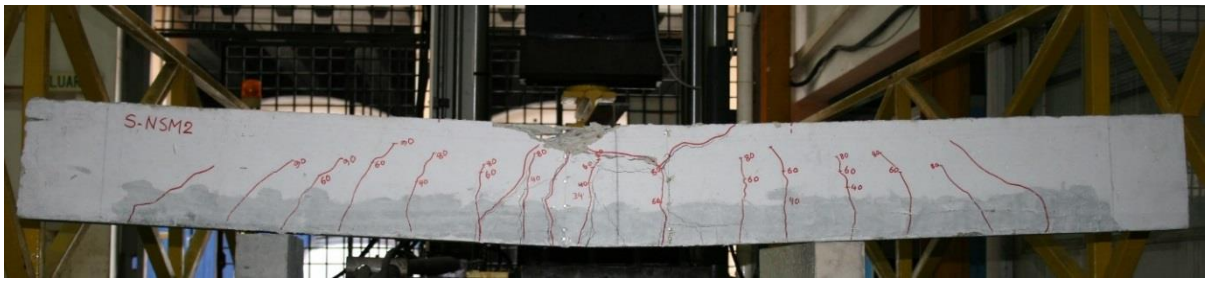

(b) SN2S8

(c) SN2S10

(d) SN2S12

Figure 5.24: Failure modes of beam specimens

5.2.6.3 COMPRESSIVE STRAIN OF CONCRETE

The load versus concrete compressive strain at midspan and top fibre of the beams is shown in Figure 5.25. The compressive strains of the concrete for all the strengthened specimens were less than the concrete compression strain of the control specimen owing to the superior stiffness of the strengthened specimens. All the strengthened specimens exhibited linear dissimilarity in strain up to yielding of the steel, except SN2S12. After the steel yielding, the concrete strain rapidly increased as a result of the strain compatibility. This shows that concrete compression failure was then followed by flexural failure. However, the SN2S12 specimen showed linear strain variation up to the peeling off failure.

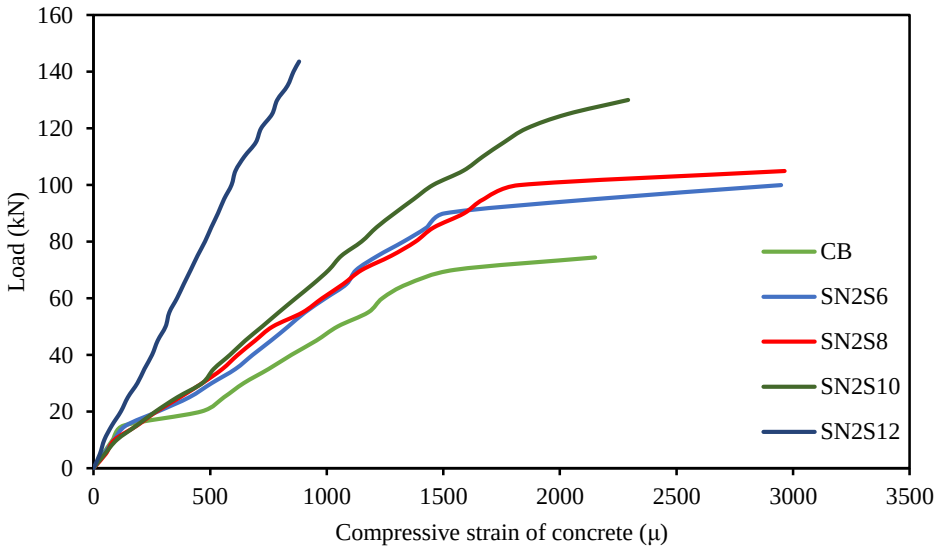

Figure 5.25: Load-compressive strain of concrete

5.2.6.4 TENSILE STRAIN OF MAIN REBARS

The load versus tensile strain of the main reinforcement is shown in Figure 5.26. After the first crack formed in the concrete sections, the tensile stresses were transferred to the steel bars. This caused an abrupt increase in the strain in the tension steel bars. The increment rate was greater for the control specimen than for the strengthened specimens owing to the larger crack width of the control specimen. All the strengthened beams showed a linear variation in strain from the first crack to steel yielding except SN2S12 specimen. After steel yielding, the tension bar strains rapidly increased. However, the SN2S12 specimen showed linear tensile strain variation up to the peeling off failure.

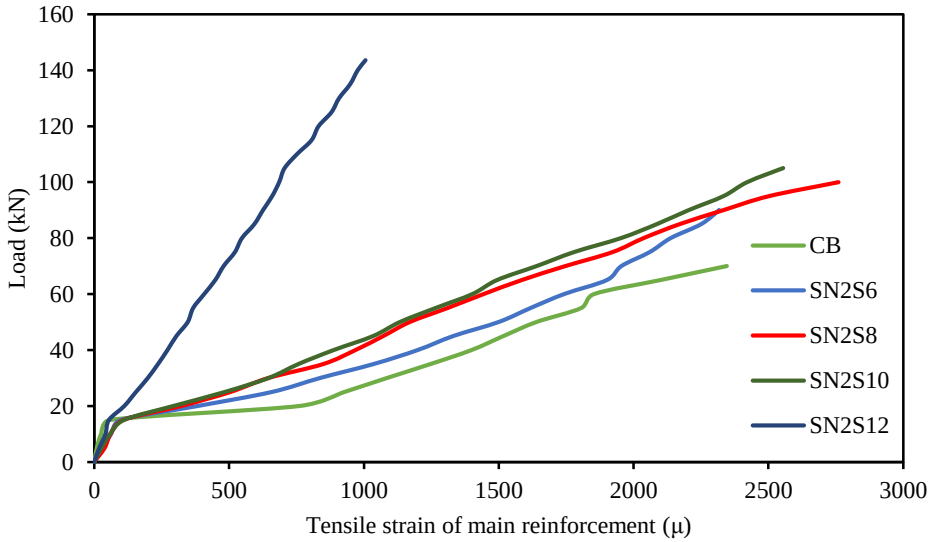

Figure 5.26: Load-tensile strain of main reinforcement

5.2.6.5 TENSILE STRAIN OF SNSM REINFORCEMENT

The load versus tensile strain of the SNSM reinforcement is shown in Figure 5.27. After first cracking, the tensile strain of the SNSM steel bars for all the strengthened beams increased significantly. The tensile strains in the steel strengthening bars were measured using strain gauges attached to the bars at mid-span. The first crack loads of SN2S8 and SN2S10 were 34.7 kN and 35 kN.

Therefore, SN2S8 and SN2S10 showed very similar linear variations in strain from first crack to failure of the SNSM steel bars. However, the SN2S6 and SN2S12 beam specimens, had a lower and higher first crack load, thus the behaviour of SN2S6 and SN2S12 differed from the other strengthened beams.

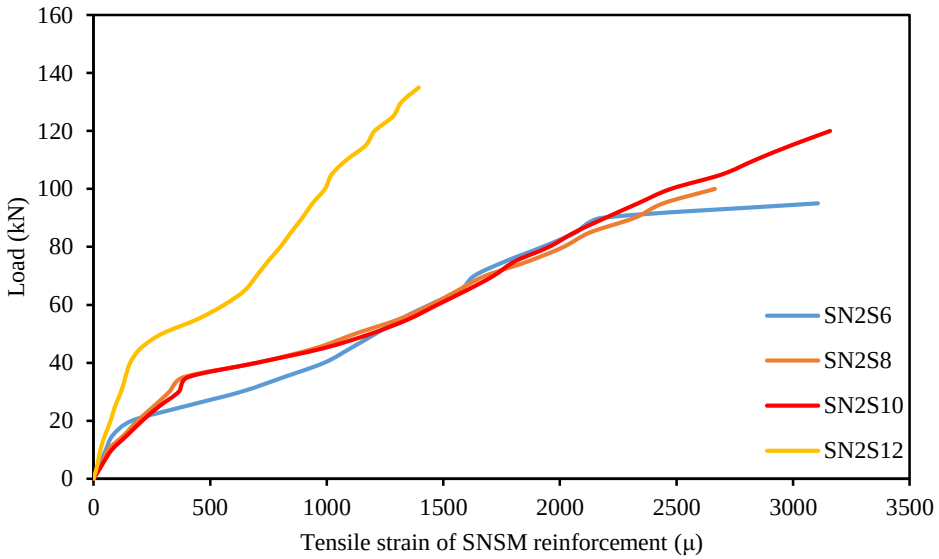

Figure 5.27: Load-tensile strain of SNSM reinforcement

5.2.6.6 SECTIONAL STRAIN VARIATION

The variations in strain over the depth of the strengthened beams SN2S6, SN2S8, SN2S10 and SN2S12 at different load levels are shown in Figure 5.28. These variations in strain were taken from the demec readings. The strain variation is linear when loading commences and increases as higher load levels are applied. The strain characteristics confirm that the SNSM steel bars were properly bonded to the concrete of the specimen and thus full composite action took place with no slip between the concrete and the SNSM steel bars.

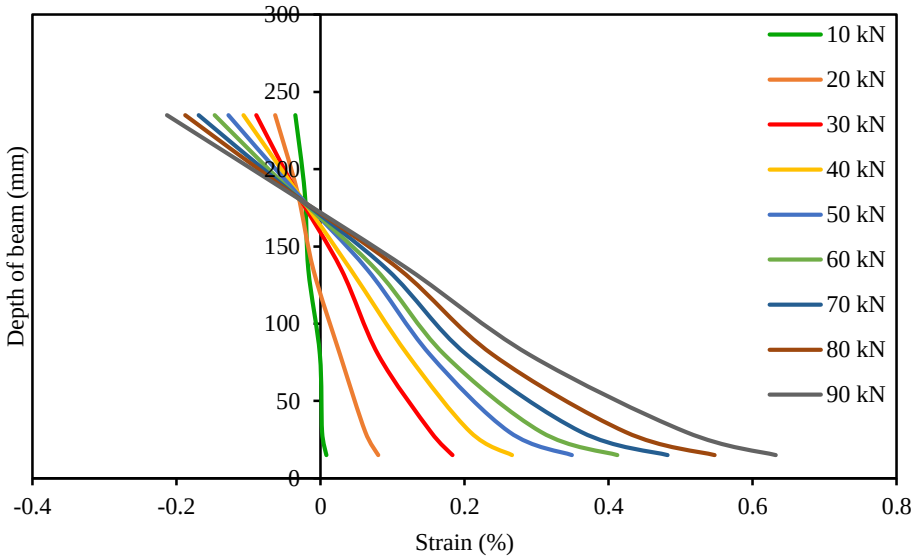

5.28 (a) SN2S6

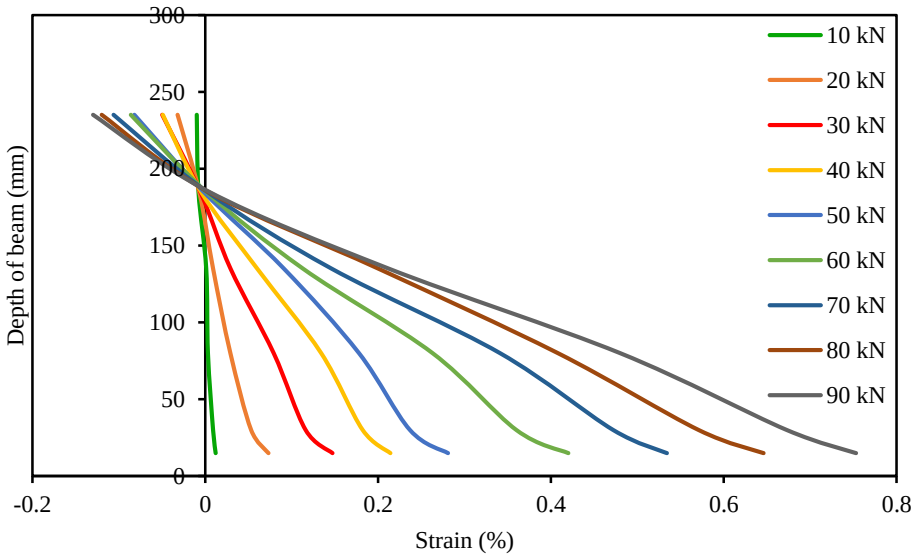

5.28 (b) SN2S8

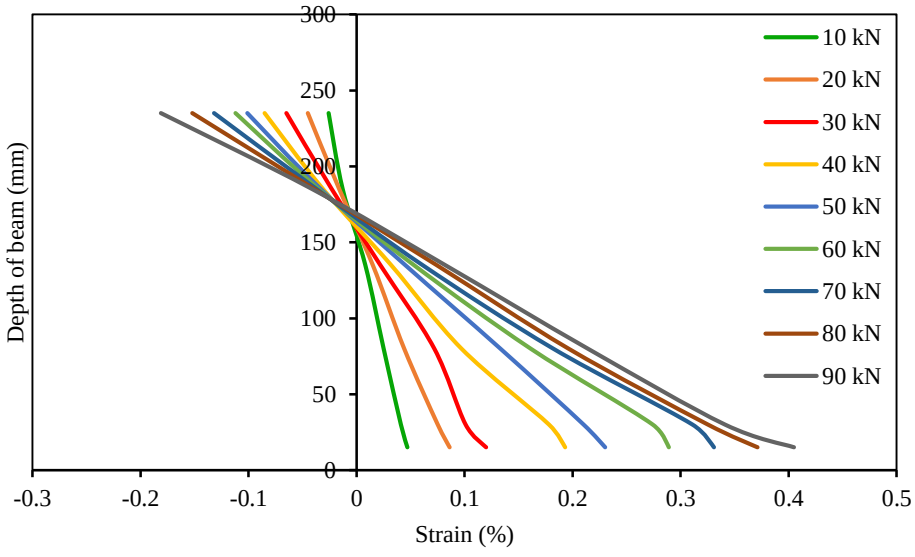

5.28 (c) SN2S10

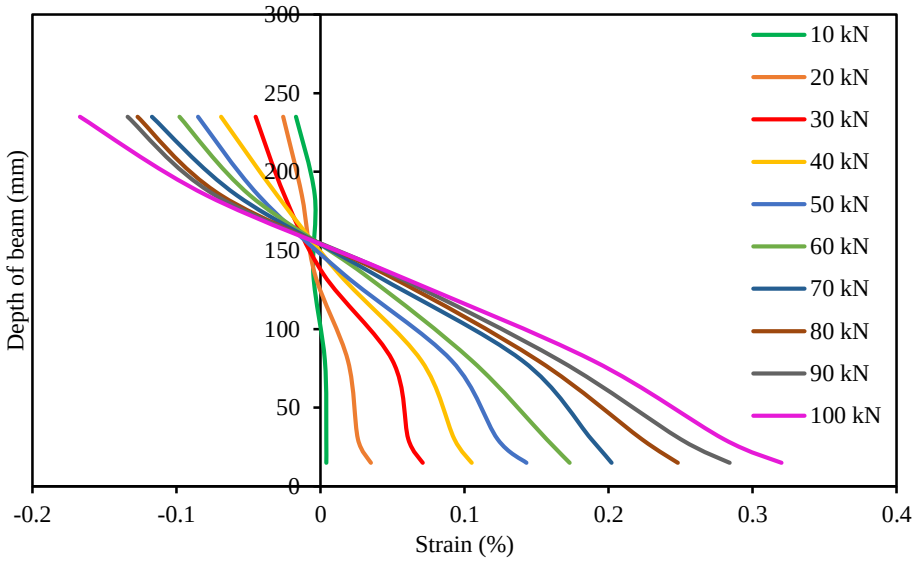

5.28 (d) SN2S12

Figure 5.28: Sectional strain variation at midspan of the strengthened beams

5.2.6.7 CRACK CHARACTERISTICS

The load versus crack widths of the specimens are shown in Figure 5.29. The first crack loads of CB, SN2S6, SN2S8, SN2S10 and SN2S12 were 15.75 kN, 27 kN, 34.7 kN, 35 kN and 50 kN, respectively. All the strengthened specimens had greater first crack loads than the control specimen. Thus, the SNSM strengthening technique noticeably increased the first crack load. The total number of cracks for CB, SN2S6, SN2S8, SN2S10 and SN2S12 were 11, 14, 15, 19 and 21, respectively, and the average crack spacing of each beam was 180 mm, 115 mm, 109 mm, 102 mm and 96 mm, respectively. Thus, the SNSM strengthening technique decreased the spacing of the cracks and increased the number of cracks. The crack widths also reduced with the increasing number of cracks.

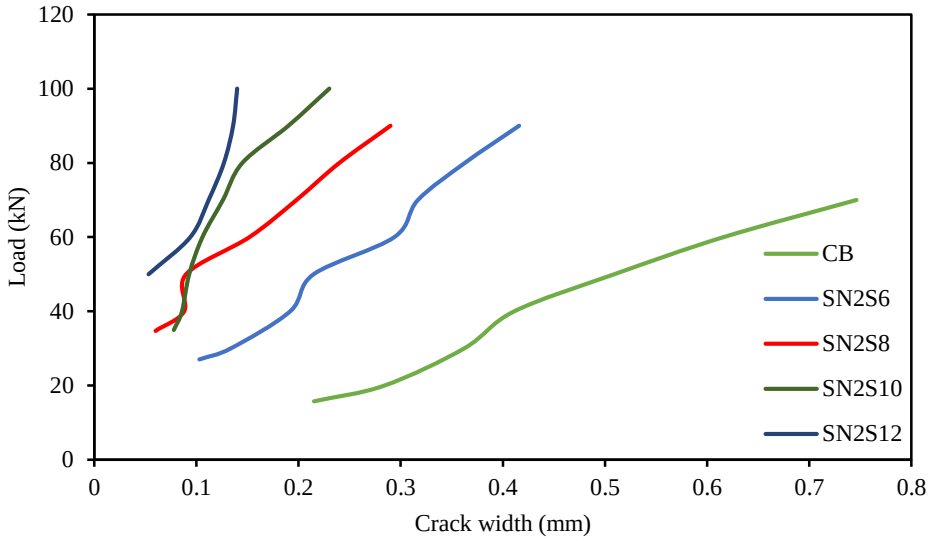

Figure 5.29: Load-crack width

5.2.6.8 THE EFFECTIVENESS OF SNSM-STEEL TECHNIQUE

The reduction in deflection due to strengthening with SNSM steel bars at 30 kN, 50 kN and 70 kN service loadings is revealed in Figure 5.30. The deflection of the strengthened specimens was reduced by a maximum of about 58%, 56% and 58% at 30 kN, 50 kN and 70 kN, respectively, compared to the control specimen, which is due to the superior stiffness of the strengthened specimens. The compressive strain of the concrete at the top fibre of the specimens and the reduction of the strain due to strengthening at 30 kN, 50 kN and 70 kN service loading are presented in Figure 5.31. The compressive strain of the strengthened specimens was reduced by a maximum of about 71%, 70% and 73% at 30 kN, 50 kN and 70 kN, respectively, compared to the control specimen. The internal reinforcing tension steel bar strain and reduction of the strain is due to strengthening at 30 kN, 50 kN and 70 kN service loading, as shown in Figure 5.32. The reinforcing bar strain of the strengthened specimens was reduced by a maximum of about 82%, 79% and 80% at 30 kN, 50 kN and 70 kN, respectively, compared to the control specimen.

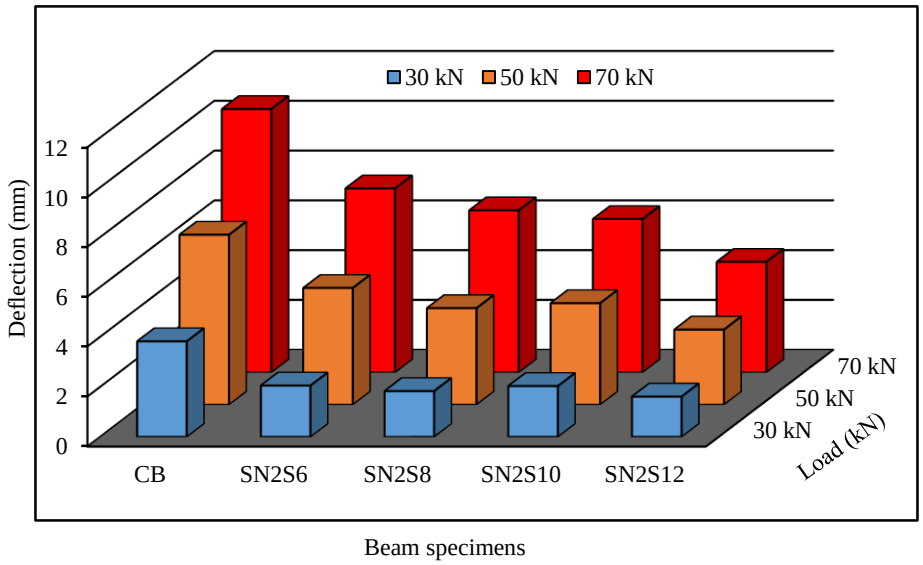

Figure 5.30: Reduction in deflection due to SNSM-steel strengthening

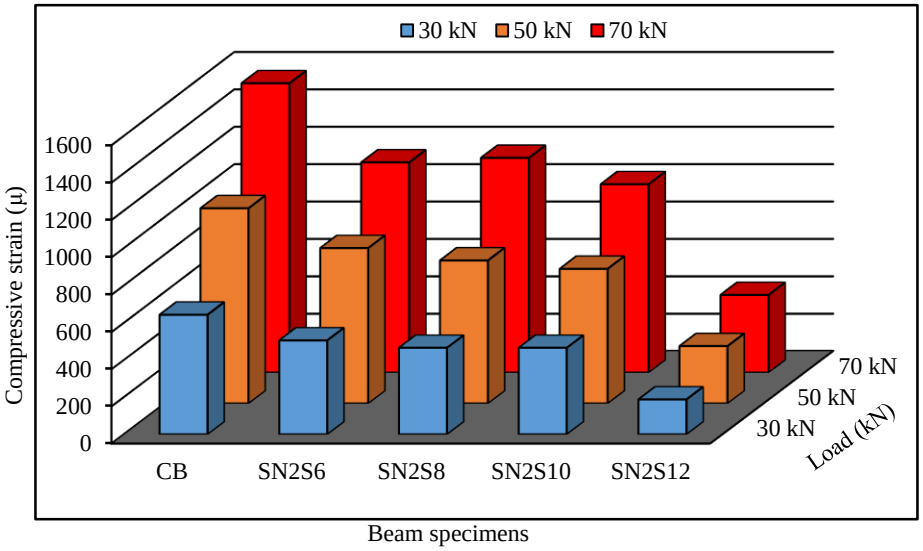

Figure 5.31: Reduction in concrete top fibre strain due to SNSM-steel strengthening

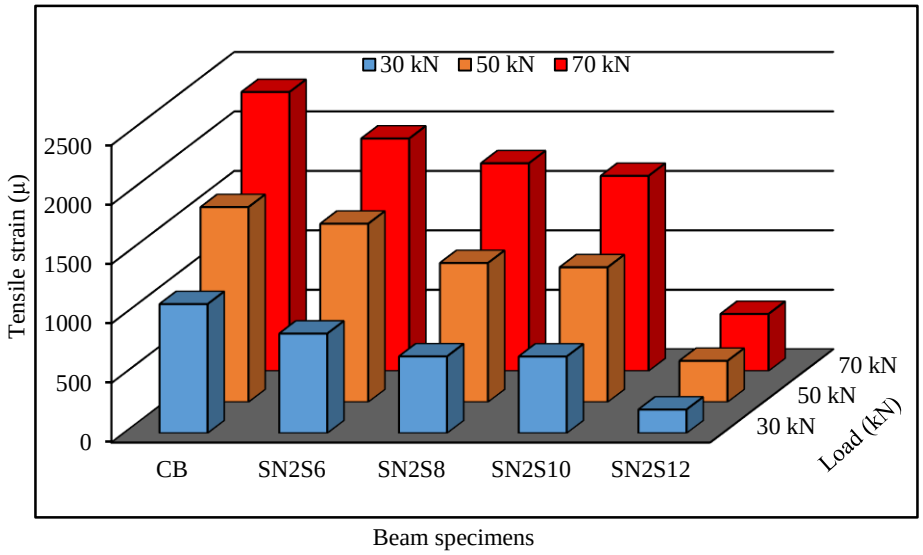

Figure 5.32: Reduction in main steel bar strain due to SNSM-steel strengthening

5.2.7 INNOVATIVE SNSM TECHNIQUE FOR ENHANCING THE FLEXURAL PERFORMANCE OF RC BEAMS STRENGTHENED WITH CFRP BARS

In this section, the experimental results obtained from the RC CFRP bars strengthened beam specimens using the side near surface mounted (SNSM) technique are compared with the control beam specimen. The results of these beam specimens are presented as below.

5.2.7.1 FLEXURAL STRENGTH AND DEFLECTION BEHAVIOUR

The experimental investigation of all tested specimens in terms of flexural strength, maximum deflection and modes of failure are demonstrated in Table 5.5. The specimens strengthened with SNSM CFRP bars showed a remarkable increase in the first crack load of 90.48%, 93.65%, and 101.90% for SN2C8, SN2C10 and SN2C12, respectively, over the control specimen. The yield load increased by 71.43%, 85.71% and 100.00%, respectively, over the control specimen. The ultimate load increased by 90.98%, 137.70% and 132.77% for SN2C8, SN2C10 and SN2C12, respectively, compared to the control specimen. However, SN2C12 showed less improvement in the ultimate load than SN2C10, since the SN2C12 specimen failed by the CFRP bars peeling off.

Table 5.5: Summary of test results for SNSM CFRP bars

Beam ID	P_{cr} (kN)	$\%P_{cr}$	P_y (kN)	$\%P_y$	P_u (kN)	$\%P_u$	Δ_{max} (mm)	Failure mode
CB	15.75	-	70.00	-	74.37	-	33.61	FL
SN2C8	30.00	90.48	120.00	71.43	142.03	90.98	24.03	FL
SN2C10	30.50	93.65	130.00	85.71	176.78	137.70	34.29	FL
SN2C12	31.80	101.9	140.00	100.00	173.11	132.77	17.20	PL

The load versus midspan deflection curves for beams CB, SN2C8, SN2C10 and SN2C12 are shown in Figure 5.33. The curves reveal an approximate tri-linear response defined by the pre-cracking, cracking and post-cracking phases. In the

pre-cracking phase, the strengthened beams showed linear elastic behaviour similar to the control specimen. The SNSM bars significantly influenced the stiffness of the strengthened beams in the pre-cracking phase (see Table 5.5 and Figure 5.33). In the cracking phase, from first cracking to steel yielding, the SNSM bars increased the stiffness and yielding load of the strengthened beams. In the post-cracking phase, from steel yielding to failure of the beam, the load increased and the deflection increased at a higher order than in the previous phases. In this phase, the SNSM bars controlled the cracks and crack widths up to failure of the beam specimens.

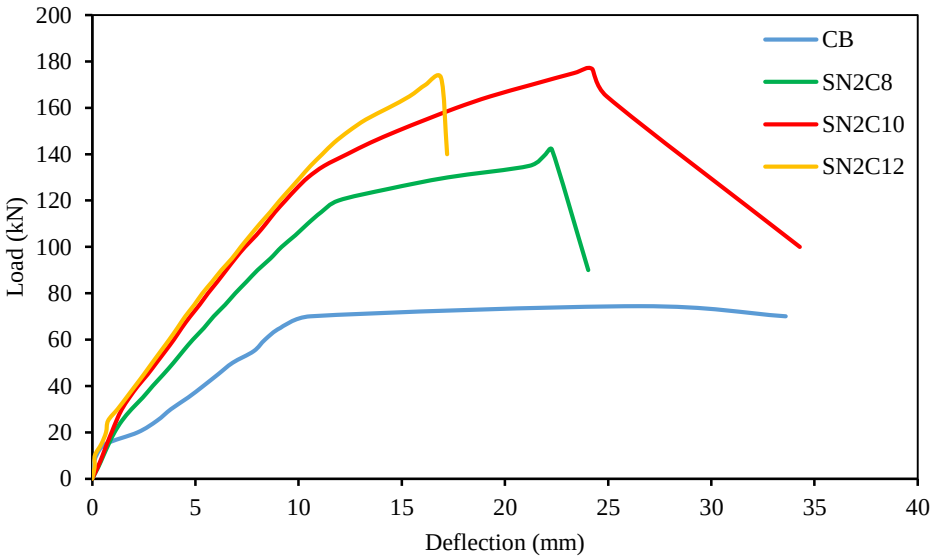

Figure 5.33: Load-midspan deflection

5.2.7.2 MODE OF FAILURE

The modes of failure of tested beams are revealed in Figure 5.34. The modes of failure of the SN2C8 and SN2C10 strengthened specimens were very similar to each other and failed in flexure. A hair crack first initiated at midspan and progressively spread towards the neutral axis of each beam. Subsequent failure occurred by concrete crushing at the extreme fibre of the beam after yielding of the main tension reinforcement and the rupture of the SNSM CFRP bars. However, the SN2C12 specimen failed due to the CFRP bars peeling off. After

yielding of the internal main reinforcement, the shear crack initiated at the completion edge of the SNSM bars and the crack width rapidly increased. Where the shear crack and the flexural cracks intersected, the CFRP bars peeled off, which encouraged the premature failure of the specimen.

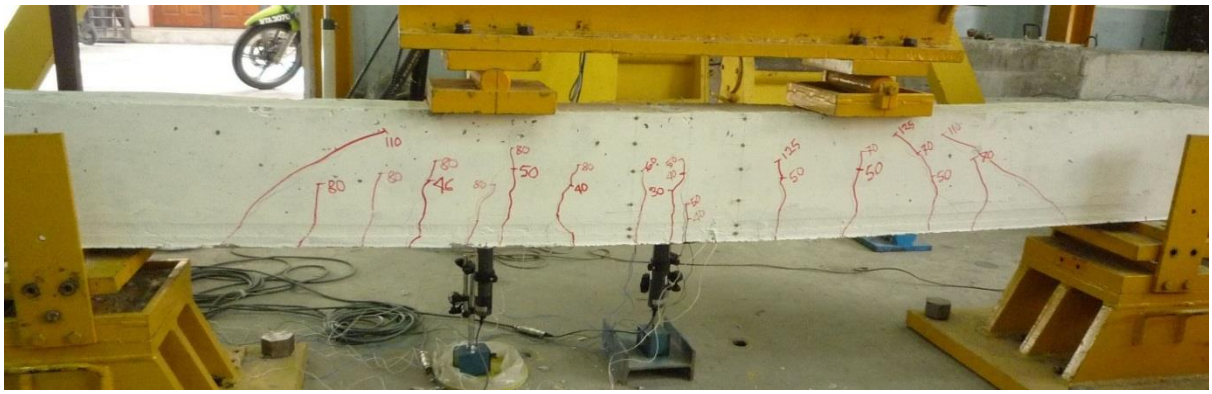

(a) SN2C8

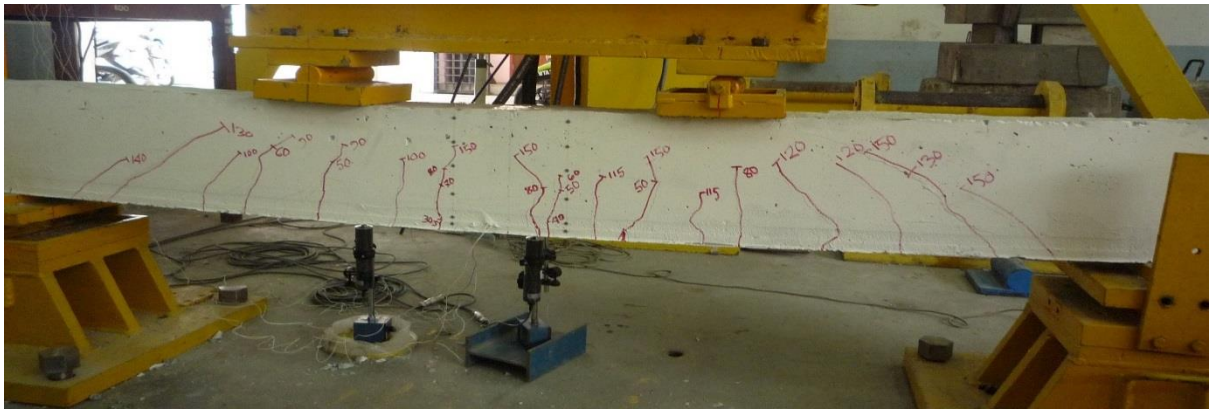

(b) SN2C10

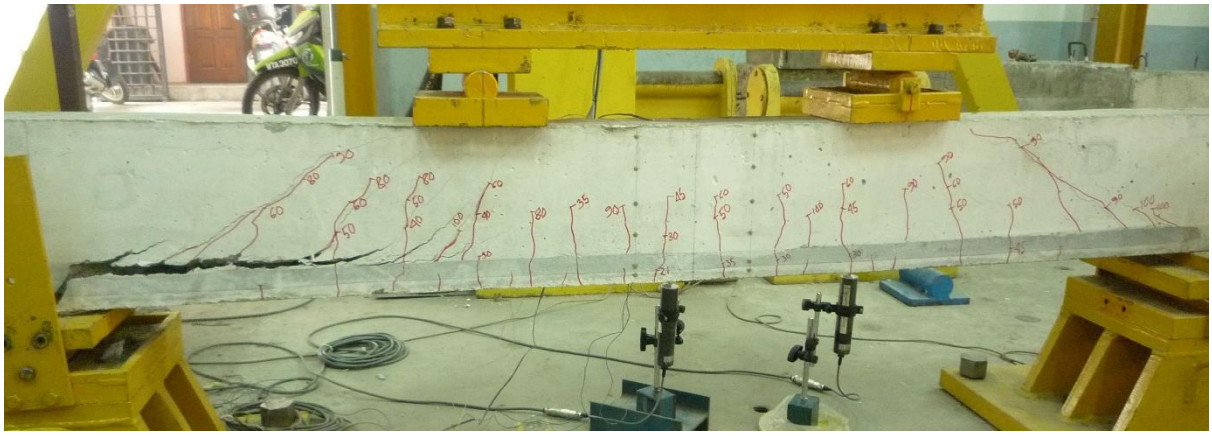

(c) SN2C12

Figure 5.34: Failure modes of beam specimens

5.2.7.3 COMPRESSIVE STRAIN OF CONCRETE

The load-compressive strains of the concrete at the extreme fibre of the specimen curves are revealed in Figure 5.35. All the strengthened specimens disclosed a linear variation in strain up to steel yielding. After steel yielding, the concrete strain quickly increased as a result of strain compatibility. Therefore, the CFRP bars gradually enhanced the failure strain except the SN2C12 specimen due to the peeling off failure.

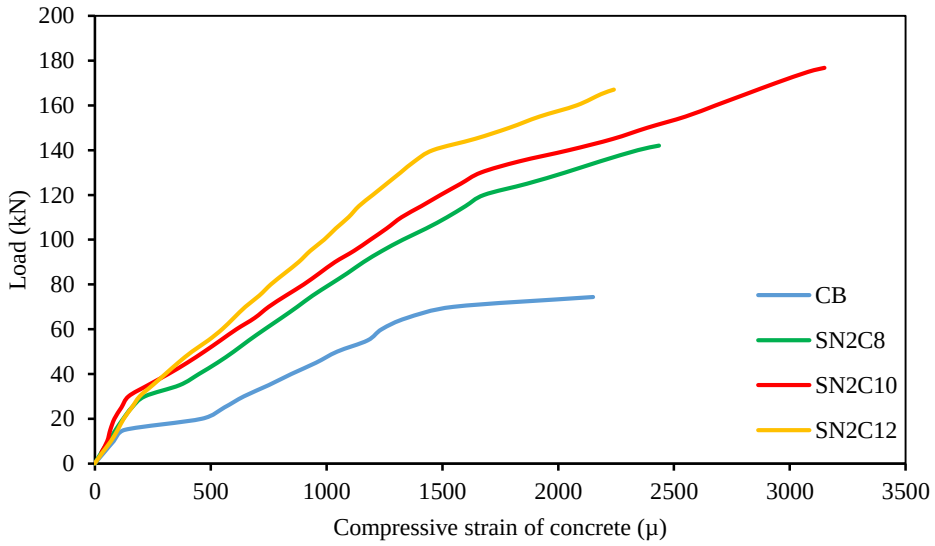

Figure 5.35: Load-compressive strain of concrete

5.2.7.4 TENSILE STRAIN OF MAIN REBARS

The load-tensile strains of the internal main reinforcement curves are demonstrated in Figure 5.36. The tension steel bars strains of all strengthened beams were less than the strains in the tension reinforcement of the control beam. Once the first crack forms in the concrete section, the tensile stresses were moved to the steel bars. This caused an immediate increase in the strain in the tension steel bars. The increment percentage of all the strengthened beams was smaller than the control beam owing to the larger crack width in the control beam. All the strengthened beams revealed a linear variation in strain from the first crack to steel

yielding. After steel yielding, the tension bar strain rapidly increased except for the SN2C12 beam due to premature failure.

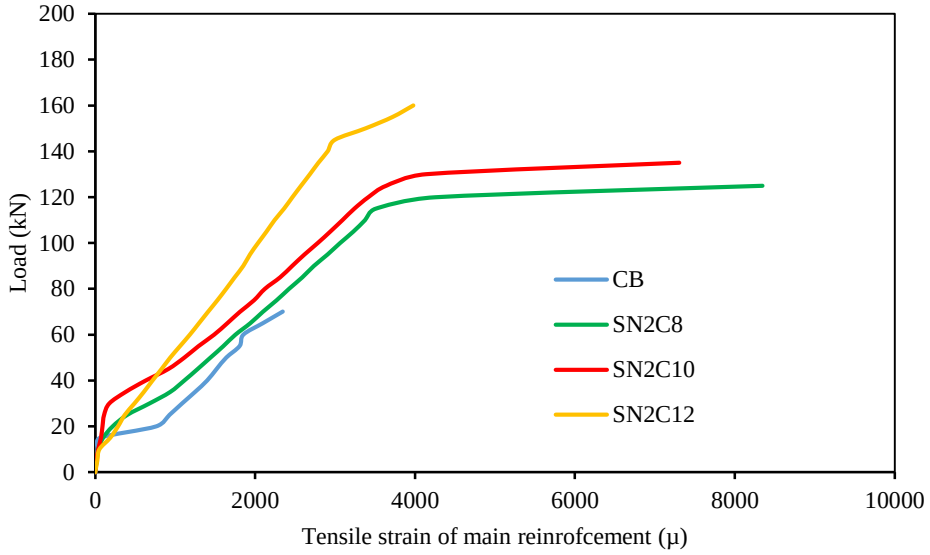

Figure 5.36: Load-tensile strain of main reinforcement

5.2.7.5 TENSILE STRAIN OF SNSM REINFORCEMENT

The load-tensile strains of the SNSM CFRP bar curves are shown in Figure 5.37. The tensile strains for the CFRP strengthening bars were measured using strain gauges attached to the bars at mid-span. The first crack loads of SN2C8, SN2C10 and SN2C12 were 30.00 kN, 30.50 kN and 31.80 kN, respectively. Hence, all the specimens showed the same linear curves up to first crack. After first cracking, the tensile strains in the SNSM CFRP bars in all the strengthened beams increased significantly. Afterward yielding, the SNSM bars strain of the SN2C8 and SN2C10 specimens gradually increased until failure of the specimens. However, the SN2C12 specimen showed different strain behaviour due to the different failure mode.

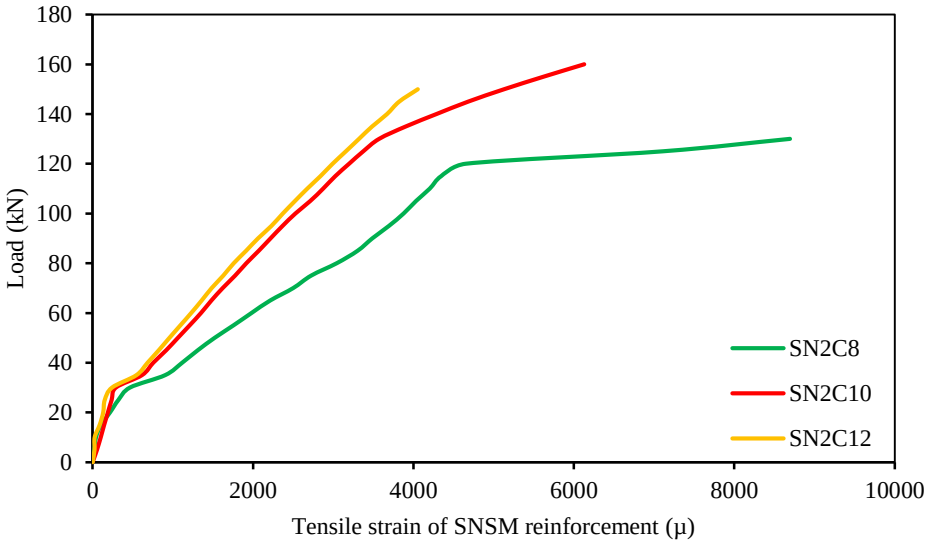

Figure 5.37: Load-tensile strain of SNSM reinforcement

5.2.7.6 SECTIONAL STRAIN VARIATION

The beam depth (h) versus strain at midspan of the beam specimens for various load levels using demec readings are shown in Figure 5.38. The strain variations of the strengthened specimens were almost linear at the lower loading stages, whereas the load increased as a result of the concrete cracking at the midspan, resulting in more strain on the CFRP bars. The strain on the CFRP bars for the SN2C12 specimen was lower than the strain on the SN2C8 and SN2C10 specimens owing to the larger area of the CFRP bars.

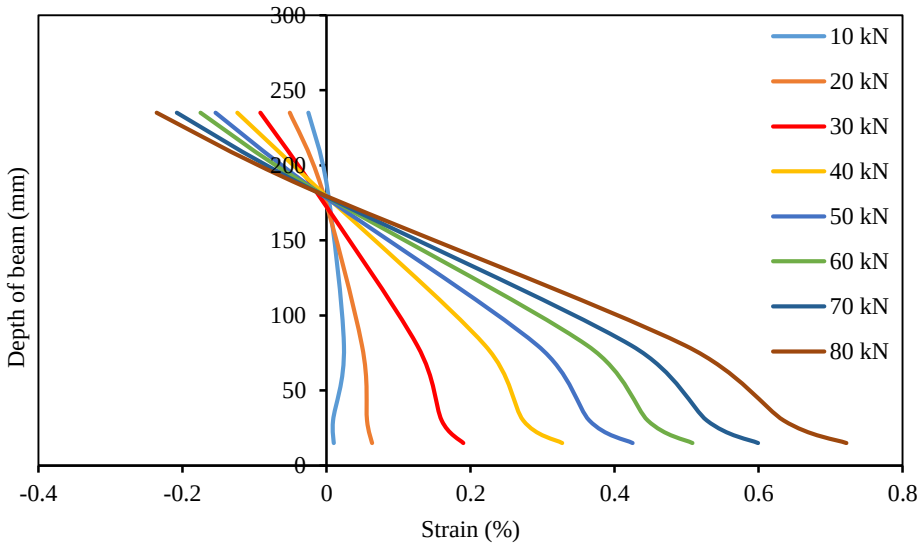

5.38 (a) SN2C8

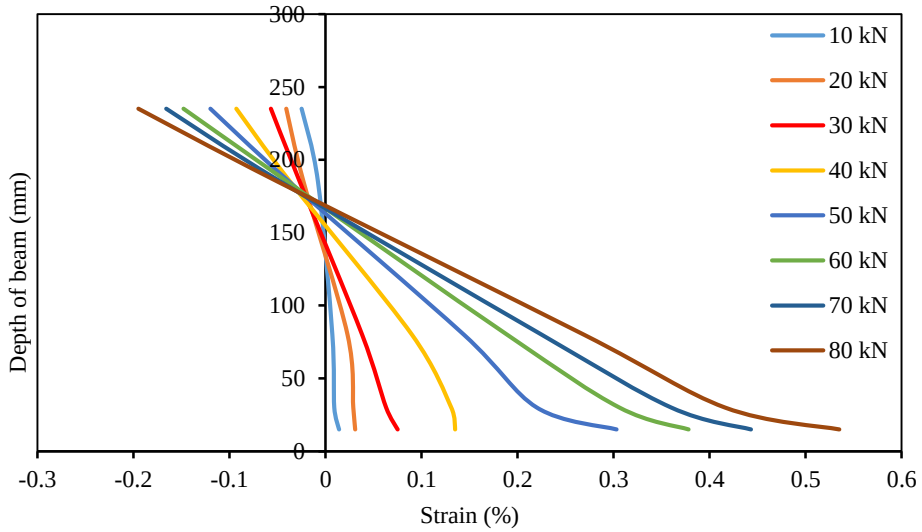

5.38 (b) SN2C10

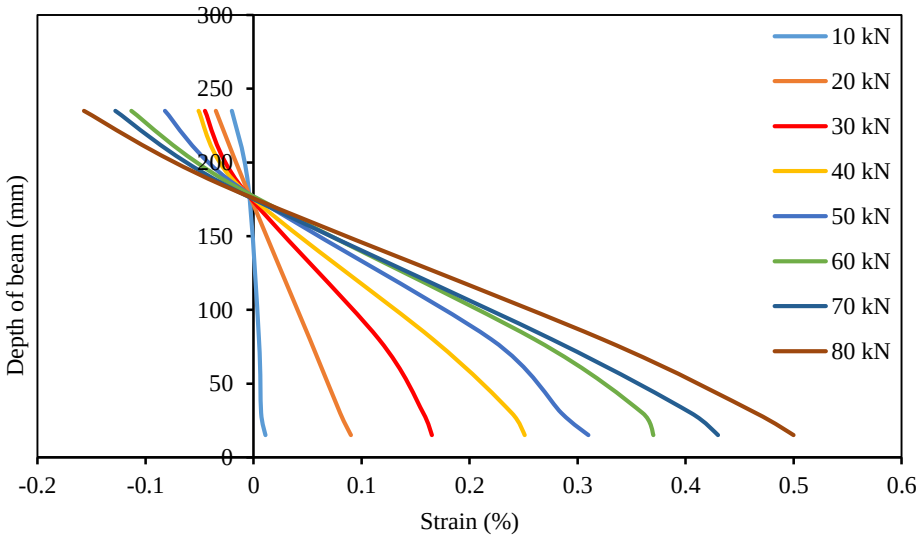

5.38 (c) SN2C12

Figure 5.38: Sectional strain variation at midspan of the strengthened beams

5.2.7.7 CRACK CHARACTERISTICS

The load versus crack width of the beam specimens is shown in Figure 5.39. The first crack loads of CB, SN2C8, SN2C10 and SN2C12 were 15.75kN, 30.00 kN, 30.50 kN and 31.80 kN, respectively. The strengthened specimens had higher first crack loads than the control beam. Therefore, the SNSM with the CFRP strengthening technique significantly increased the first crack load. The total number of cracks for CB, SN2C8, SN2C10 and SN2C12 were 11, 14, 17 and 19,

respectively, and the average crack spacing of each beam was 180 mm, 125 mm, 100 mm and 96 mm, respectively. Therefore, the SNSM CFRP strengthening technique decreased the spacing of the cracks and increased the number of cracks.

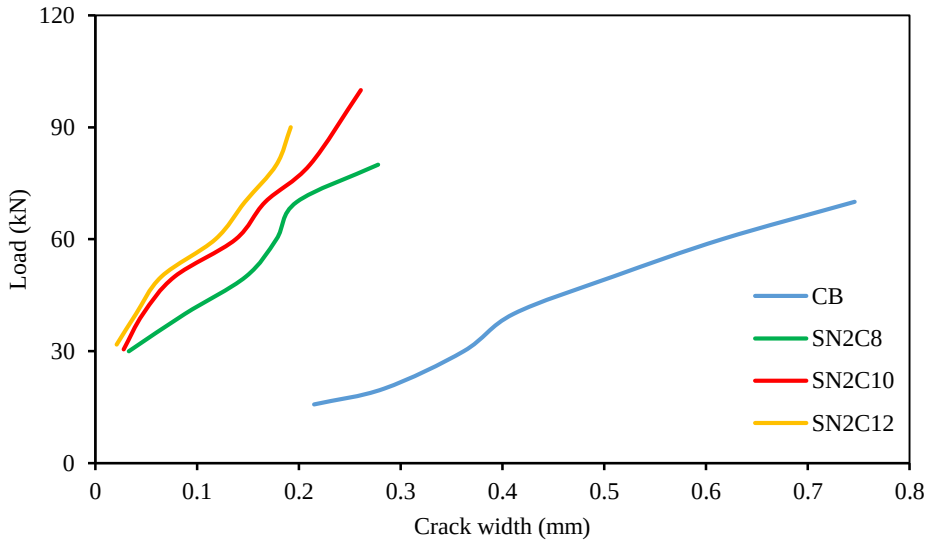

Figure 5.39: Load-crack width

5.2.7.8 THE EFFECTIVENESS OF SNSM-CFRP TECHNIQUE

The decrease in deflection due to strengthening with SNSM CFRP bars at 30 kN, 50 kN and 70 kN service loadings is revealed in Figure 5.40. The deflection of the strengthened specimens was reduced by a maximum of about 68%, 57% and 57% at 30 kN, 50 kN and 70 kN, respectively, compared to the control specimen due to the increased stiffness of the strengthened specimens. The compressive strain of concrete at the top fibre of the specimens and reduction of the strain due to strengthening at 30 kN, 50 kN and 70 kN service loading is revealed in Figure 5.41. The compressive strain of the strengthened specimens was reduced by a maximum of about 70%, 60% and 58% at 30 kN, 50 kN and 70 kN, respectively, compared to the control specimen. The internal reinforcing tension steel bar strain and reduction of the strain due to strengthening at 30 kN, 50 kN and 70 kN service loading is shown in Figure 5.42. The strain of the reinforcing bars in the strengthened specimens was reduced by a maximum of

about 55%, 43% and 40% at 30 kN, 50 kN and 70 kN, respectively, compared to the control specimen.

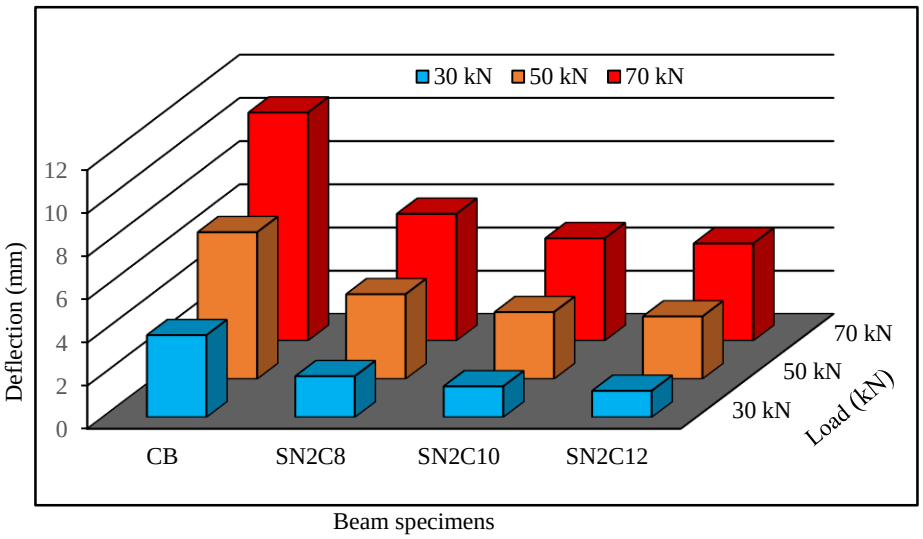

Figure 5.40: Reduction in deflection due to SNSM-CFRP strengthening

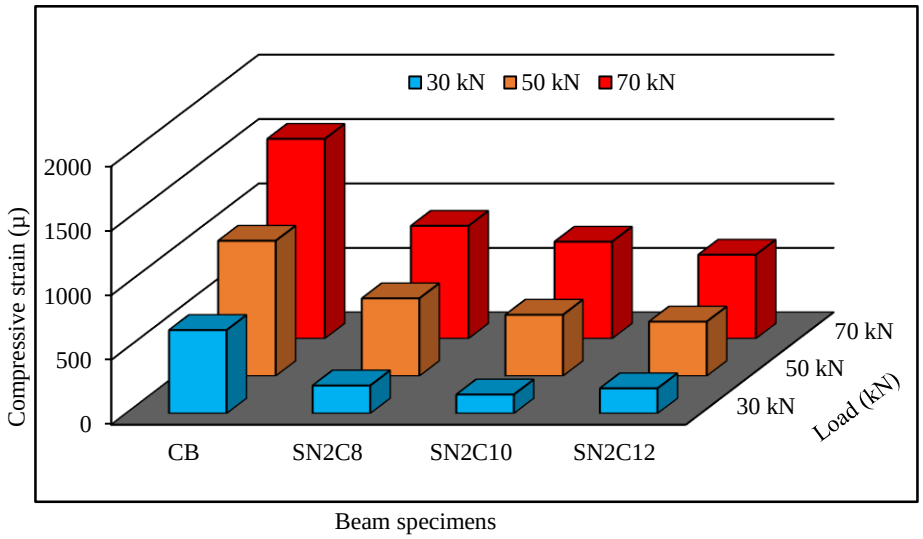

Figure 5.41: Reduction in concrete top fibre strain due to SNSM-CFRP strengthening

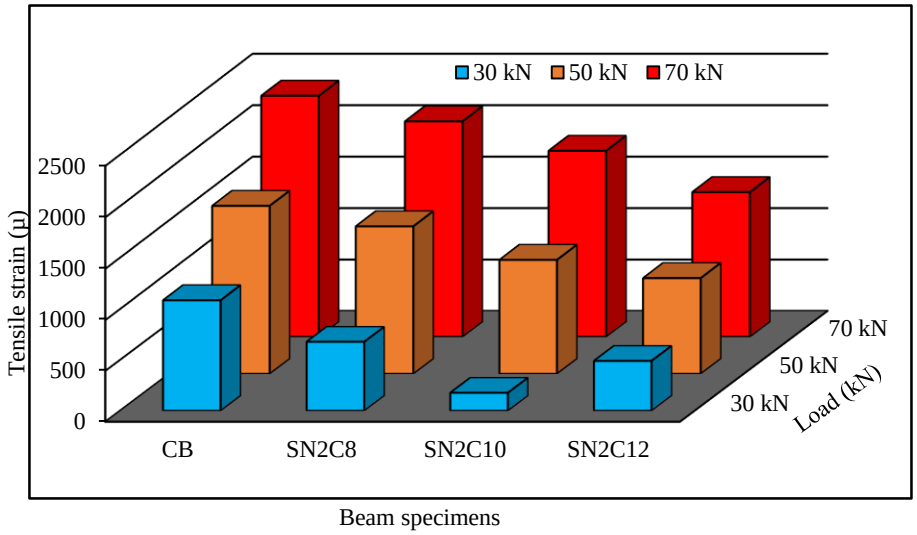

Figure 5.42: Reduction in main steel bar strain due to SNSM-CFRP strengthening

5.2.8 EFFECT OF END ANCHORAGE TO PREVENT THE CONCRETE COVER SEPARATION

In this section, the test results from eight specimens are presented. The results of the control specimen are compared with the results of the strengthened specimens. The RC beam specimens flexurally strengthened with NSM-steel bars were tested to compare the results with their corresponding U-wrap (CFRP fabric) end-anchored strengthened beams.

5.2.8.1 FLEXURAL STRENGTH AND DEFLECTION BEHAVIOUR

The test results showed that all the strengthened specimens without end-anchored NSM steel bars and those with end-anchored NSM steel bars had higher flexural strength compared to the control specimen. The comprehensive test results for strengthened beams without end-anchored and for beams with end-anchored are revealed in Table 5.6. The ultimate loads of the specimens with NSM steel bars and end-anchored were higher compared to the ultimate loads of the specimens with NSM steel bars and without end-anchored. This could be due to the presence of end anchorage, which eliminated the failure through separation of the concrete cover. The NSM steel bars and without end-anchored strengthened specimens

failed by separation of the concrete cover before the specimens could achieve their full strength. However, the specimens strengthened with NSM steel bars and with end-anchored had the full strength before failure, which enhanced the ultimate strength over the without end-anchored strengthened specimens.

Table 5.6: Summary of test results for effect of anchorage

Beam ID	P_{cr} (kN)	$\%P_{cr}$	P_y (kN)	$\%P_y$	P_u (kN)	$\%P_u$	Δ_{max} (mm)	Failure mode
CB	15.75	-	70.00	-	74.37	-	33.61	FL
N2S8	20.00	26.98	-	-	106.24	42.85	14.14	CC
N2S8U3	19.50	23.81	105.00	50.00	121.65	63.57	30.71	FL
N2S10	21.00	33.33	-	-	117.75	58.33	15.62	CC
N2S10U3	27.00	71.43	120.00	71.43	153.78	106.78	34.14	FL
N2S12	26.60	68.89	-	-	136.75	83.88	11.95	CC
N2S12U3	31.50	100.00	135.00	92.86	160.76	116.16	30.64	FL
N2S12U4	32.00	103.17	140.00	100.00	172.69	132.20	30.67	FL

The load-midspan deflection curves for the control, and the specimens strengthened with NSM steel bars with anchorage, and NSM steel bars without anchorage are shown in Figure 5.43. All the beam specimens revealed the linear elastic behaviour of deflection at the commencement followed by the first crack. Afterwards, the deflection curve developed nonlinearly as many flexural cracks were initiated. In the elastic region, the NSM steel bars and end-anchored strengthened specimens showed smaller deflections compared to the specimens strengthened with NSM steel bars but not end-anchored, except the N2S12 specimen. However, at the failure stage, the specimens strengthened with NSM steel bars and end-anchored showed more deflection compared to the specimens strengthened with NSM steel bars but not end-anchored. The reason being that the specimens strengthened with NSM steel bars and end-anchored prevented concrete failure through separation of the cover and enhanced the ultimate loads. The load-deflection behaviour difference between the N2S12U3 and N2S12U4 due to experimental scatter.

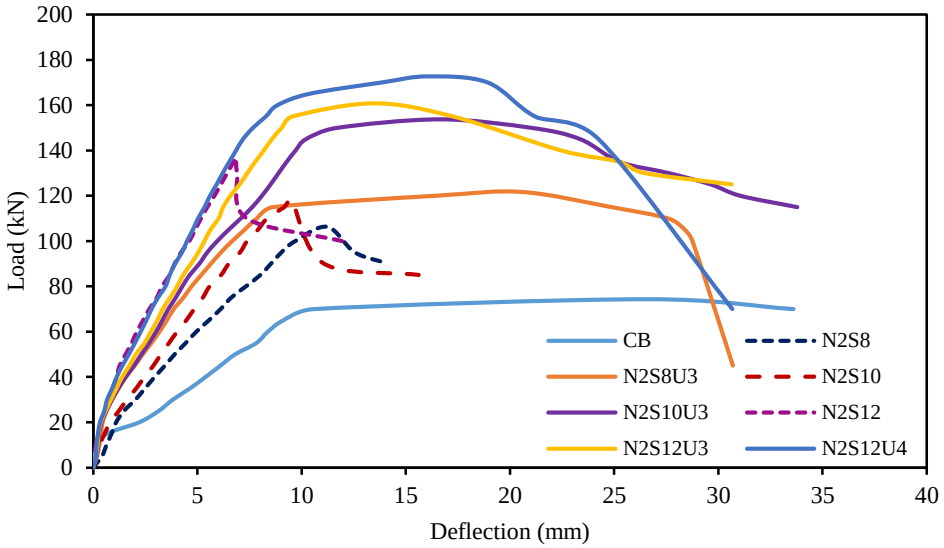

Figure 5.43: Load-midspan deflection

5.2.8.2 MODE OF FAILURE

The failure modes of end-anchored specimens strengthened without NSM steel bars (N2S8, N2S10 and N2S12) are shown in Figure 5.12 and strengthened specimens with NSM steel bars and end-anchored are revealed in Figure 5.44. The results show that the strengthened specimens without end anchorage failed by separation of the concrete cover in a brittle manner. However, the strengthened specimens with NSM steel bars and with end anchorage failed in flexure in a ductile failure mode. Hence, the failure through separation of the concrete cover of all the strengthened specimens without end anchoring due to the formation of shear cracks at the curtailment edge of the NSM steel bars. Since the U-wrap end-anchored was firmly attached at the end of the NSM steel bars, it reduced the risk of the formation of shear cracks at the end of the NSM bars curtailment. Therefore, concrete cover separation did not occur and the failure mode shows ductile characteristics.

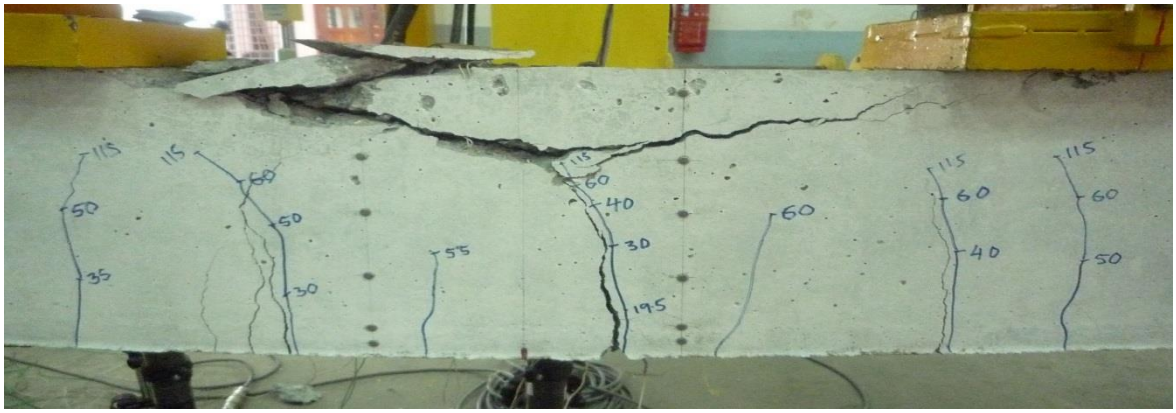

5.44 (a) N2S8U3

5.44 (b) N2S10U3

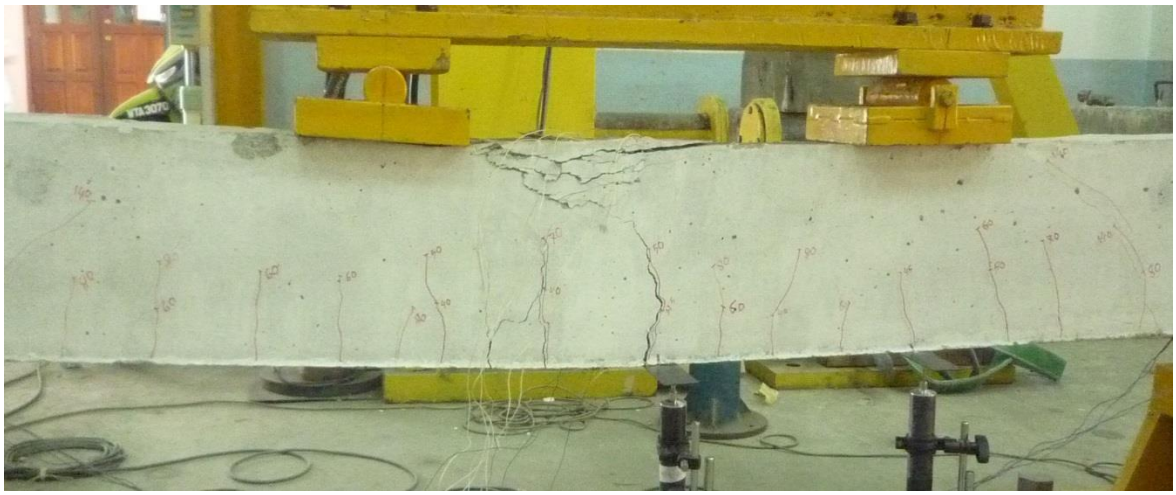

5.44 (c) N2S12U3

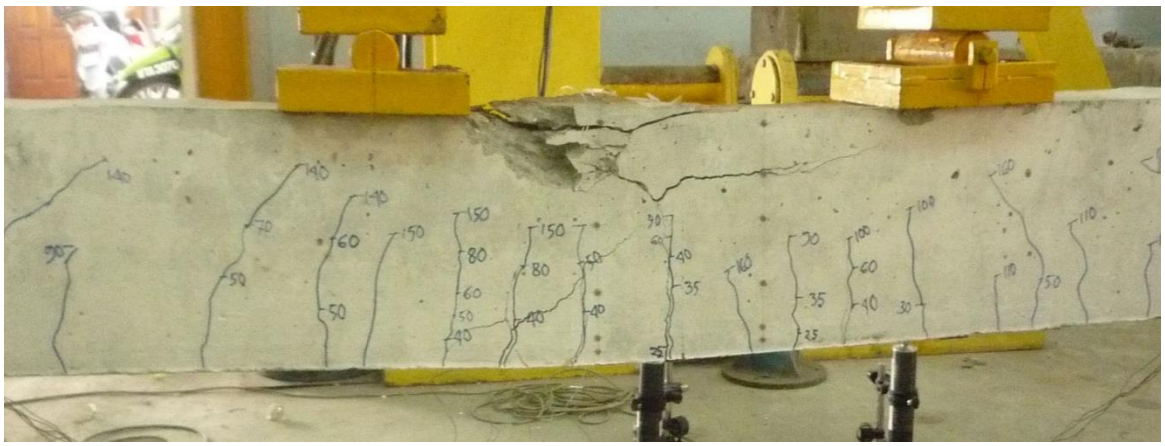

5.44 (d) N2S12U4

Figure 5.44: Failure modes of beam specimens

5.2.8.3 COMPRESSIVE STRAIN OF CONCRETE

The compressive strain of concrete at the midspan and top fibre of the beams are shown in Figure 5.45. The first crack zone of the strengthened beams without end anchorage had similar compressive strains to the concrete of the strengthened beams with end anchorage. The cracking zone of the strengthened beams without end anchorage showed higher compressive strains in the concrete than that of the strengthened beams with end anchorage. However, the strengthened beams with end anchorage showed more compressive strain in the concrete compared to those without end anchorage in the failure phase. This was because the U-wrap end anchorage prevented failure through separation of the concrete cover and achieved maximum strength.

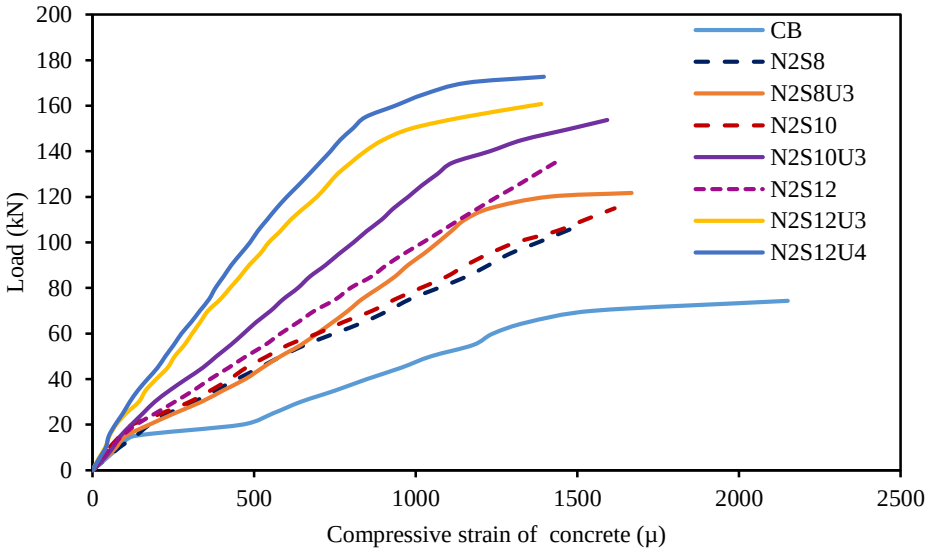

Figure 5.45: Load-compressive strain of concrete

5.2.8.4 TENSILE STRAIN OF MAIN REBARS

The tensile strain of the main reinforcement was recorded at the midspan of the beams, as shown in Figure 5.46. The tensile strain of all strengthened specimens without and with end anchorage were smaller than the control specimen. The elastic zone of the strengthened specimens without end anchorage showed more tensile strain of the main reinforcement compared to those with end anchorage except N2S12. However, the strengthened specimens with end anchorage showed more tensile strain in the main reinforcement compared to those without end anchorage at the failure stage. This is because the strengthened specimens without end anchorage failed by separation of the concrete cover in a brittle manner in contrast to the strengthened specimens with end anchorage, which failed in flexure in a ductile manner.

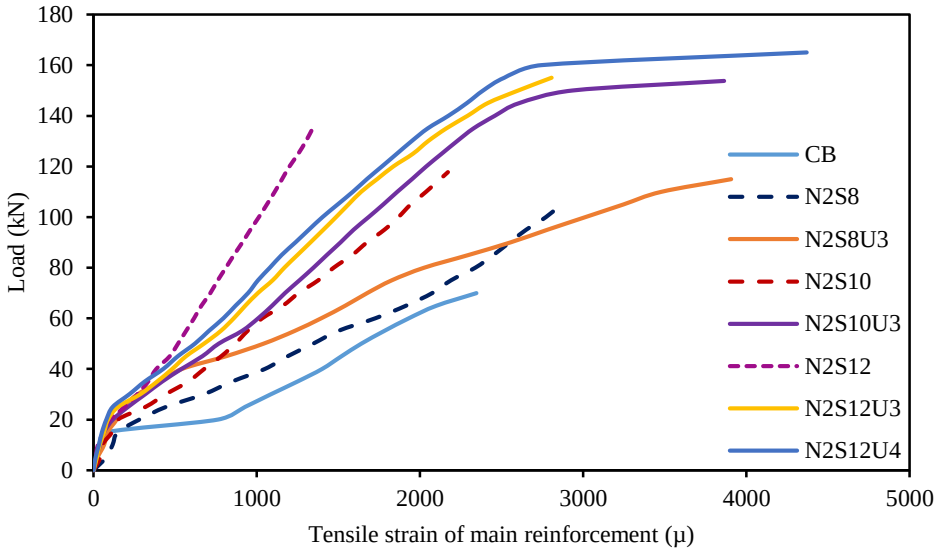

Figure 5.46: Load-tensile strain of main reinforcement

5.2.8.5 TENSILE STRAIN OF NSM REINFORCEMENT

The tensile strain of the NSM reinforcement for all the strengthened specimens is shown in Figure 5.47. The cracking zone of the strengthened specimens without end anchorage showed more tensile strain in the NSM reinforcement compared to those with end anchorage. However, at the failure stage, the specimens strengthened with NSM steel bars and end anchorage had more tensile strain of the NSM reinforcement compared to the specimens strengthened with NSM steel bars but without end anchorage. This is because the strengthened specimens with end anchorage had superior failure loads compared to those without end anchorage.

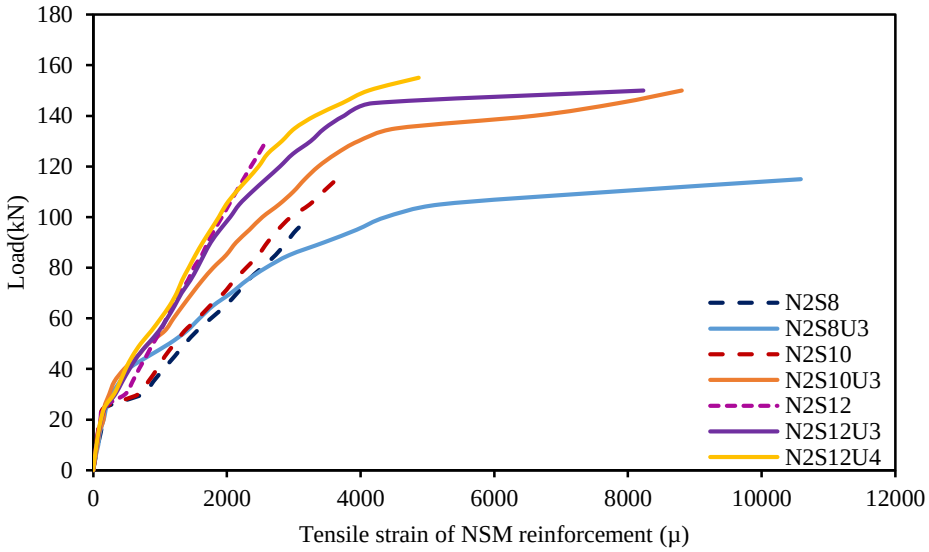

Figure 5.47: Load-tensile strain of NSM reinforcement

5.2.8.6 SECTIONAL STRAIN VARIATION

The depth of beam (h) versus strain at the midspan of the beam specimens for various load levels using demec readings for the strengthened specimens with end anchorage are shown in Figure 5.48 and in Figure 5.16 for the strengthened specimens without end anchorage. The strengthened specimens with end anchorage showed more sectional strain compared to those without end anchorage at the failure stage. This is because the strengthened beams without end anchorage failed by separation of the concrete cover, i.e. premature failure, while the strengthened specimens with end anchorage failed in flexure.

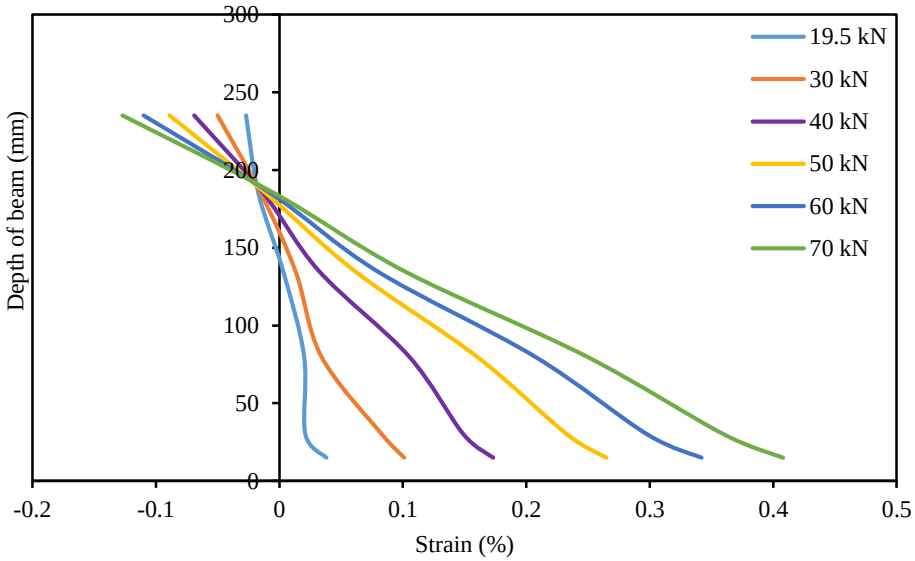

5.48 (a) N2S8U3

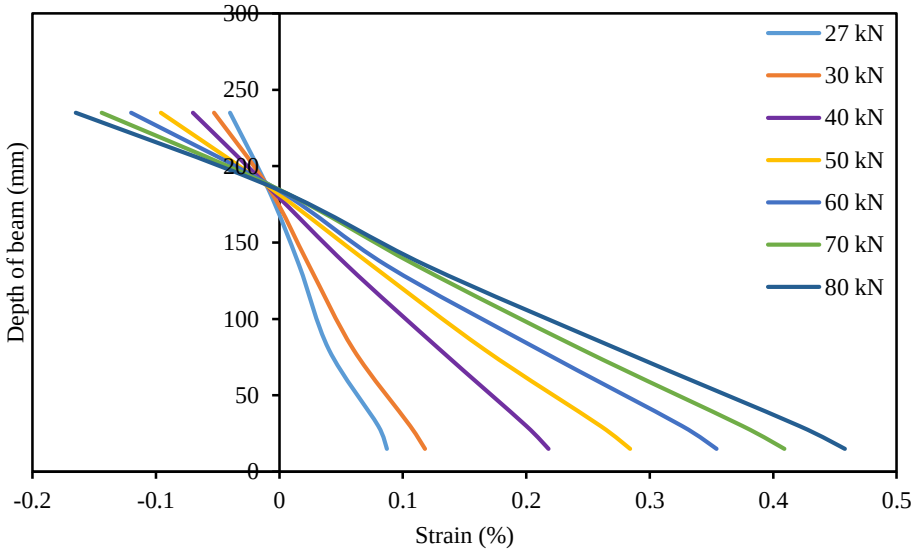

5.48 (b) N2S10U3

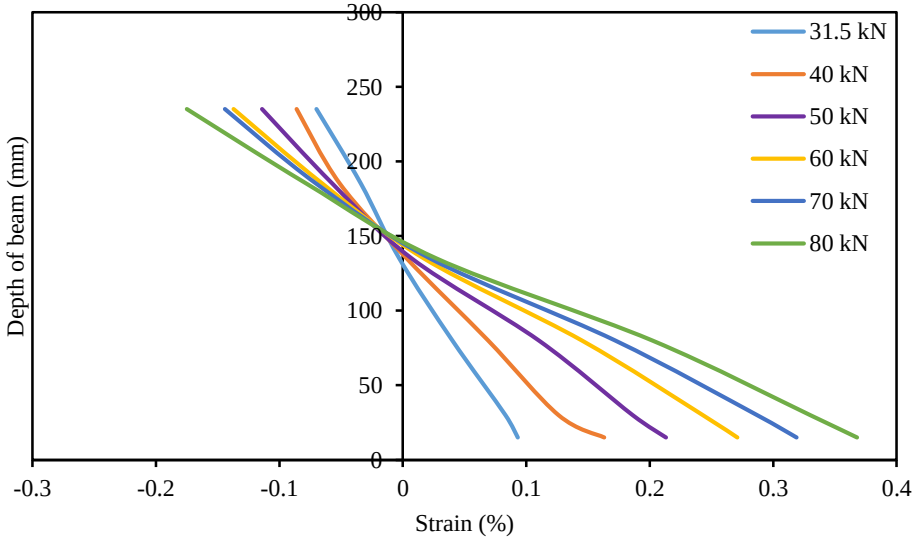

5.48 (c) N2S12U3

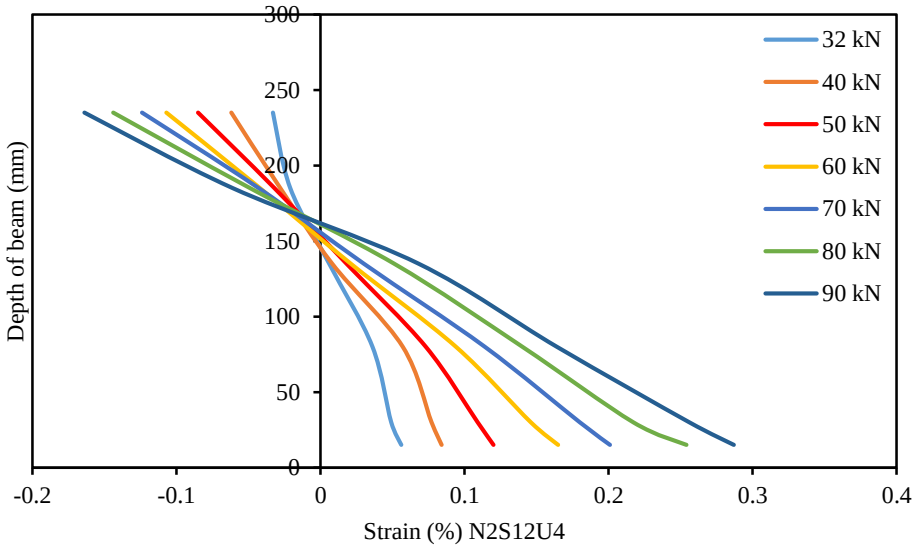

5.48 (d) N2S12U4

Figure 5.48: Sectional strain variation at midspan of strengthened beams

5.2.8.7 CRACK CHARACTERISTICS

The load-crack widths of beams CB, N2S8, N2S8U3, N2S10, N2S10U3, N2S12, N2S12U3 and N2S12U4 are shown in Figure 5.49. The experimental first cracking loads of all specimens are revealed in Table 5.6. The first cracking loads of all end anchorage strengthened beams were higher than for those without end anchorage except the N2S8U3 specimen. It was noted that the strengthened beams with end anchorage had higher stiffness compared to those without end anchorage. The total number of cracks for CB, N2S8, N2S8U3, N2S10, N2S10U3, N2S12, N2S12U3 and N2S12U4 were 11, 15, 16, 17, 18, 20, 22 and 23, respectively. The average crack spacing of those beams was 180 mm, 125 mm, 123 mm, 115 mm, 105 mm, 95 mm, 90 mm and 85 mm, respectively. The strengthened beams with end anchorage had a greater number of cracks and less crack spacing than those without end anchorage.

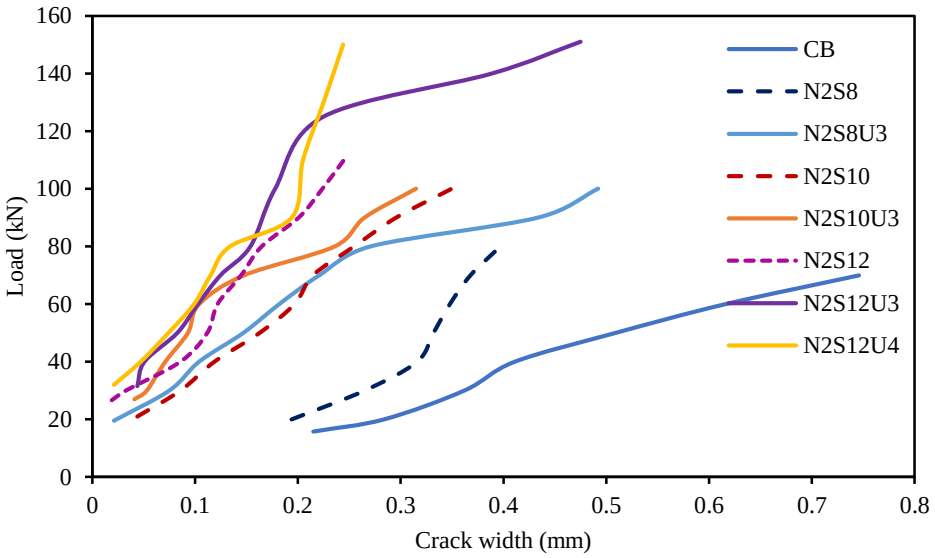

Figure 5.49: Load-crack width

5.2.8.8 THE EFFECTIVENESS OF U-WRAP END ANCHORAGE

The reduction in deflection due to strengthening with NSM steel bars and U-wrap end anchorage with CFRP fabric and strengthening with NSM steel bars and without end anchorage at 30 kN, 50 kN and 70 kN service loadings are presented in Figure 5.50. The deflection of the strengthened specimens was reduced by a maximum of about 47%, 76%, 58%, 76%, 78%, 78% and 83% for N2S8, N2S8U3, N2S10, N2S10U3, N2S12, N2S12U3 and N2S12U4, respectively, compared to the control specimen due to the increased stiffness of the strengthened specimens. The compressive strain of the concrete at the top fibre of the specimens and reduction of the strain due to strengthening at 30 kN, 50 kN and 70 kN service loading are revealed in Figure 5.51. The compressive strain of the strengthened specimens was reduced by a maximum of about 51%, 49%, 53%, 70%, 61%, 78% and 82% for N2S8, N2S8U3, N2S10, N2S10U3, N2S12, N2S12U3 and N2S12U4, respectively, compared to the control specimen. The internal reinforcing tension steel bar tensile strain and reduction of the strain due to strengthening at 30 kN, 50 kN and 70 kN service loading are shown in Figure 5.52. The reinforcing bar strain of the strengthened specimens was reduced by a

maximum of about 38%, 75%, 59%, 71%, 75%, 74% and 80% for N2S8, N2S8U3, N2S10, N2S10U3, N2S12, N2S12U3 and N2S12U4, respectively, compared to the control specimen. Therefore, the beam specimens strengthened with NSM steel bars with end anchorage showed more reduction in deflection, and compressive and tensile strain compared to the specimens without end anchorage. This is because the failure mode of the strengthened beam specimens with end anchorage was due to flexure.

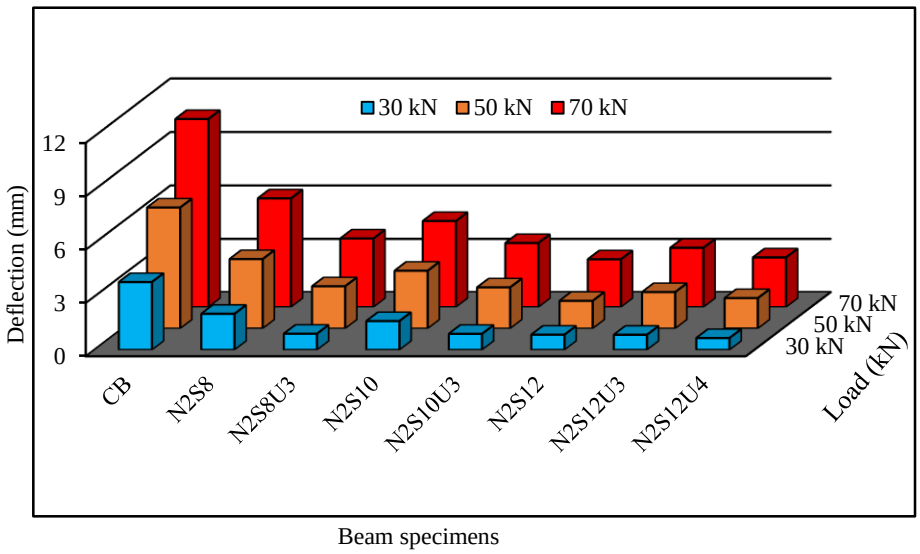

Figure 5.50: Reduction in deflection due to with and without end-anchored strengthening

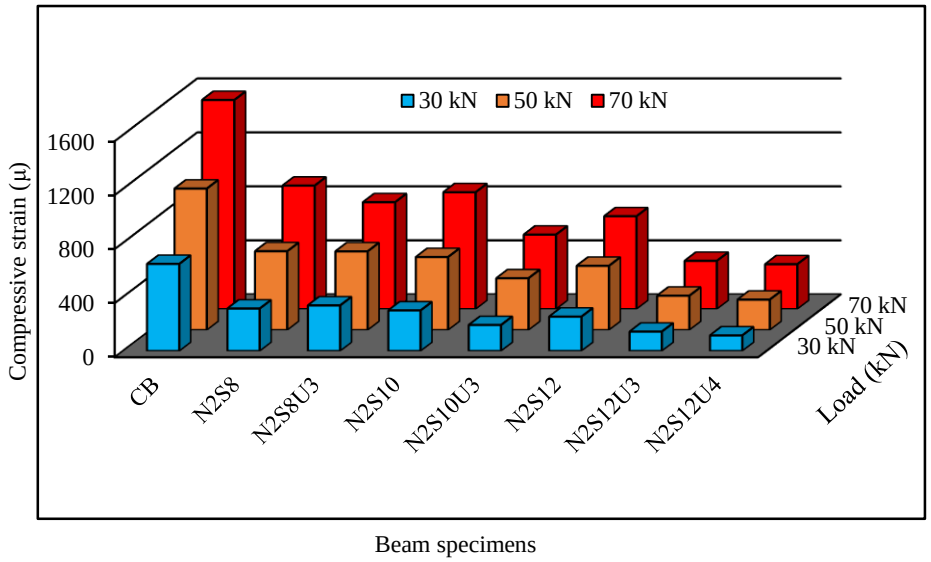

Figure 5.51: Reduction in concrete top fibre strain due to with and without end-anchored strengthening

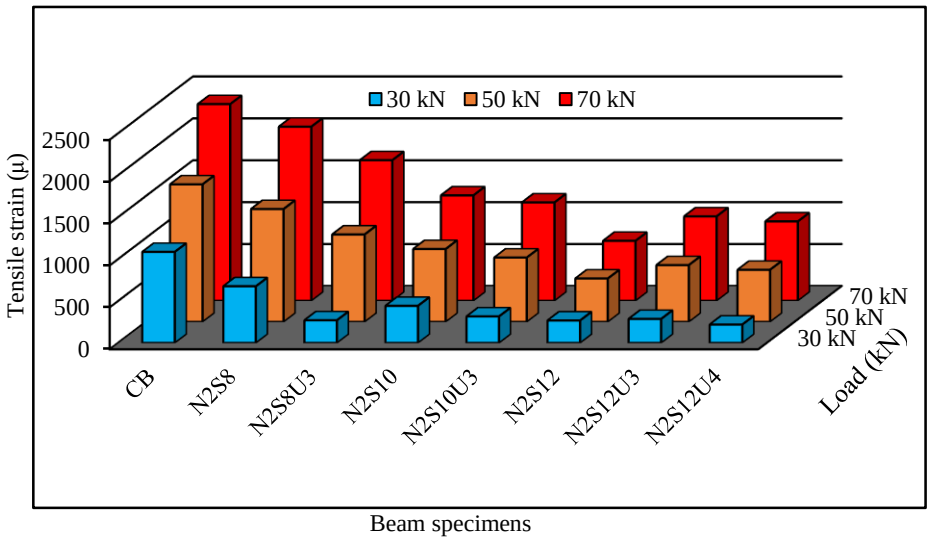

Figure 5.52: Reduction in strain main steel bar due to with and without end-anchored strengthening

5.2.9 THE BEHAVIOUR OF PRE-CRACKED RC BEAMS STRENGTHENED WITH SNSM TECHNIQUE USING CFRP BARS.

In this section, the experimental results from the flexurally strengthened pre-cracked RC beam specimens by the SNSM technique using CFRP bars are compared with the control specimen. The preloading was applied by 30%, 40% and 50% of the ultimate capacity of the control beam for PSN2C8, PSN2C10 and PSN2C12, respectively. The results of these beams are presented as shown below.

5.2.9.1 FLEXURAL STRENGTH AND DEFLECTION BEHAVIOUR

The flexural behaviour of pre-cracked beams in terms of preload, ultimate load, maximum deflection and failure modes are revealed in Table 5.7. The test results showed that all pre-cracked with side near surface mounted (SNSM) CFRP strengthened specimens had greater ultimate loads compared to the control specimen. The SNSM CFRP bars increased the ultimate load capacity by 85.58%, 130.11% and 125.10% for beams PSN2C8, PSN2C10 and PSN2C12, respectively, compared to the control beam. However, the PSN2C12 specimen

showed less ultimate loads compared to the PSN2C10 specimen due to the peeling off failure of the PSN2C12specimen. It is important to note that the ultimate capacity of the pre-cracked beams were increased remarkably by the SNSM CFRP technique. Therefore, the SNSM technique is very efficient for increasing the flexural strength of pre-cracked specimens.

Table 5.7: Summary of test results for pre-cracked beams

Beam ID	**Preload (kN)**	**P_u (kN)**	**$\%P_u$**	**Δ_{max} (mm)**	**Failure mode**
CB	-	74.37	-	33.61	FL
PSN2C8	22.50	138.02	85.58	27.78	FL
PSN2C10	30.00	171.13	130.11	21.24	FL
PSN2C12	37.50	169.41	125.10	14.23	PL

The load versus midspan deflection curves of CB, PSN2C8, PSN2C10 and PSN2C12 are shown in Figure 5.53. All the strengthened beam specimens displayed a linear behaviour of deflection at the beginning followed by preload. Thereafter, the deflection curves showed a similar trend in the elastic zone. At failure, the PSN2C8 and PSN2C10 specimens showed more deflection compared to PSN2C12 specimen. This was because the PSN2C8 and PSN2C10 specimens failed in flexure while the PSN2C12 specimen failed by the CFRP bars peeling off.

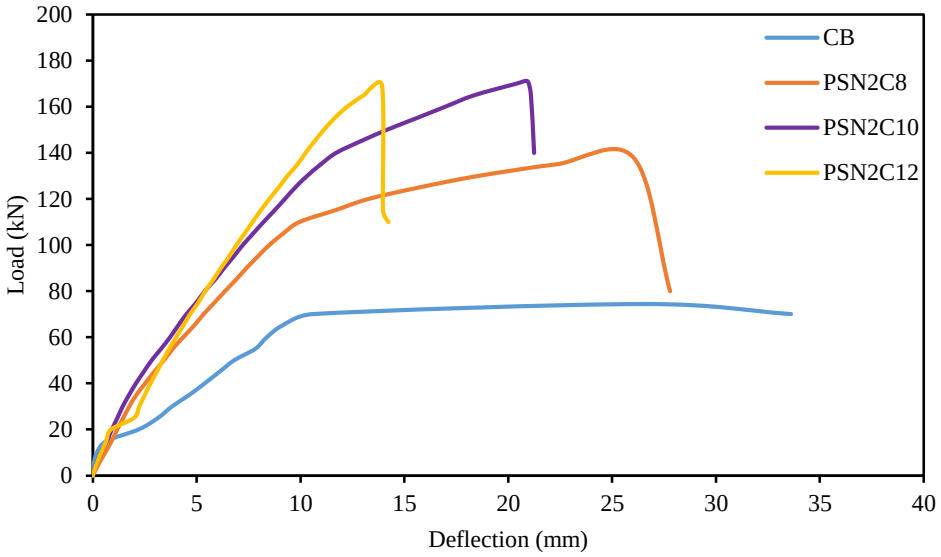

Figure 5.53: Load-midspan deflection

5.2.9.2 MODE OF FAILURE

The failure modes of the CB, PSN2C8, PSN2C10 and PSN2C12 beam specimens are shown in Figure 5.54. The modes of failure for the PSN2C8 and PSN2C10 strengthened beam specimens were in flexure with the ductile mode of failure. Flexure failure is concrete crushing followed by internal steel bars yielding and rupture of the strengthening CFRP bars. However, the PSN2C12 strengthened specimen failed by the CFRP bars peeling off. The reason being that subsequent to the yielding of the internal steel bars, the shear crack commenced at the end of the SNSM CFRP bars and the crack width increased rapidly. Where the shear and flexural cracks overlapped, the CFRP bars peeled off, which accelerated the premature failure.

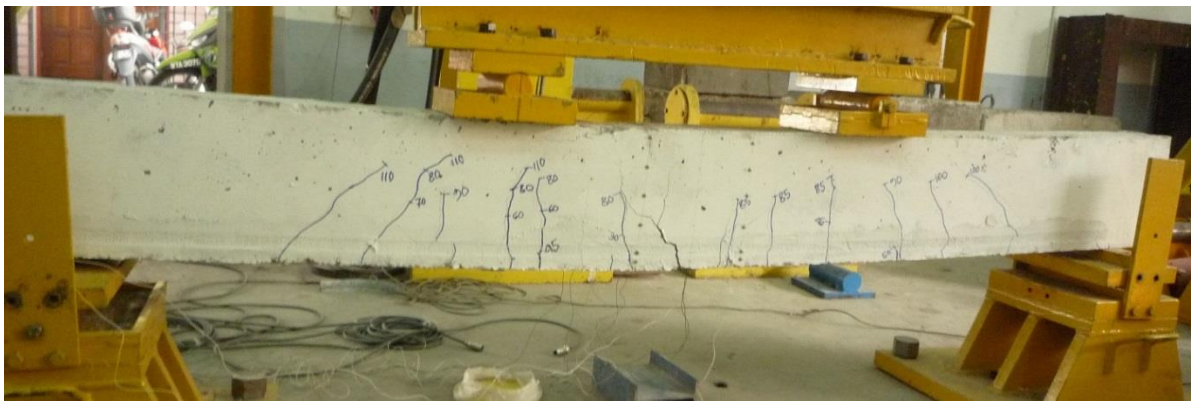

5.54 (a) PSN2C8

5.54 (b) PSN2C10

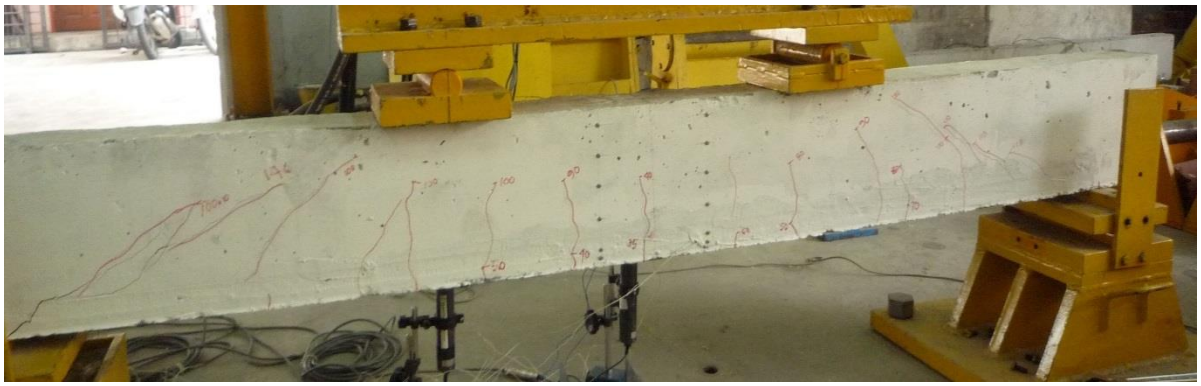

5.54 (c) PSN2C12

Figure 5.54: Failure modes of beam specimens

5.2.9.3 COMPRESSIVE STRAIN OF CONCRETE

The compressive strain of concrete measured at the midspan and top fibre of the beam specimens is shown in Figure 5.55. The concrete compressive strain of pre-cracked strengthened specimens was smaller than for the control specimen. This could be due to the greater compressive strength of the pre-cracked strengthened

beam specimens. Moreover, the PSN2C10 specimen showed more compressive strain compared to the other specimens.

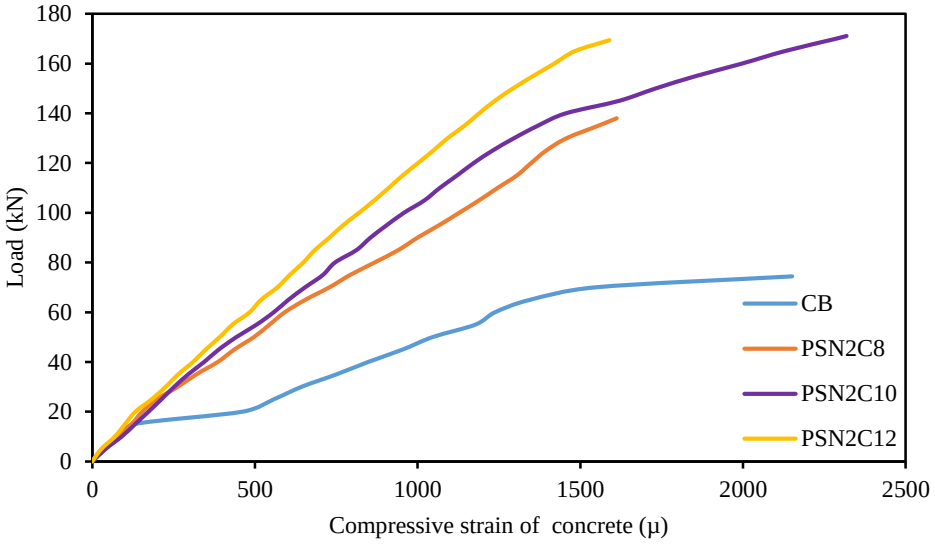

Figure 5.55: Load-compressive strain of concrete

5.2.9.4 TENSILE STRAIN OF MAIN REBARS

The load versus tensile strain of the main rebars for the beam specimens is shown in Figure 5.56. The PSN2C12 specimen had smaller tensile strain compared to the PSN2C8 and PSN2C10 specimens. This could be due to the variation in the strengthening with the CFRP bars. Furthermore, strengthening CFRP bar areas increased the stiffness of the beam specimens, thus reducing the tensile strain of the main rebars.

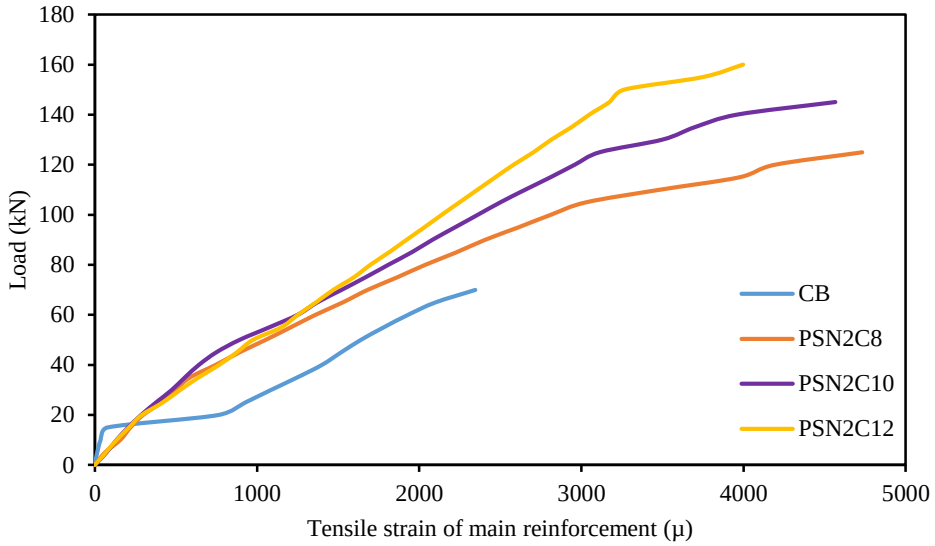

Figure 5.56: Load-tensile strain of main reinforcement

5.2.9.5 TENSILE STRAIN OF SNSM REINFORCEMENT

The load versus tensile strain of the SNSM reinforcement of the PSN2C8, PSN2C10 and PSN2C12 beam specimens are shown in Figure 5.57. It was found that the pre-cracked strengthened beam PSN2C12 had less SNSM CFRP bar strain compared to beams PSN2C8 and PSN2C10 due to premature failure of PSN2C12. At the failure stage the SNSM bar strain of beams PSN2C8, PSN2C10 and PSN2C12 were found to be 0.0102, 0.0065 and 0.0037, respectively. It was found that the peeling off failure of beam PSN2C12 was initiated at the SNSM bar strain of around 0.0037.

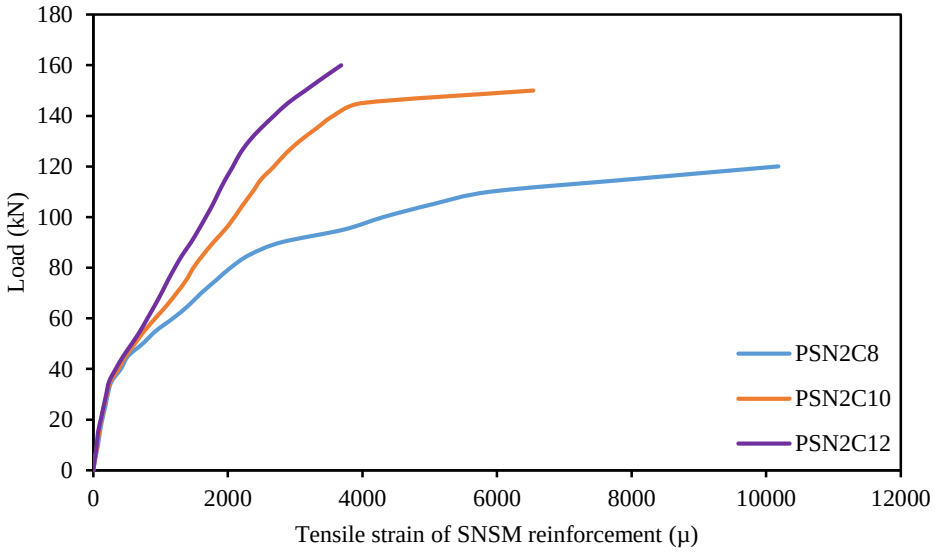

Figure 5.57: Load-tensile strain of SNSM reinforcement

5.2.9.6 SECTIONAL STRAIN VARIATION

The depth of beam versus sectional strain at midspan of the specimens at different load levels using the demec strain gauge reading for pre-cracked specimens is shown in Figure 5.58. The strain variation of the pre-cracked strengthened specimen PSN2C12 was almost linear at the lower loading stages compared to the PSN2C8 and PSN2C10 specimens, whereas the load that increased as a result of the flexural cracks also increased at the midspan, leading to more strain on the SNSM bars. It was investigated that the strain on the SNSM bars for the SN2C12 specimen was higher than the strain on the PSN2C8 and PSN2C10 specimens at higher load levels.

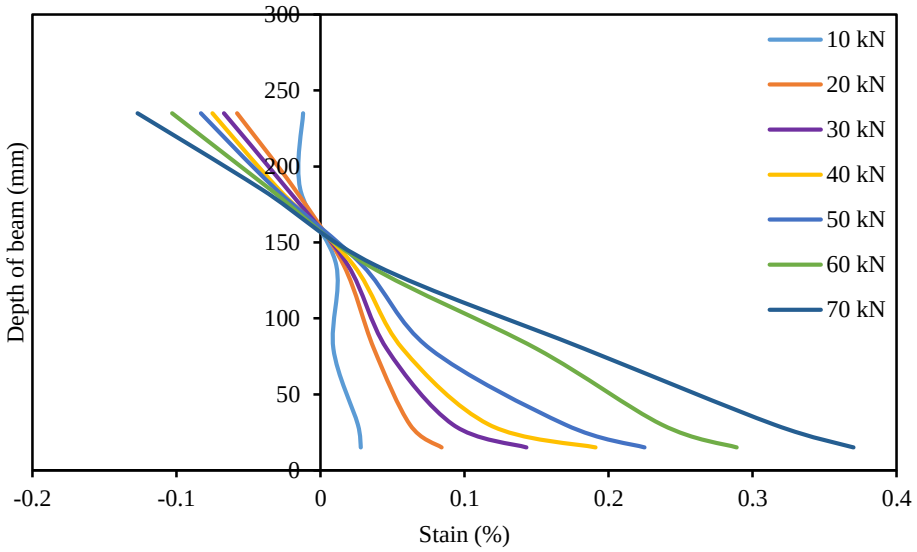

(a) PSN2C8

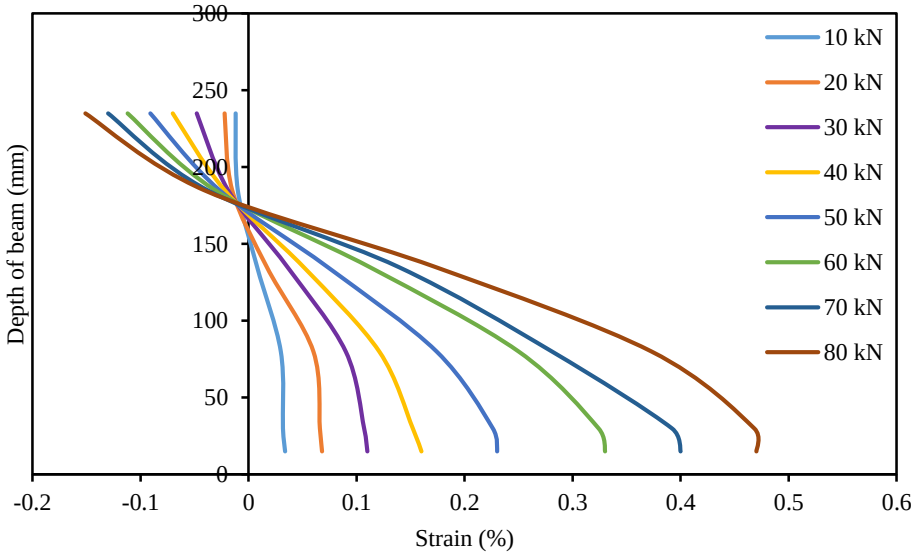

(b) PSN2C10

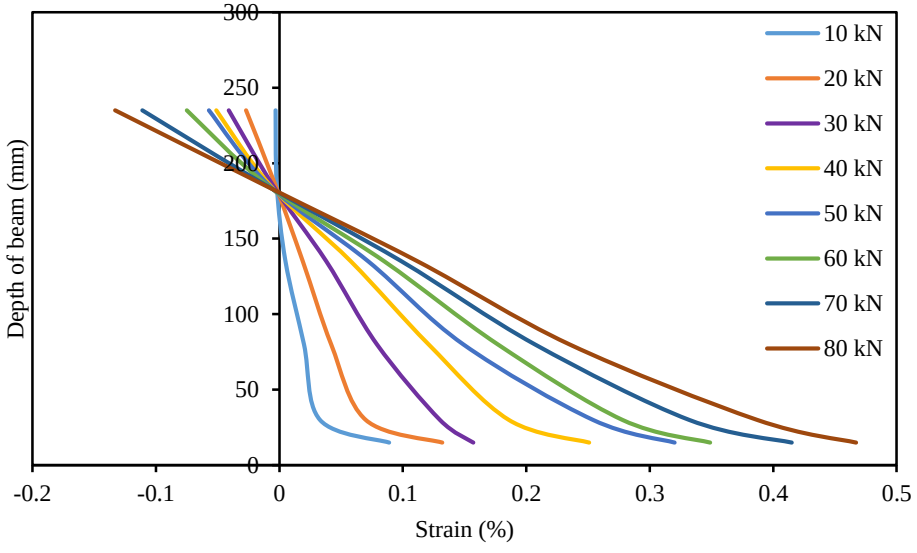

(c) PSN2C12

Figure 5.58: Sectional strain variation at midspan of strengthened beams

5.2.9.7 CRACK CHARACTERISTICS

The load versus crack width of the pre-cracked strengthened beam specimens PSN2C8, PSN2C10 and PSN2C12 are shown in Figure 5.59. The figure shows that the pre-cracked strengthened beam specimens had similar cracking pattern until failure. It was found that the increase in the amount of SNSM reinforcement, decreased the crack width correspondingly.

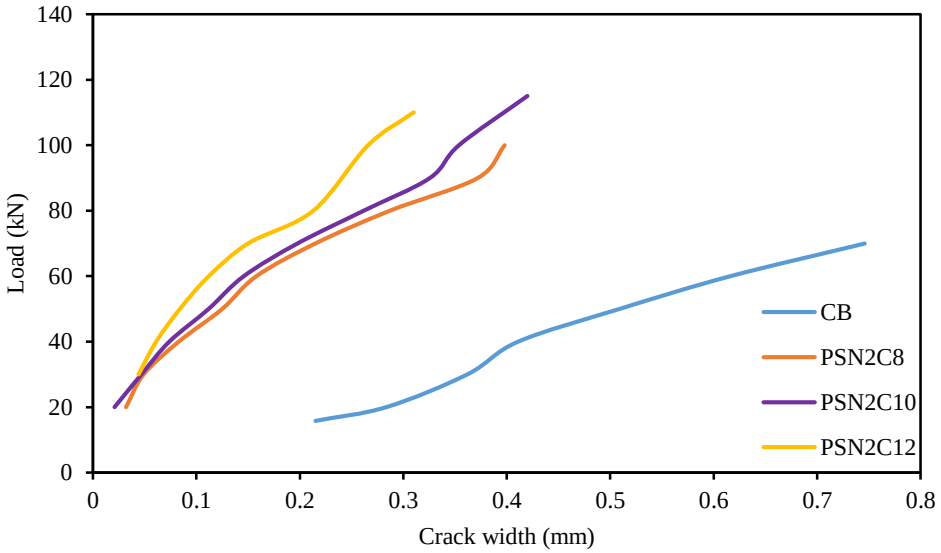

Figure 5.59: Load-crack width

5.3 VERIFICATION OF THE ANALYTICAL MODEL

5.3.1 VERIFICATION OF LOAD PEDICTION MODEL

Figure 5.60 shows a comparison between the experimental and predicted ultimate load of the strengthened beams. The figure exhibits that within the range of loads achieved in this analysis, the difference between the experimental and predicted load ranged from 1% to 7%. The prediction model is found to be very competent for predicting the ultimate load of RC beams strengthened in flexure.

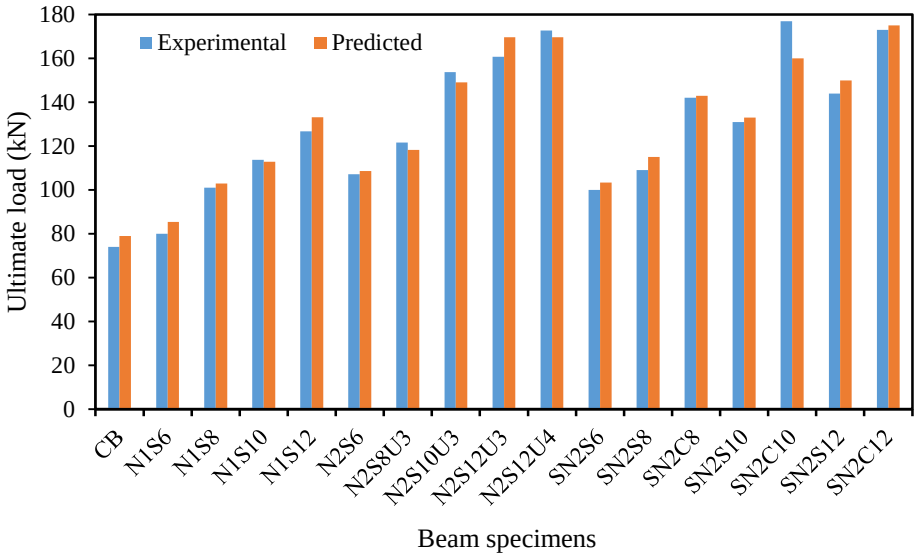

Figure 5.60: Experimental and predicted ultimate loads comparison

5.3.2 VERIFICATION OF CONCRETE COVER SEPARATION MODEL

Figure 5.61 presents a comparison between the experimental and predicted failure loads of the strengthened beams. The results in the table show that the analytical predicted loads are mostly very similar to the achieved experimental loads. Except for beam N2S8, the beams N2S10, N1S16, N2S12 and N2C12 reveal a very good agreement for the failure load. As the crack spacing for beam N2S8 was higher in the predicted model, a major upturn in ultimate load was seen, which is desirable due to cracking behaviour. However, the overall evaluation of ultimate load in both techniques is acceptable as the average deviation is trivial.

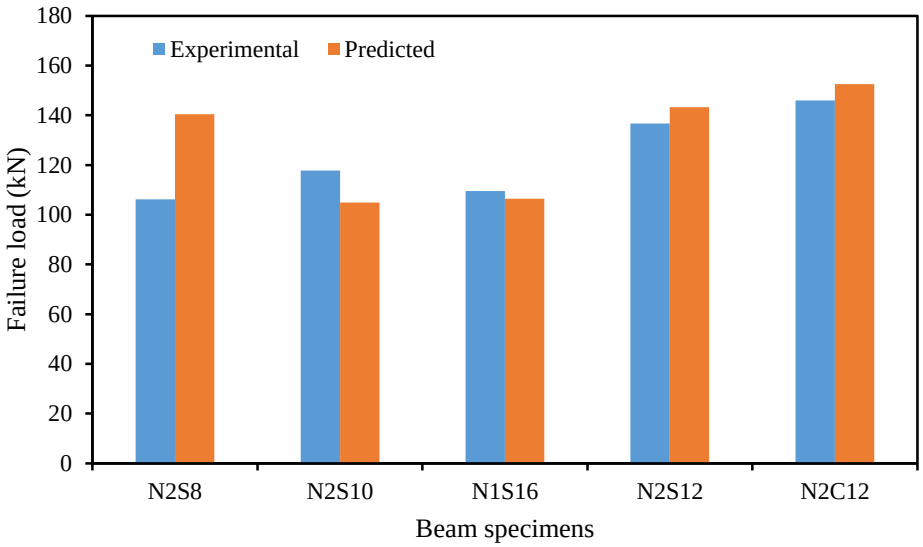

Figure 5.61: Comparison of experimental and predicted failure loads

5.3.3 VERIFICATION OF DEFLECTION PREDICTION MODEL

To verify the deflection prediction model, the load versus midspan deflection relationship during loading is compared with the analytical results found from the model. The comparison of the predicted and experimental test results in relation to the load versus midspan deflection for only CB specimen is shown in Figure 5.62. Graphs for all other specimens are appended (Appendix B). The correlation between the predicted and experimental results for the tested beam specimens are within close agreement except for the beam specimens that suffered concrete cover separation failure.

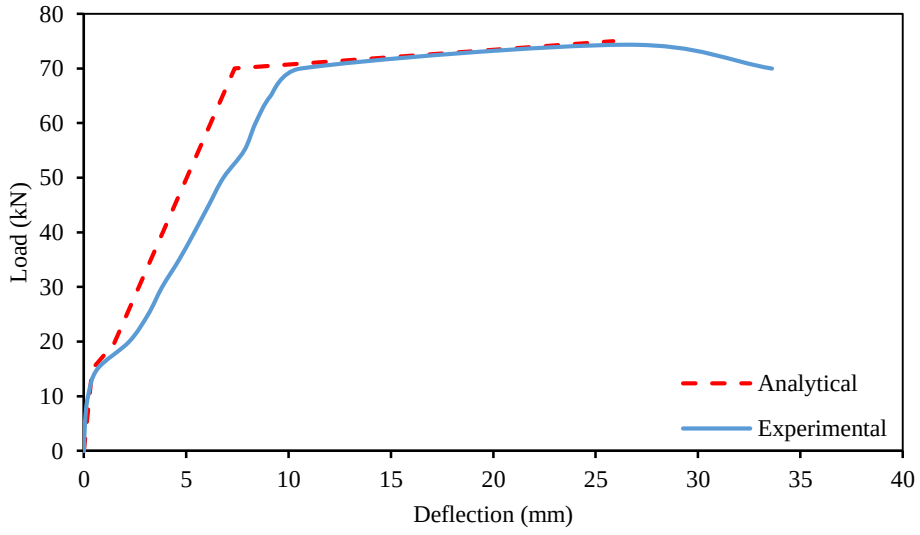

Figure 5.62: Experimental and predicted load-midspan deflection diagram (CB)

5.3.4 VERIFICATION OF CONCRETE COMPRESSIVE STAIN PREDICTION MODEL

The relationship between the predicted and experimental tested results in respect of the load versus concrete compressive strains for only CB specimen is shown in Figure 5.63. Graphs for all other specimens are appended (Appendix C). From the figures, it can be seen that there is a reasonable consensus between the predicted and experimental tested results obtained for the beam specimens.

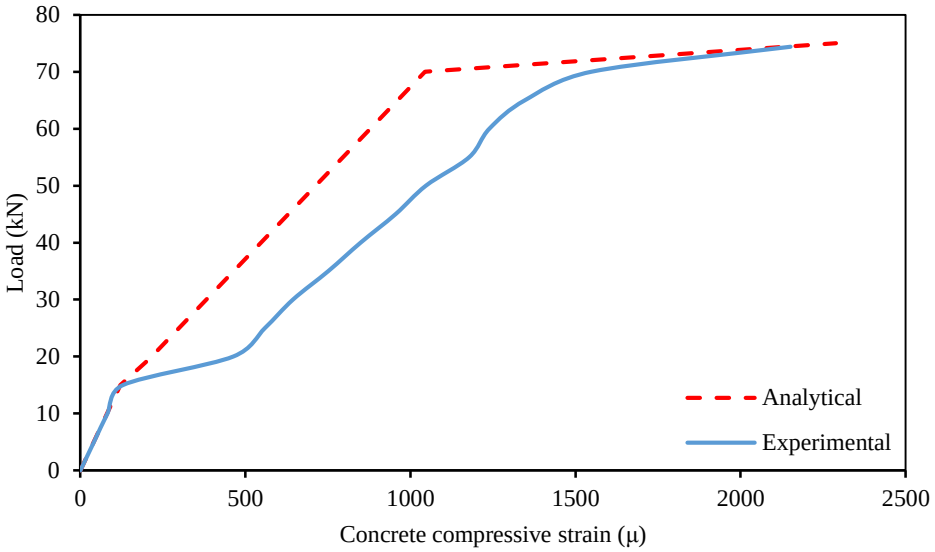

Figure 5.63: Experimental and predicted load-concrete compressive strain diagram (CB)

5.3.5 VERIFICATION OF INTERNAL REINFORCEMENT TENSILE STAIN PREDICTION MODEL

The comparison between the predicted and experimental tested results in relation to the load versus tensile strain of the main reinforcement for only CB specimen is shown in Figure 5.64. Graphs for all other specimens are appended (Appendix D). The relationship between the predicted and experimental results for all beam specimens shows good agreement.

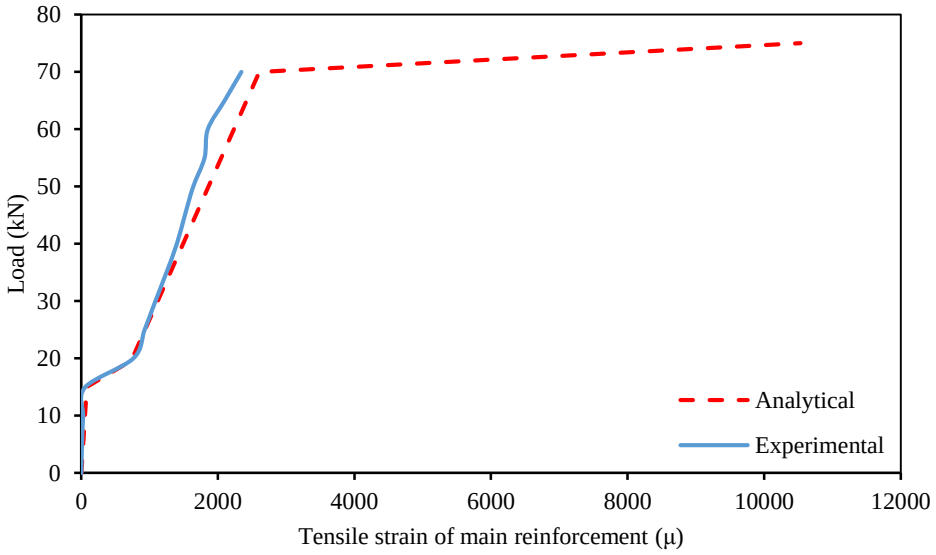

Figure 5.64: Experimental and predicted load-tensile strain of main reinforcement diagram (CB)

5.3.6 VERIFICATION OF STRENGTHENING REINFORCEMENT TENSILE STAIN PREDICTION MODEL

The correlation between the predicted and experimental tested results in relation to the load versus tensile strain of strengthening reinforcement for only N1S6 strengthened beam specimen is shown in Figure 5.65. Graphs for all other specimens are appended (Appendix E). The relationship between the predicted and experimental results for all the strengthened beam specimens shows a close agreement.

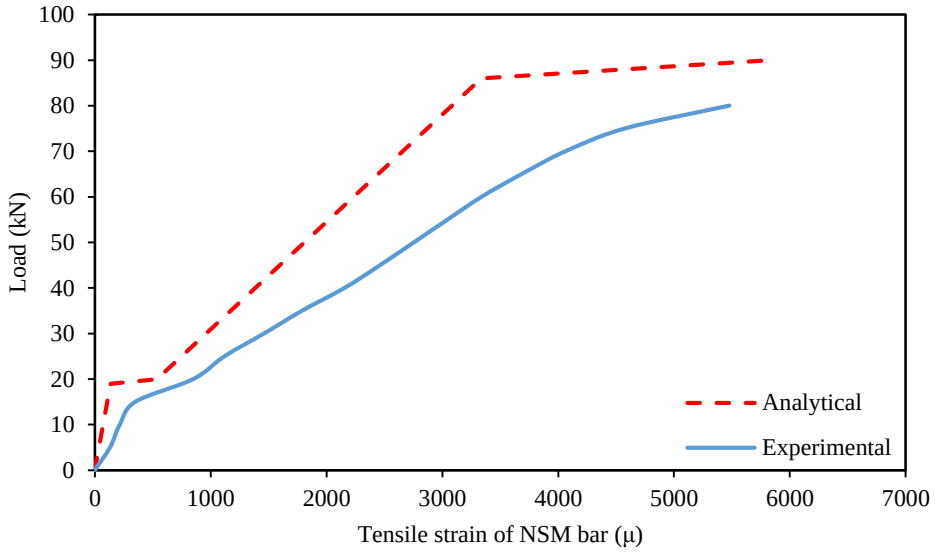

Figure 5.65: Experimental and predicted load-tensile strain of strengthening bar diagram (N1S6)

5.3.7 VERIFICATION OF CRACK SPACING PREDICTION MODEL

The relationship between the predicted and experimental test results for the crack spacing for all beam specimens except the pre-cracked strengthened beam specimens are shown in Figure 5.66. The relationship between the predicted and experimental results for all beam specimens shows very close agreement.

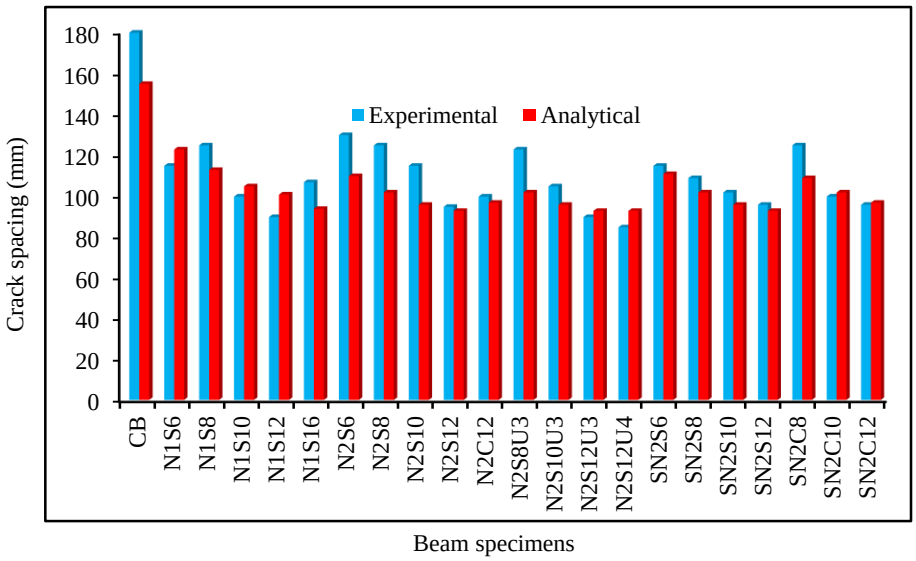

Figure 5.66: Experimental and predicted crack spacing diagram

5.4 THE EFFECTIVENESS OF SNSM TECHNIQUE

The proposed SNSM strengthening technique using CFRP and steel bars significantly enhanced the flexural strength (Figure 5.67b) of the RC beams. However, SNSM with CFRP strengthened beams showed higher flexural strength and stiffness compared to the SNSM-steel beams due to high tensile strength of CFRP bars. Up to 2.38 times and 1.76 times increment of the flexural strength with SNSM-CFRP and steel respectively, over the control beam could be attained. Whereas, in the case of NSM with steel bars strengthened beams, the flexural strength increased up to 1.58 times. Therefore, the SNSM-CFRP approach can be considered as being more beneficial. The first cracking load was higher in the SNSM technique, which consistently increased the serviceability load (Figure 5.67a). The SNSM-steel approach showed better performance in terms of the cracking loads. The higher cracking load is related to the increase in the SNSM reinforcement. The NSM-steel strengthen beams shows less deflection compared with the SNSM-steel strengthen beams due to concrete cover separation failure i.e. premature failure. Therefore, the SNSM technique very effective in terms of serviceability and flexural strength.

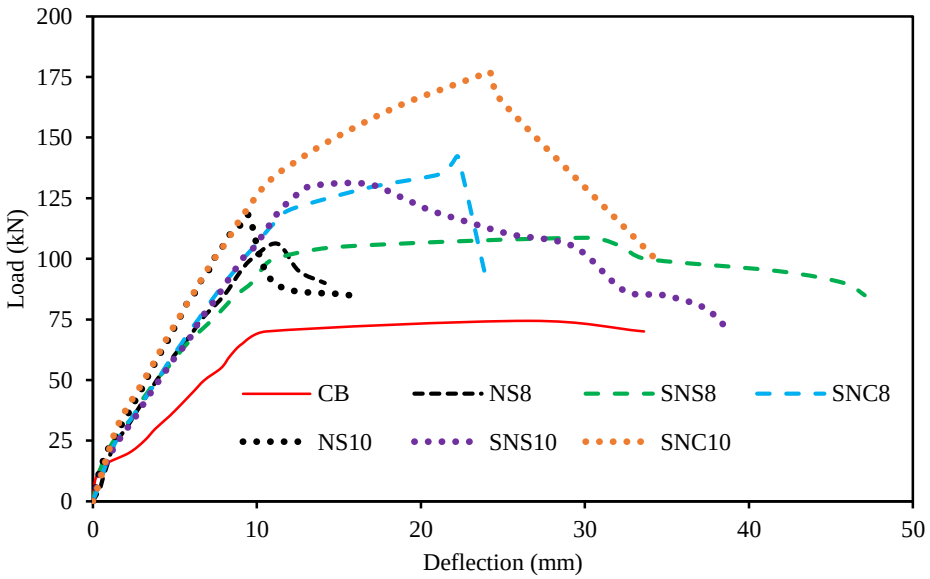

(a) Load-deflection curve comparison

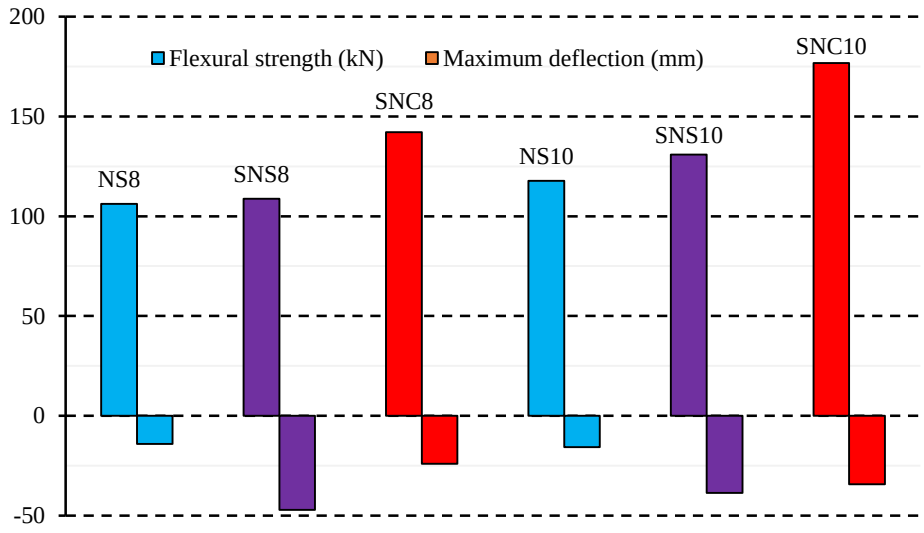

(b) Flexural strength and maximum deflection comparison

Figure 5.67: NSM and SNSM techniques comparison

6. CONCLUSIONS AND RECOMMENDATIONS

6.1 CONCLUSIONS

An experimental programme was conducted to investigate the structural behaviour of the RC beams strengthened with steel and CFRP bars using two methods – NSM and an innovative SNSM technique. The behavioural enhancement of RC beams strengthened by NSM steel bars with U-wrap (CFRP fabric) end anchorage and pre-cracked beams strengthened with SNSM CFRP bars had also been investigated. In addition, several analytical models were developed to predict the flexural responses of the RC beams strengthened using different strengthening techniques. The predicted results agreed reasonably well with the experimental results. Based on the objectives, the following conclusions can be drawn:

6.1.1 PERFORMANCE OF RC BEAMS STRENGTHENED WITH NSM-STEEL TECHNIQUE.

- The NSM steel bars significantly increased the flexural performance of RC beams.
- The beams strengthened with NSM steel bars showed higher first cracking and failure loads than control beams.
- Less deflection, crack widths, concrete compressive strains and tensile strain of the internal reinforcement were found compared to those of the control beams.

6.1.2 EFFECT OF THE NUMBER OF GROOVES AND THE AMOUNT OF NSM REINFORCEMENT.

- Increasing the number of grooves increased the ultimate load carrying capacity of the RC beams.
- For increase in the amount of NSM steel reinforcement from 28 mm^2 to 113 mm^2 the ultimate load capacity enhanced by from 8% to 70%.

6.1.3 BEHAVIOUR OF RC BEAMS STRENGTHENED WITH SNSM TECHNIQUE.

- The first cracking load delayed the SNSM strengthening technique (SNSM steel bars increased up to 217% and SNSM CFRP bars increased up to 102%), which, correspondingly, increased the serviceability load.
- The flexural strength of the strengthened beams increased by 138% for the SNSM CFRP bars and 93% for the SNSM steel bars.
- The proposed innovative approach SNSM strengthening technique effectively enhanced the flexural capacity and stiffness of the RC beams.

6.1.4 PREVENTING THE CONCRETE COVER SEPARATION WITH END ANCHORAGE.

- The proposed U-wrap end anchorage with CFRP fabric was found to be able to eliminate the concrete cover separation failure of the beams strengthened using NSM steel bars.
- The beams strengthened with NSM steel bars employing the U-wrap end anchorage were failed by flexure in a ductile manner.
- All the end anchored strengthened beams showed greater ultimate loads compared to the strengthened beams without end anchors.

6.1.5 BEHAVIOUR OF PRE-CRACKED RC BEAMS STRENGTHENED WITH SNSM TECHNIQUE.

- The ultimate load capacity of pre-cracked strengthened beams was up to 130% whereas for normal strengthened beams it was up to 138%.
- The flexural performance of the pre-cracked strengthened beams using SNSM CFRP bars did not significantly differ from the normal strengthened beams. This phenomenon appearances the advantage of the proposed SNSM CFRP technique.
- The SNSM CFRP approach gives a good enhancement of structural behaviour of pre-cracked beams when strengthened was done following the technique.

6.1.6 ANALYTICAL MODELS TO PREDICT THE FLEXURAL RESPONSES OF RC BEAMS.

- The proposed analytical model is able to predict the flexural response of all beam specimens (deflection, concrete compressive strain, internal main reinforcement tensile strain, strengthening reinforcement tensile strain and crack spacing).
- The predicted and experimental results show reasonable agreement.
- Hence both the NSM (with Steel or CFRP) and SNSM (with Steel or CFRP) techniques can be competently incorporated for strengthening RC beam elements.
- Innovative SNSM technique shows better performance in terms of flexural strength, failure modes and serviceability respectively, compared to the NSM technique.

6.2 RECOMMENDATIONS

The present study illustrates the NSM and SNSM techniques for strengthening RC beams and their practical suitability. The techniques have huge potential in the future. It is expected to greatly promote their implementations. Following are the important recommendations required to be addressed for future work in this area.

a) Further investigation is needed concerning the fatigue performance of RC beams strengthened with NSM steel bars.
b) In this research, CFRP fabric was used as a U-wrap end anchorage to prevent the concrete cover separation failure. Future investigations are required to propose a design theory for the end anchorage using CFRP fabric for eliminating the concrete cover separation.
c) The behaviour of RC beams strengthened with SNSM CFRP bars under different loading conditions, such as sustained loads and freeze thaw, could be investigated.
d) Design guidelines need to be developed for the practical application of the SNSM technique.
e) In this research, the flexural behaviour of pre-cracked beams strengthened with SNSM CFRP bars was investigated. Future works are required to investigate its fatigue performance.

REFERENCES

A615/A615M-09b, A. (2009). Standard Specification for Deformed and Plain Carbon-Steel Bars for Concrete Reinforcement.

ACI Committee 440. ACI 440.2R-08 Guide for the design and construction of externally bonded frp systems for strengthening concrete structures, American Concrete Institute, Farmington Hills, MI; 2008.

Aidoo, J., Harries, K. A., & Petrou, M. F. (2006). Full-scale experimental investigation of repair of reinforced concrete interstate bridge using CFRP materials. Journal of Bridge Engineering, 11(3), 350-358.

Al-Mahmoud, F., Castel, A., François, R., & Tourneur, C. (2009). Strengthening of RC members with near-surface mounted CFRP rods. Composite Structures, 91(2), 138-147.

Al-Mahmoud, F., Castel, A., François, R., & Tourneur, C. (2010). RC beams strengthened with NSM CFRP rods and modeling of peeling-off failure. Composite Structures, 92(8), 1920-1930.

Almusallam, T. H., Elsanadedy, H. M., Al-Salloum, Y. A., & Alsayed, S. H. (2013). Experimental and numerical investigation for the flexural strengthening of RC beams using near-surface mounted steel or GFRP bars. Construction and Building Materials, 40, 145-161.

Asplund, S. O. (1949). Strengthening bridge slabs with grouted reinforcement. ACI Structural Journal , 20(4), 397-406.

Badawi, M., & Soudki, K. (2009). Flexural strengthening of RC beams with prestressed NSM CFRP rods–experimental and analytical investigation. Construction and Building Materials, 23(10), 3292-3300.

Barros, J. A. O., and Fortes, A. S. (2005). Flexural strengthening of concrete beams with CFRP laminates bonded into slits. Cement and Concrete Composites, 27(4), 471-480.

Barros, J. A. O., Ferreira, D. R. S. M., Fortes, A. S., and Dias, S. J. E. (2006). Assessing the effectiveness of embedding CFRP laminates in the near surface for structural strengthening. Construction and Building Materials, 20(7), 478-491.

Beeby, A. W., & Narayanan, R. S. (1995). Designers' Handbook to Eurocode 2: 1. Design of concrete structures: Thomas Telford.

Blaschko, M., and Zilch, K. (1999). Rehabilitation of concrete structures with CFRP strips glued into slits. In Proceedings of the 12th international conference on composite materials, ICCM12, Paris Franća, 5-9.

BS EN 12390–3:2009 Testing Hardened Concrete: Compressive Strength of Test Specimens, Milton Keynes, UK.

BS EN 12390–5:2009 Testing Hardened Concrete: Flexural Strength of Test Specimens, Milton Keynes, UK.

Capozucca, R. (2009). Static and dynamic response of damaged RC beams strengthened with NSM CFRP rods. Composite Structures, 91(3), 237-248.

Capozucca, R. (2014). On the strengthening of RC beams with near surface mounted GFRP rods. Composite Structures, 117, 143-155.

Ceroni, F. (2010). Experimental performances of RC beams strengthened with FRP materials. Construction and Building Materials, 24(9), 1547-1559.

Choi, H. T., West, J. S., & Soudki, K. A. (2011). Partially bonded near-surface-mounted CFRP bars for strengthened concrete T-beams. Construction and Building Materials, 25(5), 2441-2449.

Committee, A., Institute, A. C., & Standardization, I. O. f. (2008). Building Code Requirements for Structural Concrete (ACI 318-08) and Commentary.

Costa, I. G., & Barros, J. A. (2010). Flexural and shear strengthening of RC beams with composite materials–The influence of cutting steel stirrups to install CFRP strips. Cement and Concrete Composites, 32(7), 544-553.

De Lorenzis, L., & Nanni, A. (2002). Bond between near-surface mounted fiber-reinforced polymer rods and concrete in structural strengthening. ACI structural Journal, 99(2), 123-132.

De Lorenzis L., Nanni A., and Tegda, La. (2000). Flexure and shear strengthening of reinforced concrete structures with near surface mounted FRP rods, Proceedings of the 3rd International Conference on Advanced Composite Materials in Bridges and Structures (ACMBS 2000) Canadian Society for Civil Engineering, Ottawa. 521-528.

De Lorenzis, L., & Teng, J. (2007). Near-surface mounted FRP reinforcement: An emerging technique for strengthening structures. Composites Part B: Engineering, 38(2), 119-143.

Eberline, D. K., Klaiber, F. W., & Dunker, K. F. (1988). Bridge strengthening with epoxy-bonded steel plates. Transport Research Record, 1180, 7-11.

El-Hacha R., Filho D. S., Melo G.S., and Rizkalla S.H. (2004). Effectiveness of near surface mounted frp reinforcement for flexural strengthening of reinforcedconcrete beams. Proceedings of the 4th International Conference on Advanced Composite Materials in Bridges and Structures (ACMBS 2004), Calgary, Ontario, Canada.

El-Hacha, R., & Gaafar, M. (2011). Flexural strengthening of reinforced concrete beams using prestressed, near-surfacemounted CFRP bars. PCI journal, 56(4), 134-151.

El-Hacha, R., and Rizkalla, S. H. (2004). Near-surface-mounted fiber-reinforced polymer reinforcements for flexural strengthening of concrete structures. ACI Structural Journal, 101(5), 717-726., 101(5), 717-726.

El-Mihilmy, M. T., & Tedesco, J. W. (2001). Prediction of anchorage failure for reinforced concrete beams strengthened with fiber-reinforced polymer plates. ACI Structural Journal, 98(3), 301-314.

Garrity, S. W. (2001). Near-surface reinforcement of masonry arch highway bridges. In Proceedings 9th Canadian Masonry Symposium, Fredericton (Canada).

Gentile, C., and Rizkalla, S. (1999). Flexural strengthening of timber beams using FRP. Technical Progress Report, ISIS Canada, University of Manitoba, Winnipeg.

Hassan, T., and Rizkalla, S. (2002). Flexural strengthening of prestressed bridge slabs with FRP systems. PCI journal, 47(1), 76-93.

Jung, W. T., Park, Y. H., Park, J. S., Kang, J. Y., & You, Y. J. (2006). Experimental investigation on flexural behavior of rc beams strengthened by NSM CFRP reinforcements. American Concrete Institute (ACI), Special Publication, SP-230-40.

Kalayci, A. S., Yalim, B., & Mirmiran, A. (2010). Construction tolerances and design parameters for NSM FRP reinforcement in concrete beams. Construction and Building Materials, 24(10), 1821-1829.

Kang, J. Y., Park, Y. H., Park, J. S., You, Y. J., & Jung, W. T. (2006). Analytical evaluation of RC beams strengthened with near surface mounted CFRP laminates,. American ConcreteInstitute (ACI), Special Publication,, SP-230-45.

Kishi, N., Mikami, H., Kurihashi, Y. and Sawada, S. (2005) Flexural behaviour of RC beams reinforced with NSM AFRP rods", Proceeding of the International Symposium on Bond Behaviour of FRP in structures (BBFS 2005), Hong Kong. 337-342.

MacDonald, M., & Calder, A. (1982). Bonded steel plating for strengthening concrete structures. International Journal of Adhesion and Adhesives, 2(2), 119-127.

Neville, A. M., & Brooks, J. J. (1987). Concrete technology: Longman Scientific & Technical Harlow.

Nordin, H., Taljsten, B., and Carolin, A. (2001). Concrete beams strengthened with prestressed near surface mounted reinforcement,. Paper presented at the Proceedings of the International Conference on FRP Composites in Civil Engineering, Hong Kong, China.

Nordin, H., & Täljsten, B. (2006). Concrete beams strengthened with prestressed near surface mounted CFRP. Journal of Composites for Construction, 10(1), 60-68.

Rasheed, H. A., Harrison, R. R., Peterman, R. J., & Alkhrdaji, T. (2010). Ductile strengthening using externally bonded and near surface mounted composite systems. Composite Structures, 92(10), 2379-2390.

Rethnasamy, C., Rajagopal, T., & Muthuraj, H. (2013). Bending behavior, deformability and strength analysis of Prefabricated Cage Reinforced Composite beams. Construction and Building Materials, 38, 482-490.

Rosenboom, O. A., Hassan, T. K., Mirmiran, A., and Rizkalla, S. (2004). Static and fatigue performance of 40 year old prestressed concrete girders strengthened with various CFRP systems. Paper presented at the Proceedings of the 2nd International Conference on FRP Composite in Civil Engineering (CICE 2004), Adelaide, Australia.

Sharaky, I. A., Torres, L., Comas, J., & Barris, C. (2014). Flexural response of reinforced concrete (RC) beams strengthened with near surface mounted (NSM) fibre reinforced polymer (FRP) bars. Composite Structures, 109, 8-22.

Sikadur®-30. Product data sheet-adhesive for bonding reinforcement. Edition: 2014-01_1.Retrieved June 02, 2014, from: http://mys.sika.com/en/solutions_products/02/02a013/02a013sa06/02a013sa06100/02a013sa06105.html

Sikadur®-330, product data sheet, 2-part epoxy impregnation resin [Edition 2012-05_1], Retrieved December 05, 2013, from: http://mys.sika.com/en/solutions_products-old/02/02a013/02a013sa06/02a013sa06100/02a013sa06105.html

SikaWrap®-301 C, product data sheet, unidirectional woven carbon fibre fabric for structural strengthening [Edition 2010-12_1], Retrieved December 02, 2013, from:http://mys.sika.com/en/solutions_products-old/02/02a013/02a013sa06/02a013sa06100/02a013sa06103.html

Smith, S. T., & Teng, J. G. (2002). FRP-strengthened RC beams. I: review of debonding strength models. Engineering Structures, 24(4), 385-395.

Soliman, S. M., El-Salakawy, E., & Benmokrane, B. (2010). Flexural behaviour of concrete beams strengthened with near surface mounted fibre reinforced polymer bars. Canadian Journal of Civil Engineering, 37(10), 1371-1382.

Tang, W. C., Balendran, R. V., Nadeem, A., & Leung, H. Y. (2006). Flexural strengthening of reinforced lightweight polystyrene aggregate concrete beams with near-surface mounted GFRP bars. Building and environment, 41(10), 1381-1393.

Yost, J. R., Gross, S. P., and Dinehart, D. W. (2004). Near surface mounted CFRP reinforcement for structural retrofit of concrete flexural members. Paper presented at the proceedings of the 4th international conference on Advanced Composite Materials in Bridges and Structures (ACMBS 2004), Calgary, Alberta, Canada.

APPENDICES

APPENDIX A – CONCRETE MIX DESIGN FOR RC BEAM

The concrete mix was prepared according to the DOE method.

Table A1:

Properties of materials	Values/Types
Coarse aggregate	crushed granite
Fina aggregate	river sand
Cement	Ordinary Portland Cement (OPC)
Maximum size of coarse aggregate (C. A.)	20 mm
The specific gravity of coarse aggregate	2.95
The maximum deflective level of C. A.	5.00
The water absorption capacity of C. A.	0.65%
The specific gravity of fine aggregate (F. A.)	2.59
The percentage of F. A. retained on 600 sieve	39%
The water absorption capacity of F. A.	0.95%
The specific strength of the concrete	27 MPa
The standard deviation	8.00

Step-wise procedures of mix design

Step - 1: Calculate the target mean strength

Target mean strength = specified strength + standard deviation x risk factor

= 27 + 8 x 1.64

= 40 MPa

Step - 2: Find the water/cement ratio

The free water/cement ratio of 40 MPa concrete is 0.50

Step - 3: Estimate the water content

The slump of concrete 60 mm

Therefore, the water content = 210 kg/m^3

Step - 4: Compute the cement content

The cement content = $\frac{210}{0.50}$ = 420 kg/m^3

Step - 5: Find the total aggregate content

The wet density of concrete = 2425 kg/m^3

Thus, the total weight of aggregate = 2425 – 210 – 420

= 1795 kg/m^3

Step - 6: Find the percentage of F. A.

The grading zone of fine aggregate 2

Hence, the proportion of F. A. = 50%

Step - 7: Calculate quantities of materials

The weight of F. A. = 1795 x $\frac{50}{100}$

= 897.50 kg/m^3

The weight of C.A. = 1795 – 897.50

= 897.50 kg/m^3

The weight of cement = 420 kg/m^3

The weight of water = 210 kg/m^3

Step - 8: Adjustment for field condition

The water absorbed by F.A. = 897.50 x $\frac{0.95}{100}$

= 8.53 kg/m3

The weight of F. A. in field conditions = 897.50 – 8.53

= 889 kg/m^3

The water absorbed by CA = 897.50 x $\frac{0.65}{100}$

= 5.83 kg/m^3

The weight of C. A. in field conditions = 897.50 – 5.83

= 892 kg/m^3

The total weight of water = 210 + 8.53 + 5.83

= 224 kg/m^3

APPENDIX B – VERIFICATION OF LOAD-DEFLECTION DIAGRAMS

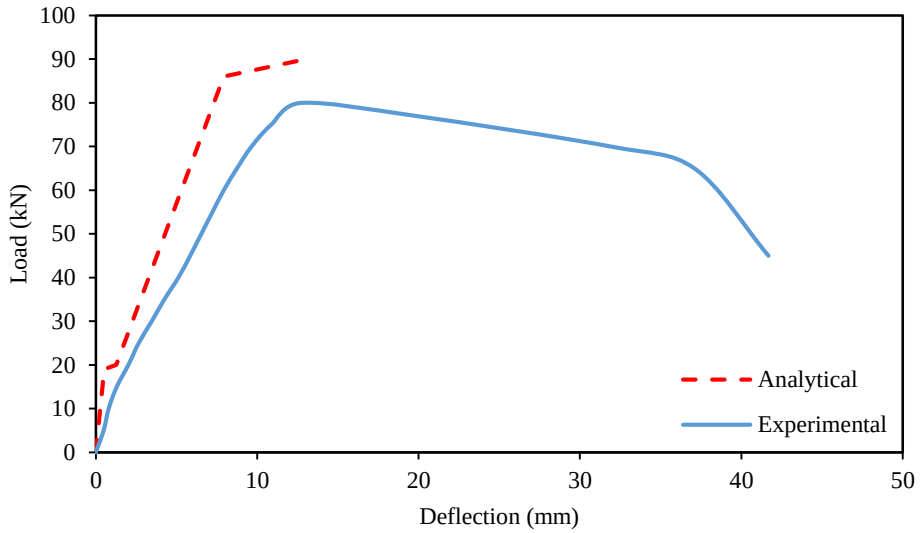

Figure B.1: Experimental and predicted load-deflection curve (N1S6)

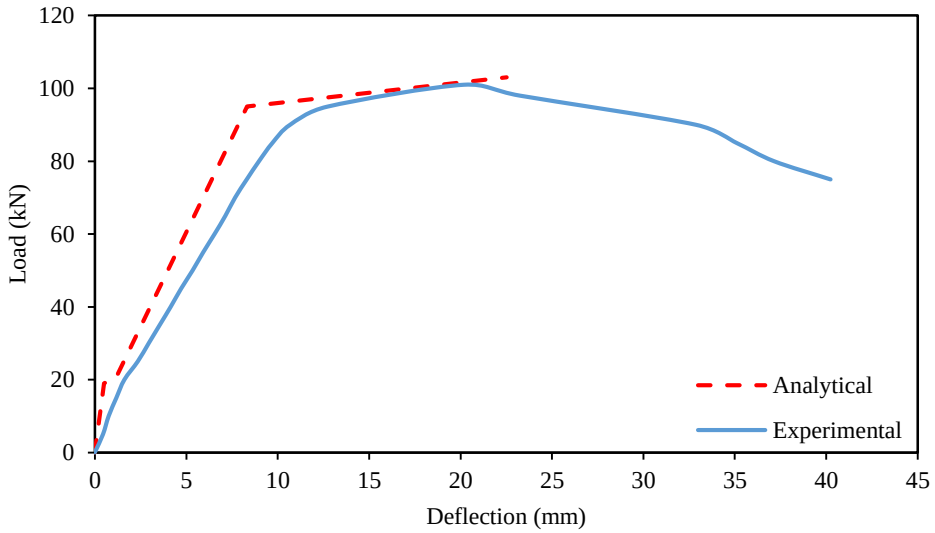

Figure B.2: Experimental and predicted load-deflection curve (N1S8)

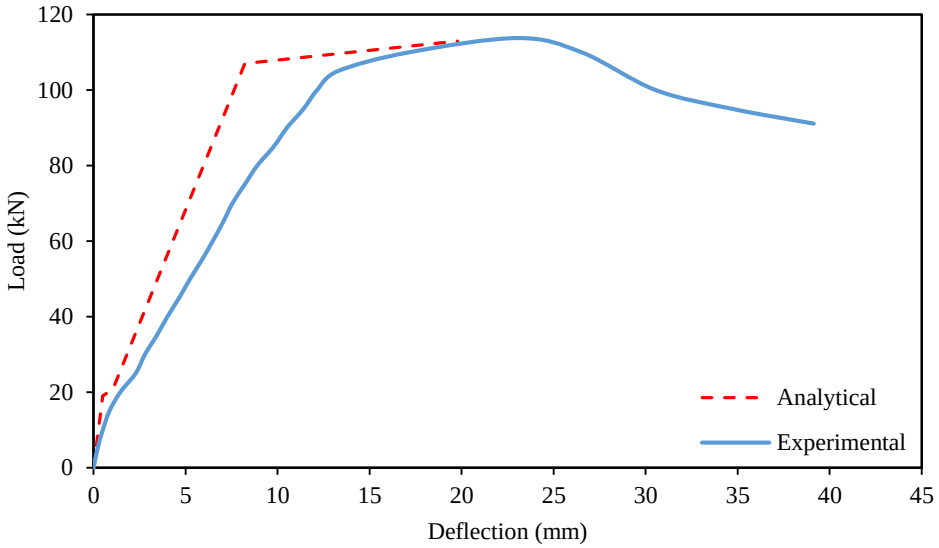

Figure B.3: Experimental and predicted load-deflection curve (N1S10)

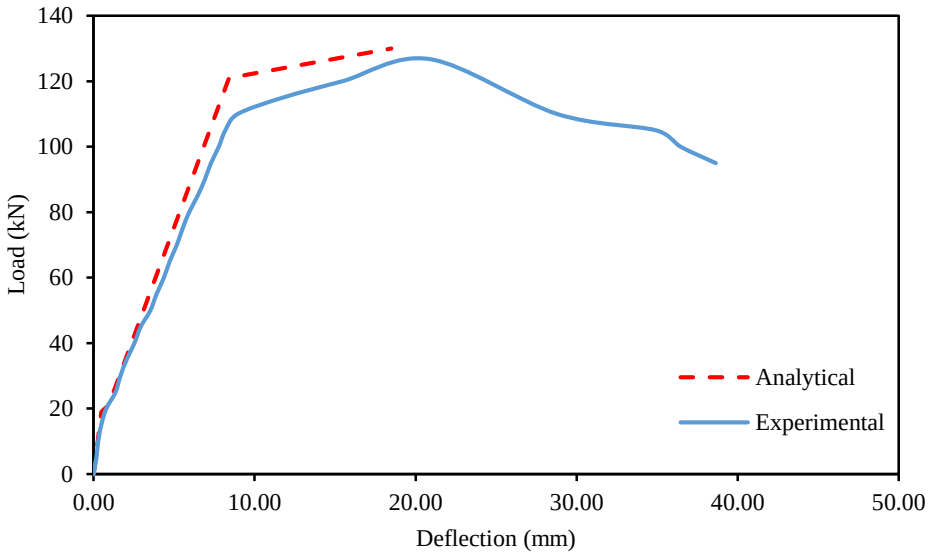

Figure B.4: Experimental and predicted load-deflection curve (N1S12)

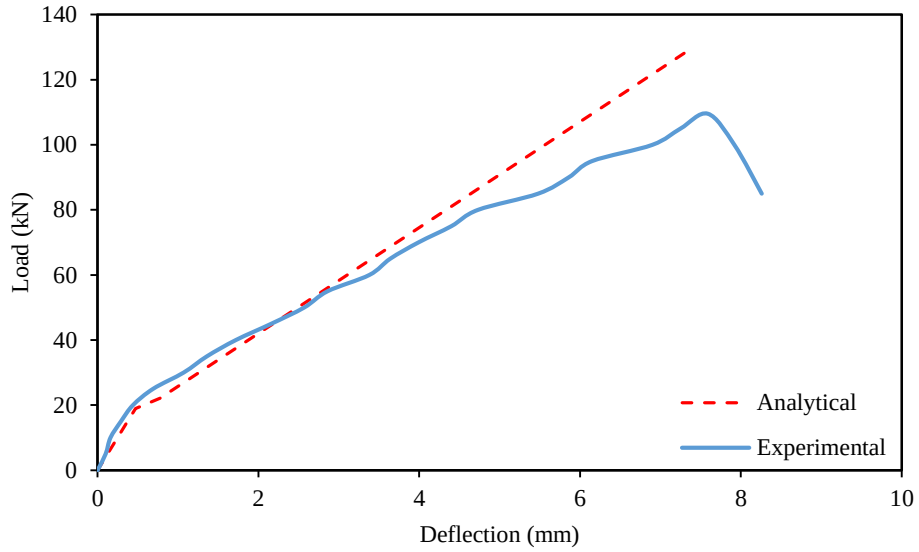

Figure B.5: Experimental and predicted load-deflection curve (N1S16)

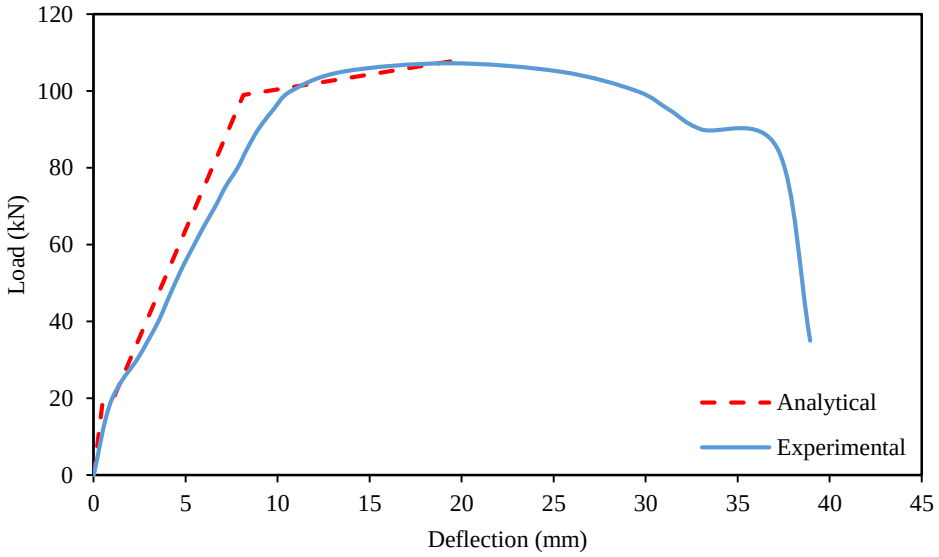

Figure B.6: Experimental and predicted load-deflection curve (N2S6)

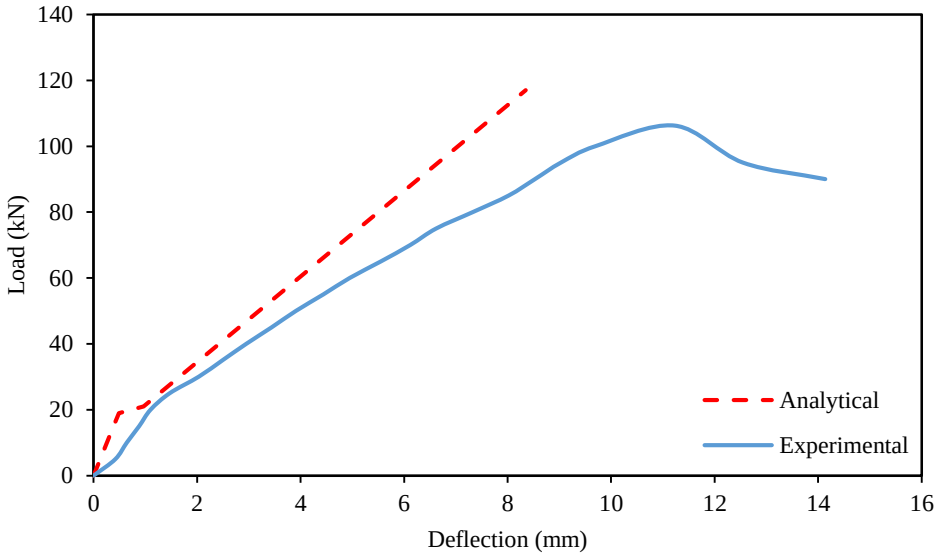

Figure B.7: Experimental and predicted load-deflection curve (N2S8)

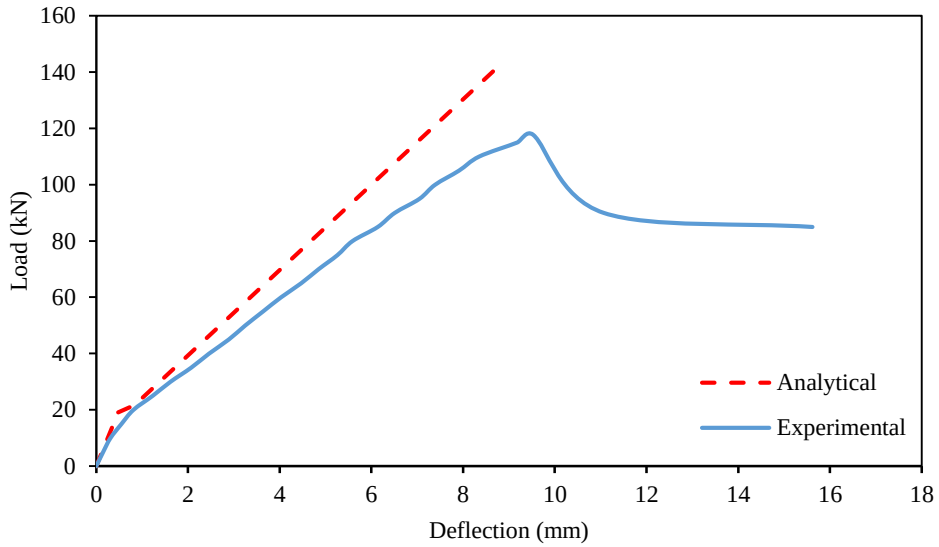

Figure B.8: Experimental and predicted load-deflection curve (N2S10)

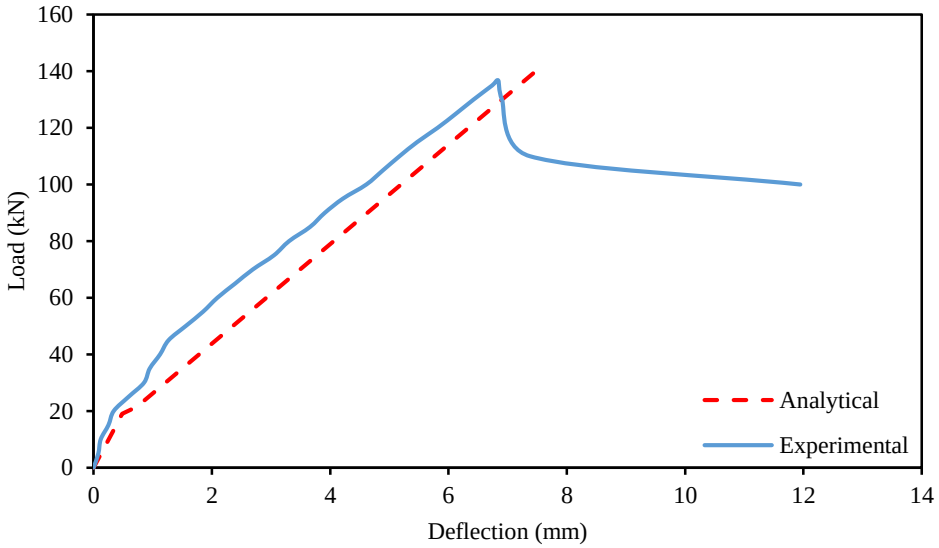

Figure B.9: Experimental and predicted load-deflection curve (N2S12)

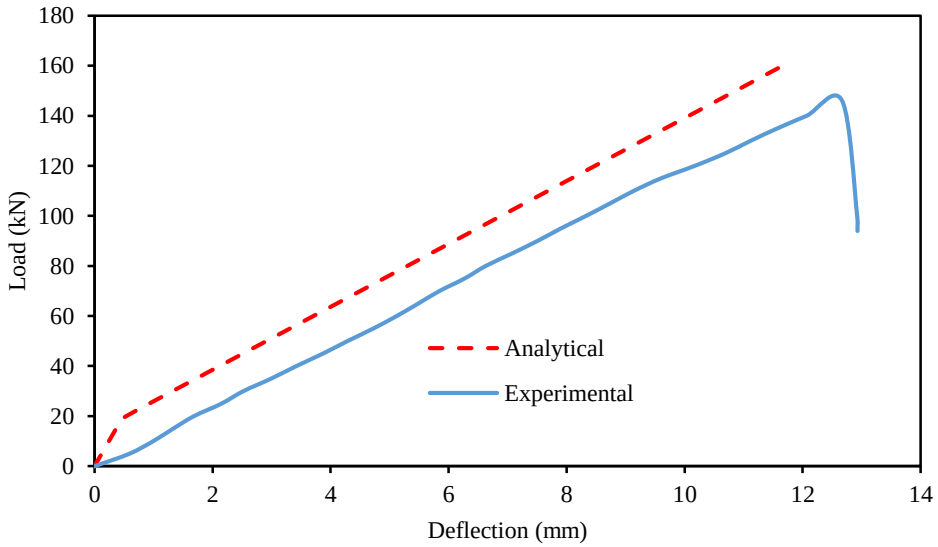

Figure B.10: Experimental and predicted load-deflection curve (N2C12)

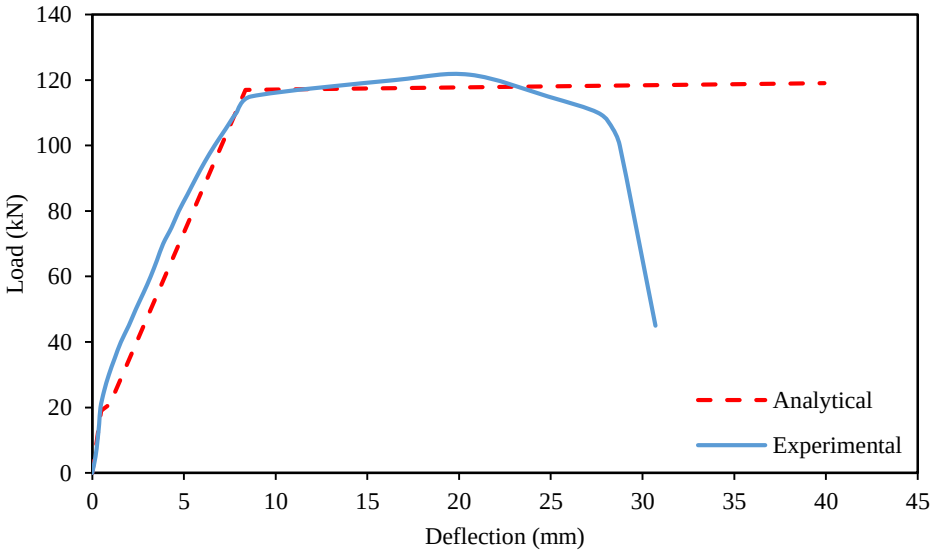

Figure B.11: Experimental and predicted load-deflection curve (N2S8U3)

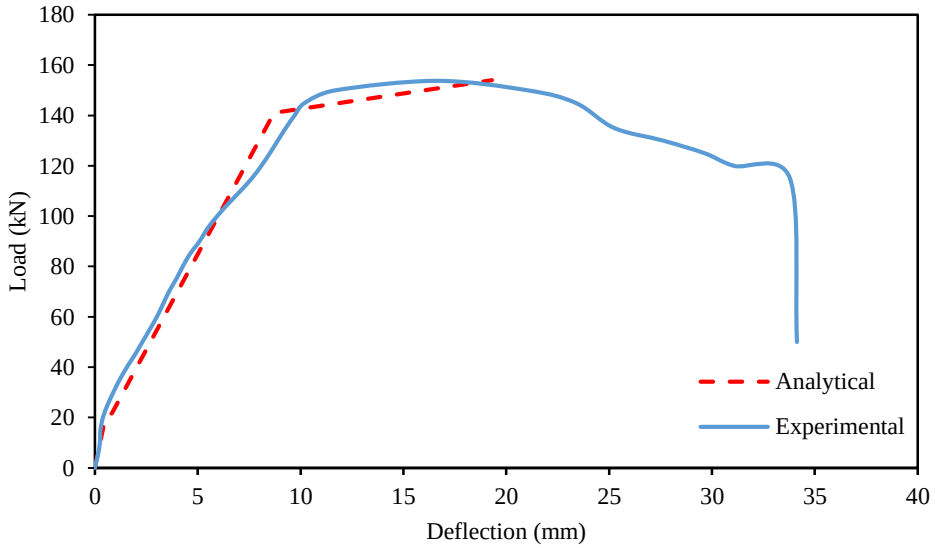

Figure B.12: Experimental and predicted load-deflection curve (N2S10U3)

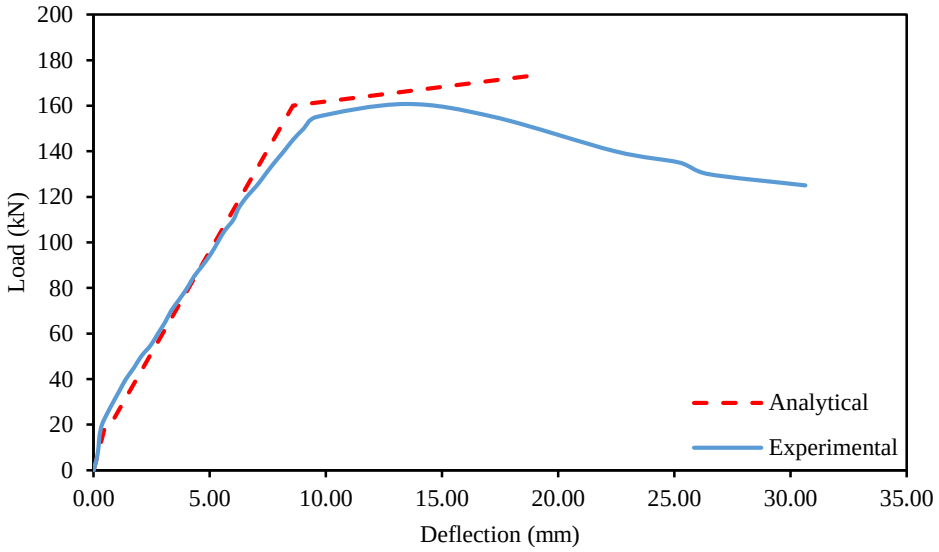

Figure B.13: Experimental and predicted load-deflection curve (N2S12U3)

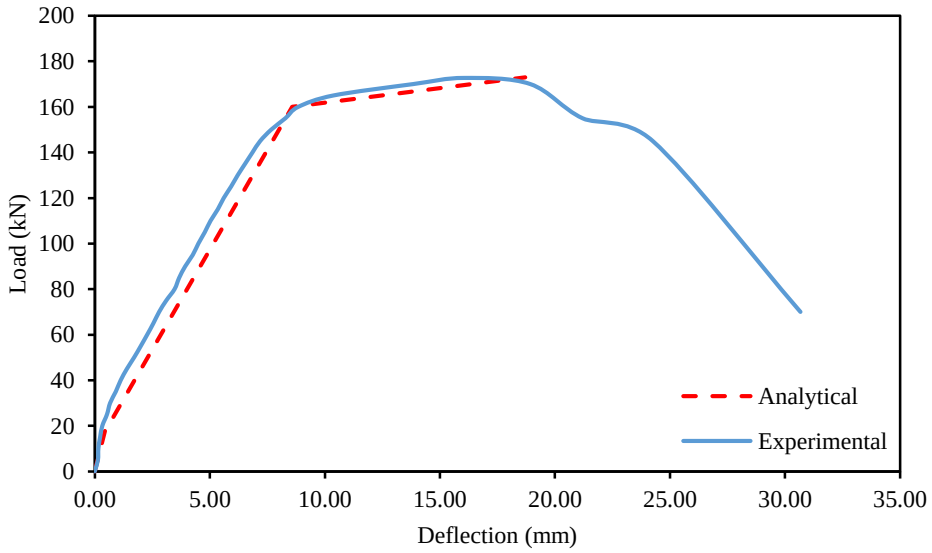

Figure B.14: Experimental and predicted load-deflection curve (N2S12U4)

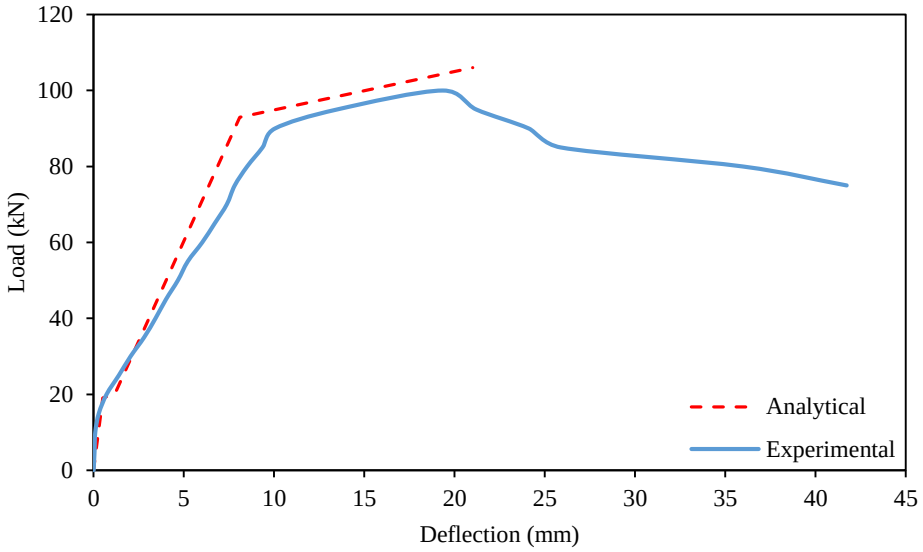

Figure B.15: Experimental and predicted load-deflection curve (SN2S6)

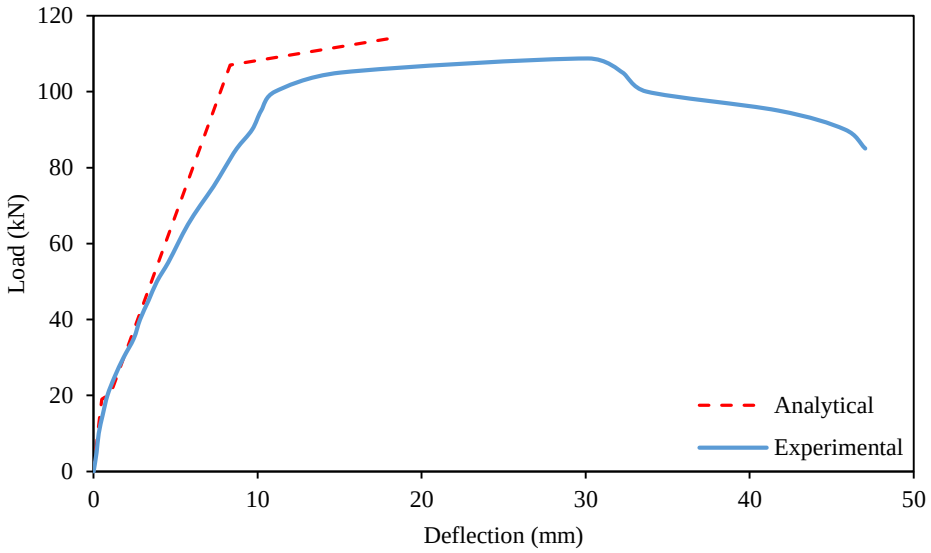

Figure B.16: Experimental and predicted load-deflection curve (SN2S8)

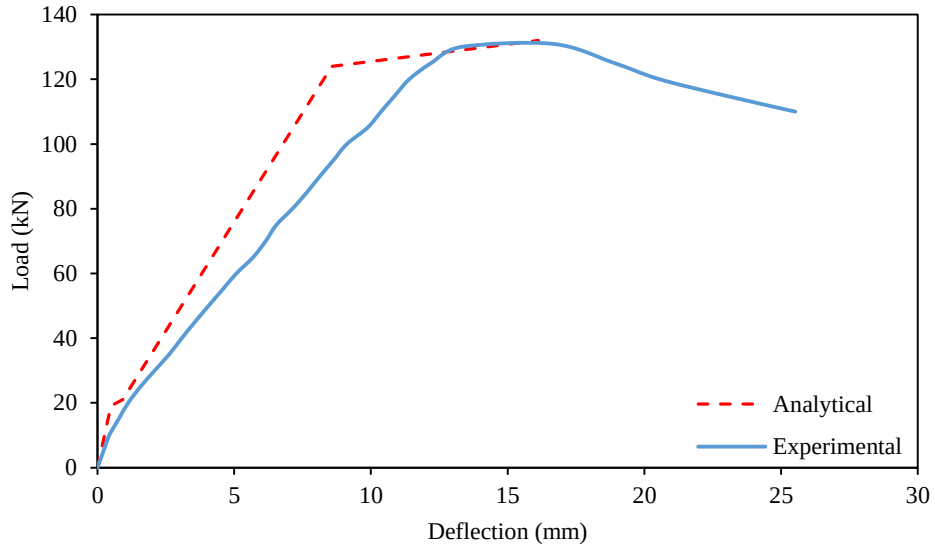

Figure B.17: Experimental and predicted load-deflection curve (SN2S10)

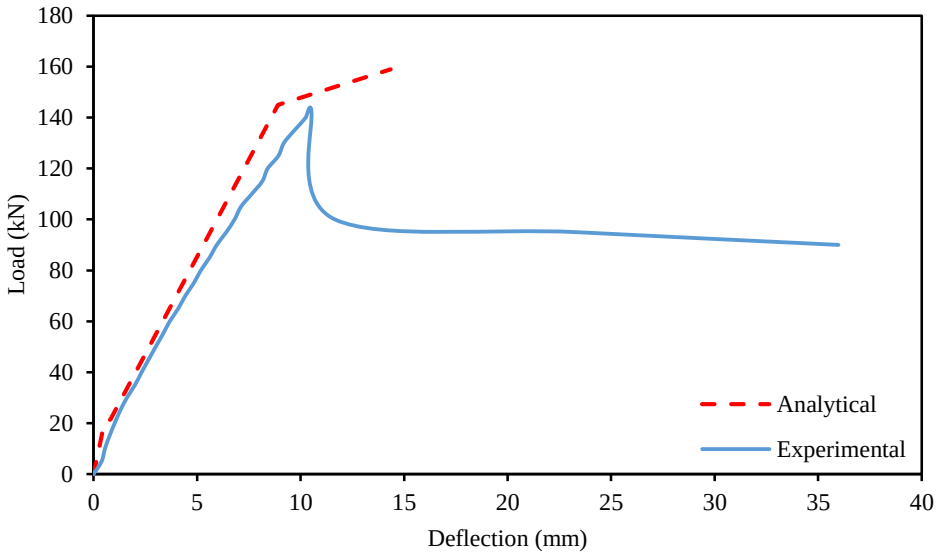

Figure B.18: Experimental and predicted load-deflection curve (SN2S12)

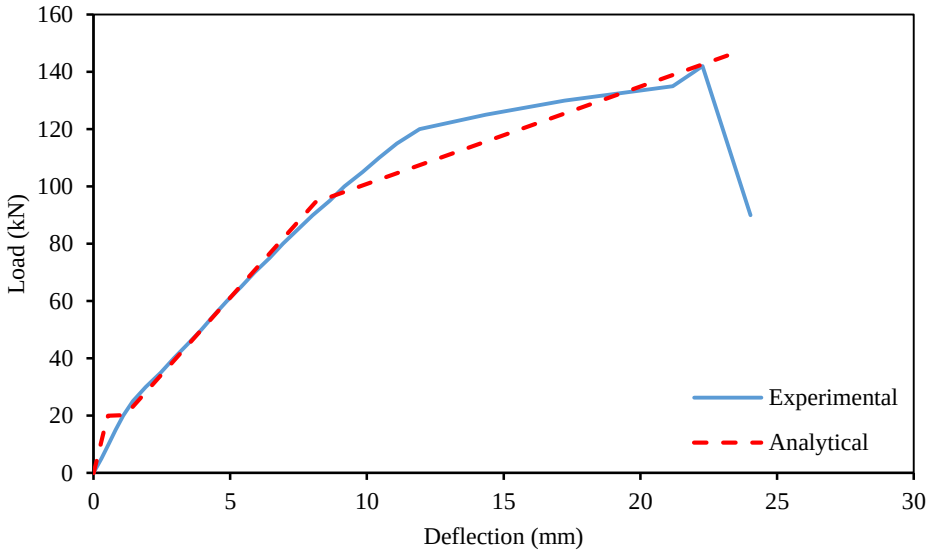

Figure B.19: Experimental and predicted load-deflection curve (SN2C8)

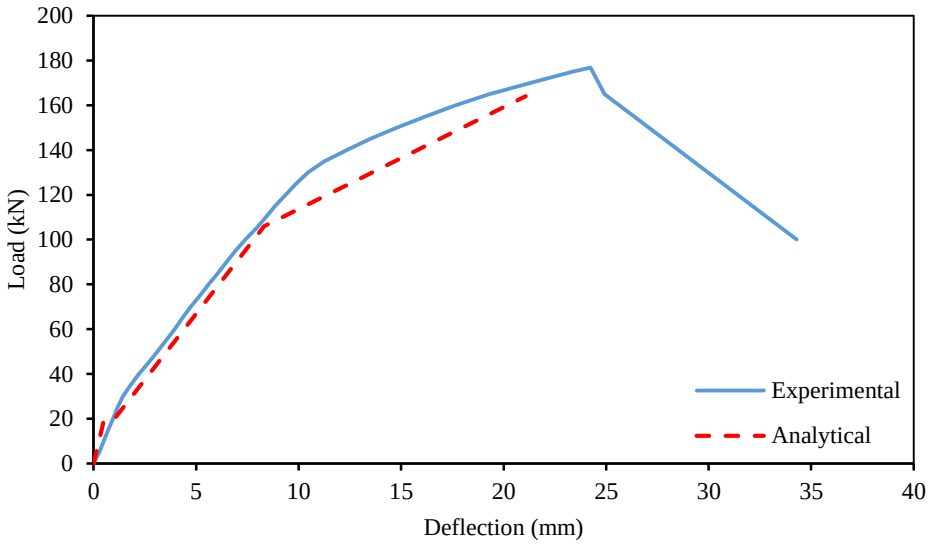

Figure B.20: Experimental and predicted load-deflection curve (SN2C10)

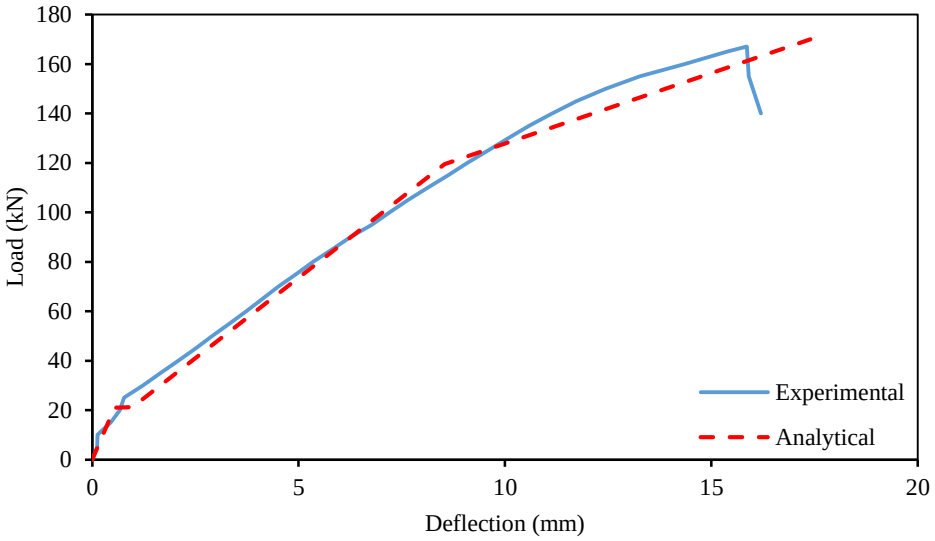

Figure B.21: Experimental and predicted load-deflection curve (SN2C12)

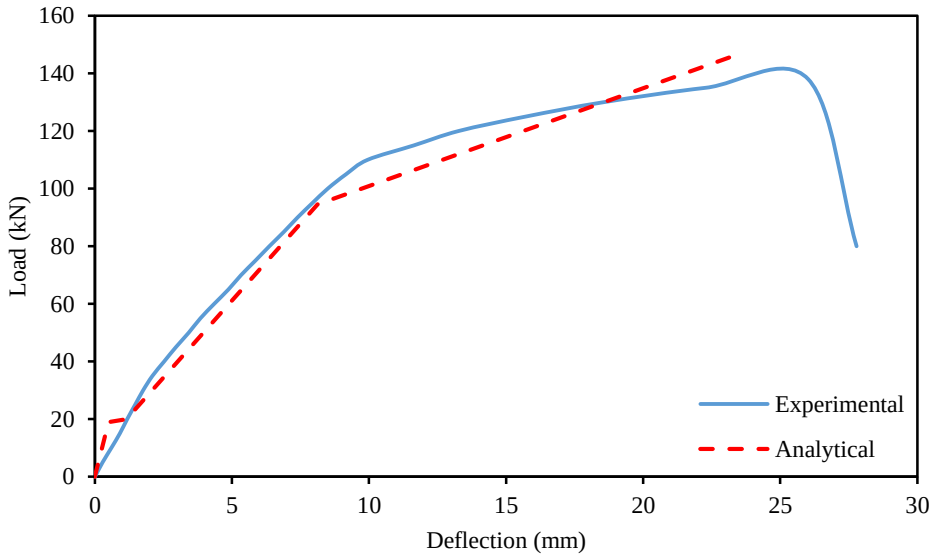

Figure B.22: Experimental and predicted load-deflection curve (PSN2C8)

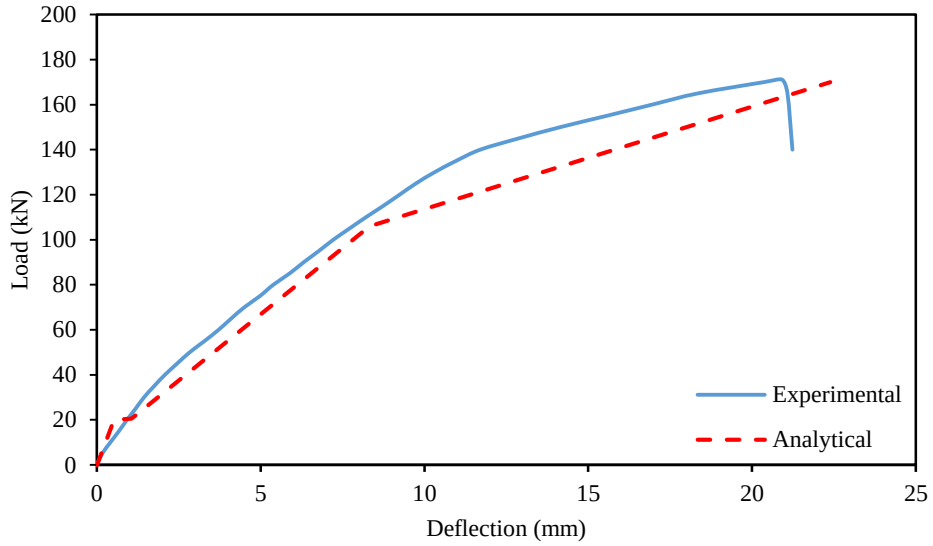

Figure B.23: Experimental and predicted load-deflection curve (PSN2C10)

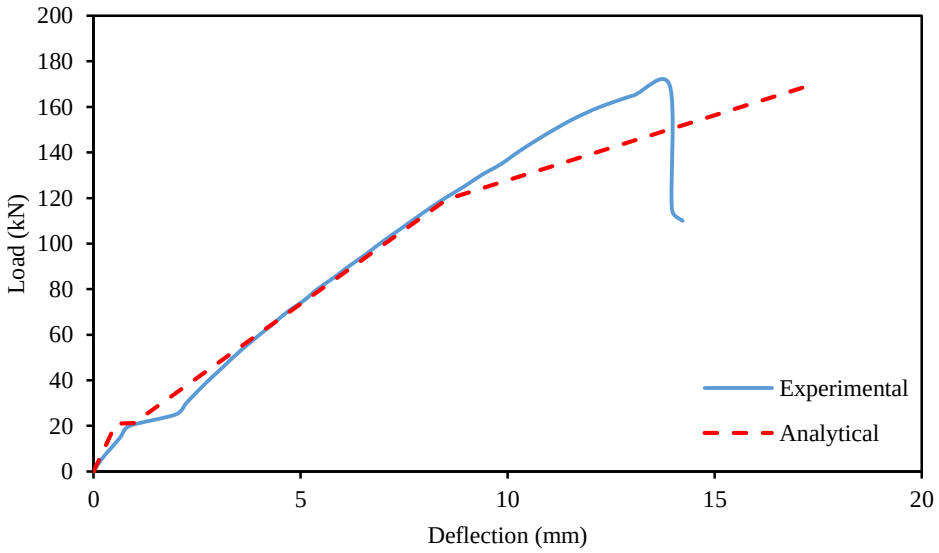

Figure B.24: Experimental and predicted load-deflection curve (PSN2C12)

APPENDIX C – VERIFICATION OF CONCRETE COMPRESSIVE STRAIN DIAGRAMS

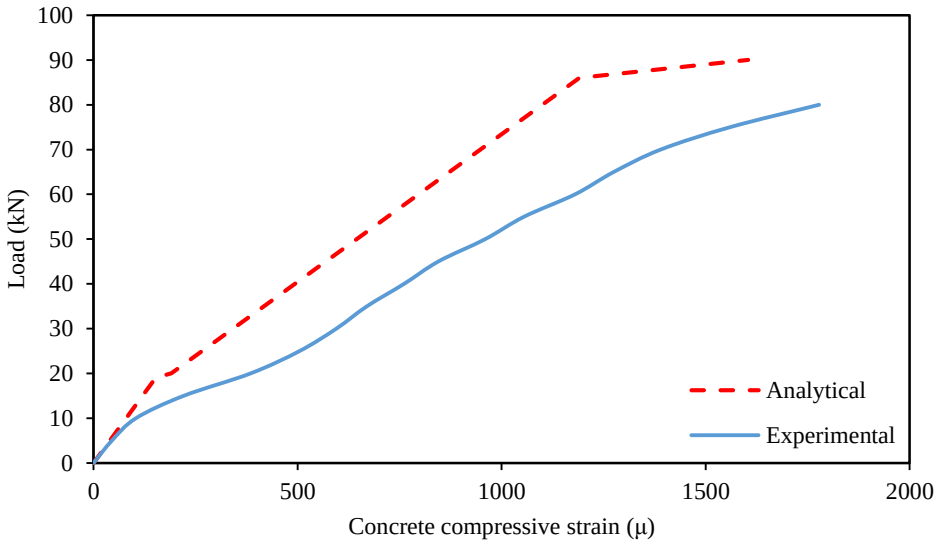

Figure C.1: Experimental and predicted load-concrete compressive strain curve (N1S6)

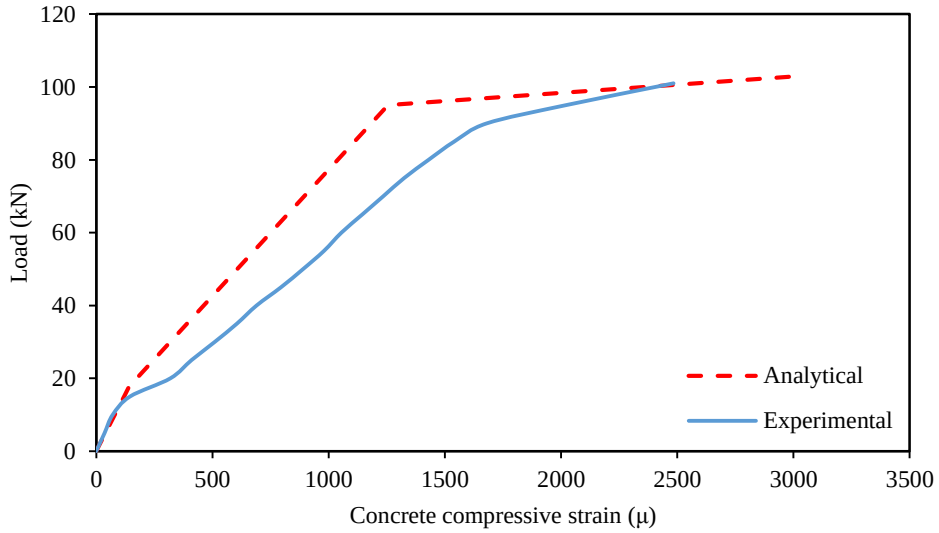

Figure C.2: Experimental and predicted load-concrete compressive strain curve (N1S8)

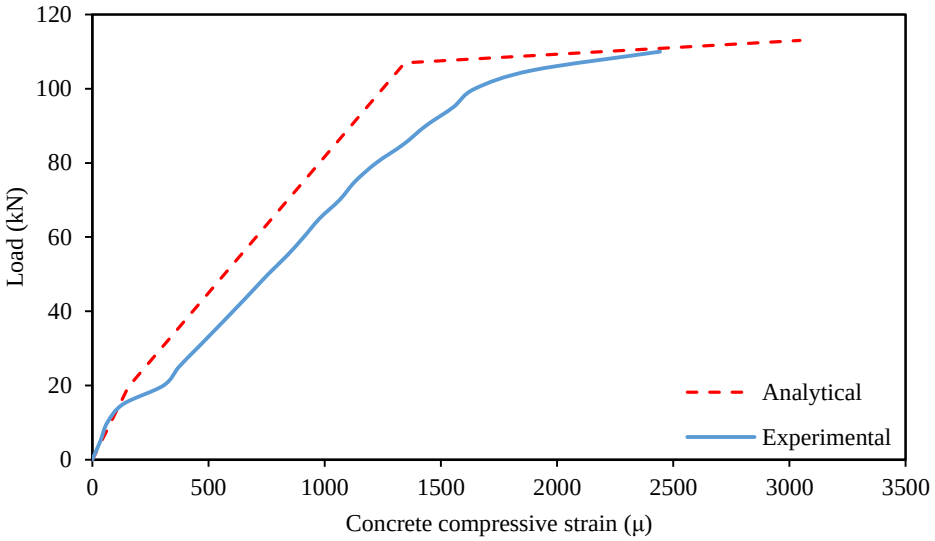

Figure C.3: Experimental and predicted load-concrete compressive strain curve (N1S10)

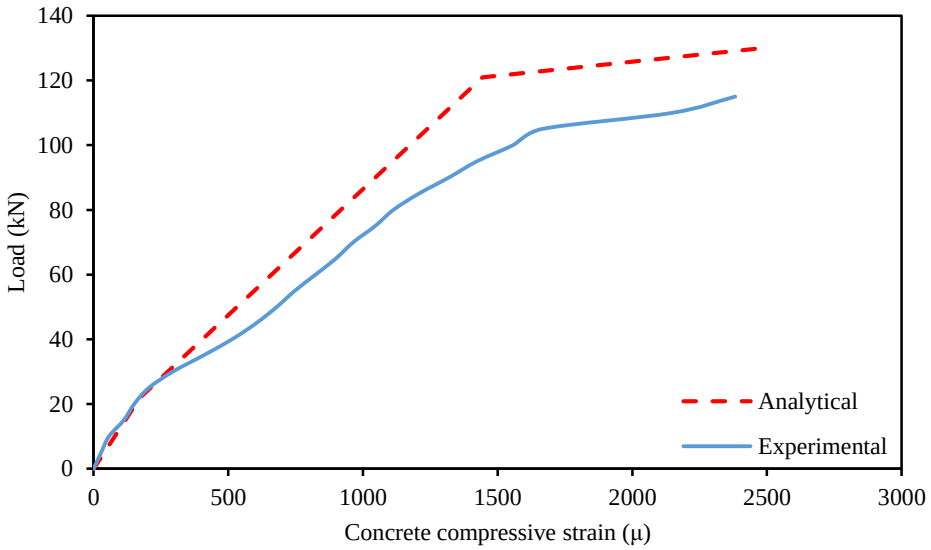

Figure C.4: Experimental and predicted load-concrete compressive strain curve (N1S12)

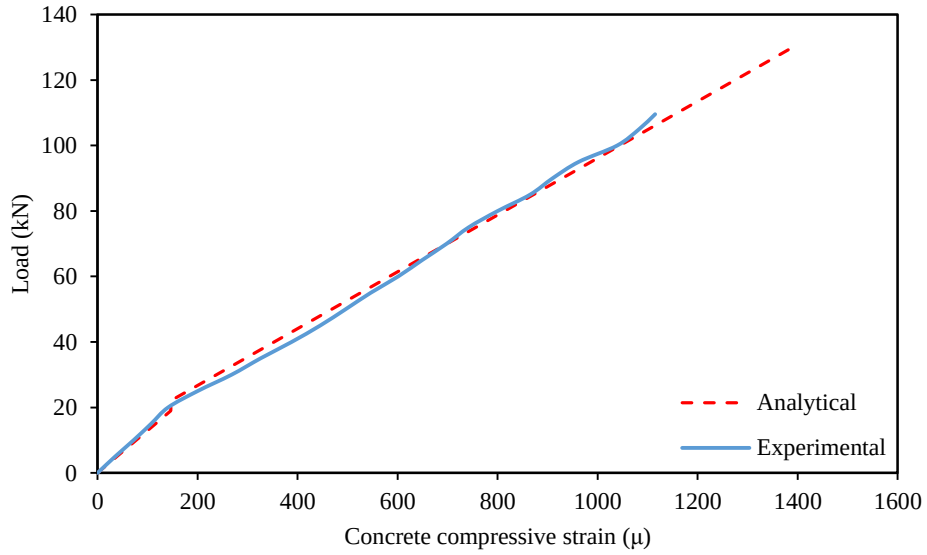

Figure C.5: Experimental and predicted load-concrete compressive strain curve (N1S16)

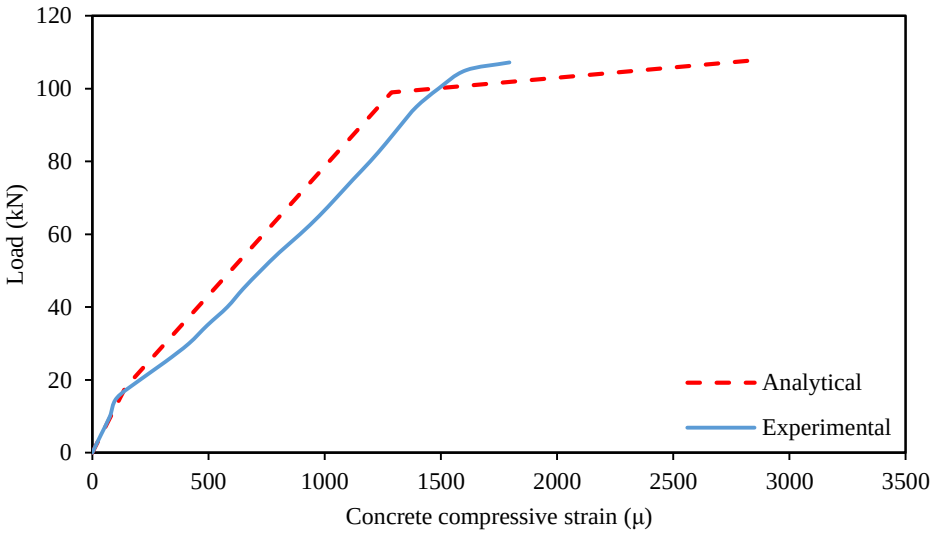

Figure C.6: Experimental and predicted load-concrete compressive strain curve (N2S6)

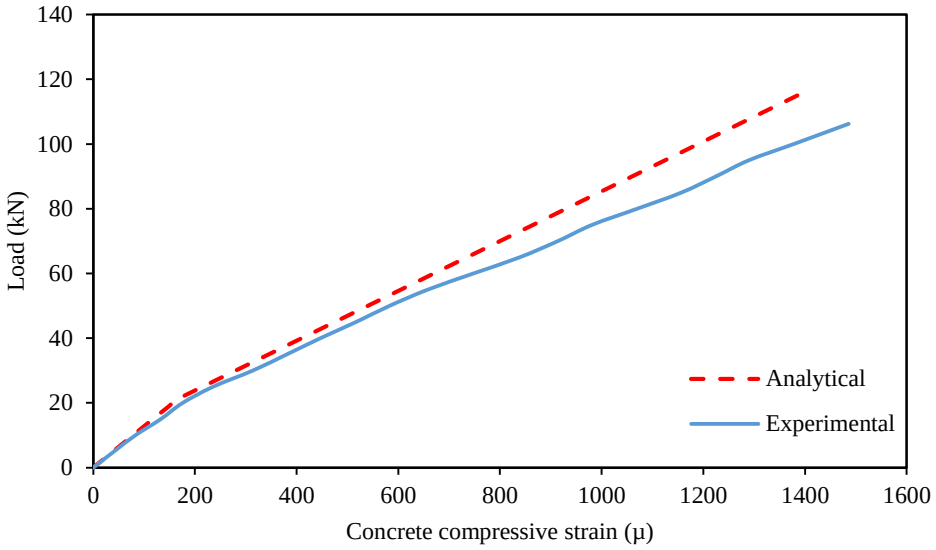

Figure C.7: Experimental and predicted load-concrete compressive strain curve (N2S8)

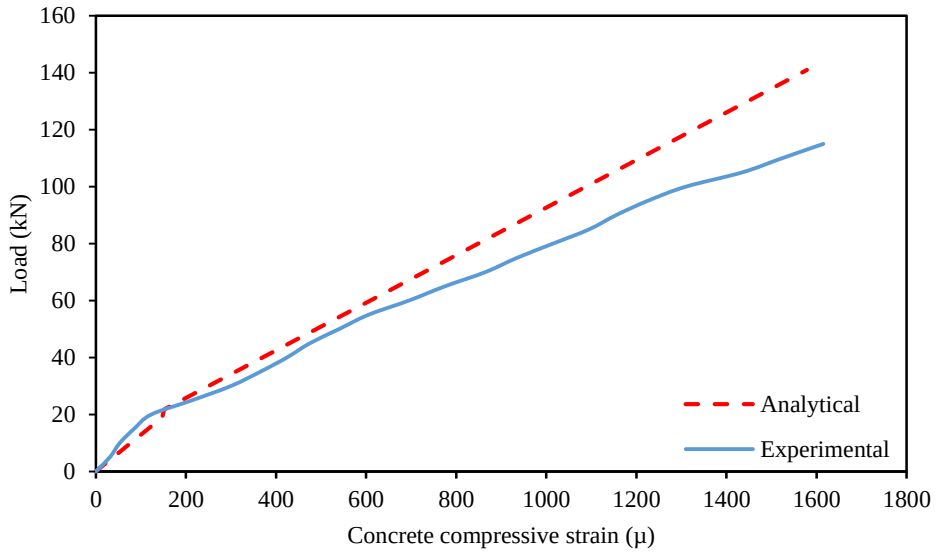

Figure C.8: Experimental and predicted load-concrete compressive strain curve (N2S10)

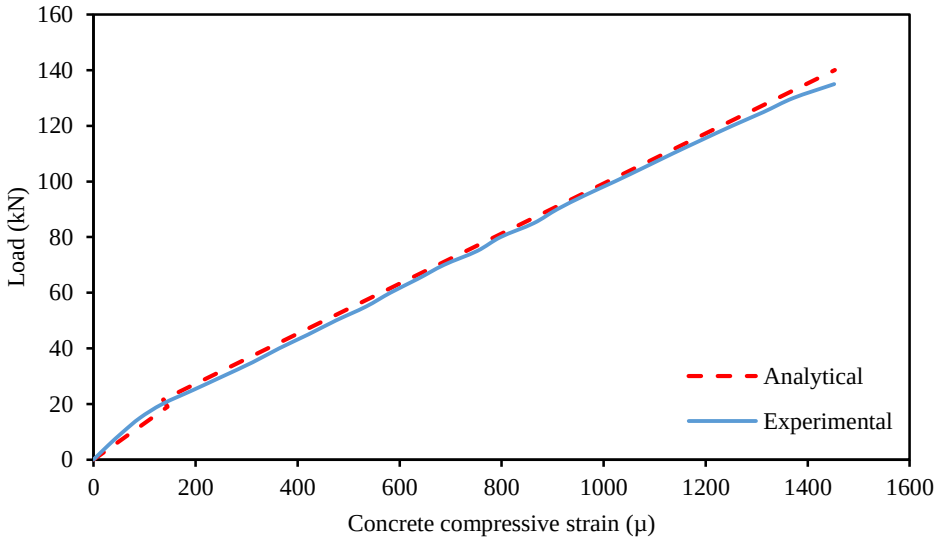

Figure C.9: Experimental and predicted load-concrete compressive strain curve (N2S12)

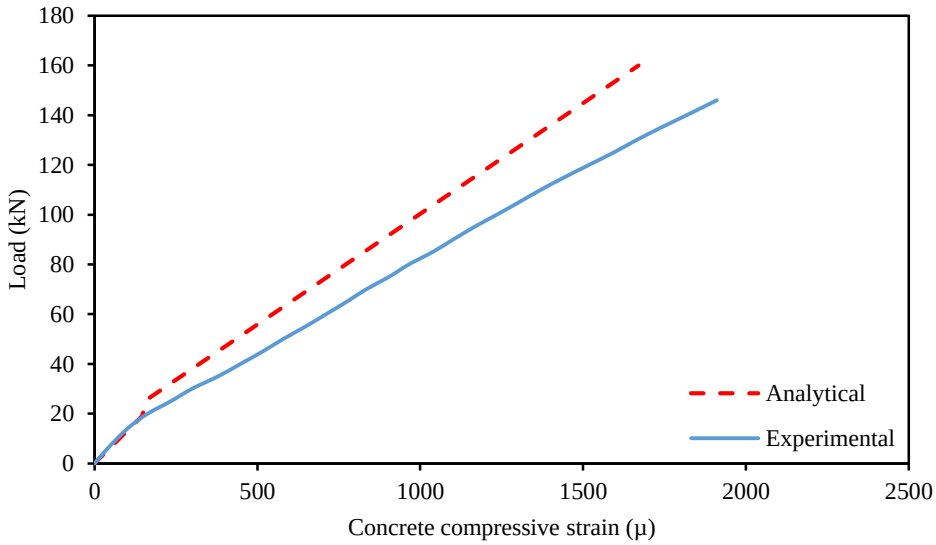

Figure C.10: Experimental and predicted load-concrete compressive strain curve (N2C12)

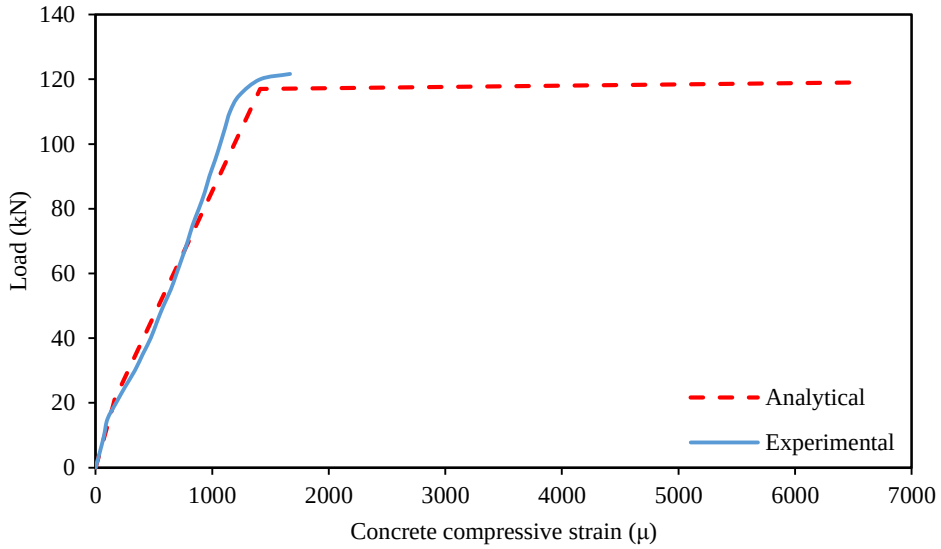

Figure C.11: Experimental and predicted load-concrete compressive strain curve (N2S8U3)

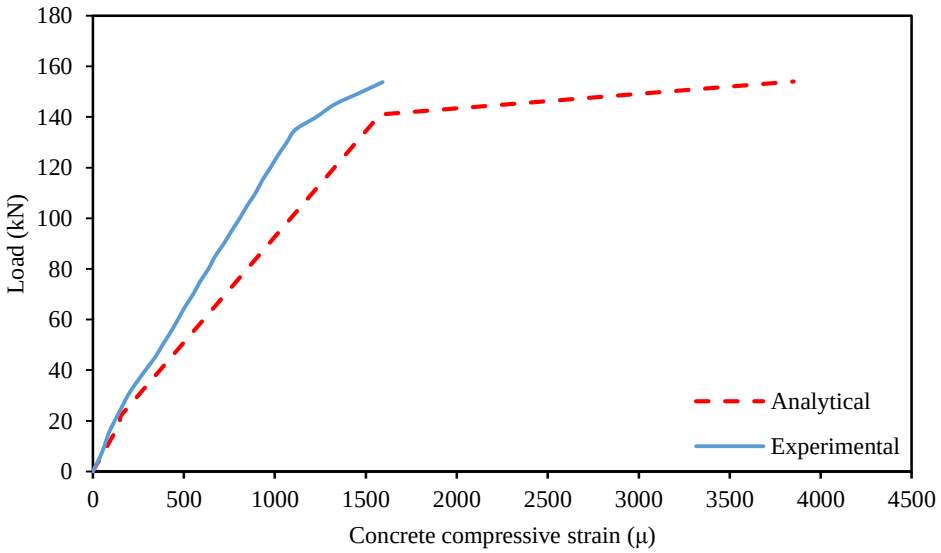

Figure C.12: Experimental and predicted load-concrete compressive strain curve N2S10U3

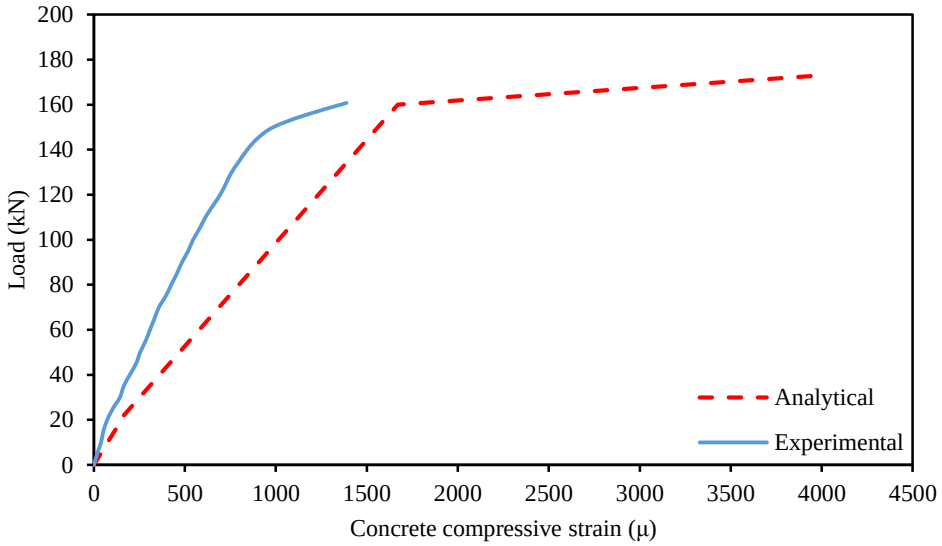

Figure C.13: Experimental and predicted load-concrete compressive strain curve N2S12U3

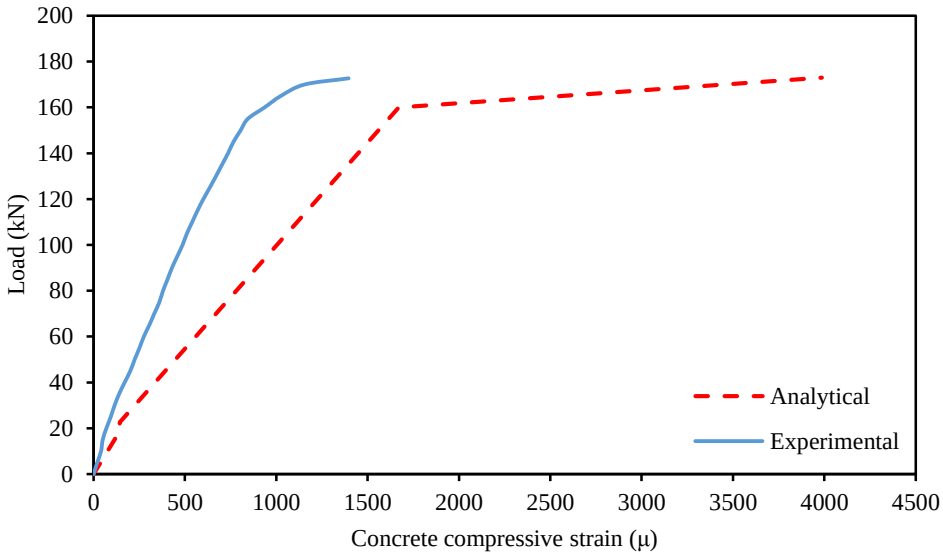

Figure C.14: Experimental and predicted load-concrete compressive strain curve (N2S12U4)

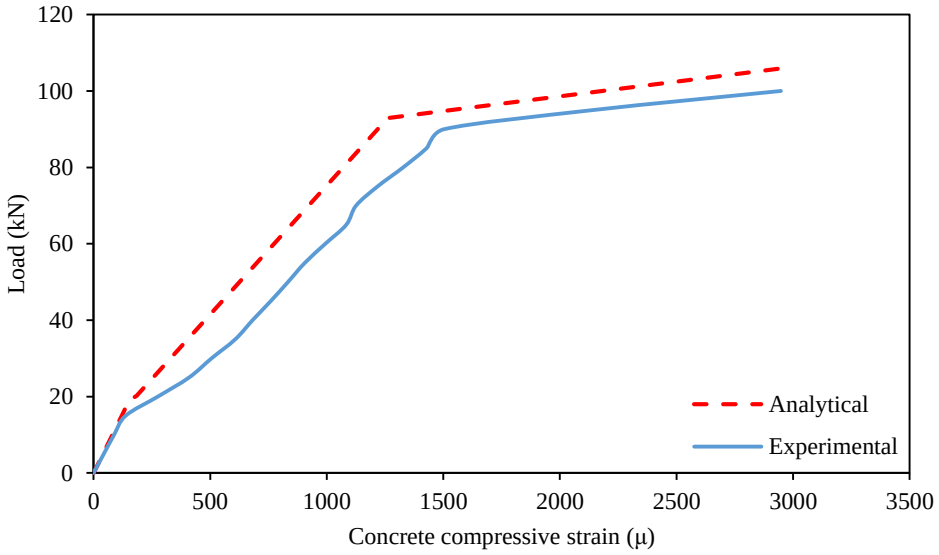

Figure C.15: Experimental and predicted load-concrete compressive strain curve (SN2S6)

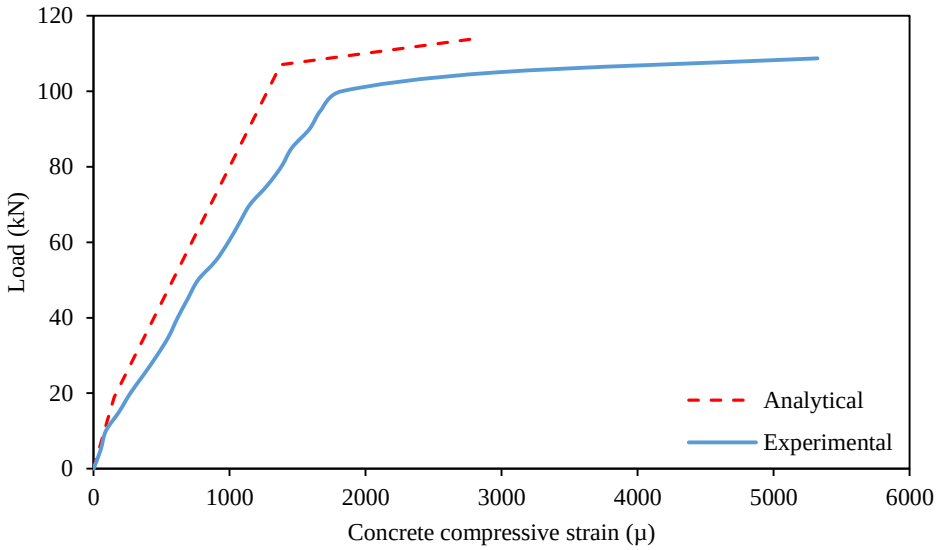

Figure C.16: Experimental and predicted load-concrete compressive strain curve (SN2S8)

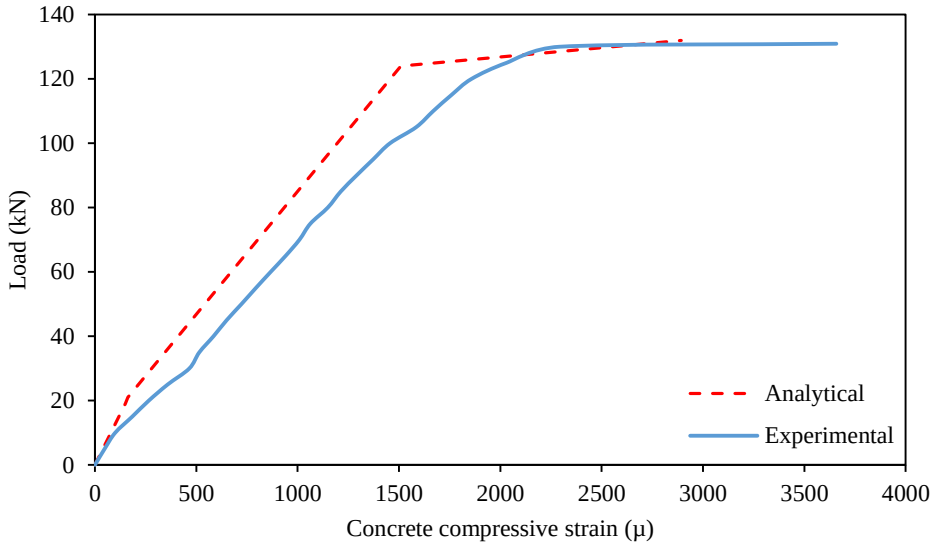

Figure C.17: Experimental and predicted load-concrete compressive strain curve (SN2S10)

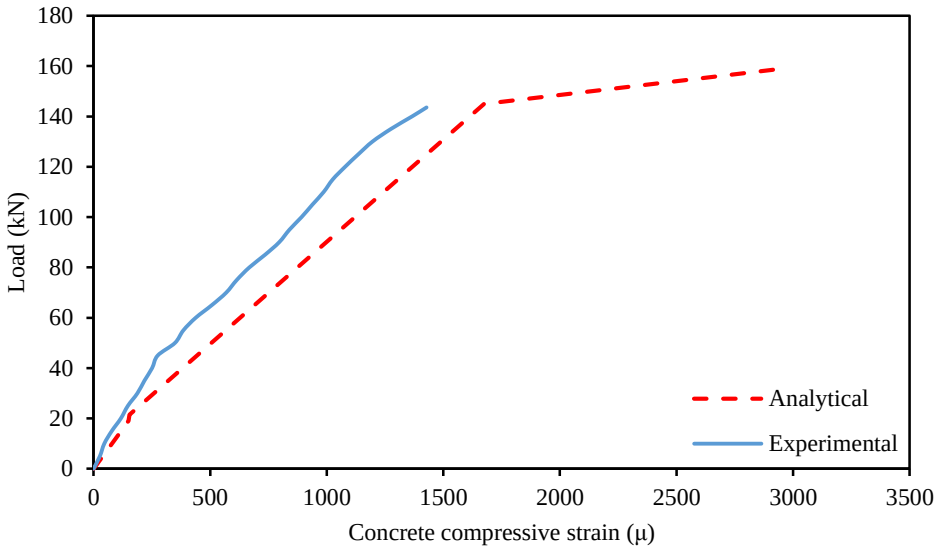

Figure C.18: Experimental and predicted load-concrete compressive strain curve (SN2S12)

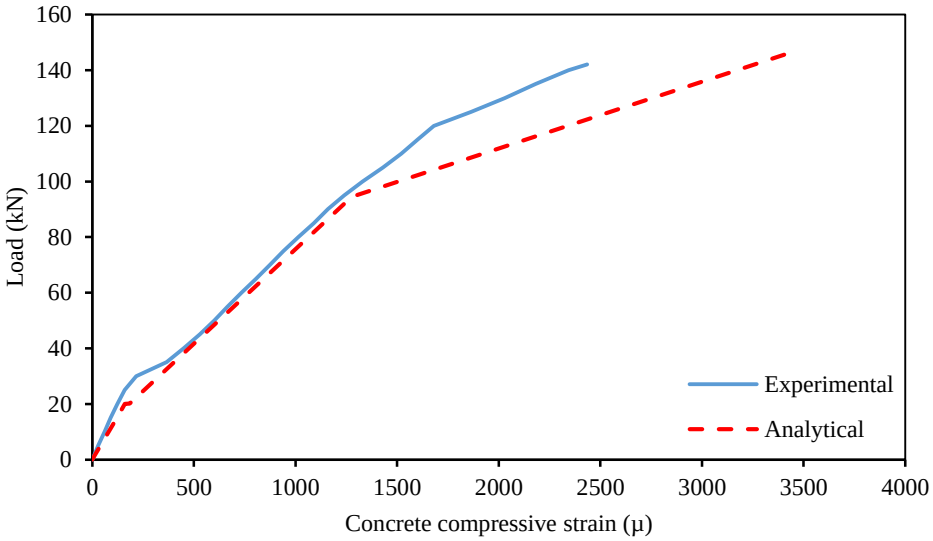

Figure C.19: Experimental and predicted load-concrete compressive strain curve (SN2C8)

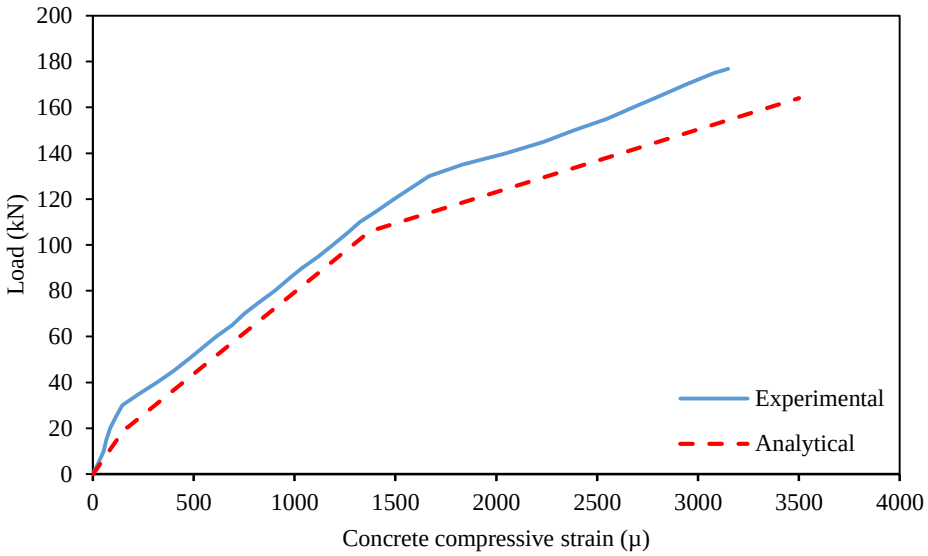

Figure C.20: Experimental and predicted load-concrete compressive strain curve (SN2C10)

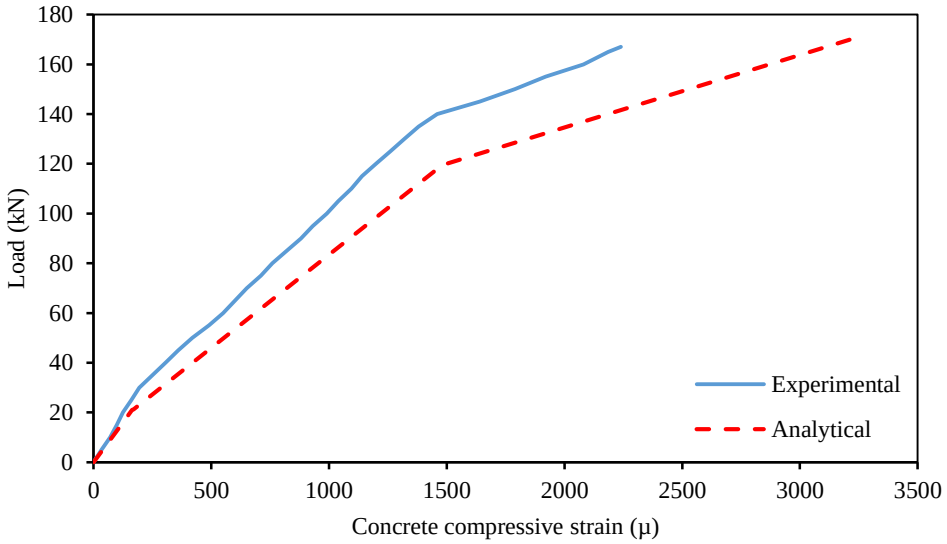

Figure C.21: Experimental and predicted load-concrete compressive strain curve (SN2C12)

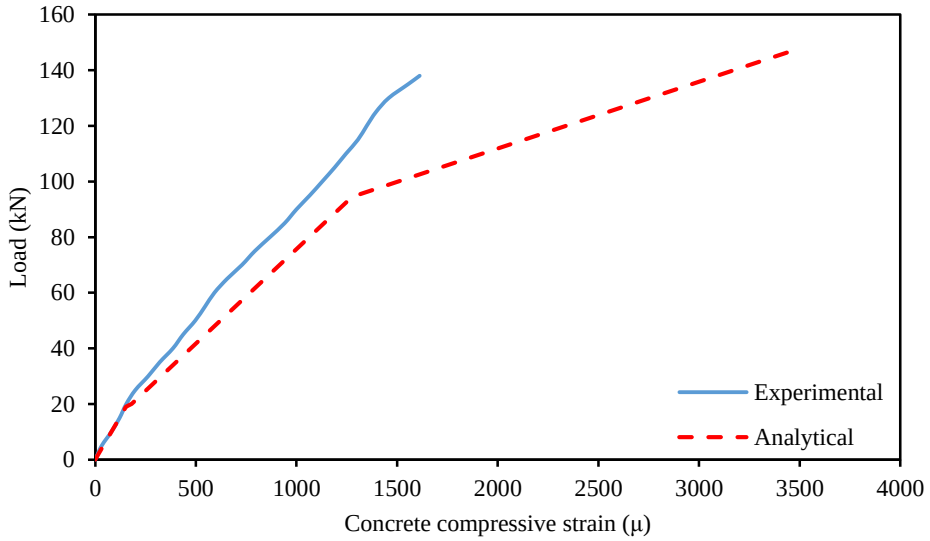

Figure C.22: Experimental and predicted load-concrete compressive strain curve (PSN2C8)

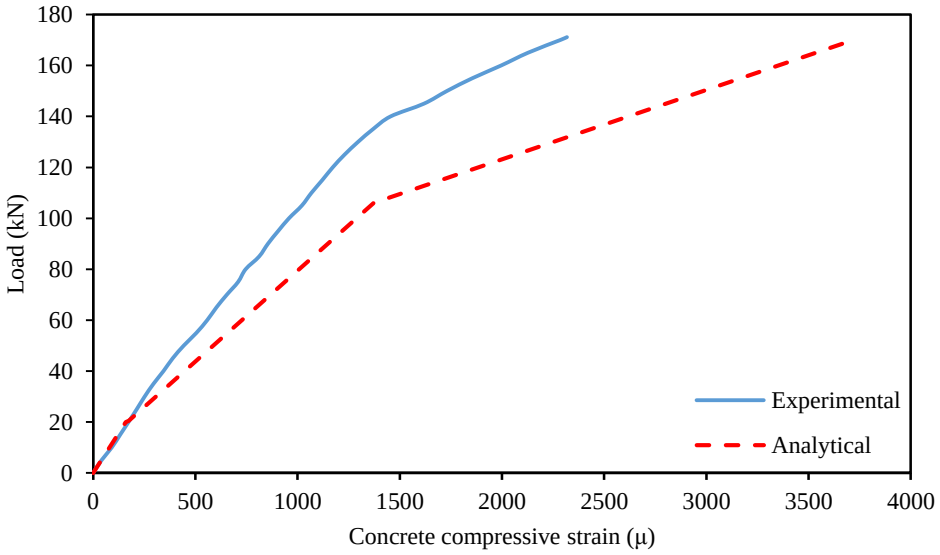

Figure C.23: Experimental and predicted load-concrete compressive strain curve (PSN2C10)

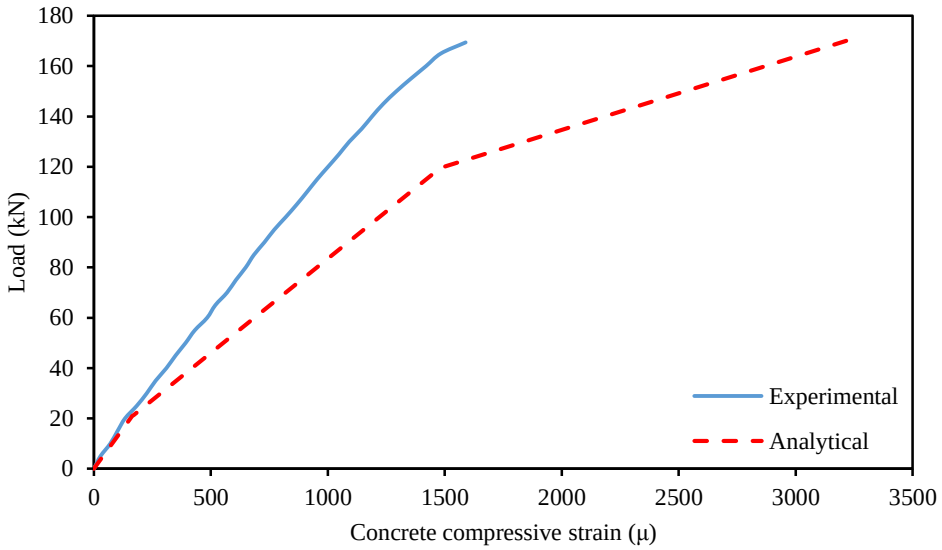

Figure C.24: Experimental and predicted load-concrete compressive strain curve (PSN2C12)

APPENDIX D – VERIFICATION OF MAIN BAR TENSILE STRAIN DIAGRAMS

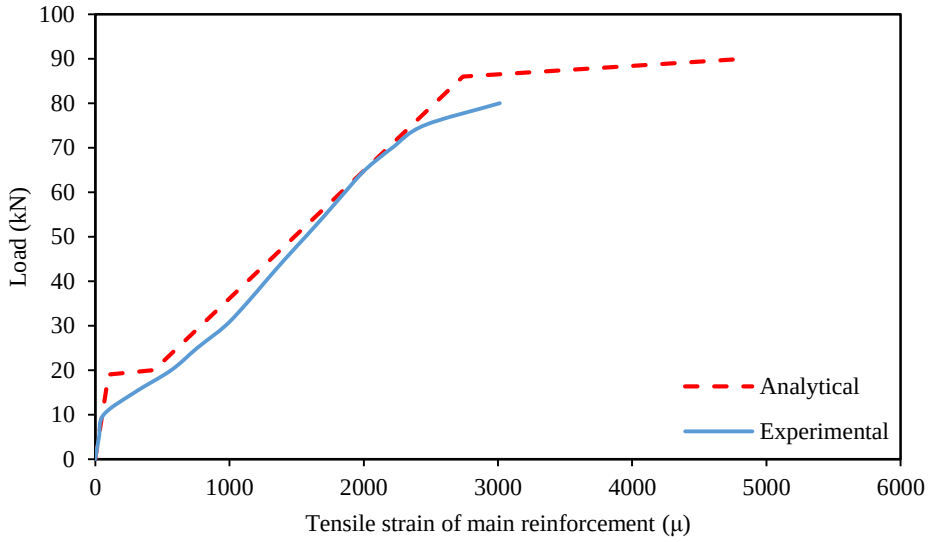

Figure D.1: Experimental and predicted load-tensile strain of the main reinforcement (N1S6)

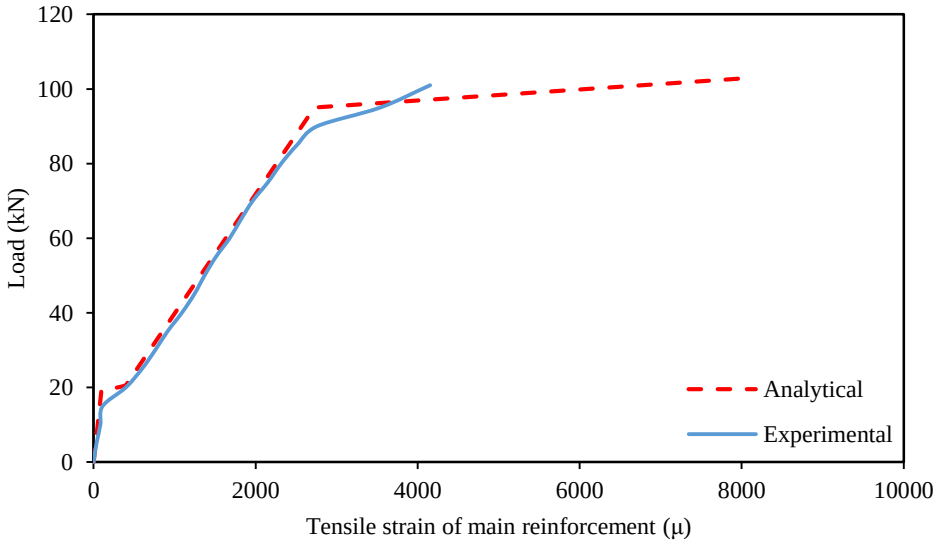

Figure D.2: Experimental and predicted load-tensile strain of the main reinforcement (N1S8)

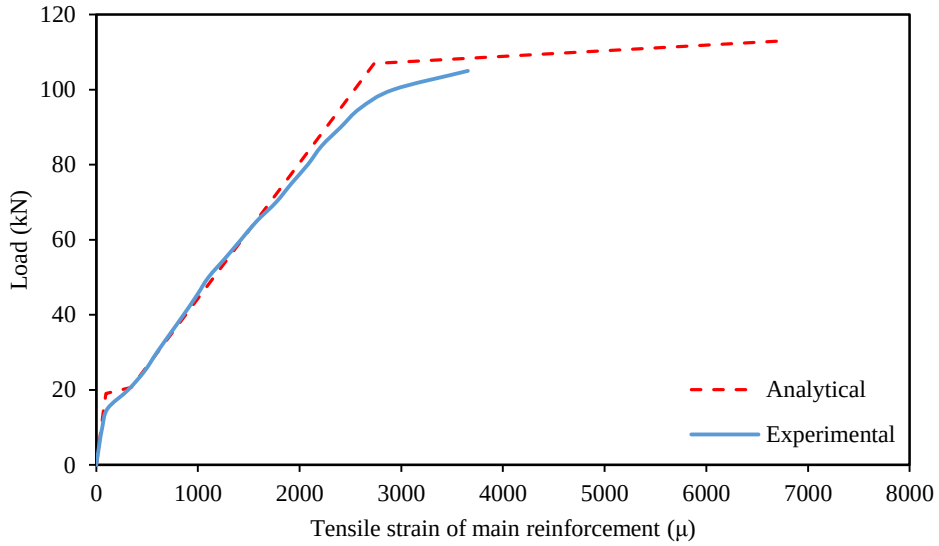

Figure D.3: Experimental and predicted load-tensile strain of the main reinforcement (N1S10)

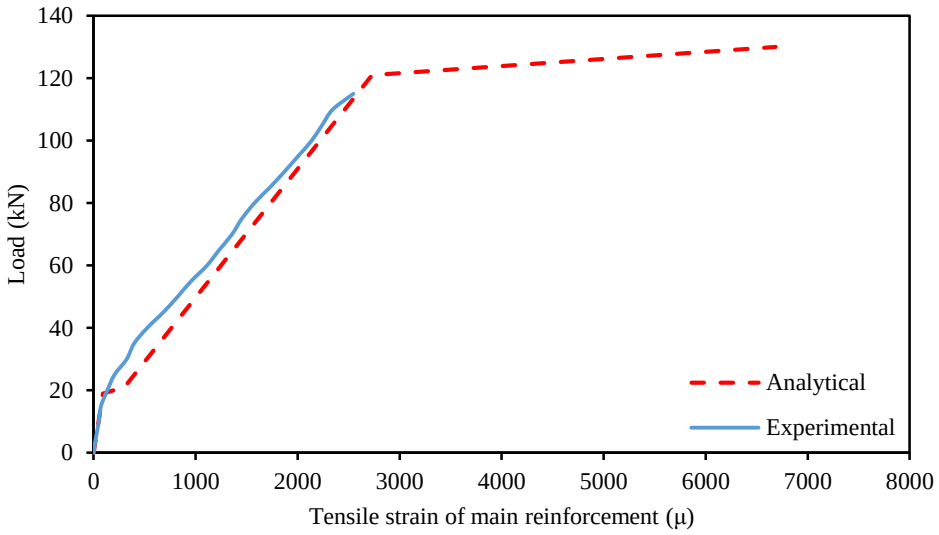

Figure D.4: Experimental and predicted load-tensile strain of the main reinforcement (N1S12)

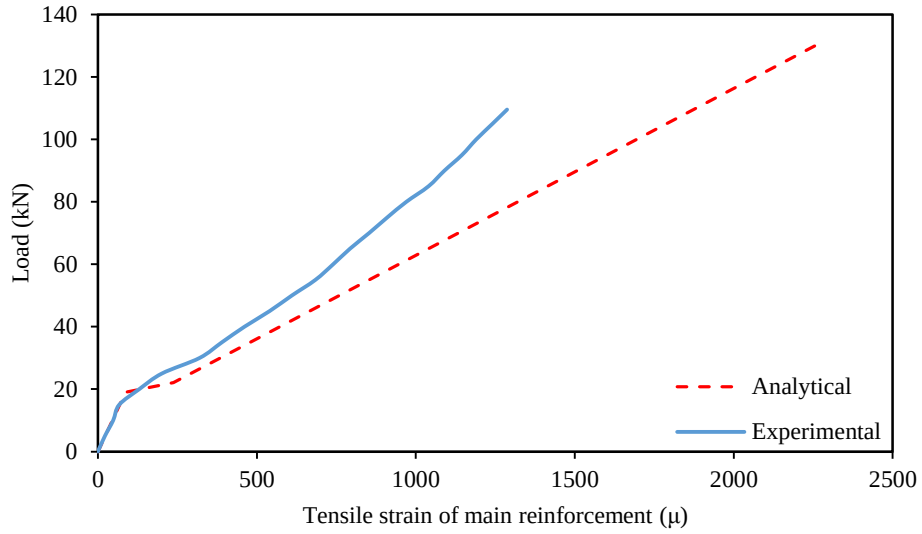

Figure D.5: Experimental and predicted load-tensile strain of the main reinforcement (N1S16)

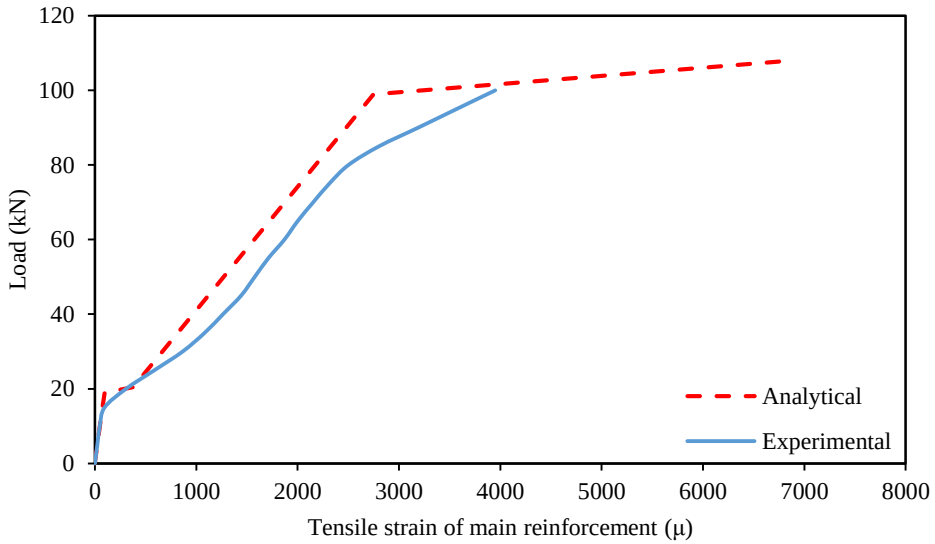

Figure D.6: Experimental and predicted load-tensile strain of the main reinforcement (N2S6)

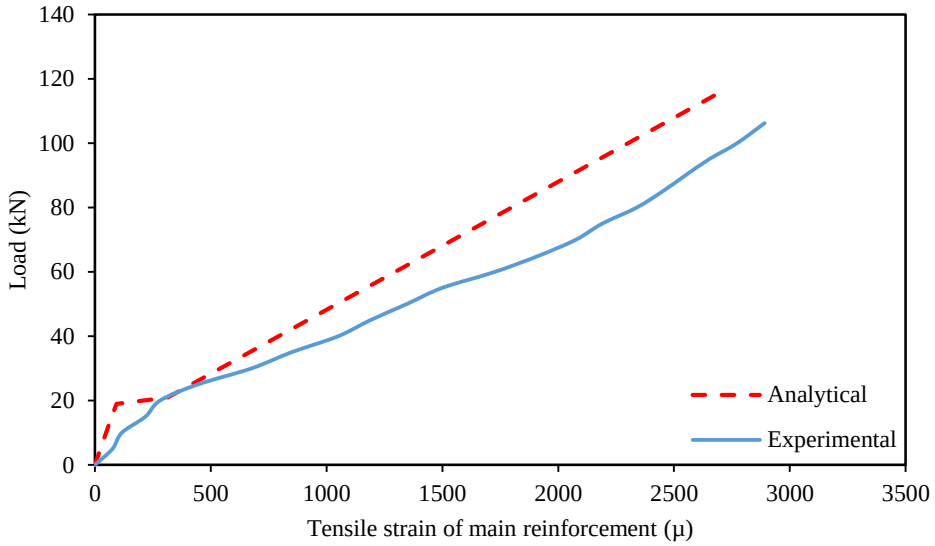

Figure D.7: Experimental and predicted load-tensile strain of the main reinforcement (N2S8)

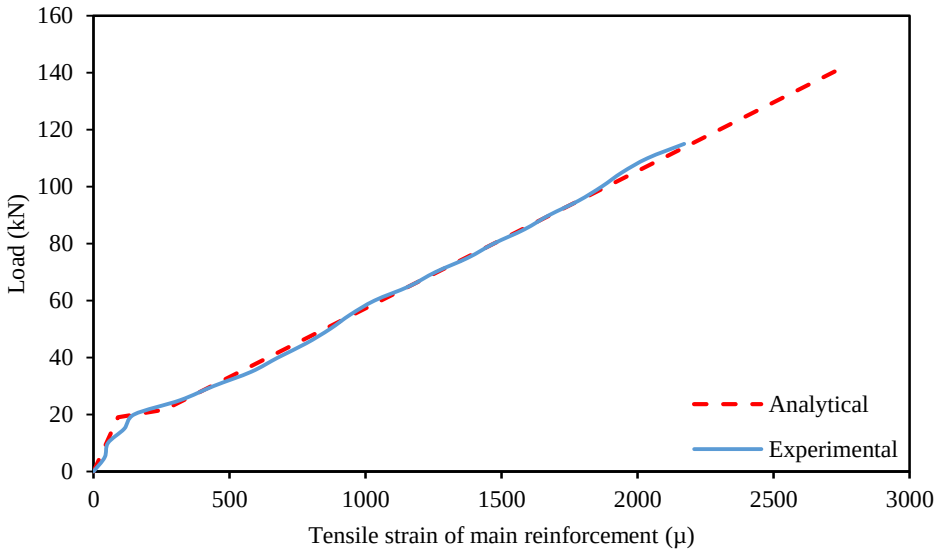

Figure D.8: Experimental and predicted load-tensile strain of the main reinforcement (N2S10)

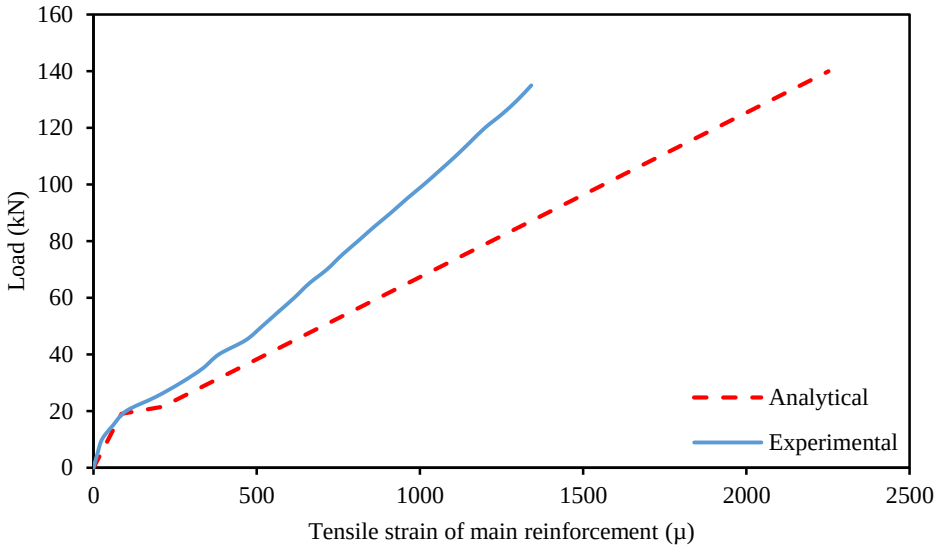

Figure D.9: Experimental and predicted load-tensile strain of the main reinforcement (N2S12)

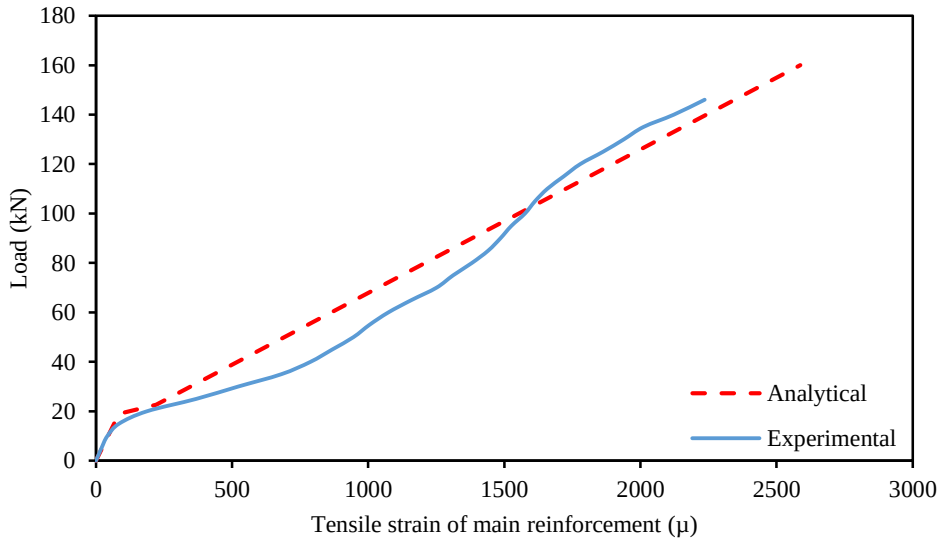

Figure D.10: Experimental and predicted load-tensile strain of the main reinforcement (N2C12)

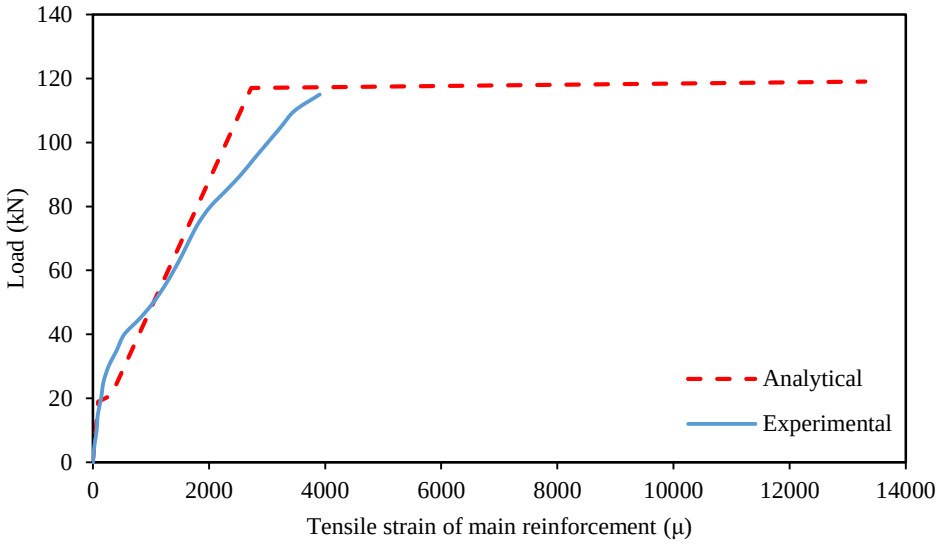

Figure D.11: Experimental and predicted load-tensile strain of the main reinforcement (N2S8U3)

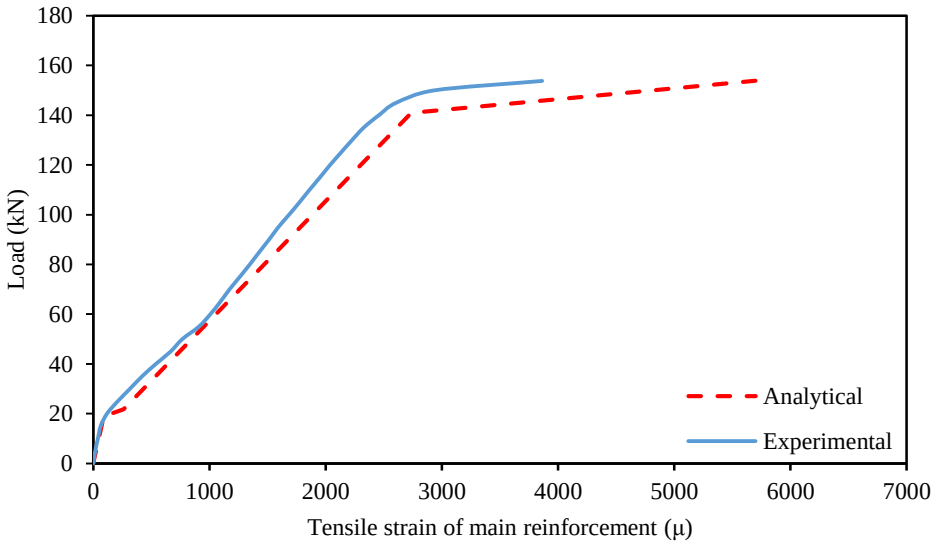

Figure D.12: Experimental and predicted load-tensile strain of the main reinforcement (N2S10U3)

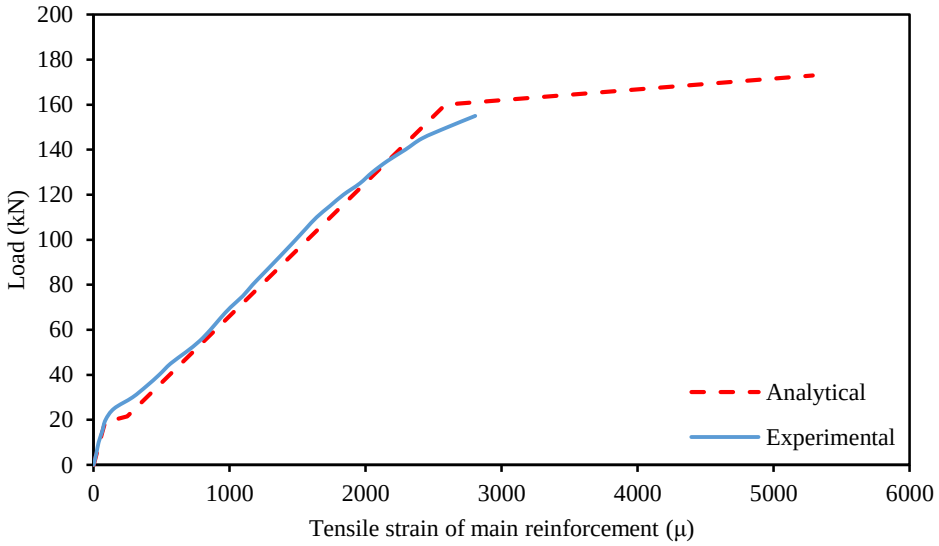

Figure D.13: Experimental and predicted load-tensile strain of the main reinforcement (N2S12U3)

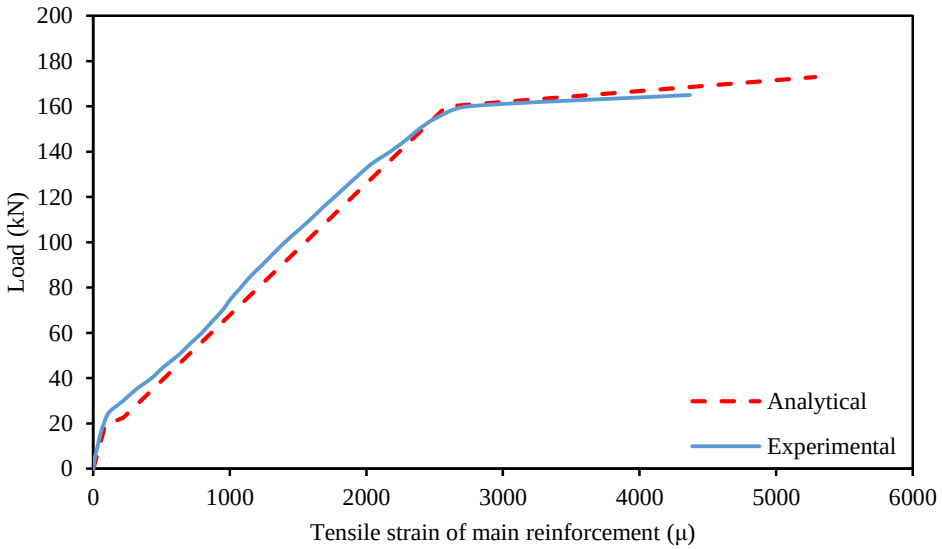

Figure D.14: Experimental and predicted load-tensile strain of the main reinforcement (N2S12U4)

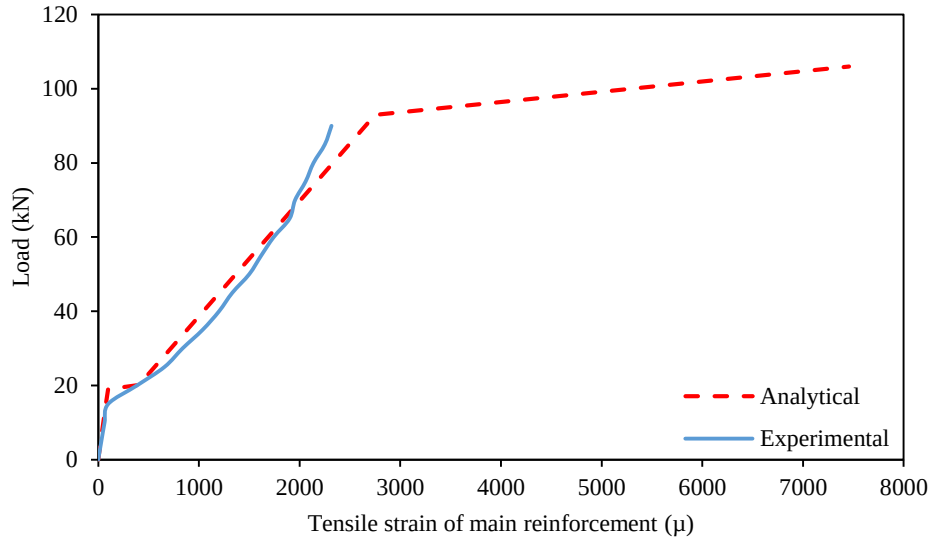

Figure D.15: Experimental and predicted load-tensile strain of the main reinforcement (SN2S6)

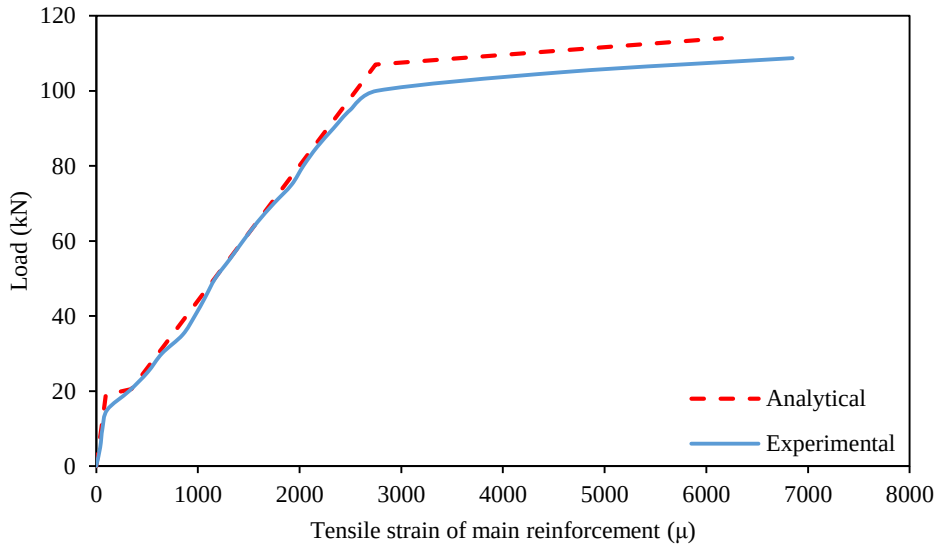

Figure D.16: Experimental and predicted load-tensile strain of the main reinforcement (SN2S8)

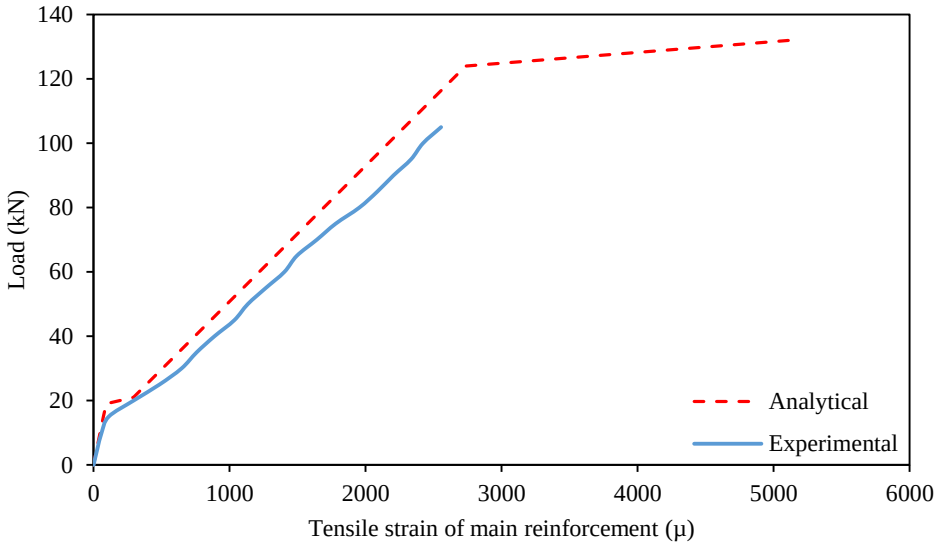

Figure D.17: Experimental and predicted load-tensile strain of the main reinforcement (SN2S10)

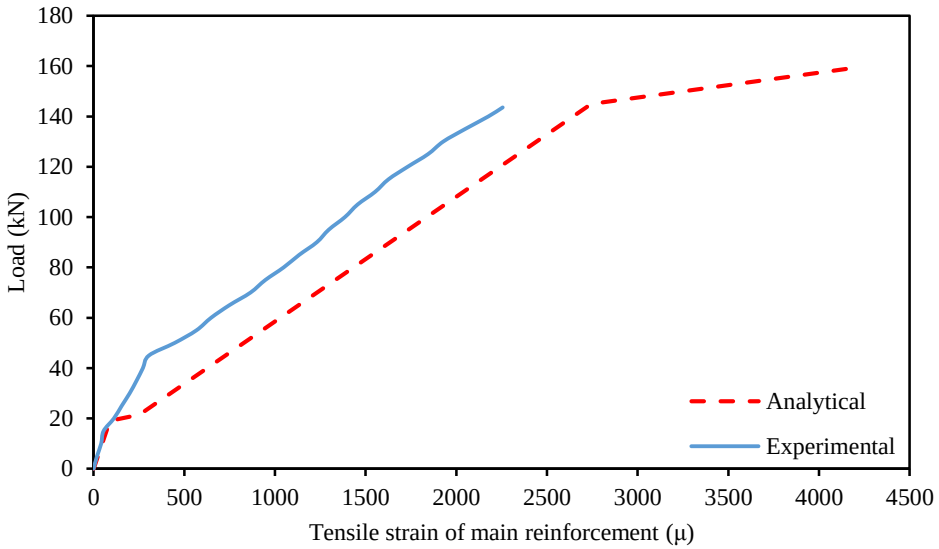

Figure D.18: Experimental and predicted load-tensile strain of the main reinforcement (SN2S12)

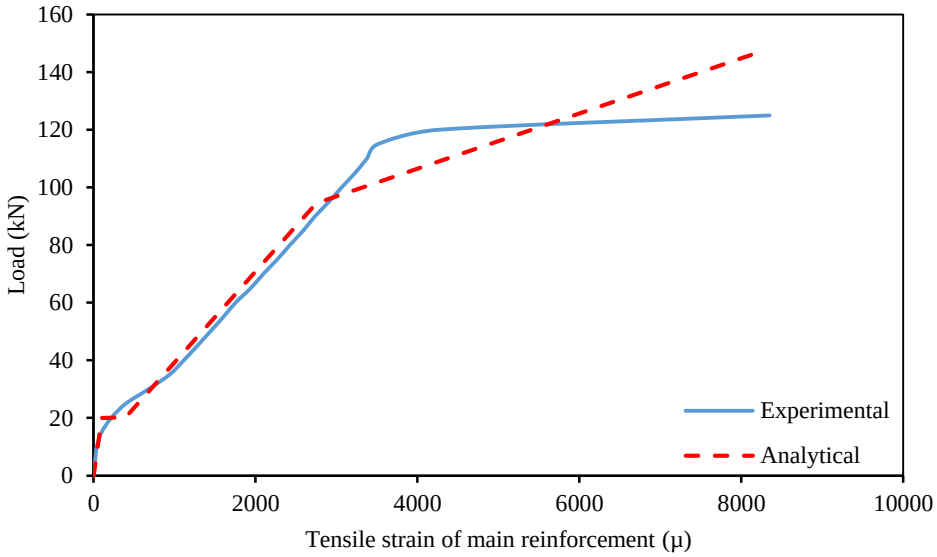

Figure D.19: Experimental and predicted load-tensile strain of the main reinforcement (SN2C8)

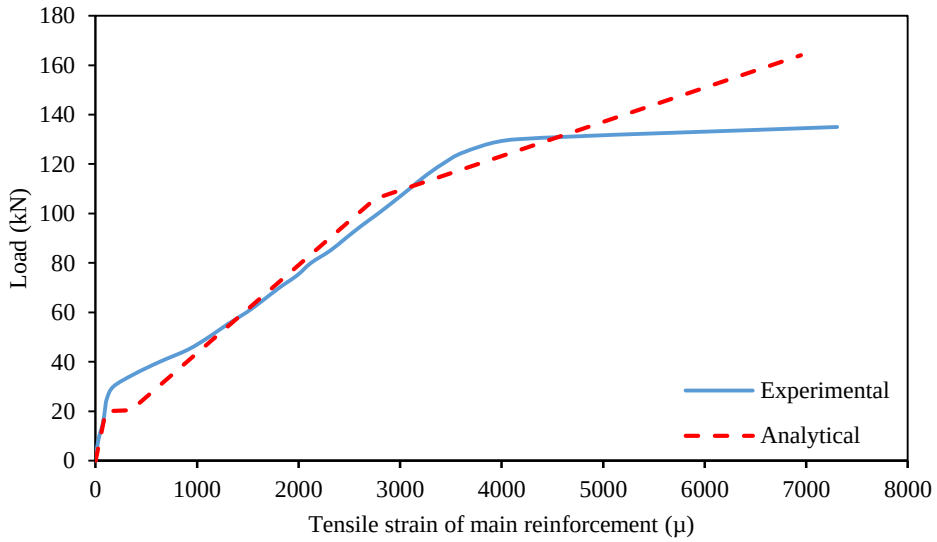

Figure D.20: Experimental and predicted load-tensile strain of the main reinforcement (SN2C10)

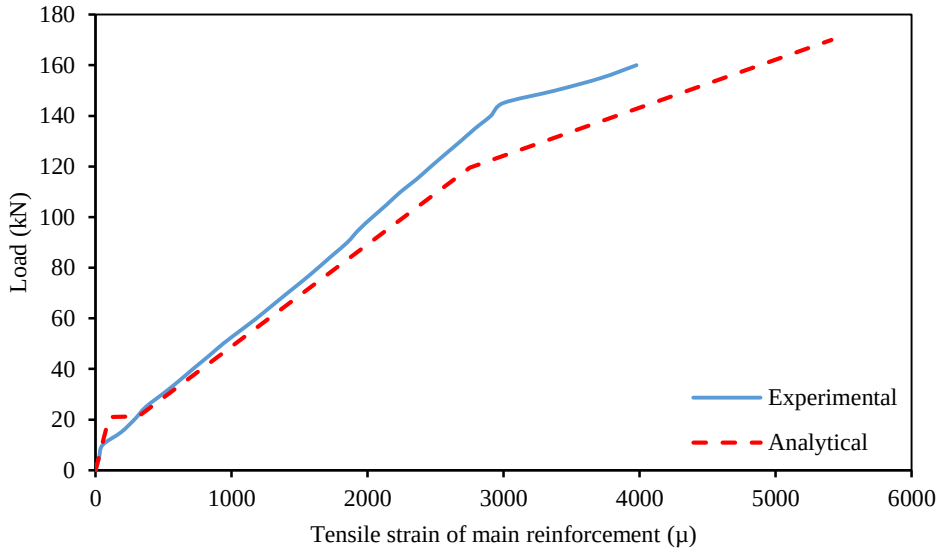

Figure D.21: Experimental and predicted load-tensile strain of the main reinforcement (SN2C12)

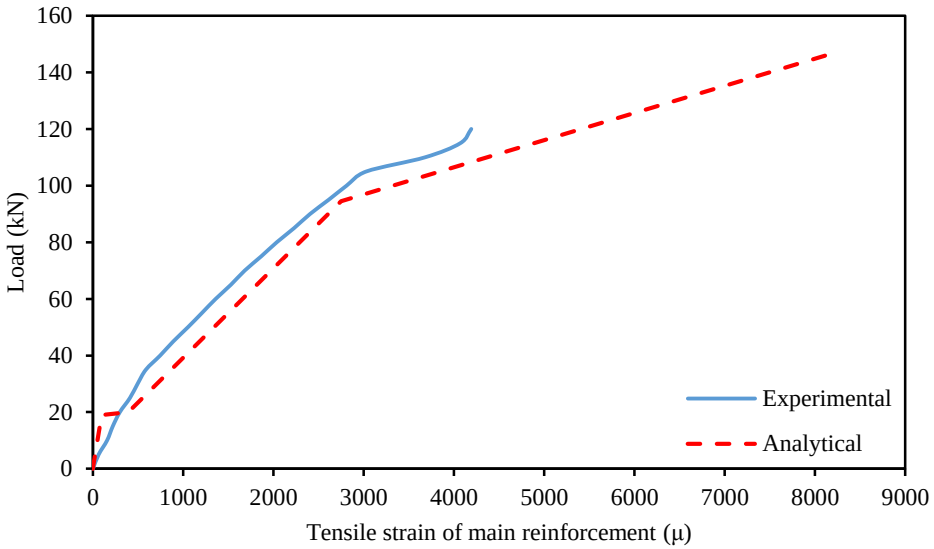

Figure D.22: Experimental and predicted load-tensile strain of the main reinforcement (PSN2C8)

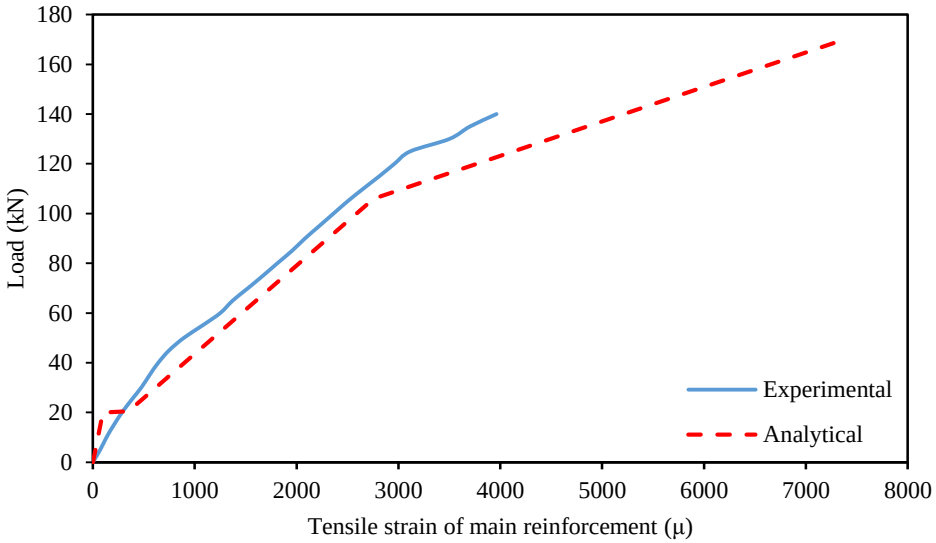

Figure D.23: Experimental and predicted load-tensile strain of the main reinforcement (PSN2C10)

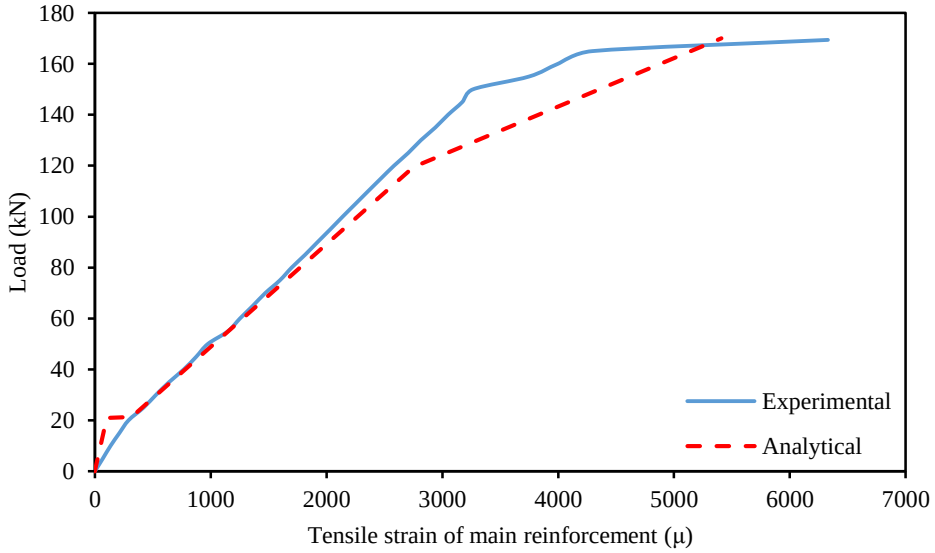

Figure D.24: Experimental and predicted load-tensile strain of the main reinforcement (PSN2C12)

APPENDIX E – VERIFICATION OF STRENGTHENING BAR TENSILE STRAIN DIAGRAMS

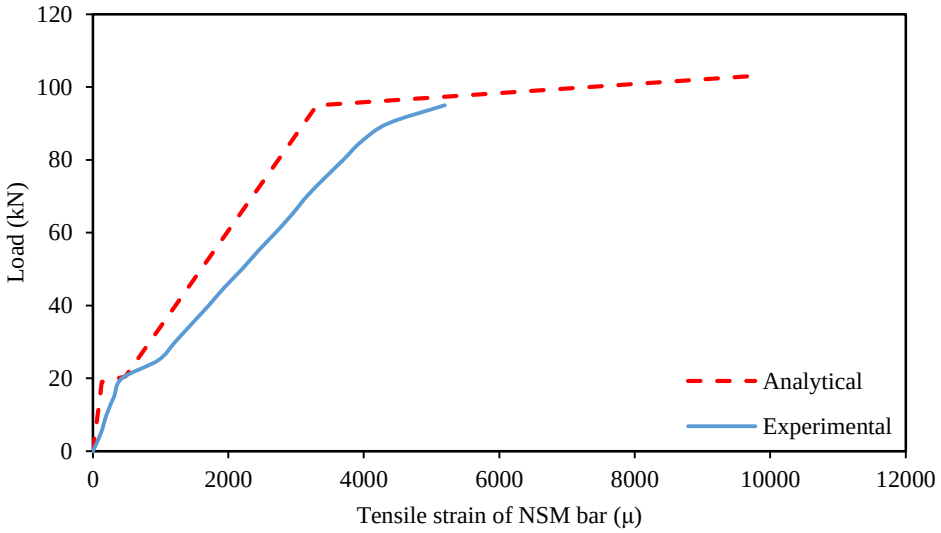

Figure E.1: Experimental and predicted load-tensile strain of strengthening bar curve (N1S8)

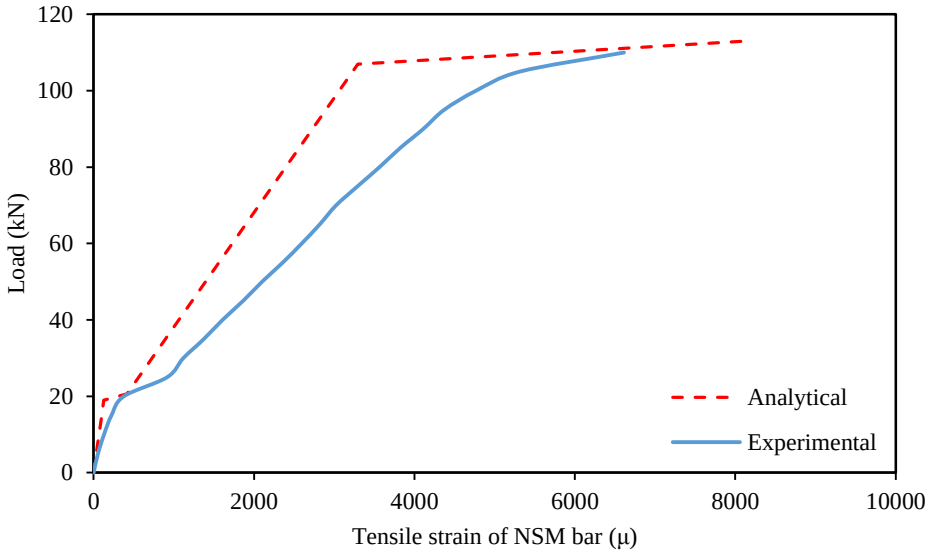

Figure E.2: Experimental and predicted load-tensile strain of strengthening bar curve (N1S10)

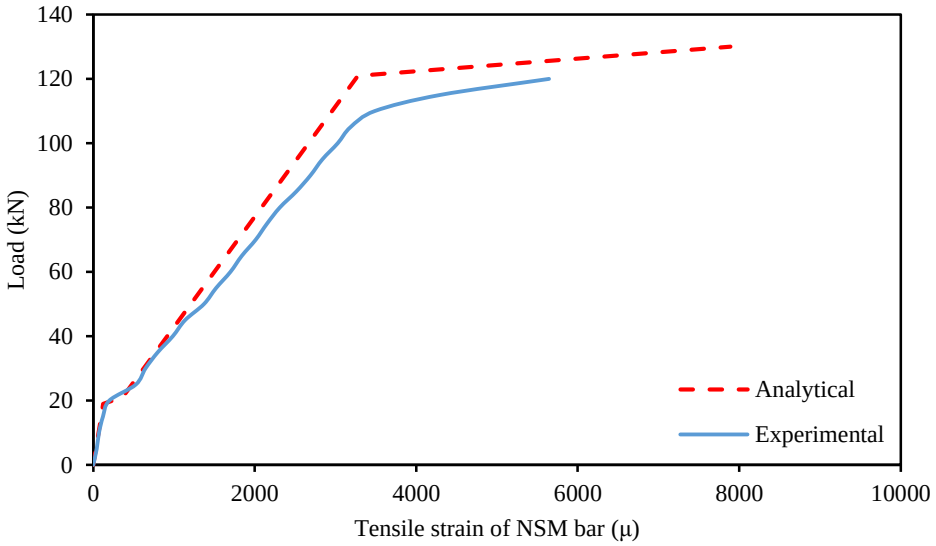

Figure E.3: Experimental and predicted load-tensile strain of strengthening bar curve (N1S12)

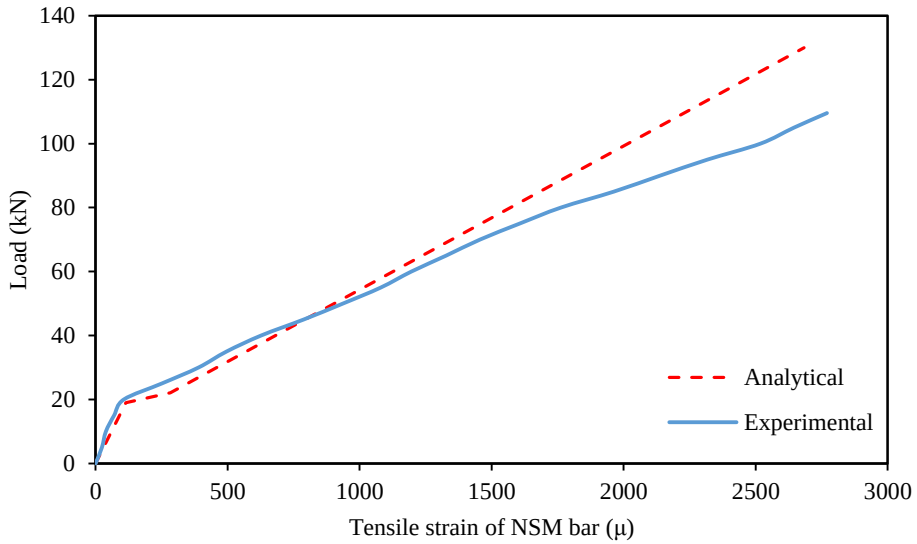

Figure E.4: Experimental and predicted load-tensile strain of strengthening bar curve (N1S16)

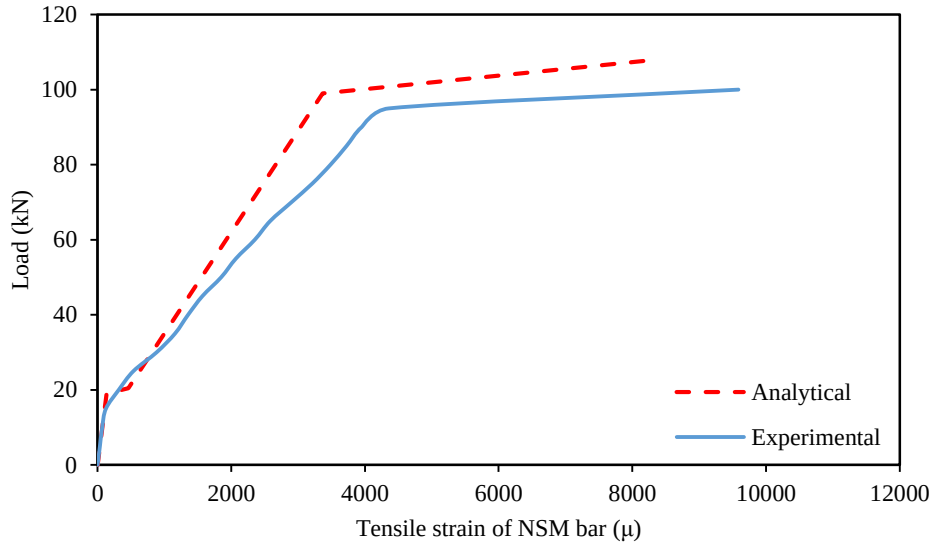

Figure E.5: Experimental and predicted load-tensile strain of strengthening bar curve (N2S6)

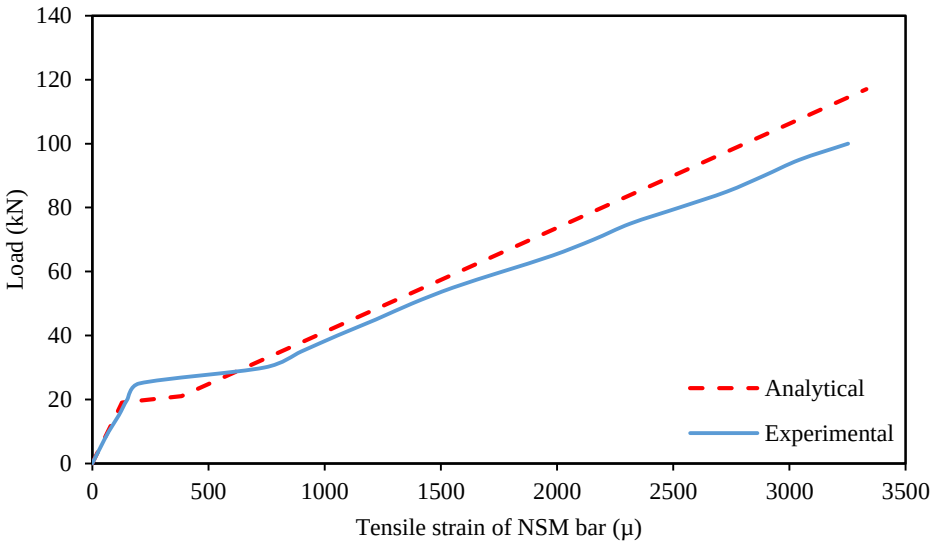

Figure E.6: Experimental and predicted load-tensile strain of strengthening bar curve (N2S8)

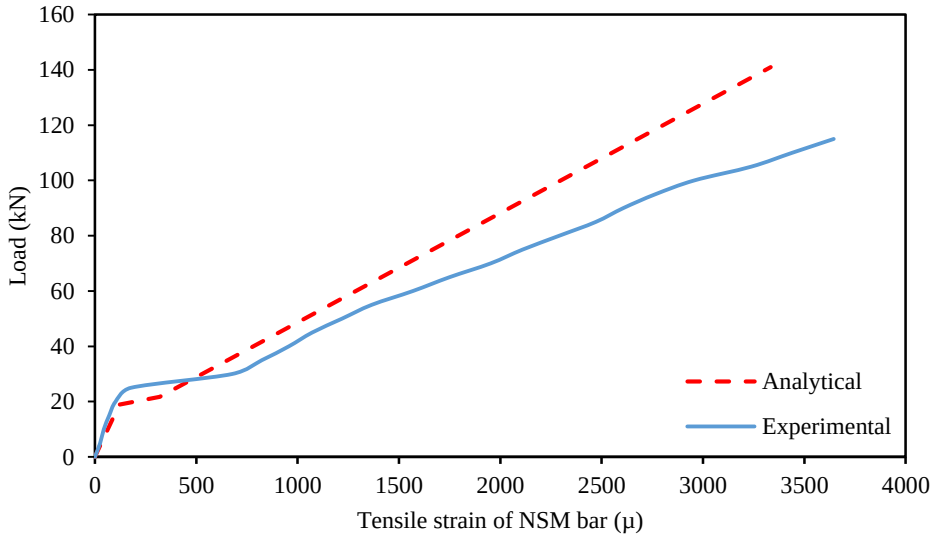

Figure E.7: Experimental and predicted load-tensile strain of strengthening bar curve (N2S10)

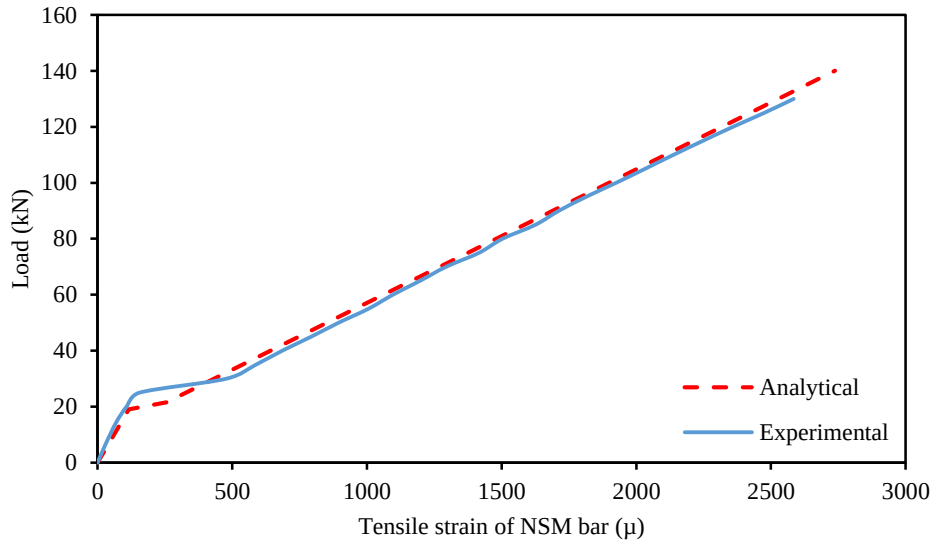

Figure E.8: Experimental and predicted load-tensile strain of strengthening bar curve (N2S12)

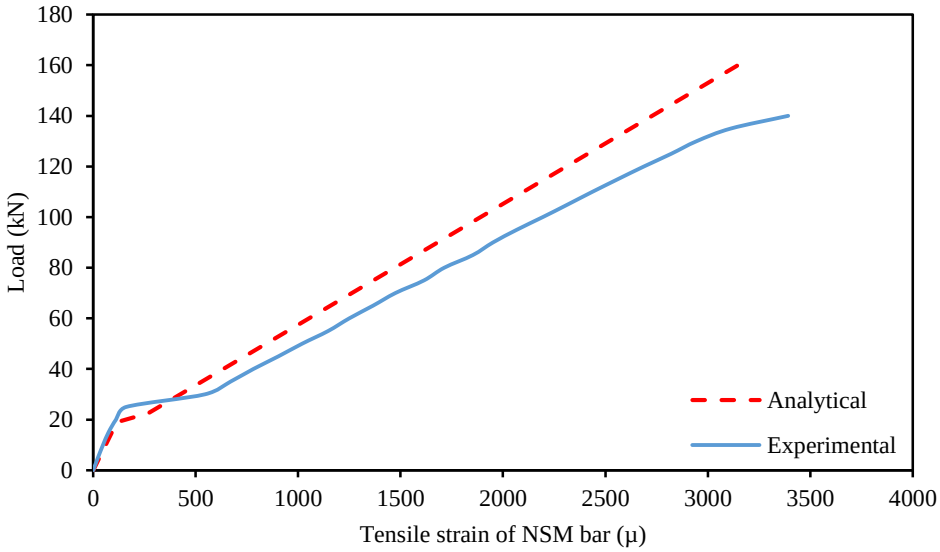

Figure E.9: Experimental and predicted load-tensile strain of strengthening bar curve (N2C12)

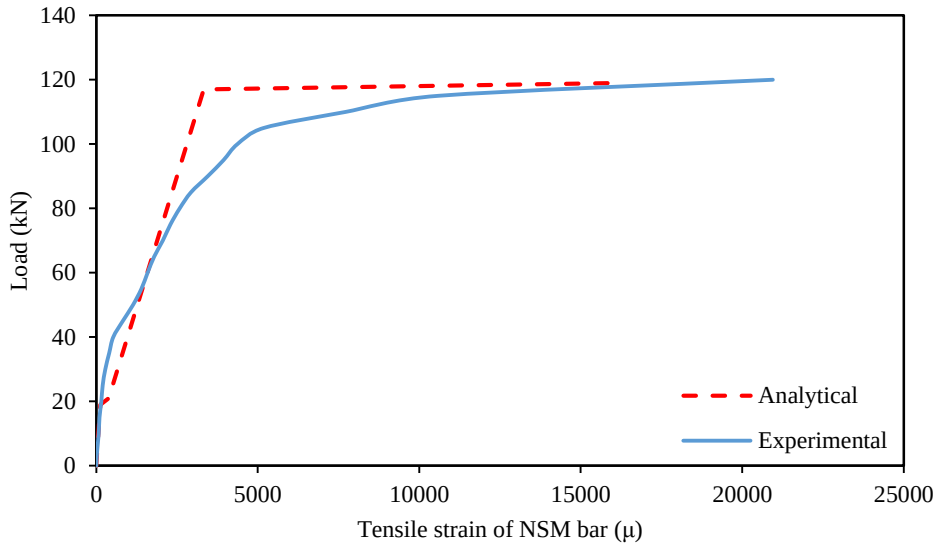

Figure E.10: Experimental and predicted load-tensile strain of strengthening bar curve (N2S8U3)

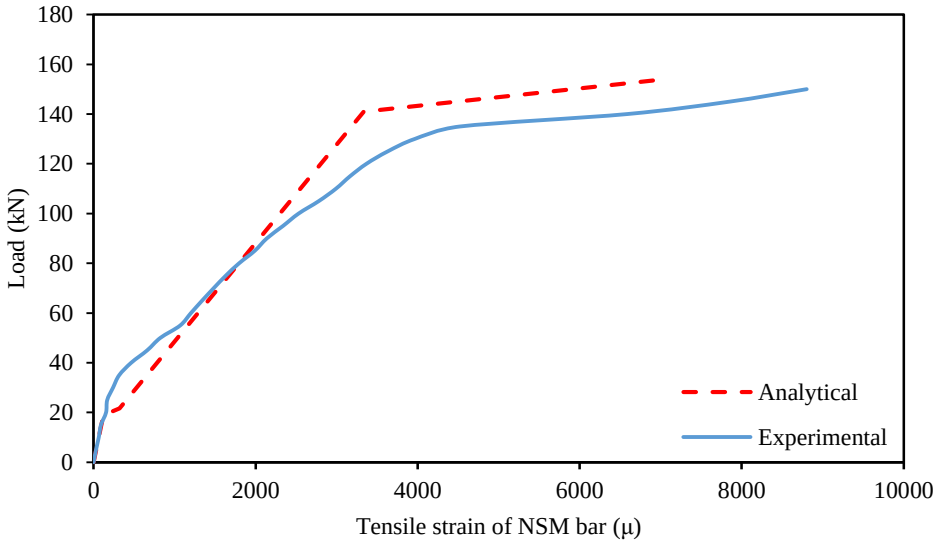

Figure E.11: Experimental and predicted load-tensile strain of strengthening bar curve (N2S10U3)

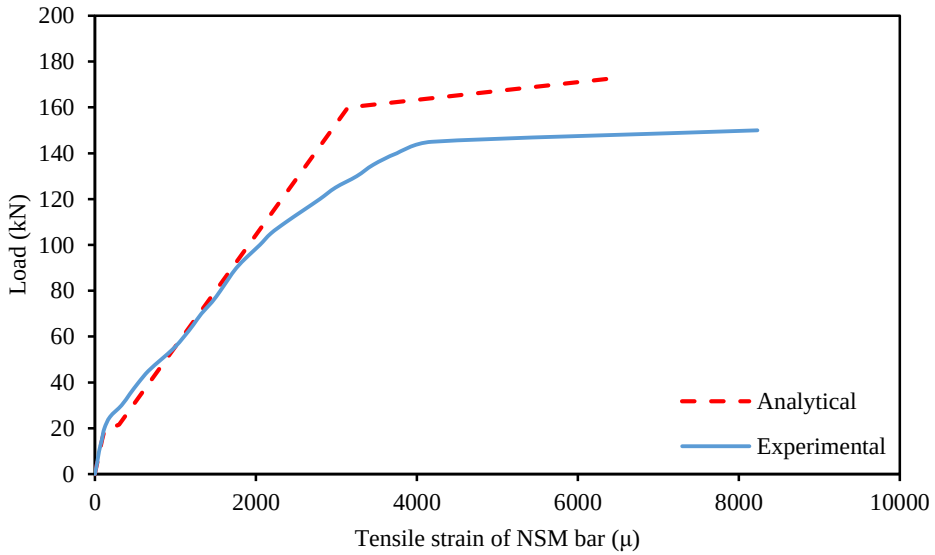

Figure E.12: Experimental and predicted load-tensile strain of strengthening bar curve (N2S12U3)

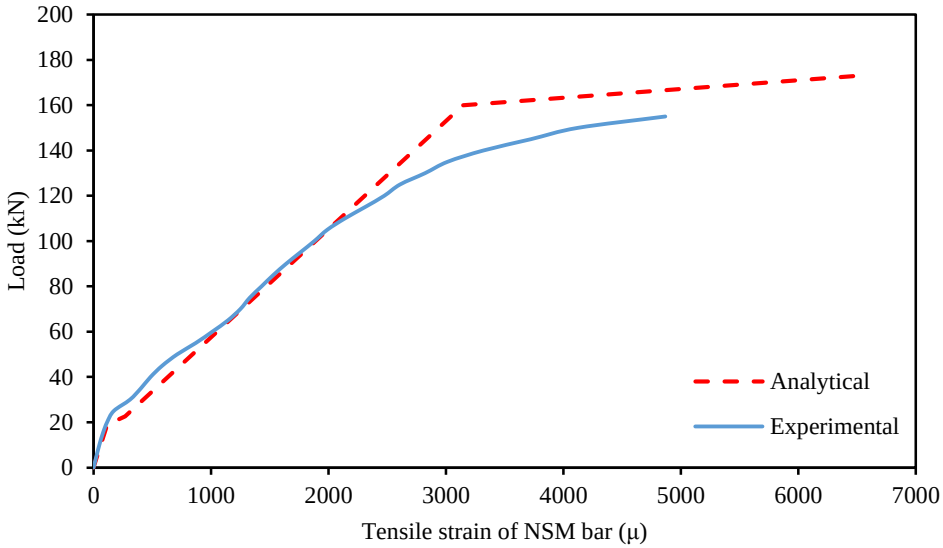

Figure E.13: Experimental and predicted load-tensile strain of strengthening bar curve (N2S12U4)

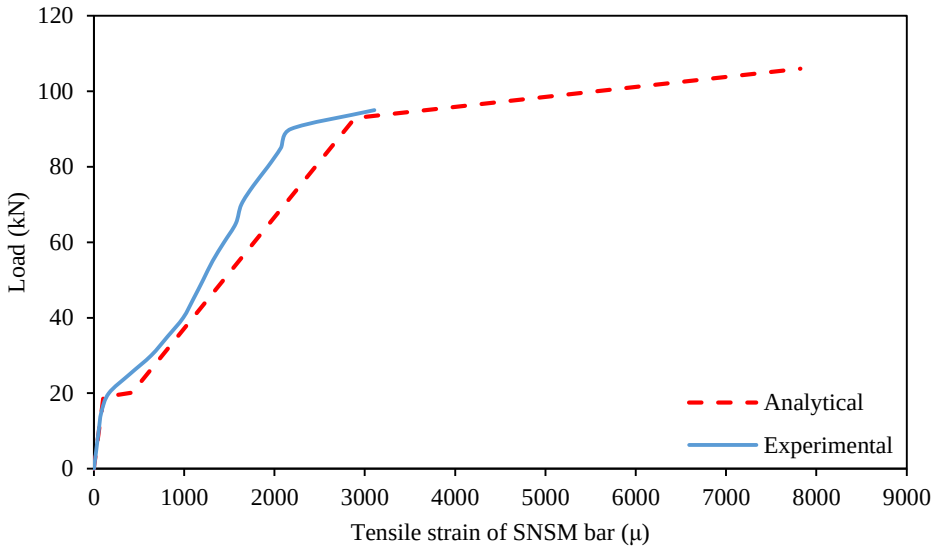

Figure E.14: Experimental and predicted load-tensile strain of strengthening bar curve (SN2S6)

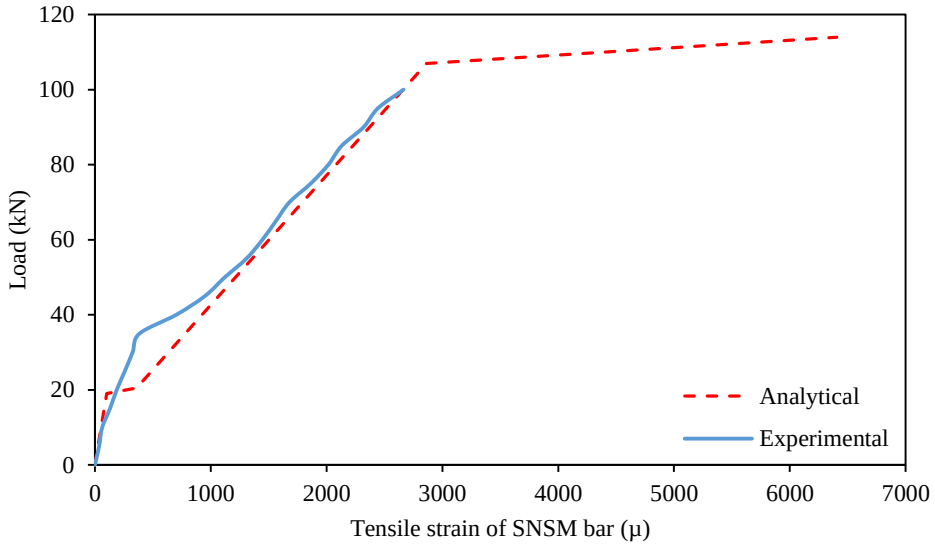

Figure E.15: Experimental and predicted load-tensile strain of strengthening bar curve (SN2S8)

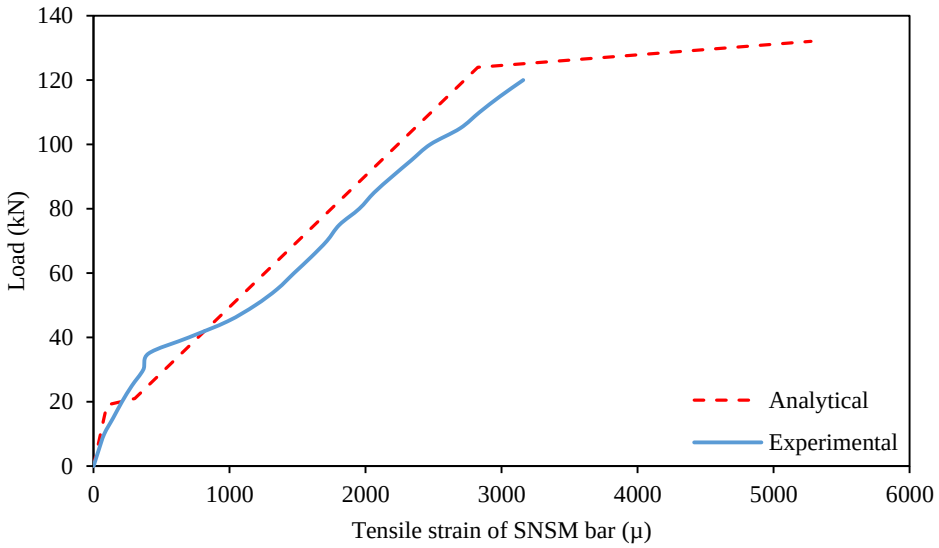

Figure E.16: Experimental and predicted load-tensile strain of strengthening bar curve (SN2S10)

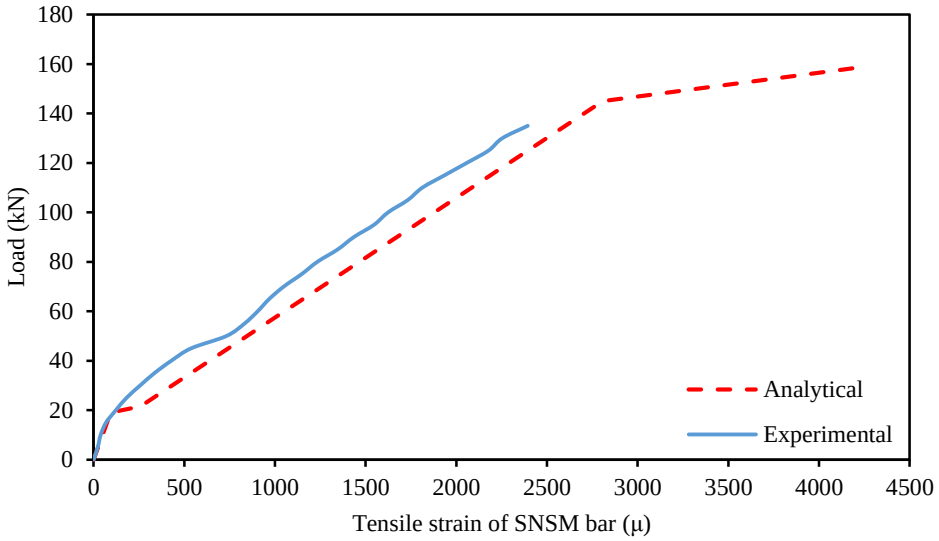

Figure E.17: Experimental and predicted load-tensile strain of strengthening bar curve (SN2S12)

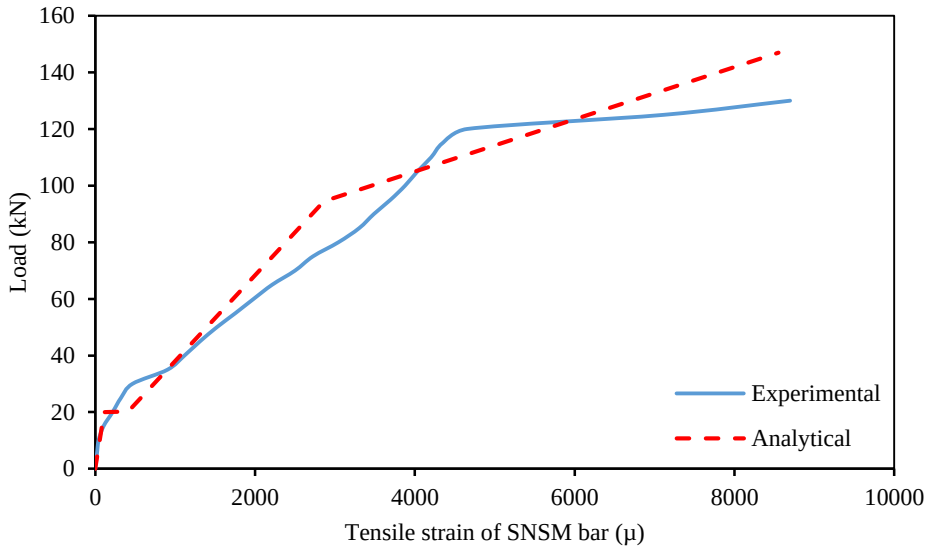

Figure E.18: Experimental and predicted load-tensile strain of strengthening bar curve (SN2C8)

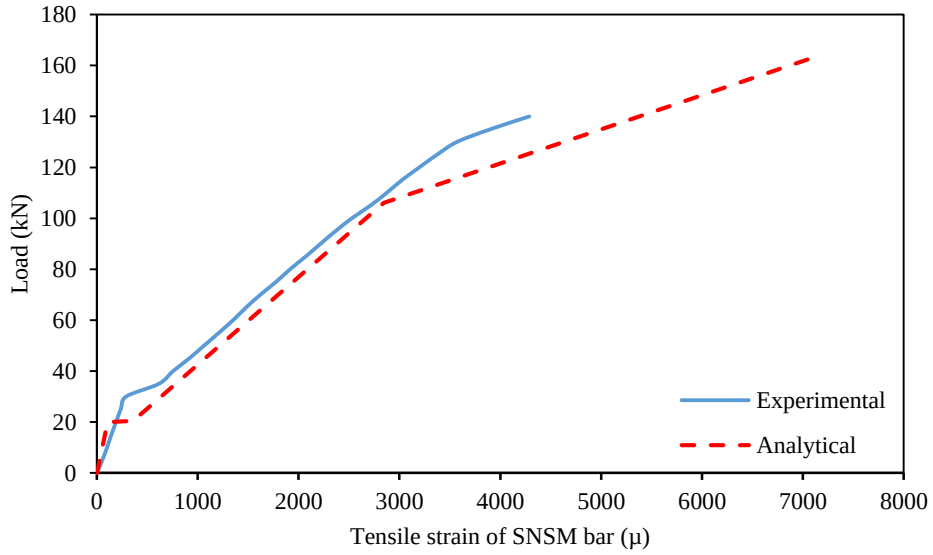

Figure E.19: Experimental and predicted load-tensile strain of strengthening bar curve (SN2C10)

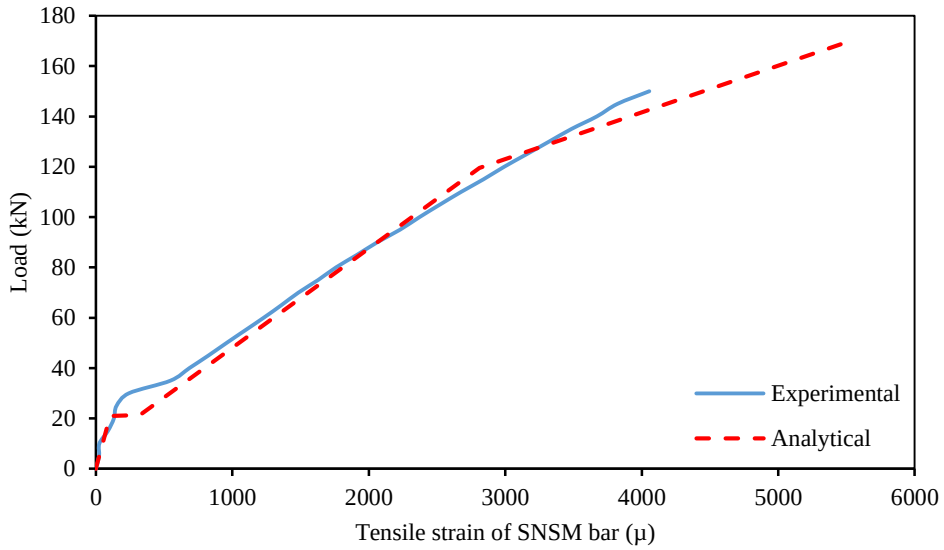

Figure E.20: Experimental and predicted load-tensile strain of strengthening bar curve (SN2C12)

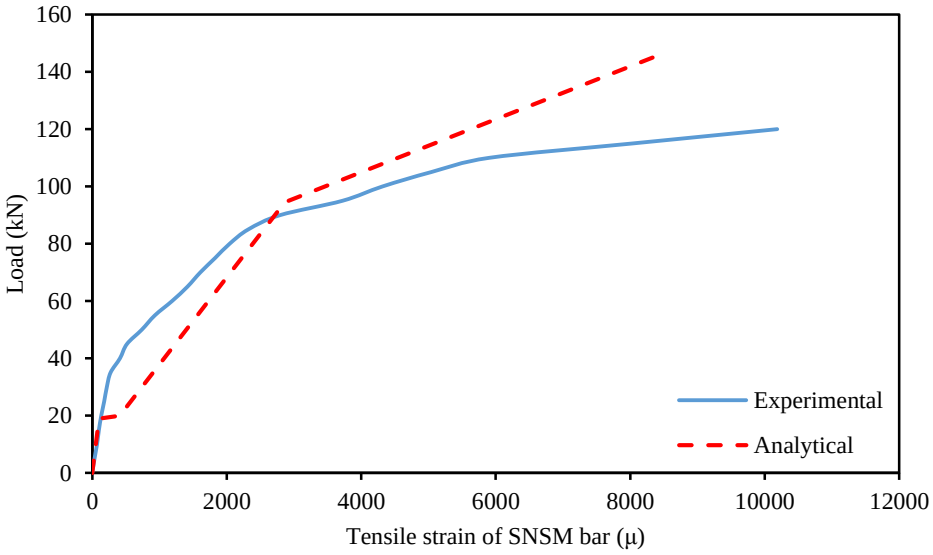

Figure E.21: Experimental and predicted load-tensile strain of strengthening bar curve (PSN2C8)

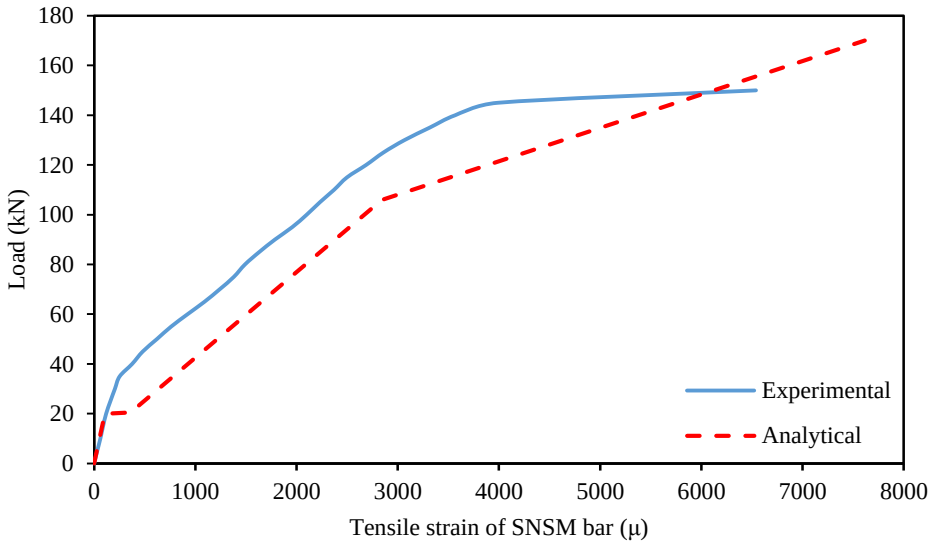

Figure E.22: Experimental and predicted load-tensile strain of strengthening bar curve (PSN2C10)

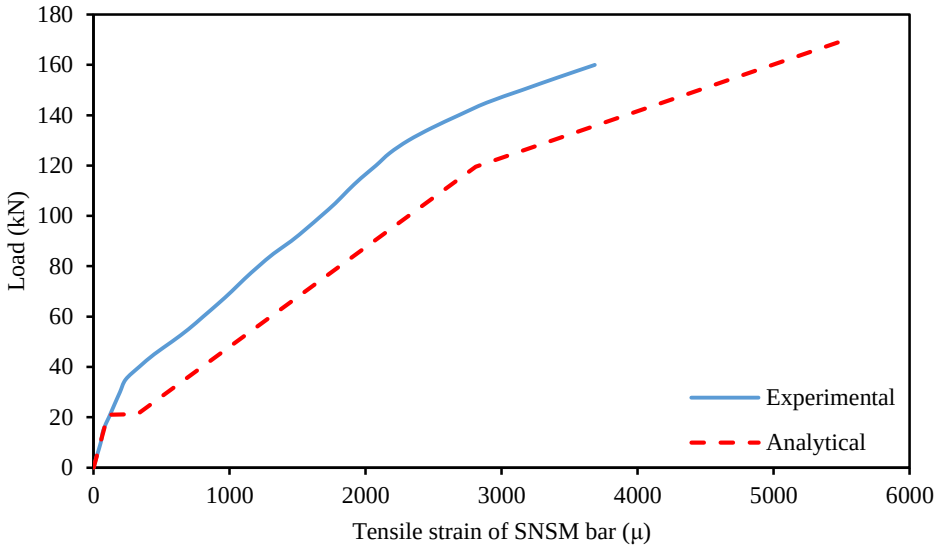

Figure E.23: Experimental and predicted load-tensile strain of strengthening bar curve (PSN2C12)

APPENDIX F – LIST OF PUBLICATIONS

Journal Articles:

Hosen, M. A., Jumaat, M. Z., and Islam, A. S. "Side Near Surface Mounted (SNSM) Technique for Flexural Enhancement of RC Beams," Materials and Design, vol. 83C, 2015, p. 587-597.

Hosen, M. A., Jumaat, M. Z., and Islam, A. S. "Inclusion of CFRP-Epoxy Composite for End Anchorage in NSM-Epoxy Strengthened Beams," Advances in Materials Science and Engineering, vol. 2015, p. 10.

Hosen, M. A., Jumaat, M. Z., Islam, A. S., & Darain, K. M. U, "Flexural Performance of RC Beams Strengthened in New S-NSM Technique using CFRP Bars – Experimental and Analytical Investigation," Science of Advance Materials (Accepted).

Hosen, M. A., Jumaat, M. Z., Darain, K. M. U., & Obaydullah, "Energy Absorption capacity of RC Beams Strengthened with NSM Technique using Ductile Materials," Engineering Structures (Under review).

Hosen, M. A., Jumaat, M. Z., and Islam, A. S. "Flexural Behavior Enhancement of RC Beams Strengthen with NSM Steel Bar: Experiment and Simulation," Structural and Multidisciplinary Optimization (Under review).

Hosen, M. A., Jumaat, M. Z., and Alengaram, U. J. "NSM Composites for Flexural Enhancement of RC Beams: Experimental and Analytical Investigation," Journal of Zhejiang University-SCIENCE A (Under review).

Hosen, M. A., Jumaat, M. Z., Alengaram, U. J., and Islam, A. S. "Flexural Enhancement of RC Beams with Side-NSM Technique and Comparison with prediction models," Materials and Structures (With editor).

Conference Proceedings:

Hosen, M. A., Jumaat, M. Z., Darain, K. M. U., Obaydullah, M., & Islam, A. S. "Flexural Strengthening of RC Beams with NSM Steel Bars," International Conference on Food, Agriculture and Biology (FAB-2014) June 11-12, 2014 Kuala Lumpur, Malaysia.

Jumaat, M. Z., Hosen, M. A., Darain, K. M. U., & Obaydullah, M. "Innovative End Anchorage for Preventing Concrete Cover Separation of NSM Steel and CFRP bars Strengthened RC Beams," The Sixth Jordanian International Civil Engineering Conference, March 10-12, 2015 Amman, Jordan.